THE UNIVERSITY *of* EDINBURGH

Genesis of Zoned Granite Plutons in the Iapetus Suture Zone: New Constraints from High-precision Micro-analysis of Accessory Minerals

THE UNIVERSITY *of* EDINBURGH

Andrew J. Miles

A Thesis Submitted for the Degree of Doctor of Philosophy

2012

Declaration

I declare that this thesis has been composed solely by myself and that it has not been submitted, either in whole or in part, in any previous application for a degree. Except where otherwise acknowledged, the work presented is entirely my own.

Andrew Miles

September 20th, 2012 (initial submission)
November 30th, 2012 (final submission)

Ignorance more frequently begets confidence than does knowledge: it is those who know little, and not those who know much, who so positively assert that this or that problem will never be solved by science.

Charles Darwin

The Descent of Man, 1871

Abstract

The Trans-Suture Suite (TSS) of granitic plutons located in Northern Britain span the Iapetus Suture and represent a particularly enigmatic stage of post-Caledonian Devonian magmatism. Despite calc-alkaline affinities, proximity to the Iapetus Suture precludes a direct relationship to active subduction. Furthermore, the absence of inherited zircons distinguishes the TSS from plutons of a similar age throughout the Scottish Highlands, and is not easily reconciled with the abundance of peraluminous and S-type granites. Micro-analytical techniques are employed to analyse accessory zircon and apatite from three TSS plutons (Criffell, Fleet and Shap) in order to investigate connections between magmatic and tectonic processes within a continental suture zone. Accessory minerals contain a robust and accessible record of magma evolution. However, their trace element compositions are shown to document the final stages of pluton emplacement only, and are determined primarily by competitive crystallisation of other accessory phases at shallow crustal levels. By contrast, whole-rock compositions record an earlier stage of magma evolution that occurred in deeper and open-system crustal hot zones. The absence of inherited zircon in the final crystal assemblage reflects resorption during rapid and potentially adiabatic ascent of super-liquidus and water-rich magmas from the crustal hot zone. The concentrations of REE in apatite inclusions decrease with increasing crystallisation of other accessory minerals and in some samples have been distinguished on the basis of their host phase. In metaluminous granodiorites, no preferred crystallisation sequence is observed between host phases. In peraluminous samples, zircon-hosted apatite compositions appear more primitive compared to those hosted by other phases and reflects earlier saturation of zircon in these magmas. The isotopic record of zircon is shown to be biased towards earlier stages of magma evolution in peraluminous magmas and provides a means of assessing zircon isotope compositions in the context of often protracted histories during silicic magma evolution. The Mn content of apatite varies independently to whole-rock composition, correlating positively with decreasing oxygen fugacity and indices of increasing reduction. Apatite is proposed as a robust and effective redox proxy with application to magmatic, detrital and lunar studies of redox conditions. Zircon O-Hf-

U-Th-Pb isotope compositions have identified increasing degrees of compositional heterogeneity in more silicic components of the TSS, including the involvement of more mafic magmas in the generation of the large S-type pluton of Fleet. Compositional trends between zircons from plutons emplaced on both sides of the Iapetus Suture are used to identify a common Avalonian component beneath the Southern Uplands and English Lake District related to Avalonian underthrusting beneath the Laurentian margin during the late Caledonian. New geochronological dating indicates that pluton emplacement occurred during periods of both pre- and post-Acadian transtension. The distinguishing characteristics of these plutons relative to other Caledonian plutons reflect their unique emplacement into the hydrated lithosphere of the Iapetus Suture Zone. Oxygen isotope disequilibrium between the magmatic compositions recorded by zircon and those of the whole-rock and some quartz crystals reflect hydrothermal alteration of the latter two archives. Hydrothermal alteration and exchange caused by ^{18}O-rich magmatic fluids has elevated the δ^{18}O compositions of the whole-rock and some quartz crystals, with most disequilibrium observed around the outer margins of the plutons due to further fluid interaction with local ^{18}O-rich sediments. The hydrothermal history of the TSS is markedly different from that of the British Tertiary Igneous Province where hydrothermal alteration resulted from circulation of meteoric water, reflecting significantly different magmatic and emplacement histories.

Acknowledgements

After three-and-a-half years' research comes an inevitable and sincere level of gratitude to a long list of individuals. My experience is no exception and I would firstly like to thank Colin Graham, who as principal supervisor of this project, has always been a tireless source of inspiration, available at all times for impromptu discussions and has remained enthusiastic after countless manuscript iterations.

Martin Gillespie has sacrificed many hours from his numerous commitments at the BGS to guide, offer advice and most importantly offer clarity during times of seemingly immense complexity. Chris Hawkesworth has never ceased in providing prompt, constructive and invaluable advice with a brilliant ability to quickly identify new and intriguing lines of research. Chris' dedication is perhaps best reflected by an almost unbroken record of 5.00am emails and a constant hunt for that 'killer diagram'! Richard Hinton together with John Craven have always provided encyclopaedic knowledge of all things ion probe-related and it is no overstatement to say that this project would simply not have been possible without them.

Funding for this PhD has been provided by NERC, a BGS BUFI grant and the School of GeoSciences at Edinburgh, without whom, this project would not have been possible. NERC are also thanked for funding analytical time on the ion probe.

Amongst the 'hard-rock' group at Edinburgh, Godfrey Fitton, Simon Harley, Thor Thordarson, Geoff Bromiley, Barry Dawson, Brian Upton, John Dixon, Ian Butler and Ian Parsons have provided what is collectively a geological treasure trove of experience and advice. Ed Stephens deserves special thanks for some fascinating discussions related to Caledonian granites over many long and enjoyable lunches in St Andrews, and has kindly provided some whole-rock analyses for this project. Nigel Woodcock and Sally Gibson have always been keen to learn of progress, while Nigel has provided useful advice about the regional aspects of British Caledonian geology. Matthew Thirlwall advised on aspects of the Lake District igneous rocks. Calvin Miller has always given constructive and thoughtful reviews that have greatly improved a number of chapters. Nigel Harris and a number of anonymous reviews have provided valuable feedback that has significantly improved the thesis.

I have been fortunate enough to have used many of the most sophisticated analytical instruments available during this project. From Edinburgh, I would again like to thank Richard and John for their help with SIMS analysis, Chris Hayward for assistance with electron probe analysis, Nicola Cayzer and Rosie Jones for guidance on the SEM, Nic Odling for XRF analyses and Mike Hall for thin sections of the highest quality. Bruno Dhuime and Stuart Kearns both kindly sacrificed their weekends to assist with laser and electron probe work respectively at Bristol. Angus Calder and Donald Herd provided training for heavy mineral separation at the Heavy Mineral Separation Facility in St Andrews. Tony Fallick and Chris Taylor helped with whole-rock oxygen isotope work at SUERC, East Kilbride.

My enthusiasm for Geology is without a doubt a reflection of the passion I saw in my many supervisors and demonstrators during four year of undergraduate study at Cambridge. I've been fortunate enough to have been involved in teaching eight different year groups at Edinburgh and it is with fond memories that I look back on many a fieldtrip to Mull and Inchnadamph where that same degree of passion for geology has flourished. Many of those students, I now have the pleasure of sharing the PhD office with. I hope in demonstrating, I have taken just a small step in repaying that debt of gratitude I owe my supervisors.

Edinburgh has of course been more than just a place of work and I am grateful for having met many colleagues and friends with whom I share so many common sporting and academic interests. Thank you for your friendship over the years and in particular to Nick, Simon, Rob, Dan, Jenny, Caroline, Ruth, Gijs, Louise, Margaret, Rhian, Jen R, Rosie, Niklas, Gillian, Tom, Matt H, Rosie, Alex, Theresa, Darren, Romesh, Matt B, Jamie and Mark. Thanks also to all flatmates of the Viewforth 'Geoflat', including Steven, Margaret, Alex, Jennifer, Lofty and both Matts. The attic pets and geo-mascots, Sophie and Milo have provided welcome distractions on many occasions! A big thank you of course goes to Elizabeth who has provided great support for the last couple of years.

And finally to both my parents who, with every conviction, have supported my interest in geology and have always gone beyond the call of duty in trying to understand and share my interest in a subject with which they have no background. It is through your support that my education has been possible. Thank you.

Contents

Chapter 1

Introduction

1. Introduction

The Earth's continental crust is distinct from that of other planets in the Solar System (Rudnick and Gao, 2003). Its uniquely silicic composition results from a combination of melt extraction and subsequent differentiation that have in turn both modified and regulated the compositions of the atmosphere (e.g Garrels and Perry, 1974; Zhang and Zindler, 1993; Lowe and Tice, 2004) together with the mantle from which it is derived (Taylor and McLennan, 1985; Windley, 1995; Condie, 1993; Jacobsen and Wasserburg, 1979; O'Nions et al. 1980; Allègre et al. 1983). It is also chemically and physically distinct from the oceanic crust, its greater buoyancy serving to ensure its longevity and resistance to subduction and recycling (Cloos, 1993). It is thus the single most complete archive of Earth's history (Hawkesworth et al. 2010).

As a major component of the upper continental crust, granites are the manifestation of crustal evolution (e.g. Atherton and Petford, 1993; Chappell and White, 1974; 2001; Gray, 1984; Keay et al. 1997; Collins, 1998; 1999; Kemp et al. 2007). Their study has helped shape and guide geological research for over 200 years and is today proving vital in unravelling the early evolution of the Earth (see Hawkesworth et al. 2010 and references therein). Their accessory minerals have provided a much sought-after window into the processes of silicic magma generation in the last few decades, and have revived what was otherwise a neglected field of research. With increasing levels of spatial resolution and analytical precision, the isotope and trace element compositions of accessory minerals are providing new, detailed and perhaps most crucially, reliable archives of sources and processes now overprinted and lost from the whole-rock record (e.g. Coleman et al. 2004; Hawkesworth and Kemp,

2006, Kemp et al. 2007; Matzel et al. 2006; Appleby et al. 2008; 2010). Their use has however raised new questions, the foremost being how this new chemical archive relates to more established records based around bulk-rock compositions. At issue is whether these 'time capsules' provide a complete or biased record of magma evolution and whether any such bias is different in magmas of different compositions.

This study applies recently developed micro-analytical techniques to measure the isotope and trace element compositions of accessory zircon and apatite from a suite of Devonian granitic plutons in Northern Britain. Through integrating the accessory mineral record with whole-rock and other mineral records, the relationships between different magmatic archives is investigated. Furthermore, constraints are placed on the extent to which accessory minerals retain evidence for different stages of magma history in plutons of different composition. New opportunities for using accessory minerals to investigate the redox states of different magmas are also investigated. A new geochronological framework is proposed on the basis of new U-Pb ages, with further insights into magmatic processes investigated using the oxygen and hafnium isotope compositions of zircon. It is shown that contrary to previous suggestions, the Trans-Suture Suite (TSS) plutons of northern Britain were emplaced during multiple periods of transtension and not transpression. Finally, the hydrothermal history of the Trans-Suture plutons is investigated using oxygen isotope compositions in zircon, quartz and whole-rocks. The results indicate that hydrothermal processes were dominated by magmatic fluids, with a distinct absence of meteoric water. These conclusions are contrasted with hydrothermal activity around the British Tertiary Igneous Province where meteoric waters have been shown to dominate the final magmatic evolution of the province. These differences are used to reveal fundamental differences in the emplacement history of the two magmatic episodes.

2. On the Origin of Granites

In recent decades, granites and their constituent minerals have played an important role in unravelling the processes associated with the formation, evolution and preservation of the continental crust. Their historic significance has however helped shape philosophies far beyond the realm of Geology. Granites have proved revolutionary in rejecting the 18th century religious dogmas on the age of the Earth, while the early pioneering work of James Hutton in particular arguably defined the birth of modern Geology. This section presents a review of granite research and recognises how the granite story with its connections to Edinburgh University has transformed scientific thinking and helped establish geology as a respected and fundamental discipline of the natural sciences.

The twentieth century abounds with important discoveries relating to the origins of granites. In the interest of brevity, only a selective coverage is presented, focussing mainly on the landmark work of Tuttle, Bowen and Chappell. The final part of this section looks at the contributions made by accessory minerals to the study of granite genesis and how the analysis of progressively smaller constituents has led to a better understanding of crustal evolution on a planetary scale.

2.1 Early Ideas

The 'Neptunist' theory proposed by Abraham Werner (1749-1817) maintained that different rock types were deposited sequentially from a primeval ocean, with granites followed by metamorphic rocks, chemical precipitates and other rock layers as water levels fell. Werner's ideas flourished, reflecting his profound ability to communicate science to his many students. In 1785, James Hutton (pictured left) presented his *Theory of the Earth* to the Royal Society of Edinburgh, proposing that granites and basalts solidify from a molten state. This idea was to spark what became one of the greatest scientific debates of the Scottish

Enlightenment era between Werner's Neptunist and Hutton's Plutonist theories. Hutton's ideas, and particularly those made at Glen Tilt, were rooted in the same careful observations, evidence and logic that had vindicated Newton's laws of motion over a century before and would later support Darwin's theories of biological evolution by means of natural selection later in the nineteenth century. Key aspects of Hutton's theory include the suggestion that heat and pressure from deep within the Earth were vital for granite genesis and that the intrusive nature of granites meant that they were younger than the rocks into which they were emplaced. It cannot go without mention that these same direct observations also supported the idea of unconformities and 'missing time' in the geological record, reflecting repeated processes of burial, uplift and erosion over millions rather than thousands of years. Acceptance of Hutton's ideas took time, hindered in no small way by his poor ability to communicate his work. Jack Repcheck (2003) argues that had Hutton's communication skills been better, then his name would now rank amongst the likes of Newton, Darwin and Einstein. John Playfair (1748-1819), Professor of Natural Philosophy at Edinburgh, is credited with bringing Hutton's ideas to full fruition with his publication of '*Illustrations of the Huttonian Theory*' in 1802.

Observations underpin and also test scientific theories. However, acceptance relies on replication, often by experiment. Hutton's ideas of granite formation were no exception, but despite this, Hutton was no proponent of experimental methods, and credit for this goes instead to his younger colleague, James Hall (1761-1832) (pictured left). The relationship between Hutton and Hall and the delay in developing experimental models for granite formation are outlined by Hall himself. Hall was:

"…convinced that the chemical effects ascribed by him to compression, ought, in the first place, to be investigated… established in a direct manner by experiment", and he "urged him to make the attempt; but he always rejected this proposal, on account of the immensity of the natural agents, whose operations he supposed to lie far beyond the reach of our imitation…I considered myself bound, in practice, to pay deference to his opinion, in a field which the prosecution of some experiments with compression, which I had begun in 1790. In 1798 [following Hutton's death], I resumed the subject with eagerness, being still of opinion, that the chemical law which forms the basis of the Huttonian Theory, ought, in the first place, to be investigated experimentally. "

Hall's experiments on granites used feldspar as a form of flux to melt a mixture of crushed quartz and feldspar. However, many of his ideas have been traced to an accidental experiment at a glass manufacturer when a large volume of glass was left to cool slowly. Hall realised that had the glass been allowed to cool very slowly, it would have crystallised to produce granite similar to that initially melted. These experiments led to the idea of cotectic (or eutectic) melting and crystallisation, which also led to a mechanism for generating coarse crystals during slow cooling and a finer groundmass as a result of later and more rapid cooling. Despite Hall's experiments, plutonism remained controversial, as is evident from the published work of Charles Lyell in '*The Principles of Geology*' of 1830 to 1833.

Further controversy followed in the pursuit of understanding granite genesis, particularly once the important effect of water at high temperatures was recognised. 'Magmatists' supported Hutton and Hall in suggesting that granites formed by the slow crystallisation of molten magmas. 'Granitisers', however, appealed to granitic juice, or 'ichor' that was assumed to be capable of 'granitising' large volumes of rock. Many petrologists argued that the transition from metamorphic rocks through migmatites to large granite plutons provided strong evidence for this transition. The idea of 'dry granitisation', developed in the 1930s and 1940s, suggested that metasomatic fronts moved through large bodies of rock by diffusion on a regional scale, transforming large volumes of rock into granite in the solid state. Doris

Reynolds (1899-1985) (University of Edinburgh), wife of Arthur Holmes, proposed that 'acid fronts' introduced ions such as Si, Na and K and thereby converted existing rocks into granites with non-granitic components such as Ca, Fe and Mg expelled in 'basic fronts'. Many petrologists such as Norman Bowen (1887-1956) opposed the idea of acid fronts and many continued to be sceptical of experimental studies conducted at atmospheric pressure. Many of the concerns regarding experimental approaches went beyond the use of only low pressures and questioned whether the experimental systems used were too simple and whether the lack of volatiles undermined their significance. Although the ternary residua system $NaAlSi_3O_8$-$KAlSi_3O_8$-SiO_2 (Albite-Orthoclase-Quartz) represents > 90% of the normative components of many granites, it remained difficult to assess phase relationships at atmospheric pressures due to slow reactions and high viscosities.

Controversy about the origins of granites continued until 1950 when experiments were developed to simulate the effects of water at high pressure. O.F. Tuttle developed a cold-seal pressure vessel that allowed experimental studies on the melting of granitic minerals and rocks in the presence of water under high pressures (up to 4 kbars). Tuttle and Bowen's landmark publication '*Origin of granite in light of experimental studies in the system* $NaAlSi_3O_8$-$KAlSi_3O_8$-SiO_2-H_2O' in 1958 showed how water has a large effect on the kinetics of reactions in silicic melts. Their results showed that dissolved water was able to lower the granite liquidus by hundreds of degrees and would permit the precipitation of both plagioclase and K-feldspar (sanidine) instead of a single feldspar solid solution in granitic magmas. It would later be shown that the two (subsolvus) or one feldspar (hypersolvus) nature of granitic rocks depends on two principal factors: water vapour pressure which lowers the crystallisation temperature of silicate magmas significantly, and the Ca content of the magma, which raises the temperature of the solvus, so that granite with a small proportion of anorthite in its K-feldspar will be subsolvus at a much lower water vapour pressure than a hypothetical Ca free feldspar. Nonetheless, this calibration led to an acceptance of the idea that granites are essentially magmatic rocks. Most natural granite compositions were found to cluster around the temperature minimum on the liquidus surface (Fig. 1.1), suggesting that felsic granites formed by processes

involving equilibrium between melts and crystals and must therefore be of magmatic origin. Bowen was a strong advocate of the idea that most granites represent the final products of fractional crystallisation from more primitive magmas, though acknowledged the possibility that they may also result from partial melting. Subsequent work has revealed that most granites are the product of partial melting and not fractional crystallisation. Three main lines of evidence have been put forward to support this opinion:

1. Studies on high grade metamorphic granulites have shown that heat accumulated from the decay of radioactive elements may heat the crust to temperatures capable of causing partial melting. Migmatites provide direct evidence of these processes.
2. The dominance of granites over more primitive rocks, particularly in continental regions, is difficult to reconcile with fractional crystallisation, through which only small volumes of highly fractionated material form.
3. The chondrite-normalised trace element compositions of granites are often smooth and not highly fractionated, suggesting that granites represent primary or close to primary magmas.

Tuttle and Bowen's landmark findings are seminal to our modern understanding of granite formation.

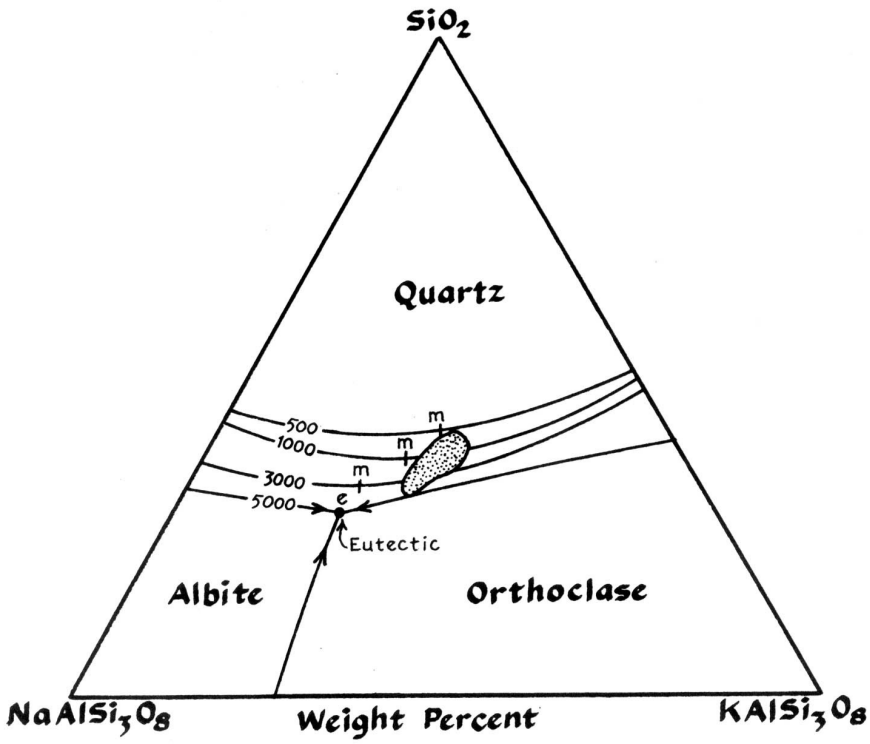

Fig. 1.1 The granite system quartz-albite-orthoclase. Phase boundaries are for P_{H2O} = 500 to 5000 bars (0.05 to 0.5MPa). The temperature minimum (m) on the quartz-feldspar cotectic separates the two feldspars at this pressure. The stippled field represents the compositions of granites with >80% normative quartz + albite + orthoclase. After Tuttle and Bowen (1958).

2.2 Into the Modern Era: Acceptance of the magmatist theory

Following wide acceptance of the work of Tuttle and Bowen, a popular view developed that granites were solely derived from the melting of sedimentary rocks. In 1957, Read proposed that a series of granites could be recognised that developed through time and at progressively higher levels in the crust, suggesting that most granites were derived from melting in the upper crust. Early isotopic results however showed that some granites have more mantle-like and primitive isotopic compositions than others and it was soon realised that hornblende-bearing granites rich in Ca and Na could not form directly from melting of sediments containing significant amounts of weathered material. This arises because weathering preferentially destroys minerals that are unstable at the Earth's surface, leading to the formation of clay minerals. Elements such as Ca and Na that are not incorporated

into clay minerals are gradually lost from mantle-derived rocks during weathering and are lost in solution. These elements are therefore not available during the partial melting of sedimentary rocks. Partial melting of such rocks leads to oversaturation in Al relative to Ca and Na and to the formation of peraluminous magmas. Chappell and White (1974) recognised a distinction between granites derived mainly from the melting of greywackes, containing quartz, feldspars and clays and known as 'S-type' granites, and amphibole-bearing granites that can only have formed from the melting of sources not significantly modified by chemical weathering. This latter group are derived mainly from partial melting of igneous precursors and have become known as the 'I-type' granites (Table 1.1).

A further important finding from the early work of Chappell and White was that I-type plutons display more regular inter-element variations than S-type plutons. This observation was further developed in 1984 by Chappell and White, when it was proposed that the I-type source rocks of the Lachlan Fold Belt (Australia) are relatively more homogeneous than those from which S-type granites are derived. I-type granites were therefore considered to have formed at deeper levels in the crust and from sources produced by earlier underplating of the crust. These distinctions reveal fundamental differences in the origins of the source rocks themselves, with S-type granites derived from sources formed by deposition of reworked crustal material and I-type granites derived from sources that represent net accretion to the crust from the mantle. The 'I' in I-type therefore came to represent igneous or infracrustal while the 'S' in S-type was associated with sedimentary or supracrustal sources. These findings signalled an important step forward in our understanding of granite genesis and showed for the first time that the two different groups of granite correspond to different sources and have markedly different implications for the net proportions of new crustal growth represented by both suites.

Table 1.1 Differing characteristics of I- and S-type granites according to Chappell and White, 2001.

I type granites	S-type granites
Relatively high Na, Na_2O typically > 3.2 % in felsic varieties decreasing to >2.2 % in mafic samples	Relatively low Na, Na_2O typically < 3.2 % in rocks with c. 5 % K_2O, decreasing to <2.2 % in rocks with c. 2 % K_2O (due to removal of Na into sea water (or evaporites) during sedimentary fractionation)
Mol. $Al_2O_3/(Na_2O+K_2O+CaO)$ <1.1	Mol. $Al_2O_3/(Na_2O+K_2O+CaO)$ >1.1
CIPW normative diopside or < 1 % normative corundum	> 1 % CIPW normative corundum
Broad spectrum of compositions from felsic to mafic	Relatively restricted in composition to high SiO_2 types
Regular inter-element variations within plutons; linear or near linear variation diagram	Variation diagrams more irregular
Hornblende common	Muscovite, up to 35 % biotite (in more mafic S-types), garnet and cordierite common, no hornblende
Sphene; apatite inclusions in biotite and hornblende	Monazite, apatite in larger discrete crystals
$(^{87}Sr/^{86}Sr)_i$ = 0.704-0.706 (generally)	$(^{87}Sr/^{86}Sr)_i$ >0.708
Mafic hornblende-bearing igneous enclaves	Metasedimentary xenoliths

Independent of the I- and S-type classification and without reference to it, Shunso Ishihara identified the magnetite- and ilmenite-series of granites in 1975, a finding later published in 1977. The magnetite series of granites contains magnetite ± ilmenite and the ilmenite series contains only ilmenite. The fundamental importance of this series was to acknowledge the higher Fe^{3+}/Fe^{2+} ratio of the magnetite series and that this in some way reflects the oxygen fugacity (fO_2) of the magma. The more oxidised magnetite series granites were proposed to have formed from mantle-derived material, while the ilmenite series was proposed to have formed by late-stage processes such as the interaction between magmas and graphite-bearing wall rocks.

Many would no doubt now question this interpretation, but the underlying significance that different source rocks have different compositions and Fe^{3+}/Fe^{2+} ratios that are imparted into granites formed by partial melting is similar to the conclusions of Chappell and White (1974). The significance of Ishihara's findings relates principally to the association between the different series and the presence or absence of economically important ore deposits. In particular, the magnetite series is often associated with vein deposits of scheelite-molybdenite, gold and porphyry copper-molybdenite deposits. Likewise, the ilmenite series is often associated with cassiterite-wolframite veins.

In what appears as a prelude to the future direction that granite research was to follow, Ishihara (1977) stressed in his opening remarks that accessory minerals are commonly ignored in granitic rocks but that they may contain important information about the petrogenesis of granites.

2.3 The role of zircon and other accessory minerals in the granite story

Zircon and other accessory minerals have been extensively used to extend our knowledge of granite petrogenesis at previously inaccessible scales. These developments have come about due to a revolution in micro-analytical techniques, but the importance of zircon in particular to understanding granites and obtaining reliable estimates for the age for the Earth has been known for much longer.

Inspired by Rutherford's suggestion that the decay of accumulated radioactive elements could be used to determine rock ages, John Strutt (Lord Rayleigh) was the first to attempt to measure He (a product of radioactive decay) in uraniferous substances, including zircon in 1909. Strutt acknowledged the importance of He loss from zircon, but was the first to suggest zircon inheritance in some granites and to recognise that zircon showed great promise because of its inertness. The method involved fusing zircon with borax in a Pt crucible, with dissolution achieved using HCl. At this time, attempts were also made to date zircon using pleochroic halos (Joly, 1909) in thin section, but were seriously undermined by an absence of U data

in the inclusions. In 1911, Arthur Holmes, a graduate student of Strutt at Imperial College, suggested that the most reliable means of determining ages was to measure Pb accumulation in high-U minerals (Holmes, 1911). Although using uraninites, Holmes was able to construct a Palaeozoic to Precambrian time scale that remains remarkably accurate to the present day. However, despite high concentrations of U in zircon, its presence in trace amounts meant that for a further forty years, U-Pb ages were determined by chemical analyses of total U and Pb contents in more radioactive minerals.

Interest in zircon was limited until 1952 when Larsen et al. (1952) recommended zircon as a geochronometer because of its high (although trace) U content, resistance to alteration and the large difference in ionic radii between Zr^{4+} (0.84Å) and Pb^{2+} (1.32Å) in 8-fold coordination. The importance of this was that zircon should not contain any primary Pb. Despite the advent of quantitative mass spectrometry in 1938 by Alfred Nier to measure isotope abundances, it was still necessary to use ~ 100g of zircon in order to obtain several milligrams of Pb for analysis. Most early studies therefore used total emission atomic methods that required only small volumes of zircon but had a precision of only ~ 10%. George Tilton was the first to pioneer the use of thermal ionisation mass spectrometry (TIMS) for zircon dating in the mid 1950s. The TIMS method marked an important step forward as it permitted accurate Pb isotope measurements using only micrograms of zircon. The volumes of material needed became progressively smaller as the TIMS method was developed, but it was still susceptible to the effects of inheritance and discordance. These limitations drove the need for direct U-Pb measurements at the intra-grain level using secondary ion mass spectrometry (SIMS). The method uses a focused beam of high energy ions to ablate a small area (~20 μm) on polished surfaces, with secondary ions analysed for their compositions. The method was first developed by Andersen and Hinthorne in 1972. With further refinement, Hinton and Long (1979) showed that chemical zoning in zircon was capable of retaining age data from a variety of geological events and processes, with particular relevance for the study of zircon inheritance in granites.

The presence of inherited zircons, often found only as cores around which magmatic zircon has grown, led to the recognition of inheritance rich and inheritance poor granites (Pidgeon and Aftalion, 1978; Chappell et al. 2004; Miller et al. 2003). This work built on previous studies into zircon saturation and the development of the zircon saturation thermometer (Watson and Harrison, 1983). Watson and Harrison established that the solubility of zircon in non-peralkaline intermediate to felsic magmas depends on two parameters: temperature and melt composition. The compositional dependence is related principally to silica content and the aluminium saturation index (ASI = mole $Al_2O_3/(CaO+Na_2O+K_2O)$). The importance of this thermometer was in showing that zircon solubility increases with temperature but decreases with increasing SiO_2 and ASI. Inheritance-poor plutons were shown to have mean zircon saturation temperatures of ~ 837^oC and were referred to as 'hot' granites by Miller et al. (2003), while inheritance-rich granites became known as 'cold' granites with estimated zircon saturation temperatures of only ~ 766^oC. These distinctions, like those recognised three decades earlier by Chappell and White (1974) between I- and S-type plutons, are said to reflect fundamental differences in the mechanisms of magma generation, transport and emplacement. Inheritance-poor, hot granites are thought to reflect advective heat input to the crust and are said to have been undersaturated in zircon at source. By contrast, 'cold', inheritance-rich granites are thought to require fluid influxes, are richer in crystals and are considered to be less likely to erupt (Miller et al. 2003). Later in this thesis, it is proposed that these classifications may have underestimated the significance of water contents in determining zircon inheritance in granitic magmas.

2.4 From tiny zircons to global crustal evolution

The proliferation and ease of access to micro-analytical techniques world-wide has led to an explosion in the abundance of zircon data from a variety of granites over the last two decades. As a direct result of this and the use of other radiogenic (Lu-Hf) and stable (oxygen) isotope systems, zircon can now be used not only to investigate the magmatic processes relevant to individual granites, but to globally significant processes of crustal formation, evolution and preservation throughout Earth history.

This section introduces fundamental ideas related to the formation of the continents and the role that granites and zircon have played in unravelling the dynamics of crustal evolution.

The depletion of the upper mantle in incompatible elements is likely to reflect prolonged and extensive melt extraction (Jacobsen and Wasserburg, 1970; O'Nions et al. 1980; Allègre et al. 1983). The enrichment of the continental crust in these same elements reflects an intrinsic chemical relationship between these complementary chemical reservoirs and it seems inescapable that the continents are the product of melt extraction from the mantle (Campbell and Taylor, 1983; Jacobsen and Wasserburg, 1979; O'Nions et al. 1980; Allègre et al. 1983). The continental crust constitutes only ~ 40% of the surface area of the Earth, but represents ~ 70% of the total crustal volume. Its composition is on average andesitic, its thickness ranges between 25 km and 70 km and its density is less than that of the oceanic crust. These differences have long been known to reflect different mechanisms of formation. While basaltic oceanic crust forms by the partial melting of passively upwelling mantle in areas of plate divergence, the continental crust has strikingly similar trace element properties to the magmatic rocks formed in modern arcs and related to plate subduction (Rudnick, 1995). Unlike oceanic crust, it seems highly likely that subduction related processes have been responsible for the generation of most new continental material. A key aspect of the resulting buoyancy contrasts between the continents and oceans is that they form part of what is a fundamental driving force for the continued actions of plate tectonics, subduction and the generation of new continental crust (Cloos, 1993). Beyond this, the continental crust, and specifically the chemical weathering of the continents, has regulated global climate, serving as a sink for CO_2 (e.g. Garrels and Perry, 1974; Zhang and Zindler, 1993; Lowe and Tice, 2004) and has arguably helped maintain the relatively stable climatic conditions required for the advanced evolution of life on Earth.

More contentious issues are the dynamics of crustal formation, the question of when and how most crustal material formed and whether the processes responsible for crustal formation have been continuous or episodic over time. Several different

models of continental growth have been proposed (Fig. 1.2) and are divisible into four groups based on their different methods of calculation (Rino et al. 2004). The first group use forward modelling of the thermal evolution of the earth and propose rapid crustal growth during the Hadean and Early Archean (e.g. Fyfe, 1978). Other studies (e.g. Reymer and Schubert, 1984) that fall within this group also suggest only limited crustal growth during the Phanerozoic based on calculations of crustal recycling caused by subduction erosion. A second group of models based on the age distribution of juvenile continental crust at present advocates gradual crustal growth since the Archean, with significant growth during the Phanerozoic (e.g. Hurley and Rand, 1969). These methods neglect the effects of crustal recycling and therefore provide minimum estimates of continental growth. A third group of models is based on the evolution of the isotopic composition of the depleted mantle (calculated using greenstones of various ages) and assumed a complementary relationship between the depleted mantle and continental crust (e.g. O'Nions et al. 1979). In these models, continental growth is estimated from the secular variation of the degree of depletion of the mantle from the evolution of isotopes such as Nd, Sr and Pb. The results of these models suggest steady crustal growth throughout most of Earth's history (unlabelled curve in Figure 1.2). The fourth group of models is based on the analyses of the compositional changes of sedimentary rocks, both clastic (e.g. Taylor and McLennan, 1985) and pelagic (e.g. Veizer and Compston, 1976). These models suggest that most crustal growth occurred ~ 3.0 Ga.

As a significant component of the upper continental crust, granites represent archives of the processes that underpin crustal formation and evolution, including melt extraction from the mantle and lower crust together with differentiation. The isotopic composition of zircon is now intrinsic to an understanding of the dynamics of crustal formation. However, the investigation of crustal evolution on timescales of billions of years has required a global archive less punctuated and spatially restricted than granite plutons alone can provide. In response to this need, zircon studies have increasingly turned to what is the most complete geological archive of Earth evolution: the sedimentary record and its cargo of detrital zircons derived from igneous precursors (mostly granitic) long since lost to the geological cycle (e.g.

Taylor and McLennan, 1991; Condie, 1993). This approach has revolutionised crustal studies and is continuing to do so to this day, but has also revealed new and apparently false paradoxes.

A principal paradox has become apparent from global compilations of zircon U-Pb crystallisation ages, which show marked peaks around 2.7 and 1.9 Ga, with some evidence of a third peak around 1.2 Ga but none after 1.0 Ga (see Condie, 2005) (Fig. 1.2). These peaks are present in both the igneous and detrital records (Fig. 1.3) and suggest that detrital zircons offer a representative record of magmatic history (Hawkesworth et al. 2010). Fundamentally, these peaks represent periods of enhanced magmatic activity but are in stark contrast to the smooth growth curves generated using the Nd and Hf compositions of the sedimentary record over time (e.g. O'Nions et al. 1983; Jacobsen and Wasserburg, 1979). This latter archive describes increases in the volumes of stable continental crust preserved in the geological record. With strong evidence for the involvement of subduction in the formation of new crust, the zircon record is also at odds with the more continuous actions of plate subduction that are unlikely to result in significant changes in the rates of crustal formation. Some suggest that these age peaks represent the actions of superplumes, with subduction only dominating in the last 1.0 Ga when peaks are absent (e.g. Condie, 2004). Others suggest that they are artefacts of preservation in the geological record (e.g. Gurnis and Davies, 1985; 1986; Hawkesworth et al. 2009). Resolving these issues is difficult from U-Pb dating alone, but with the benefit of Lu-Hf and O isotope systems, the distribution of zircon crystallisation ages has been investigated further.

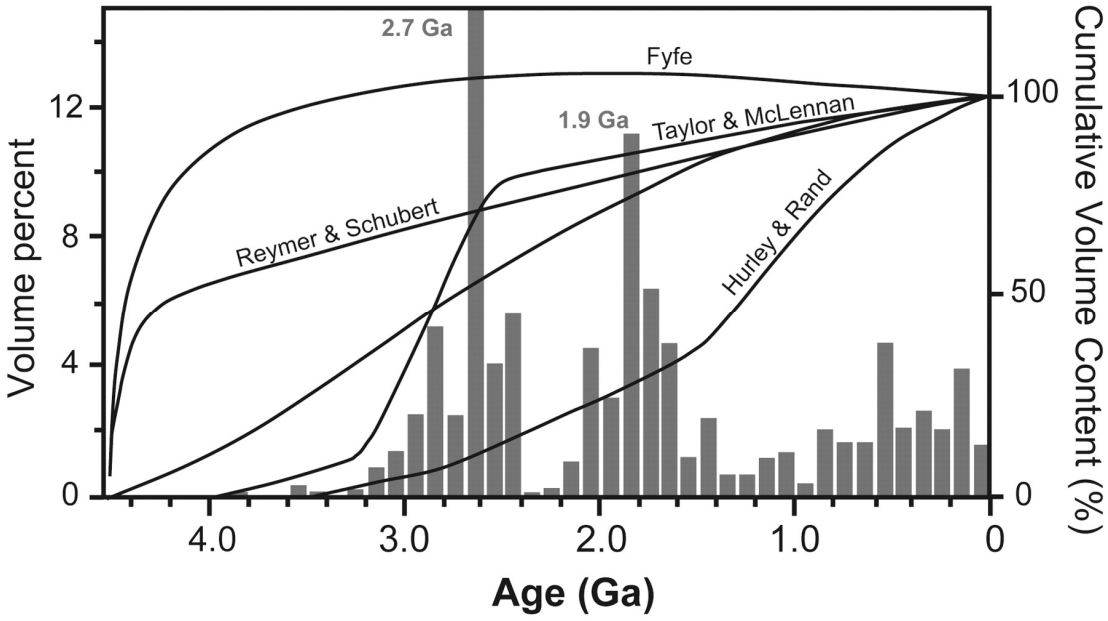

Fig. 1.2 Histogram of the volume distribution of juvenile continental crust based on a compilation of U-Pb zircon ages integrated with Nd isotope ratios and lithological associations. Crustal growth curves from various models are included where 100% represents the present-day cumulative volume of crust. Unlabelled curve is from O'Nions et al (1979) and is based on the isotopic evolution of the depleted mantle through time estimated from the chemistry of greenstones (from Hawkesworth et al. 2010).

2.4.1 Beyond U-Pb: crustal formation and preservation using Lu-Hf and O in zircon

The Lu-Hf isotope system has provided an additional and independent means of assessing the history of crustal growth. Radiogenic ^{176}Hf is produced by ß$^{-}$ decay of ^{176}Lu with a half-life of 37.2 Gyrs. Due to Hf being more incompatible than Lu during melting of spinel and garnet peridotite, the continental crust has over time developed a non-radiogenic $^{176}Hf/^{177}Hf$ composition, while the mantle has evolved towards more radiogenic $^{176}Hf/^{177}Hf$ compositions (Patchett et al. 1981). High Hf concentration in zircon results from its compatibility in the zircon crystal structure and is in contrast to the relatively low concentrations of REE such as Lu (Lu/Hf ratios are generally < 0.001). Hf isotope corrections due to *in situ* radiogenic growth are therefore negligible and zircon retains close to initial $^{176}Hf/^{177}Hf$ compositions inherited from the magma at the time of crystallisation. The robust nature of zircon together with Hf concentrations of ~ 1% mean that it is largely immune to the effects of weathering, deformation and alteration, all of which are widely thought to re-set

the analogous Sm-Nd isotope system in bulk analyses. It follows that Hf isotopes may be used to measure the residency of crustal rocks and the time at which they were extracted from the mantle, termed 'model ages'. However, sediment model ages are likely to represent hybrid ages between all contributing sources and it is necessary to distinguish model ages that are derived from sedimentary and igneous sources. Oxygen isotopes have paved the way to enable such distinctions in the zircon record.

$^{18}O/^{16}O$ ratios (or $\delta^{18}O$), expressed relative to Vienna Standard Mean Ocean Water (VSMOW) are determined by low temperature fractionation of heavy and light O isotopes. Under the low temperature conditions experienced by sediments at the Earth's surface or around shallow hydrothermal systems on the ocean floor, $\delta^{18}O$ compositions increase (*c*. 7 to 25 ‰; Eiler, 2001) due to the removal of light oxygen isotopes. By contrast, rocks that undergo only high temperature processes experience comparatively little fractionation. This effect combined with the large volume of mantle rocks explains how mantle compositions have remained largely buffered with respect to $\delta^{18}O$ over geological time, with $\delta^{18}O$ compositions of 5.3 ± 0.3‰ (Valley et al. 1998). Zircon retains a robust record of the $\delta^{18}O$ compositions of the melts from which they crystallise due to slow O diffusion rates (Peck et al. 2003) and therefore record the involvement of supracrustal components in the evolution of their host magmas. High precision (<0.5‰), *in situ* measurements of oxygen isotopes using multi-collector ion microprobes can now be integrated with U-Pb and Lu-Hf isotope measurements in zircon. This integrated isotopic approach has also enabled granites that represent new crustal growth to be distinguished from those that represent recycling of pre-existing crust (e.g. Kemp et al. 2007). The same outcomes can also be achieved by examining the extent to which peaks in U-Pb age distributions represent net additions to the crust. Detrital zircon compositions from Australia (Kemp et al. 2006b; Pietranik et al. 2008) that have been filtered using all three isotope systems reveal far fewer and less well defined peaks in Hf model ages than in U-Pb age distributions (Fig. 1.3). This evidence indicates that, like the Nd isotope compositions of shales (Allègre and Rousseau 1984), zircons provide a record that is dominated by crustal reworking. Igneous and sedimentary rocks

therefore provide different records and perspectives on the evolution of the continental crust (Hawkesworth et al. 2010).

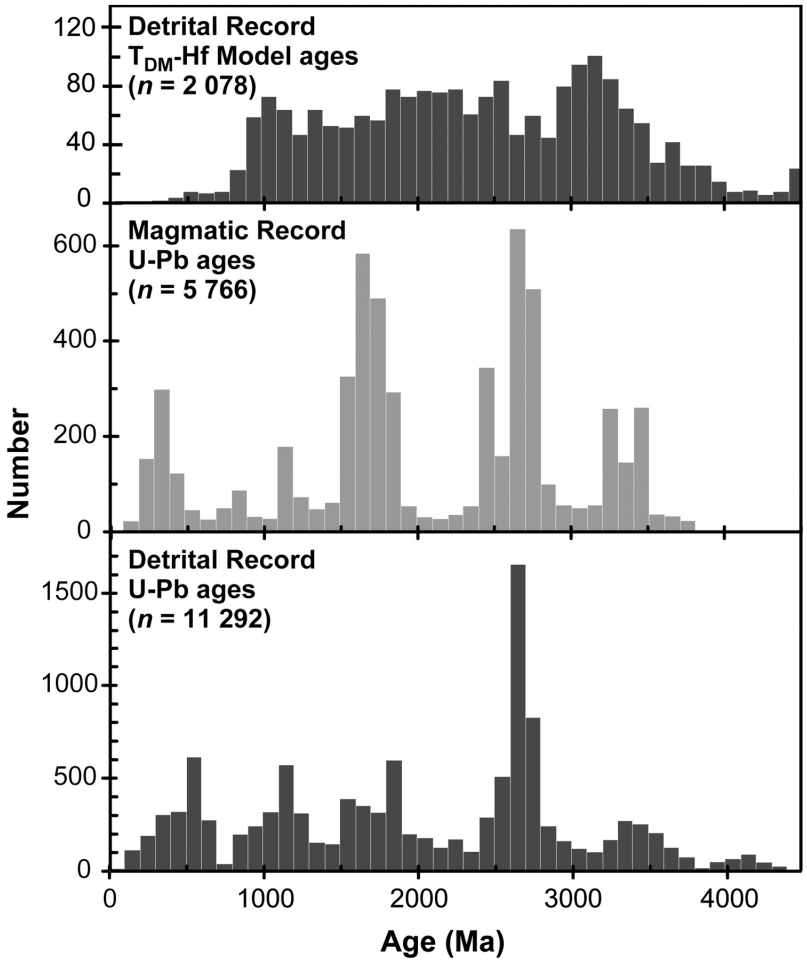

Fig. 1.3 U-Pb crystallisation and Hf model ages of zircons from Australia in magmatic rocks and as detrital grains. Of note are the distinctions between the contrasting peaks of crystallisation ages in the detrital and magmatic plots (from Hawkesworth et al. 2010).

A further clue to the origin of zircon U-Pb age peaks has been the discovery that they coincide with the formation of global supercontinents (Fig. 1.4) (e.g. Taylor and McLennan, 1995; Condie, 1998; Campbell and Allan, 2008; Rino et al. 2008).

In order to investigate this connection, Hawkesworth et al. (2009) have studied the igneous record associated with the development and break-up of supercontinents during different stages of evolution. The supercontinent cycle is regarded in three distinct phases:

1. Amalgamation associated with subduction-related magmatism
2. Collisional orogens, crustal thickening and heating
3. Break-up and extensional magmatism

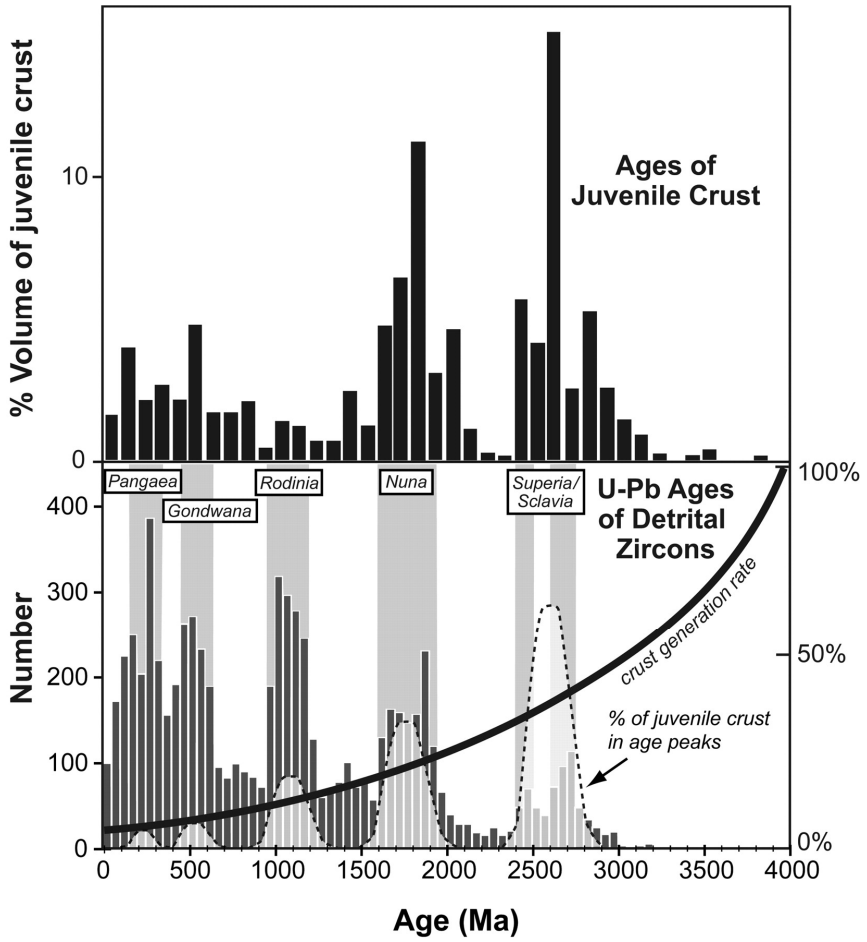

Fig. 1.4 Age distribution of relative volumes of juvenile continental crust (from Condie 2005) and of crystallisation ages for over 7000 detrital zircons (Campbell and Allen 2008). Peaks in U-Pb ages can be seen to coincide with times of supercontinent amalgamation. The crust generation rate curve illustrates a model in which the volume of new crust generated decreases with age, and the lightly shaded peaks schematically illustrate the relative volumes of new crust that might consequently be associated with each peak of zircon crystallisation ages.

The extent to which each stage of supercontinent evolution is recorded in the geological record, including in the detrital zircon record, depends on the volumes of magmatism and the preservation potential of each phase. The preservation potential of newly accreted crust created during subduction is low, with Scholl and von Huene (2007; 2009) showing that global rates of removal of continental and island arc crust through subduction erosion are similar to the rates at which new crust in created at

modern arcs (~ 2.5 km^3 a^{-1}). Most economically mined volcanic units around active continental arcs are also <100 Ma and reflect rapid uplift and denudation (Kesler and Wilkinson, 2006; Bierlein et al. 2009), consistent with the poor preservation of arc magmatic rocks.

By contrast, the collisional stage of supercontinent assembly is often dominated by partial melting of pre-existing crust and the formation of mostly S-type granites (though I-type and more mafic magmas are known from areas of continental collision), similar to granites seen in the Himalayas (e.g. Harris et al. 2000). The volumes of igneous material generated during this stage are generally small, but are more easily preserved in the geological record due to their formation within the core of the newly formed supercontinent (Hawkesworth et al. 2009). Furthermore, evidence is emerging from zircon oxygen isotope compositions for the involvement of mafic magmas in the formation of some S-type plutons (Appleby et al. 2010; Kemp et al. 2008; this study), with some representing up to 30% new crustal growth (Kemp et al. 2009). Erosion of this material forms a significant component of surrounding sedimentary basins and is a major source of detrital zircon in the sedimentary record (Hawkesworth et al. 2009; 2010).

The final break-up phase of the supercontinent cycle is dominated by extensional magmatism and mafic rocks where most erosional products enter ocean basins and are soon lost from the geological record due to subduction. Hawkesworth et al. (2009) conclude that peaks in U-Pb ages represent periods of supercontinent formation that do not result from the generation of substantial volumes of new crust but from selective preservation in the geological record.

Further evidence has emerged from integrating regional tectonic studies and zircon isotope compositions in granites from the Lachlan Fold Belt for close feedbacks between tectonic activity and magma sources (Kemp et al. 2009). In a region dominated by repeated episodes of extension and collision, zircon and whole-rock εNd-εHf-$\delta^{18}O$ compositions define secular trends that correlate with deformational events, reflecting changes in magma source during tectonic activity. Most magmatic

activity that produced juvenile magmas was shown to be associated with periods of back-arc extension that followed crustal thickening (Kemp et al. 2009). This evidence was used to draw a direct link between slab roll-back and continental growth. Throughout contractional regimes, S-type magmatism dominated, re-working sedimentary units deposited in earlier back-arc basins under granulite-facies conditions. Despite evidence for only 30-40% new crustal growth in the S-type granites (compared to 70% growth in the I-type granites formed during extension), their greater volumes mean that a larger proportion of new crust was generated during S-type magmatism (Kemp et al. 2009). Further evidence for the importance of back-arc environments in the formation of stable continental crust is seen in the Hidaka metamorphic belt in NE Japan (Kemp et al. 2007). Synchronous zircon crystallisation in back-arc gabbros and granulites has been linked to lithospheric thinning during back-arc extension. Granulite formation in the Hidaka belt has been shown to result from the reworking of older protoliths, but resulted from the enhanced heat flux caused by the addition of juvenile crust during slab roll-back. There is a growing consensus that back-arc environments provide important conditions for granulite formation and that the ages of granulite-facies terranes correlate with periods of accelerated continental growth (Collins, 2002, Brown, 2007; Kemp et al. 2007). Granulites and extensional regimes may therefore be intrinsic during tectonically-driven mantle differentiation processes and continental growth.

The apparent paradox presented by zircon crystallisation ages therefore reflects the actions of dynamic plate motions and the changing rates of crustal formation and preservation that follow such changes in tectonic regimes. During the Archean and earlier, preservation potential appears systematically poor, with few peaks and a generally low number of preserved zircons (Fig. 1.4). It is only during the late Archean that crustal evolution appears to be controlled by the competing effects of crustal preservation and generation. Although not providing proof of the absence of plate tectonics, the limited detrital material from this time may reflect more effective crustal recycling on a hotter Earth and/or the effects of frequent meteorite bombardments (Hawkesworth et al. 2010). However, there is a convergence of

opinion suggesting that a marked change occurred around 3.0 Ga and that this change signalled the onset of modern plate tectonics. Shirley et al. (2011) reported that before 3.2 Ga, only diamonds with peridotitic inclusions formed, whereas after 3.0 Ga, eclogitic inclusions within diamonds became prevalent. It is suggested that the capture of eclogitic and diamond-forming fluids occurred in response to the onset of subduction and continental collision, marking the beginning of modern plate motions and the Wilson cycle. In an independent study, Dhuime et al. (2012) used an integrated O-Hf-U-Pb approach to distinguish zircons that represent new crustal growth from those that result from magmas formed by crustal recycling. Their results identified a marked decrease in the rate of crustal growth at ~ 3.0 Ga that is said to signal the onset of subduction-driven plate tectonics.

The study of crustal evolution is revealing information that only a decade ago would have been unthinkable. The preceding section illustrates how granites and their assemblage of accessory minerals have shaped this study from its very beginnings and continues to do so to the present day.

2.5 Magma generation, ascent and emplacement

The large numbers of granite batholiths found throughout the continents has long raised questions about how such large volumes of silicic magma are generated and how they eventually become emplaced in the upper crust.

Many consider granitic plutons as being largely molten during emplacement (e.g. Buddington, 1959; Pitcher and Berger, 1972; Paterson et al. 1996), allowing for silicic compositions to evolve by fractional crystallisation. However, in order to produce silicic rocks with a composition of 60wt % SiO_2, approximately twice the volume of mafic material is required (Annen et al. 2006a). Furthermore, decreases in seismic P and S wave velocities in areas of partial melt are rarely greater than a few percent (e.g. Zandt et al. 2003) and do not support the idea of large magma chambers. These findings mirror developments in the study of magmatism around mid ocean ridges, where seismic evidence has also consistently failed to image large bodies of molten magma (Detrick et al. 1990). Instead, accretion of the oceanic crust

is now envisaged in terms of small ephemeral magma bodies (Sinton and Detrick, 1992).

New geochronological evidence from high precision U-Pb dating also indicates that many granitic batholiths grow over time periods of ~ 10 Myrs, too long to sustain single molten magma chambers in the crust (Coleman et al. 2004). The alternative is that plutons assemble incrementally (but potentially rapidly) via the emplacement of discrete magma batches (e.g. Glazner et al. 2004). These findings have significant implications for traditionally held views on pluton emplacement and in particular for models of diapirism, ballooning and stoping, many of which have been developed from studies on the Criffell pluton and other Caledonian granitoids in Scotland (e.g. Phillips, 1956; Courrioux, 1987; Fowler et al. 1995; Paterson et al. 1996). These processes require that plutons represent frozen magma chambers with at least 50 vol % liquid throughout a volume comparable to the size of the pluton (Glazner et al. 2004) and is not compatible with models of incremental assembly. Small, metre-scale chemical and textural variations in some plutons also allude to the incomplete mixing and emplacement of small melt batches during incremental assembly (Petford et al. 1993; Lipman 2007).

On the basis of thermal and fluid-dynamical analysis, Petford et al. (1993) suggested that for viscosities (10^6 Pa·s) and density contrasts (~ 200 kgm^{-3}) spanning the range considered typical for many calc-alkaline granitoids, dyke ascent is a viable mechanism for the transport of large volumes of granitoid melts through the crust. It is suggested that the critical dyke width required in order to prevent melts from freezing is ~ 2m to 7m, indicating that peak batholith-filling rates are orders of magnitude greater than mean cavity-opening rates (~ 0.7cm/yr, Tikoff and Teyssier, 1992) based on estimated fault slippage and pluton assembly times. These results are therefore consistent with incremental magma supplies that are likely to reflect decreasing volumes of granitoid melts available for extraction from the source regions (Petford et al. 1993).

Incremental assembly of granitic batholiths is consistent with the crustal hot zone model proposed by Annen and Sparks (2002) and Annen et al. (2006a). In this model, magmas of silicic and intermediate composition are generated through the repeated intrusion of sills formed from mantle melts that differentiate and cause partial melting of pre-existing host rocks and sills (Fig. 1.4). A wide range of WR trace element and isotopic compositions can then be generated through the mixing of residual mafic melts and crustal partial melts. The volumes and rates of melt production depend largely on the volumes of intruded mantle-derived material, the distribution of sills and how readily the crust fuses. The latter is broadly dependent on the depths of sill emplacement, crustal composition and water activity. Mafic sills act primarily as a heat source for subsequent melt generation, and as such may not be a dominant component in the newly formed silicic magmas. The crustal hot zone model is therefore able to reconcile the absence of large melt volumes at any particular time and evidence for the incremental assembly of large plutons (Wiebe and Collins, 1998; Glazner et al. 2004; Coleman et al. 2004; Glazner and Bartley, 2006; Lipman, 2007; Miller, 2008; Kemp et al. 2006; Appleby et al. 2008).

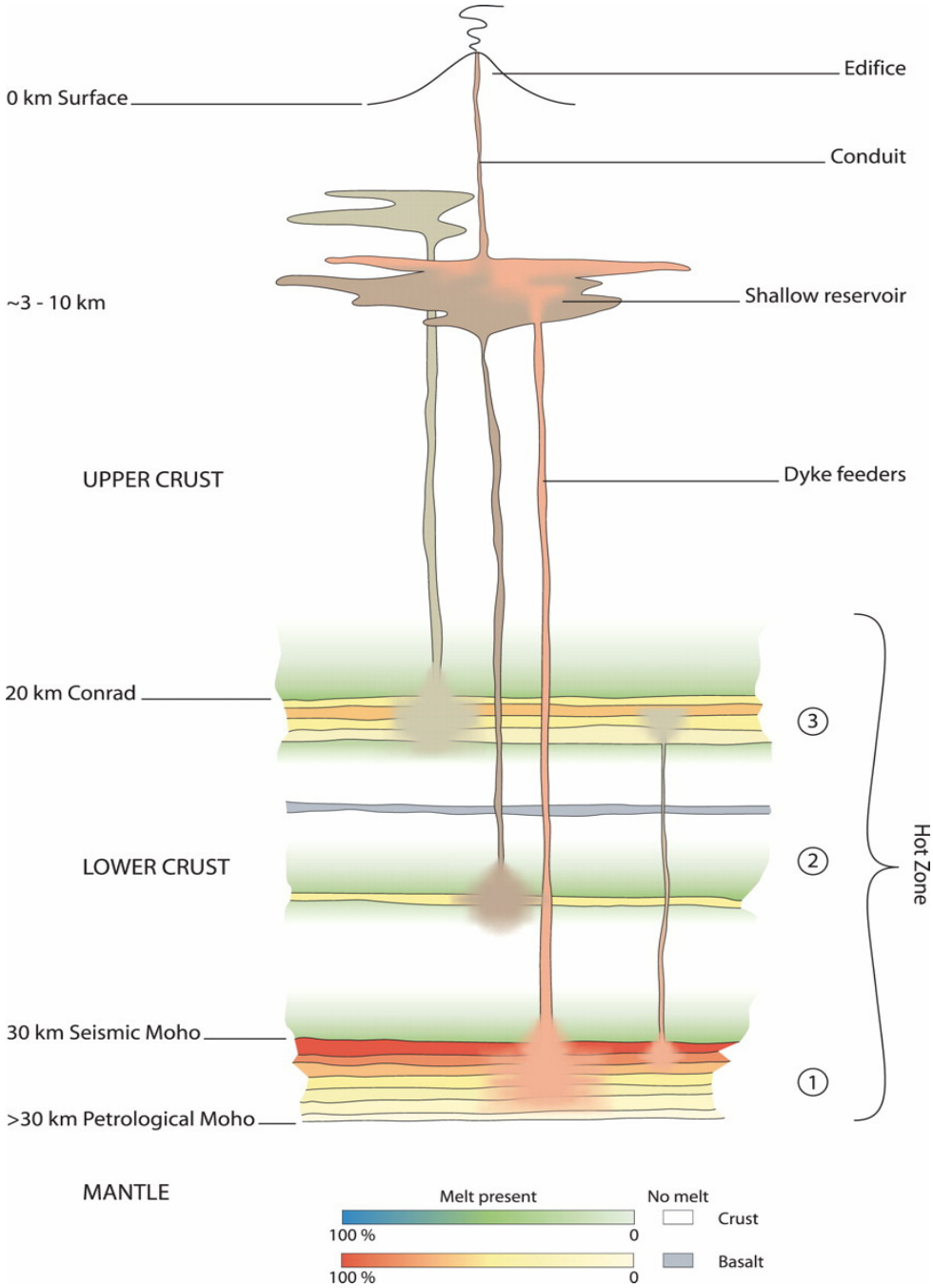

Fig. 1.4 Crustal hot zone model of Annen et al. (2006a) illustrating the emplacement of mafic sills into the lower crust and their subsequent differentiation to generate silicic melts. Sills are also predicted to initiate crustal melting. Silicic melts ascend from the hot zone, leaving residual dense refractory material in the lower crust. Chemical diversity is acquired at depth within the hot zone while magma mixing may occur at any stage along the ascent path.

3. Geological Setting: The British Caledonian

The granites investigated as part of this thesis represent some of the final geological events associated with the collision of Avalonia and Laurentia and generally referred to as the Caledonian Orogeny. This section looks at the tectonic events that led up to final closure of the Iapetus Ocean, the amalgamation of Laurentia and Avalonia and the associated igneous activity.

3.1 Loss of the Iapetus Ocean and the Caledonian Orogeny

The Iapetus Ocean formed during the late Proterozoic Eon (~650 Ma) by rifting of the Rodinia supercontinent. By the beginning of the Ordovician (~510 Ma), the ocean was at its widest, possibly up to 5,000km (Stephenson, 1999). The ocean was bounded by the continents of Laurentia (represented today by the Precambrian basement rocks of North America, Greenland and northern Britain), Gondwana (represented by the basement rocks of South America, Africa, India, Australia, East Antarctica, Western Europe and southern Britain) and Baltica (the basement of Scandinavia and Russia). In Scotland, rift and passive margin sediments related to the final break-up of Rodinia and opening of the Iapetus Ocean are represented by the Ardvreck Group (previously the Eriboll Group) and Dalradian Supergroup (Cawood et al. 2007). These sediments were deposited in basins separated by a supposed rift shoulder formed during opening of the Iapetus Ocean (Cawood et al. 2007) and are separated today by the Moine Thrust and Great Glen Fault. Convergence between these plates began in the early Ordovician, signalling the onset of new magmatic and tectonic processes that define the beginning of the Caledonian Orogeny.

The earliest stages of Caledonian convergence were marked by subduction of the Iapetus Ocean crust beneath oceanic island arcs and continental margins and there is little remaining evidence of this stage of Iapetus closure other than where obduction took place (Fig. 1.5). The earliest orogenic events in Scotland were associated with closure of a small back-arc basin and collision of the continent-facing Midland

Valley arc (Bluck, 1983) with the Laurentian margin to the north during the Grampian Orogeny (470-460 Ma).

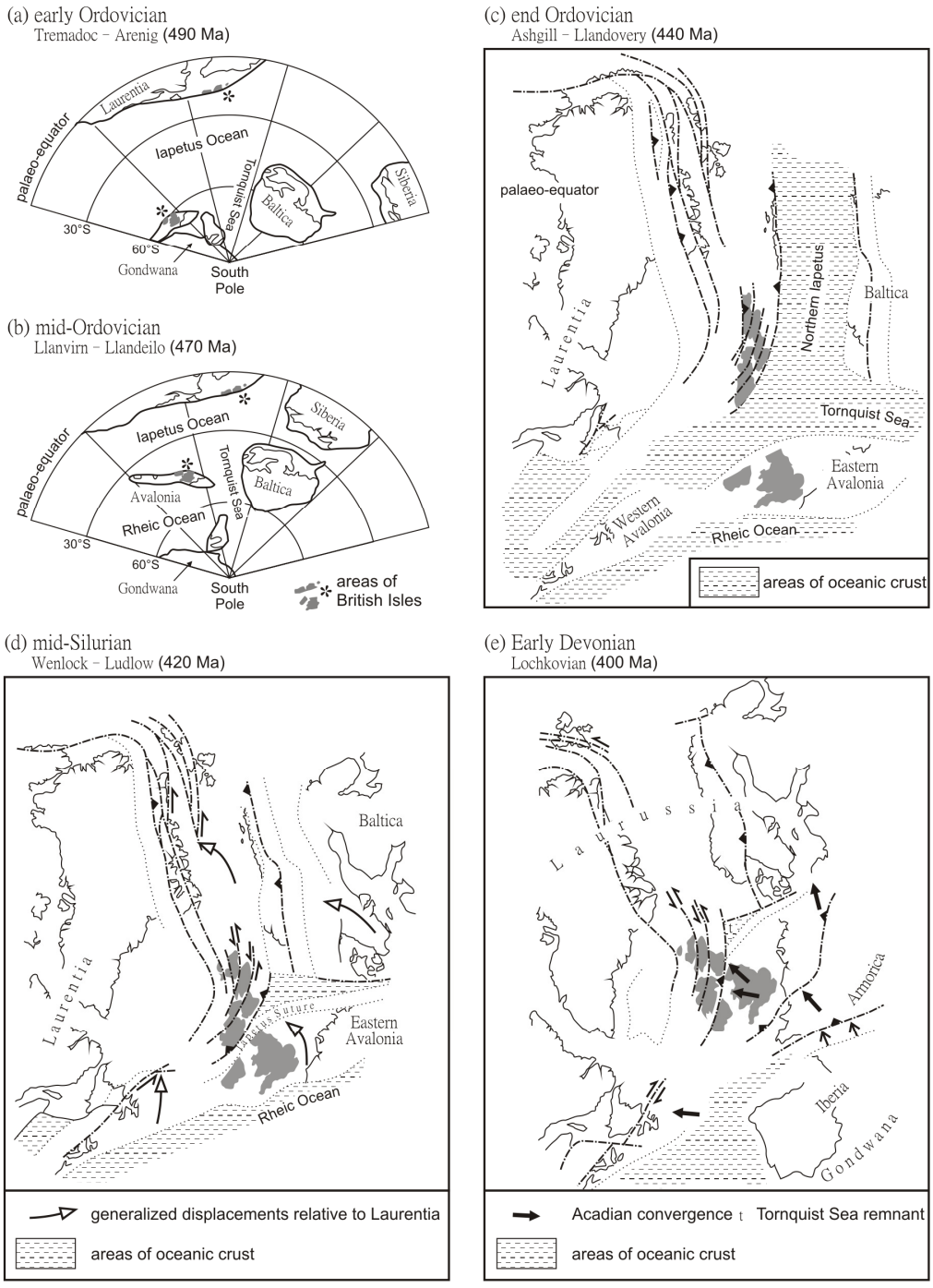

Fig. 1.5 Reconstructions of the movements of the continents bordering the Iapetus Ocean during the Caledonian Orogeny. (a) and (b) provide broad overviews during the early to mid Ordovician. (c), (d) and (e) show narrowing of the oceanic areas towards the end of the Orogeny together with continental collision and strike-slip re-alignment of terranes. From Stephenson (1999) and adapted from Soper et al. 1992.

Southward subduction of Iapetus Ocean crust ceased following arc collision and subsequent northward-directed subduction beneath the accreted arc marked the beginning of closure of the Iapetus Ocean beneath Laurentia (Leggett et al. 1983). Northward subduction was associated with propagation of the Southern Uplands–Longford Down accretionary prism in the hanging wall of the suture zone (Barnes et al. 1989).

On the adjacent Avalonian margin, final closure of the Iapetus Ocean was signalled by deposition of the Windermere Supergroup (late Ordovician to end Silurian in age) within an associated flexural basin (Kneller, 1991). Reduced accretionary deformation in the Southern Uplands accretionary prism is evident during the late Wenlock period (422 - 428 Ma), signalling a slowing of Iapetus subduction (Kemp, 1987). Iapetus subduction is thought to have completely ceased by *c.* 420 Ma (Kemp, 1987; Soper and Woodcock, 2003; Brown et al. 2008). Further constraint on the cessation of convergence has been presented using the K-Ar ages of unfoliated lamprophyre dykes within the Southern Uplands accretionary prism (Rock et al. 1986). These ages suggest that convergence and deformation had stopped by 418 Ma. Together, biostratigraphic and geochronological evidence suggest that convergence ceased between 424 Ma and 418 Ma (Soper and Woodcock, 2003). Subsequent deformation during the Early Devonian is inferred to have been predominantly caused by sinistral transtension (Dewey and Strachan, 2003; Soper and Woodcock, 2003) during oblique convergence of Laurentia and Avalonia. Subsequently, regional folding, faulting and cleavage formation are evident, particularly in the Lake District, towards the early Devonian, with broader folding identified north of the Iapetus Suture. The coeval nature of this deformation with the Acadian Orogeny in the Canadian Appalachians led Soper (1987) to refer to this as the Acadian Event in Britain, which has been linked to further compression of Eastern Avalonia and Laurentia caused by collision of the Armorica microcontinent (Soper, 1986; Soper et al. 1992).

3.2. Post Caledonian Magmatism

Despite evidence that subduction of the Iapetus Ocean had ceased by ~ 420 Ma (Brown et al. 2008; Kemp, 1987), plutonic and volcanic calc-alkaline magmatism with subduction-like geochemical characteristics became prevalent, particularly in the Laurentian terranes, at this time and continued until the early Devonian (Fig. 1.6). The volcanic rocks have particularly high K_2O contents, are mainly silica saturated, have high Mg, Ni, Cr and V and have been attributed to the mixing of primitive mantle melts and sediments thought to be subducted lower Palaeozoic greywackes (Thirlwall, 1982, 1983, 1986).

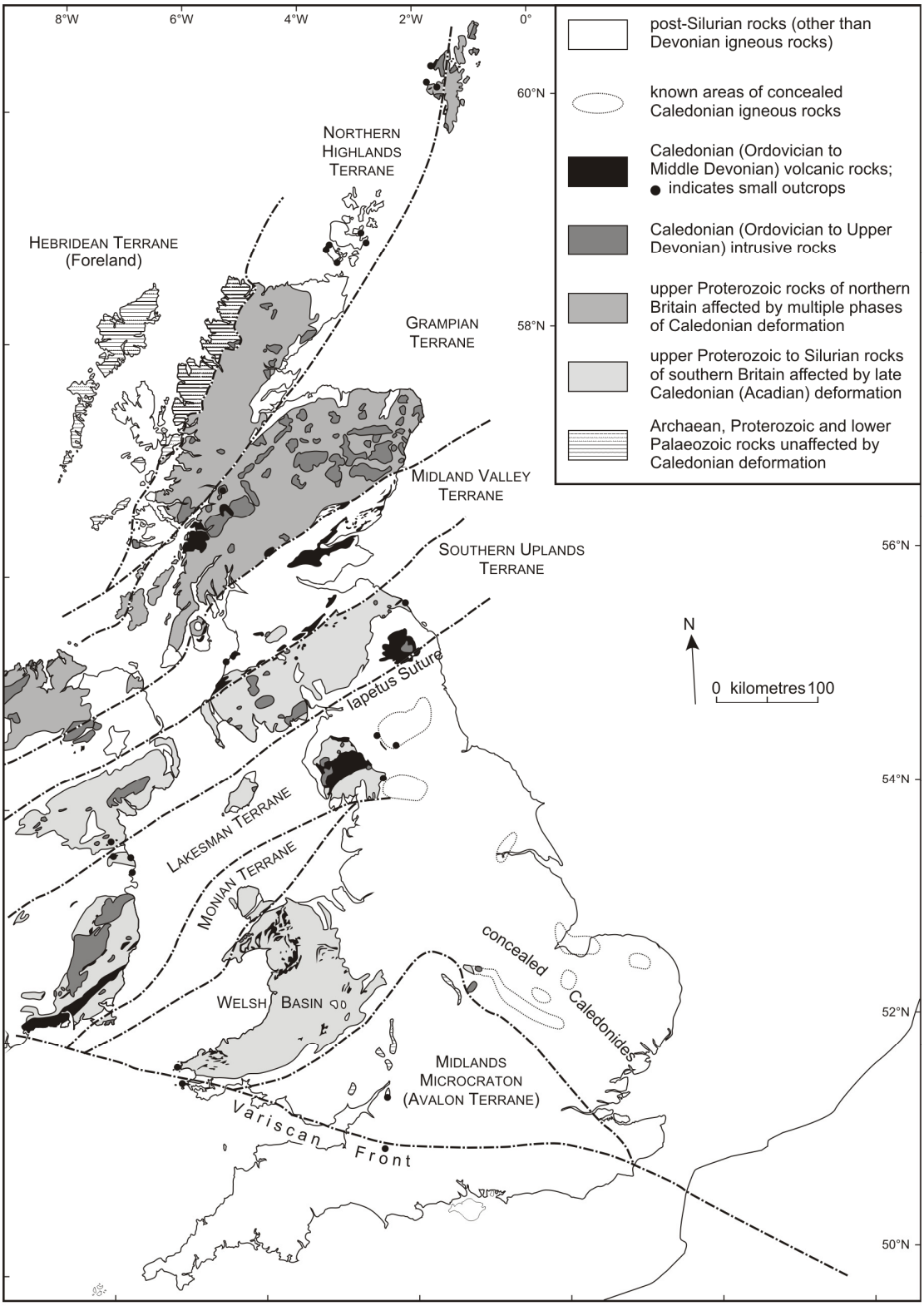

Fig. 1.6 Caledonian related intrusive and extrusive igneous rocks of Great Britain together with major terrane boundaries. Note that Caledonian is used as a group term for all Ordovician to Middle Devonian igneous rocks in this figure. Taken from Stephenson (1999).

Broad, systematic variations in the compositions of volcanic rocks were found perpendicular to the main Caledonian structural trends (Thirlwall, 1981) that were later found to be mirrored by plutonic rocks of a similar age (Stephens and Halliday, 1984). These variations are consistent with a WNW-dipping subduction zone beneath Scotland, where the depth of melting increased away from the Iapetus Suture Zone (Thirlwall, 1982). Although successful in accounting for many of the overall geochemical patterns observed throughout the magmatic suites, continued subduction remains at odds with independent evidence for the cessation of Iapetus subduction by ~ 420 Ma (Brown, et al. 2008).

A number of alternative tectonic models have been proposed to reconcile apparently conflicting evidence. These include volatile loss from a stationary slab (similar to the Cascades of California and Oregon; Thirlwall, 1981) and fluxing of the overlying mantle wedge by active subduction followed by later shearing, extension and mantle melting (Hutton and Reavy, 1992). Freeman et al. (1988) suggested that the Avalonian subcontinental mantle became detached from its overlying crust and continued to subduct despite the crust having ceased subducting, while Neilson et al. (2009) and Oliver et al. (2008) proposed slab break-off following orogenic thickening to account for voluminous I-type magmatism and rapid uplift. The latter authors suggested that slab break-off resulted in asthenospheric upwelling and melting of the subcontinental lithosphere to form lamprophyric underplate that subsequently led to the re-melting of the lower crust through thermal advection and conduction (Atherton and Ghani, 2002). These models invoke a genetic link between the regional occurrence of lamprophyric magmas and much larger volumes of calc-alkaline plutonic and volcanic material.

The plutonic and volcanic rocks that straddle the Iapetus Suture (referred to as the Trans-Suture Suite, TSS) have proved particularly difficult to reconcile with regional tectonic models at the end of the Caledonian Orogeny, primarily because of their proximity to the suture zone (Fig. 1.6). It also remains unclear whether, at a regional scale, the small degrees of melting involved in the formation of lamprophyric magmas are capable of producing the much larger volumes of magma represented by

broadly contemporaneous plutonism and volcanism. Brown et al. (2008) proposed a transtensional model for the formation of the TSS, drawing particular attention to the coeval deposition of the Old Red Sandstone sediments in apparently transtensional basins during the early Devonian on both sides of the suture zone. Their deposition has been shown to require tectonic subsidence linked to enhanced palaeogeothermal gradients in the Welsh slate belts due to extension and passive mantle upwelling (Soper and Woodcock, 2003). Extension or transtension are also consistent with the concurrent intrusion of the regional K-lamprophyre dykes formed following small amounts of lithospheric thinning and adiabatic mantle melting between 420 Ma and 400 Ma (Brown et al. 2008; Dewey and Strachan, 2003). Other mechanisms capable of resulting in extension include those proposed further north in Scotland, including slab-break off and crustal delamination discussed previously (Neilson et al. (2009) and Oliver et al. (2008)). However, the low metamorphic grade of Southern Uplands sediments (Kemp, 1897) suggest no significant crustal thickening while the emplacment of plutons on both sides of the suture makes slab-break off unlikely. We therefore adopt the more likely transtensional model of Brown et al. (2008) to account for regional extension.

3.3 The Trans-Suture Suite (TSS) granites

The predominantly I-type, late- to post-Caledonian Scottish granites were distinguished from the older and more S-type granites found in northern Scotland by Read (1961). Further subdivision by Stephens and Halliday (1984) into the Argyll, Cairngorm and South of Scotland suites followed from compositional distinctions relating to different sources in various tectonic terranes (Fig. 1.7). The South of Scotland Suite was subdivided into granites with low initial $^{87}Sr/^{86}Sr$ north of the Orlock Bridge Fault (e.g. the Loch Doon pluton; Fig 1.7) and those with high initial $^{87}Sr/^{86}Sr$ compositions south of the fault, including the TSS (Stone et al. 1997) that are likely to reflect increased contamination by a sedimentary component. It has also been noted that the southern subdivision of the South of Scotland plutons (e.g. the Criffell and Fleet plutons) share many compositional characteristics with plutons of similar age in the English Lake District (e.g. Shap pluton), emplaced within

Avalonian crust to the south (Harmon and Halliday 1980b; Harmon et al. 1984; Highton, 1999; Stephens, 1988; Thirlwall, 1989).

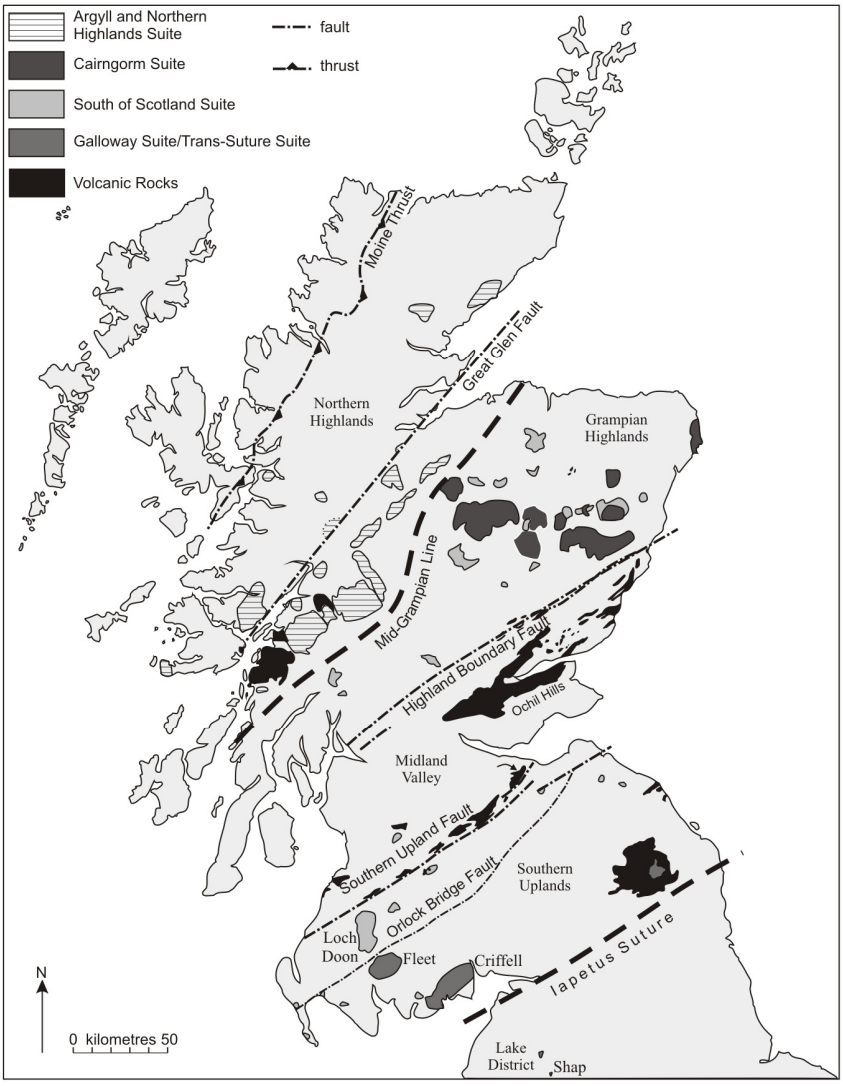

Fig. 1.7 Modified map of late Caledonian plutonic and volcanic rocks (black) in the northern United Kingdom, modified from Highton (1999). Plutons are classified according to the geochemical parameters outlined by Read (1961), Stephens and Halliday (1980) and Stone (1997).

Because of the absence of inherited detrital material (Pidgeon and Aftalion, 1978), U-Pb dating of magmatic zircons from plutons south of the Highland Boundary Fault constrains emplacement ages only. By contrast, plutons north of the Highland Boundary Fault commonly contain a significant proportion of inherited zircons, many with Archean ages consistent with underlying basement of a similar age. Pidgeon and Aftalion (1978) attributed these differences to an absence of older basement material south of the Highland Boundary Fault.

3.3.1 The Criffell Pluton

A Rb-Sr age suggests that the Criffell pluton was emplaced at ~397 ± 2 Ma (Halliday et al. 1980) into low-grade wackes and pelites of Llandovery to Wenlock age (444 to 423 Ma) that form part of the Southern Uplands accretionary prism in southern Scotland (Fig. 1.7). The pluton is of global significance as a classic example of a normally zoned pluton (Fig. 1.8) (Stephens and Halliday, 1980; Stephens et al. 1985). Outer zones (1 and 2) are of metaluminous granodiorite (~ 59 to 69 wt % SiO_2) containing primary hornblende (with occasional cores of clinopyroxene), biotite, plagioclase, potassium feldspar, quartz and accessory sphene, zircon, apatite, allanite and magnetite (with very minor hematite) (Table 1.2; Appendix C). Inner zones (4 and 5) are of peraluminous granite (~ 69 to 73 wt % SiO_2) that contains primary muscovite but lack hornblende, sphene and the abundant zircon and magnetite that characterise the granodiorites.

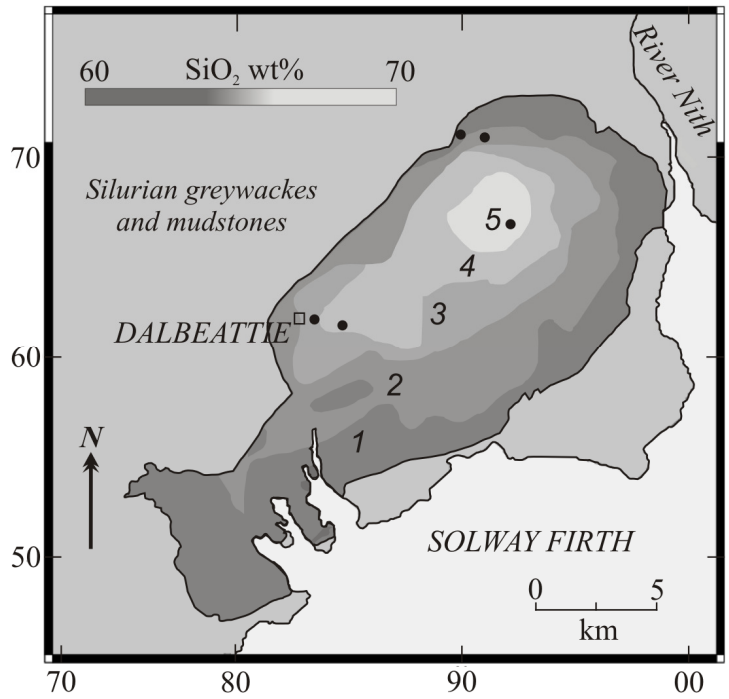

Fig. 1.8 Map of the Criffell pluton. Paler shading reflects increasing WR SiO_2. Zone mineralogy is as follows: 1) clinopyroxene-biotite-hornblende granodiorite; 2) biotite-hornblende granodiorite; 3) biotite granite; 4) muscovite-biotite granite 5) biotite-muscovite granite. Minerals listed in order of increasing modal abundance (Stephens et al.. 1985). Black points denote the locations of samples collected for this study.

Mineralogical zoning is accompanied by isotopic zoning, with outer granodiorites having initial $^{87}Sr/^{86}Sr$ ratios of 0.7052, εNd values of -0.6 and $\delta^{18}O$ values of 8.5 ‰ (Halliday, 1984; Halliday et al. 1980). Inner granites have initial $^{87}Sr/^{86}Sr$ ratios as high as 0.7073, εNd values of -3.1 and $\delta^{18}O$ values of 11.9 ‰. Simultaneous variations in isotope and Rare Earth Element (REE) compositions were interpreted by Stephens et al. (1985) as resulting from assimilation and fractional crystallisation (AFC) involving both mafic lower crustal/mantle and sedimentary components. The absence of local melting in surrounding country rocks indicates that adjacent sediments were not a major source of contamination. Pluton assembly occurred via incremental assembly of multiple batches of magma. This is supported by the alignment of minerals and mafic enclaves in the outer zones of the pluton interpreted to result from the later intrusion of the more evolved central zones (Stephens et al. 1985).

Mafic enclaves are a common feature in the outer three zones of the pluton. Oscillatory zoned plagioclase within the enclaves provides evidence for a magmatic origin (Holden et al. 1987). The enclaves have been variously interpreted to represent residual components following partial melting of the crust, restite from a basic precursor, cognate material, congealed syn-plutonic injections of basic magmas or segregated immiscible liquids (see Holden et al. 1987). Initial Nd isotope ratios of the mafic enclaves (ε_{Nd}: -0.7 to +1.6) are consistently higher than those of their host rocks (ε_{Nd}: -2 to +0.6), indicating that they were out of equilibrium with their hosts (Holden et al. 1987). By contrast, Sr isotopes show only limited variations between hosts and enclaves (0.7051-0.7061) that may reflect partial re-equilibration of the main Sr repository phases, particularly plagioclase. The higher initial Nd ratios of the enclaves suggest a non-cogenetic relationship with their hosts. Mafic enclaves may thus reflect syn-plutonic injections of mantle-derived magma into the host granodiorite magma or entrained cognate material.

3.3.2 The Fleet Pluton

The ~ 10 km by 12 km Fleet pluton intrudes the Llandovery age sediments (428 to 444 Ma) of the Central Belt of the Southern Uplands and is situated south of the Orlock Bridge fault (Fig. 1.7). Pidgeon and Aftalion (1978) reported a zircon U-Pb age of 396 ± 6 Ma, consistent with a Rb-Sr mineral-whole-rock age of 392 ± 2 Ma that lies within analytical error (Halliday et al. 1980). A fabric related to ductile deformation wraps around cordierite porphyroblasts in the aureole and is cut by the granite contact, reflecting syn-tectonic emplacement of the pluton during reactivation of the Moniaive Shear Zone during Acadian deformation (Barnes et al. 1995; Brown et al. 2008; Stone et al. 1997). Gravity anomalies suggest that the pluton extends to a depth of ~ 11 km beneath the current surface (Parslow, 1973). SiO_2 contents vary from 69 to 76 wt% and are on average more evolved and S-type than other TSS granites.

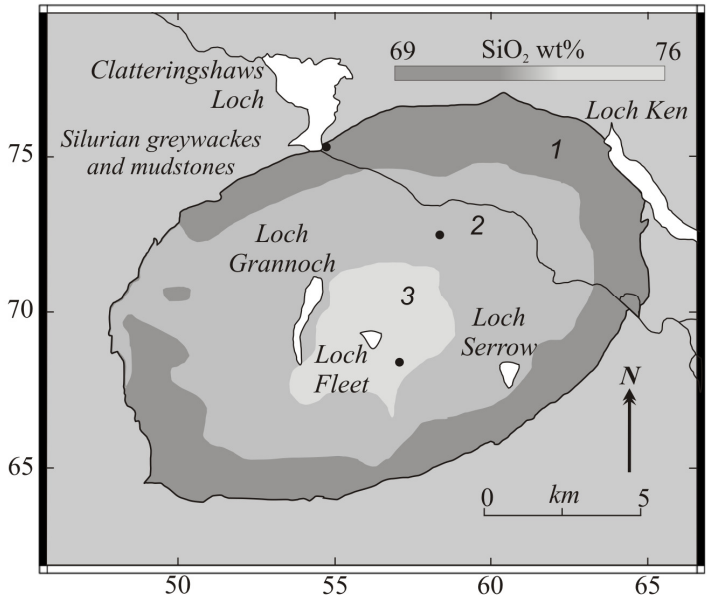

Fig. 1.9 Map of the Fleet pluton. Paler shading reflects increasing WR SiO_2. Zone mineralogy is as follows: 1) coarse-grained biotite granite; 2) coarse-grained biotite-muscovite granite; 3) fine-grained biotite-muscovite granite. Minerals listed in order of increasing modal abundance (Stephens et al.. 1985). Black points denote the locations of sample collected for this study.

Petrologically, the pluton has two main granite facies, including an outer biotite granite and inner biotite-muscovite granite (Fig. 1.9). The latter facies has been subsequently subdivided into fine and coarse grained units (Parslow, 1968) (Table 1.2; Appendix C).

Elevated initial $^{87}Sr/^{86}Sr$ ratios of 0.7062 to 0.7083 and low εNd values of -3.0 to -3.4 (Stephens and Halliday, 1984) also reflect the predominantly S-type characteristics of the Fleet pluton, with evolved whole-rock $\delta^{18}O$ values of ~11‰ indicative of a large sedimentary component (Halliday, 1984; Halliday et al. 1980; Stephens and Halliday, 1984). The Fleet pluton has previously been shown to share many geochemical similarities with plutons in the Lake District that also post-date Iapetus closure (Stephens and Halliday, 1984; Thirlwall, 1989).

3.3.3 The Shap Pluton

The Shap pluton was emplaced into the Caradoc (~ 455Ma) volcanics of the Borrowdale Volcanic Group (BVG) in the English Lake District (Fig. 1.7, Fig. 1.10). Pidgeon and Aftalion (1978) reported a zircon U-Pb age of 390 ± 6 Ma, while Wadge (1978) reported an age of 394 ± 3 Ma based on a whole-rock-feldspar isochron, similar to the 397 ± 7 Ma age estimated from K-Ar biotite dating (Rundle, 1992). Davidson et al. (2005) reported an older single mineral Sr isochron age of 405 ± 2 Ma.

Stephenson (1999) noted three distinct stages of pluton growth based primarily on the modal abundance of large K-feldspar megacrysts now thought to be igneous in origin (Lee and Parsons, 1997). Stage 1 (10% volume of the pluton) is represented by the outer margins of the pluton with 15% pink, Carlsbad-twinned orthoclase-perthite megacrysts up to 5 cm in size. The groundmass consists of orthoclase, plagioclase (zoned from andesine to albite), quartz and biotite. Accessory minerals include sphene, apatite, magnetite, zircon, fluorite, monazite, allanite, amphibole and pyrite. The dominant stage 2 granite (90% of the pluton) is broadly similar to the stage 1 granite but contains 30% orthoclase and reduced proportions of biotite. This trend continues into the final (stage 3) granitic veins with up to 60% orthoclase megacrysts (Table 1.2; Appendix C).

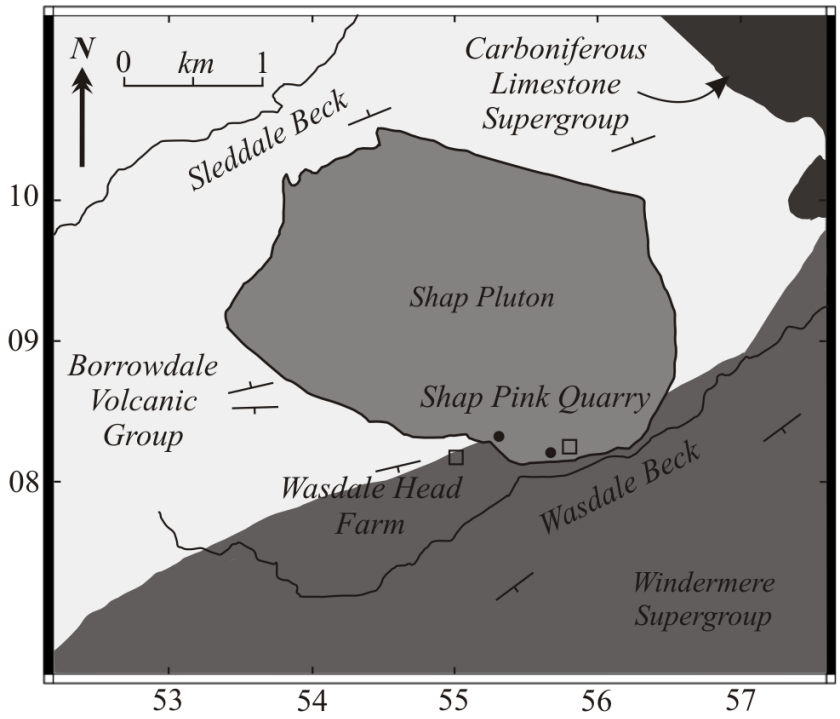

Fig. 1.10 Map of the Shap pluton and surrounding geological units. Black points denote the locations of sample collected for this study.

Significant assimilation and contamination by local Skiddaw Group sediments are thought to be indicated by relatively high $\delta^{18}O$ values of ~11‰, initial $^{87}Sr/^{86}Sr$ values (0.707) and low εNd (-2.0). However, the predominantly I-type mineralogy of the Shap granites indicates that crustal fluids may have significantly altered the isotopic composition of the pluton with enrichment in ^{18}O either during or post emplacement (Halliday, 1984).

Abundant megacryst-bearing microdioritic inclusions up to 2m in size occur in addition to country rock xenoliths in the Shap pluton. Many authors have suggested that such features represent injections of mafic magma, possibly related to the regional K-lamprophyre dyke swarm (Granthem, 1928; Stephenson, 1999), although a widely-accepted interpretation is still lacking.

A summary table of key mineralogical characteristics in each of the plutons, their zones and their enclaves is included below for reference. Full petrological descriptions are included in Appendix C.

Table 1.2 Summary table of the key minerals identified by this study and others in respective zones of the Criffell, Fleet and Shap plutons and associated mafic enclaves.

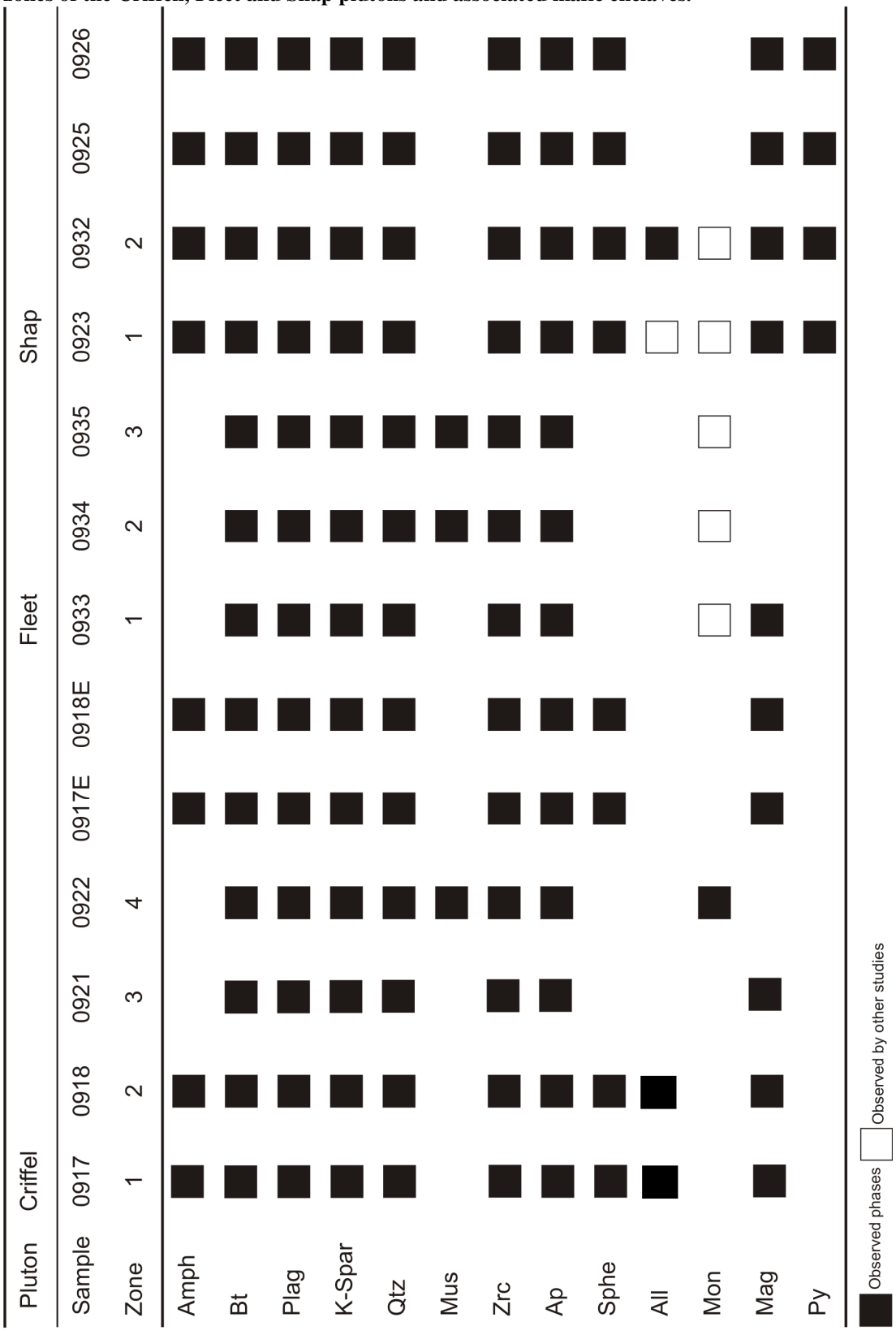

3.4. Lithospheric Structure of the Iapetus Suture

During the 1970s and 1980s a large seismic reflection profiling programme was conducted by the British Institutes Reflection Profiling Syndicate (BIRPS) to image the continental shelf around the British Isles in order to provide better geological constraints on the formation and locations of economically important hydrocarbon reservoirs. A number of these seismic profiles have revealed important information about the Iapetus Suture zone. The suture is present as a shallowly northwards dipping (~ 20-30^{o}) reflector in a number of seismic lines, but is best seen in the NW-SE NEC line (Freeman et al.1988) located offshore eastern Britain between Arbroath and Middlesbrough. The same boundary has also been imaged along the WINCH profile that runs broadly NW-SE from west of the Outer Hebrides, through the North Channel to the Isle of Man (Brewer and Smythe, 1983) and the N-S WIRE profile west of Ireland (Klemperer et al. 1991). In all, the suture has been tracked for some 900 km from the Atlantic continental shelf west of Ireland to the North Sea (Klemperer et al. 1991 and references therein).

The reflector is interpreted to represent Avalonian crust underthrust beneath the Laurentian margin and is seen to flatten to the north (Freeman et al. 1988). Brown et al.. (2008) suggest that flattening of subducting Iapetus oceanic lithosphere occurred in response to the subduction of progressively younger and more buoyant lithosphere up to 420 Ma. The geometry of the suture zone close to the Moho is less certain, but it appears to flatten and merge with a set of strong sub-horizontal reflections in the lower crust beneath the Midland Valley, interpreted as Iapetus oceanic crust or imbricated basement and sedimentary cover from the continent-ocean margin of Avalonia (Soper et al. 1992). The location of these reflectors indicates that underthrust Avalonian crust extends at least as far north as the Midland Valley. The occurrence of Avalonian sediments beneath the Southern Uplands is consistent with the high $^{207}Pb/^{204}Pb$ ratios of the Southern Uplands granites; the ratios have previously been attributed to the presence beneath the Southern Uplands of Ordovician Skiddaw Group sediments, which are exposed across the Iapetus Suture in the English Lake District (Thirlwall, 1989).

4. Thesis Motivation, Objectives and Layout

In the past decade, the growing numbers of zircon studies that integrate O-Hf-U-Th-Pb isotope analyses have re-kindled interest in what was a neglected area of geological research. The chemical and isotopic record held in zircon crystals has allowed magmatic processes and sources to be investigated at all scales, at high spatial and temporal resolution and in a manner that is largely immune from the effects of alteration. Studies of zircon have produced many important insights but they have also raised new questions. In particular, the question of how zircon isotope compositions relate to those obtained from other chemical archives is often neglected and it remains unclear how the processes inferred from zircon compositions can be related to those that are deduced from whole-rock and other mineral and textural records. Furthermore, it is unclear whether zircon records the same stages of evolution in magmas of different composition. Apatite is an equally ubiquitous mineral in many silicic rocks. A comparatively small number of studies have alluded to the ability of apatite trace element compositions to provide a sensitive and robust record of magma evolution, and only a handful of studies have attempted to integrate the chemical information retained by apatite and zircon.

The magmatic bodies chosen to investigate these issues are the end Caledonian Trans-Suture Suite (TSS) of granitic plutons located around the Iapetus Suture zone in northern Britain. In a general sense, these plutons offer an opportunity to investigate what information is recorded by apatite and zircon in calc-alkaline magmas. At a regional scale, this study is the first to apply micro-analytical techniques to a suite of rocks that have themselves posed a number of regional tectonic problems to the understanding of post-orogenic processes at the end of the British Caledonian orogenic cycle.

The primary objectives of this thesis have been to:

- Investigate the magmatic evolution of a suite of enigmatic calc-alkaline Devonian plutons that post-date Iapetus subduction and have previously

been shown to lack zircon inheritance despite whole-rock isotopic evidence for significant sedimentary involvement.

- Constrain the timing of zircon crystallisation in I- and S-type magmas in order to determine the stage of magma evolution recorded by zircon and other accessory minerals.
- Compare and contrast the stages of magma history archived by whole-rock and accessory mineral records.
- Compare the compositions and ages of crustal sources sampled by plutons lying north and south of the Iapetus Suture in order to determine their relationship to crustal structure.
- Attempt to quantify the roles of crustal and mantle sources in granite genesis, and establish whether the plutons represent net crustal growth or crustal differentiation.
- Use different scales of isotopic and elemental heterogeneity to test models of incremental pluton assembly and their geological timescales.
- Determine the petrogenetic significance of wide-ranging I-S characteristics in closely related plutons, and any relationship to spatially related mafic lamprophyres.

These objectives have been addressed in five data chapters that are a compilation of five unpublished papers. The first two chapters begin by investigating what stages of magma evolution are recorded by accessory minerals and whole-rocks and the relative timing of accessory mineral crystallisation in metaluminous and peraluminous magmas. Apatite is proposed as an additional proxy for examining magma processes and as a valuable index of magma redox conditions. Regional aspects of granite petrogenesis around the Iapetus Suture are investigated and the implications for end-Caledonian tectonic and magmatic processes are discussed. The post-emplacement thermal histories of the plutons are investigated by examining the extent of oxygen isotope equilibrium between different isotopic archives and compared with those of the younger British Tertiary granites. U-Pb ages obtained from detrital zircons found in a Devonian basaltic vent and inherited from the local Southern Uplands accretionary prism are presented in Appendix A. These are

compared with larger data-sets from the older northern province of the accretionary prism to reveal similar provenance histories and deposition within an active-margin trench environment. A summary of the main conclusions from each data chapter is included below.

1. ***Chapter 2*** investigates the processes that result in the attainment of whole-rock and accessory mineral compositions in the zoned Criffell pluton. Whole-rock Pb isotopes and geophysical/geological constraints are used to show that WR chemistry was determined at depths of > 11km and records the actions of open system magma differentiation together with significant contributions from sedimentary components. By contrast, the REE compositions of apatite crystals are shown to document the crystallisation history of incrementally assembled magmas at depths of ~ 4 to 6 km, constrained by geobarometry. The identity of competing accessory minerals is shown to differ from those that controlled WR compositions, and it is proposed that accessory mineral compositions record a distinct stage of magma history to that of the WR. The absence of inherited crystals from both country rocks and earlier stages of magma evolution is attributed to the ascent of wet super-liquidus magmas and resorption of entrained crystals. These properties reflect the rapid, adiabatic ascent of low viscosity, silicic magmas that result from high water contents during magma evolution in crustal hot zones.

2. ***Chapter 3*** looks at the timing of zircon crystallisation relative to other minerals and whether this differs in response to changing magma compositions. This is achieved by identifying host-dependency amongst the compositions of apatite inclusions in different minerals, including zircon. Two distinct trends are identified from apatite compositions, one characterised mainly by decreases in Ce that results from allanite crystallisation in metaluminous zones, the other by consistently low concentrations of Ce caused by early saturation of monazite and depletion in HREE in peraluminous magmas. Apatites formed during the earliest stages of crystallisation have the highest concentrations of REE. Host minerals that

encapsulate only the most REE-rich apatites are also likely to have formed during the early stages of crystallisation. Varying degrees of host dependency are identified in the apatites that define these trends in the Criffell pluton. In metaluminous zones, apatite inclusions in all phases (including zircon) show similar degrees of compositional heterogeneity and suggest no clear crystallisation order. In peraluminous zones, apatites hosted by zircon have consistently higher concentrations of REE, reflecting earlier crystallisation of zircon in these magmas. In a transitional metaluminous to peraluminous zone, only zircon-hosted apatites plot on the metaluminous trend. Apatites hosted by other minerals follow a similar trend to those in more peraluminous zones. This transitional zone reflects the first appearance of monazite and is the most primitive zone to show evidence that the composition of zircon is biased towards earlier stages of crystallisation.

3. ***Chapter 4*** presents evidence that the Mn concentration of apatite can be used as a proxy for the oxidation states of magmas. Increasing concentrations of Mn are identified in apatites formed from more reduced magmas in the Criffell pluton despite decreases in the Mn concentration of the magmas from which they crystallised. These trends are attributed to increasing Mn^{2+}/Mn^{3+} in reduced magmas that result in greater Mn substitution for Ca^{2+} in the apatite structure. These data are compared with the results of the recent zircon redox calibration that use Ce anomalies (Trail et al. 2011). The latter calibration is sensitive to the effects of LREE-rich mineral inclusions and the naturally low concentrations of such elements in zircon. Despite general agreement between the two methods, apatite is proposed as a potentially more robust and widely applicable redox proxy with applications to the detrital record, lunar magmas and granite petrogenesis.
4. ***Chapter 5*** integrates zircon O-Hf-U-Th-Pb isotope data from the Criffell, Fleet and Shap plutons. New zircon U-Pb ages are used to present a new geochronological framework, showing for the first time that all three of the plutons studied were emplaced during multiple phases of pre- and post-Acadian transtension. Zircons from different zones of the Fleet pluton also reveal protracted and incremental assembly of the pluton over ~ 23 Ma.

Increasing levels of oxygen isotope heterogeneity amongst zircon populations from more evolved zones of the plutons are also identified. These heterogeneities, and particularly the presence of zircons with mantle-like $\delta^{18}O$ compositions, indicate that more primitive magmas were involved in the formation of apparently S-type granites. Hf isotope compositions are used to identify potential source regions beneath the Iapetus Suture and reveal two stages of mixing between a juvenile source(s) and Avalonian basement, with further mixing between these magmas and Avalonian sedimentary component(s). The coincident intrusion of hydrous lamprophyric magmas indicates melting of hydrated mantle lithosphere and may in part explain the high water contents of these granites, which in Chapter 2 is inferred to reflect resorption of inherited crystals during magma ascent. These characteristics are likely to reflect the emplacement of these granites into a suture zone located close to a previous area of slab dehydration.

5. ***Chapter 6*** investigates the later hydrothermal stages of pluton evolution. Zircon oxygen isotope compositions are shown to represent magmatic compositions, while those of the whole-rock suite together with quartz reflect later hydrothermal alteration and exchange respectively with ^{18}O-rich magmatic fluids that underwent further enrichment due to exchange with ^{18}O-rich local sediments. The quartz and whole-rock compositions of outer zones show greater oxygen isotope disequilibrium at depth due to circulation of fluids further enriched by interaction with ^{18}O-rich sedimentary rocks. The enrichment in ^{18}O caused by hydrothermal processes is contrasted with the depletion in ^{18}O caused by hydrothermal processes around the shallower granites of the British Tertiary Igneous Province and reflects fundamentally different depths and processes of emplacement in markedly different tectonic settings.

5. Methodology

Analytical methods now enable *in situ*, high precision measurements of isotope ratios and element concentrations. This study integrates micro-analysis of zircon and apatite crystals using ion microprobes, electron microprobes and a laser ablation-multi-collector ICP-MS (LA-MC-ICPS). In addition, bulk-rock major and trace element compositions have been analysed using standard X-ray fluorescence (XRF) techniques, while bulk-rock oxygen isotope compositions were analysed using laser fluorination methods. This section presents a summary of the techniques and methods used. A detailed account of analytical set-ups is included in Appendix B.

5.1 Whole-rock major and trace element concentrations

XRF analyses were carried out in the Grant Institute of Earth Science at the University of Edinburgh. The techniques used are similar to those described by Fitton et al. (1998), with modifications noted by Fitton and Godard (2004). Fist-sized rock samples were crushed, milled and homogenised by coning and quartering to ensure sampling of representative compositions. Glass discs were produced after fusion with lithium borate flux and pressed-powder discs made for trace element analysis. The fused and pressed samples were analysed using a PANalytical PW 2404 automatic X-ray fluorescence spectrometer with a Rh-anode X-ray tube.

Oxygen isotope analyses of whole-rock samples were carried out at the Scottish Universities Environmental Research Centre (SUERC) at East Kilbride. The method followed the Macaulay et al. (2000) modification of the laser fluorination method of Sharp (1990). A Micromass PRISM 3 duel inlet, triple collector mass spectrometer was used to analyse the oxygen isotope composition.

5.2 Zircon preparation

Rock samples of approximately 5 kg from different zones of all the plutons studied were crushed and sieved to < 500 μm prior to density separation using a Wilfley

Table at the University of St Andrews separation facility. Heavy liquids, including tetrabromoethane (TBE) and methylene iodide were used for further mineral separation. Non-magnetic fractions were separated using Frantz magnetic separators at the universities of St Andrews and Edinburgh. Approximately 100 zircon crystals were picked from each sample and mounted in epoxy (Araldite/Epothin) blocks with fragments of 91500 zircon standard positioned at the centre of each block. Polished mounts were imaged by back-scattered electron and cathodoluminescence (CL) methods using a Phillips XL30CP Scanning Electron Microscope (SEM) at the University of Edinburgh to establish the positions of inclusions, cracks and internal compositional zoning.

5.3 Zircon oxygen isotope analysis

The fractionation of oxygen isotopes between coexisting minerals increases with decreasing temperatures, with Si-rich phases being more enriched in ^{18}O relative to Fe-rich and Si-poor phases. The abundance of Si-rich minerals in the upper continental crust therefore contributed to its elevated ^{18}O composition relative to that of the mafic mantle. Oxygen isotopes are preserved in zircon due to slow diffusion rates (Watson and Cherniak, 1997) and are insensitive to the effects of fractional crystallisation because melt-zircon fractionation factors increase in parallel with the oxygen isotope composition of the melt (Valley et al. 1994). High mantle temperatures mean that oxygen isotope values have remained largely buffered throughout Earth history ($\delta^{18}O$ = 5.3 ± 0.3‰; Valley et al. 1998), and zircon therefore provides a robust method for examining supracrustal contributions to silicic magmas.

Zircon oxygen isotope analyses were carried out using a Cameca ims 1270 ion microprobe at the University of Edinburgh Ion Microprobe Facility (EIMF) following the methods of Cavosie et al. (2005) and Kemp et al. (2006b) with data reported as per mil (‰) values relative to Vienna Standard Mean Ocean Water (VSMOW). Analytical pits were generally ~20 μm wide and ~ 1μm deep. Following corrections for instrument drift, unknown zircon analyses were normalised to an

average daily $^{18}O/^{16}O$ value for zircon standard 91500. Analytical precision (2σ) from session to session was generally between ± 0.3 and 0.6 ‰.

5.4 Zircon U-Th-Pb analysis

Zircon is the most widely used crystal for U-Pb dating, based on the radioactive decay of U and Th to stable isotopes of Pb. Zircon readily incorporates the parent isotopes U and Th. However, substitution of the decay product, Pb is highly limited due to large differences in the ionic radii of Zr and Pb. Thus, due to the inert nature of zircon, it may often be considered as a closed system and it can be assumed that all measured Pb results from the decay of U and Th, allowing precise estimates of crystallisation ages (see Faure and Mensing, 2004).

U-Th-Pb dating was carried out following oxygen isotope analysis using a Cameca ims 1270 ion microprobe at the University of Edinburgh. A 4 to 5 nA primary O^{2-} beam was used for zircon analysis with 22.5 keV impact energy following the method of Kelly et al. (2008). Pb ion yields were increased by a factor of ~ 2 by flooding the sample surface with oxygen. As a result, all oxygen isotope analyses were carried out prior to U-Pb dating. Analytical pits were ~20μm wide and ~ 3μm deep. Analytical precision was generally ~ ± 3 to 4 Ma (1σ).

5.5 Zircon Hf isotope analysis

During mantle melting, ^{176}Hf, the stable decay product of ^{176}Lu, is more incompatible than Lu, leading to depletion in Hf in the residual mantle and enrichment in the crust (Patchett et al. 1981). The originally uniform chondritic Lu/Hf ratio of the Bulk Silicate Earth has therefore been progressively modified by the extraction of basaltic magmas from the mantle (Kinny and Maas, 2003). Zircon can be regarded as a zircon-hafnon solid solution, with most natural zircon having ~ 0.5 to 5wt % HfO_2, with most between 1 and 2 wt % (Hoskin and Schallegger, 2003). The greater abundance of Zr relative to Hf reflects naturally high Zr/Hf ratios in all magmas. Zircon is ideally suited to the investigation of radiogenic Hf isotopes because of its inertness and low $^{176}Lu/^{177}Hf$ ratios (< 0.0005). *In situ* decay of ^{176}Lu therefore has

only a negligible effect on the Hf compositions in zircon and can be regarded as a reliable indicator of magma compositions at the time of crystallisation.

Zircon Lu-Hf isotope compositions were obtained using a ThermoFinnigan Neptune multicollector inductively-coupled plasma mass spectrometer (MC-ICP-MS) coupled with a New Wave Research UP193HE laser at the University of Bristol. Similar sites to those used for oxygen isotope analyses were chosen using a spot size of 40 or 50μm. Corrections for interferences and mass bias followed the University of Bristol procedure outlined by Hawkesworth and Kemp (2006) and Kemp (2009). Epsilon Hf values are reported relative to initial Chondritic Uniform Reservoir (CHUR) values calculated from present day values of $^{176}Lu/^{177}Hf = 0.0336$ and $^{176}Hf/^{177}Hf = 0.282785$ (Bouvier et al. 2008). A ^{176}Lu decay constant of $\lambda = 1.867 \times 10^{-11}$ yr^{-1} (Scherer et al. 2001) was used. Analytical errors were ~ ± 0.8 (2σ) epsilon units.

5.6 Zircon trace element analysis

Zircon incorporates up to 25 different elements, the most abundant being Hf, Y, REEs, P, U and Th. These elements require simple or coupled substitution to archive charge balance and their concentrations have often been shown to remain largely similar in zircons from a wide range of magmas (see Hoskin et al. 2000). When chondrite normalised, zircon REE patterns typically show steeply rising slopes from LREE to HREE, a positive Ce anomaly (Ce/Ce*) and negative Eu anomaly (Eu/Eu*) due to differences in compatibility (Hoskin and Shaltegger, 2003).

A Cameca ims-4f was used to measure trace element (including REE) concentrations at the University of Edinburgh Ion Microprobe Facility (EIMF). Analytical methods and procedures followed those described by Hinton and Upton (1991) and resulted in a 20μm wide, 5μm deep analytical pit. Analytical precisions depend on the concentration measured and are generally ~ 2% at 100 ppm and increase to 10% at 1 ppm and 100% at 10 ppb.

5.7 Apatite trace element analysis

Apatite is a common repository for trace elements, including REEs in silicic rocks. Unlike zircon, apatite chondrite normalised REE patterns differ depending on the compositions of the magmas from which they crystallised (e.g. Sha and Chappell, 1999). This has led to small number of studies that use apatite as a robust and sensitive indicator of magma petrogenesis and as a reliable provenance indicator in sedimentary rocks (Nash, 1984; Shnukov et al. 1989; Sha and Chappell, 1999; Hoskin et al. 2000; Belousova et al. 2001; 2002; Chu et al. 2009). Apatites from more primitive silicic magmas (< ~ 68 wt % SiO_2) have generally smooth trends that range from 10^3 times chondritic values of LREE to 10^2 times chondritic values of HREE with little evidence of Eu anomalies. By contrast, apatites that crystallise in peraluminous magmas show maximum concentrations of MREE, lower concentrations of LREE and HREE, and often large negative Eu anomalies.

Apatite compositions were determined primarily by a Cameca SX-100 electron probe supported for comparative purposes by ion microprobe analyses using a Cameca ims 4f at the EIMF. Good agreement was observed between the two methods. Zircon-hosted apatite was analysed in zircons mounted in epoxy blocks. Back-scattered electron (BSE) and cathodoluminescence (CL) images were taken on polished surfaces using a Philips XL30P Scanning Electron Microscope (SEM) at the University of Edinburgh. Apatite hosted by other phases was analysed directly in polished thin sections.

A wavelength dispersive method (WDS) was used for electron probe analysis of apatite using PC0, LTAP, LPET and LIF dispersion crystals. Beam conditions were 20 kV and 60 nA for trace and most major elements, with a 10 nA defocused beam used to minimise loss of alkalis during analysis.

Apatite inclusions were analysed using the Cameca ims4f ion microprobe, with a 5 nA $^{16}O^-$ primary ion beam with 15 keV net impact energy and a spot size of approximately 15 μm.

5.8 Quartz oxygen isotope analysis

Similarly to zircon, quartz has been proposed as an additional and potentially reliable archive of magmatic oxygen isotope compositions (Valley and Graham, 1996; Appleby et al. 2008). Isotope exchange may occur by rapid solution/re-precipitation along cracks, fractures and crystal boundaries and slow temperature-dependent volume diffusion (Valley and Graham, 1996; Appleby et al. 2008).

Quartz standards were mounted in polished thin sections using a new approach involving coring selected polished thin sections using an ultrasonic drill. Quartz standards were crushed and mounted in epoxy prior to emplacement and further polishing. The oxygen isotope compositions of quartz grains were determined using the Cameca ims 1270 ion microprobe, using the same instrument set-up as that used for zircon oxygen isotope analyses. External precision varies between 0.2 ‰ and 0.4 ‰ from session to session.

Chapter 2

Evidence for distinct stages of magma history recorded by the compositions of accessory apatite and zircon[†]

Abstract

Accessory minerals contain a robust and accessible record of magma evolution. However, they may reflect relatively late stage conditions in the history of the host magmas. In the normally zoned Criffell granitic pluton (Scotland), whole-rock (WR) compositions reflect open system assimilation and fractional crystallisation at depths of > 11 km, whereas amphibole barometry and the absence of inherited zircon suggest that the observed mineral assemblages crystallised following emplacement of magmas with little or no crystal cargo at depths of 4 to 6 km. The crystallisation history is documented by large trace element variations amongst apatite crystals from within individual samples: decreasing LREE and Th concentrations in apatite crystals from metaluminous samples reflect broadly synchronous crystallisation of allanite, whereas lower LREE and Th, and more negative Nd anomalies in apatites from peraluminous samples reflect the effects of monazite crystallisation. WR evolution is likely to have occurred within a deep crustal hot zone where H_2O-rich (~ 6wt %), low viscosity magmas segregated and ascended adiabatically in a super-liquidus state, leading to resorption of most entrained crystals. Stalling, emplacement and crystallisation resulted from intersection with the H_2O-saturated liquidus at ~ 4 km. H_2O contents are as important as temperature in the development of super-liquidus magmas during ascent, blurring distinctions between apparently 'hot' and 'cold' granites. The trace element contents of most accessory minerals are controlled by competitive crystallisation of other accessory minerals in small melt batches, consistent with the incremental assembly of large granitic plutons.

[†] Co-authors: Colin Graham – *University of Edinburgh*; Chris Hawkesworth – *University of St Andrews*; Martin Gillespie – *British Geological Survey*; Richard Hinton – *University of Edinburgh*; EIMF

1. Introduction

The bulk compositions and differentiation of silicic magmas may be governed by a range of factors, including source rock composition, magma mixing, assimilation of country rocks, fractional melting, fractional crystallisation, water activity and the pressure and temperature pathways of magma evolution (e.g. Bowen, 1928; DePaolo, 1981; Stephens et al. 1985; Gardner et al. 1995; Kemp et al. 2007). However, in order to account for the volumes of silcic rocks and absecne of significant mafic cumulates in the upper crust, it has been proposed that these differentiation processes operate mainly at lower crustal depths (Debari and Coleman, 1989; Kay and Kay, 1993; Müntener et al. 2001; Jull and Keleman, 2001; Coleman et al. 2004; Annen et al. 2006a; Appleby et al. 2008; Kemp et al. 2006b; Ulmer, 2007). This has since been supported by numerical simulations of heat transfer (Annen and Sparks, 2002) and high-temperature experiments (Müntener et al. 2001; Prauteau and Scaillet, 2003) that demonstrate that silica-rich magmas can be generated by incomplete crystallisation of hydrous basalts at lower crustal depths. Furthermore, the liquid-lines-of-descent represented by the whole-rock (WR) compositions of some batholiths can only be simulated by phase equilibria models at lower crustal depths where plagioclase crystallisation is delayed because of elevated pressures (Ulmer, 2007). Differentiation and the determination of bulk magma compositions is thought to occur within hot zones composed of nested sill complexes or small magma chambers (Annen and Sparks, 2002; Annen et al. 2006a; Annen et al. 2006b). By contrast, the mineral assemblages in many volcanic rocks (e.g. Bacon 1983; Bacon and Druitt, 1988; Druitt and Bacon, 1989; Harford et al. 2002; Blundy and Cashman, 2005) have been shown to crystallise in the shallow crust. Experimental data have shown that the observed phase proportions and their compositions in calc-alkaline magmas are best simulated with near-closed system, polybaric crystallisation of initially fully molten magmas and H_2O-saturated conditions without necessarily requiring significant decreases in magma temperatures (Blatter and Carmichael, 1998; Martel et al. 1999; Couch et al. 2003; Rutherford and Devine, 2003; Costa et al 2004; Blundy and Cashman, 2005). In many cases, crystallisation is therefore mainly a consequence of decompression rather than decreases in temperature and has been

successfully demonstrated by mineral thermometry (e.g. Colima andesite, Moore and Carmichael, 1998), plagioclase compositions (e.g. Soufriere Hills andesite, Higgins and Roberge, 2003; Couch et al, 2003; Rutherford and Devine, 2003) and phenocryst-hosted melt inclusion compositions (e.g. Mount St. Helens, Blundy and Cashman, 2005).

It is therefore likely that WR compositions reflect magmatic processes at depth, while the elemental compositions of most observed mineral phases, including accessory minerals, are mainly determined by the re-distribution of elements between crystallising phases after the emplacement of magma batches at shallower depths.

Accessory minerals such as zircon have been shown to provide a robust record of the evolution of the magmas from which they crystallised, yielding valuable insights into the processes associated with silicic magma genesis and crustal evolution (e.g. Kemp et al. 2006b; Eiler, 2007; Kemp et al. 2007; Appleby et al. 2008; Claiborne et al. 2010; Hawkesworth et al. 2010; Bradley, 2011; Roberts, 2012). Apatite has also been shown to document prolonged compositional changes in silicic magmas (Nash, 1984; Shnukov et al. 1989; Sha and Chappell, 1999; Hoskin et al. 2000; Belousova et al. 2001; Belousova et al. 2002; Chu, et al. 2009). However, the relationship between the trace element compositions recorded in accessory minerals at the crystal scale and those of the WR on a pluton-wide scale is uncertain. Here we examine the processes that control trace element compositions at the WR scale and accessory mineral scale in the normally zoned Criffell pluton, in southern Scotland. We show that in this pluton, accessory mineral crystals and WR trace element compositions appear to record largely different stages of magma history. Based on the observed mineral assemblages, geothermobarometry is used to estimate the temperatures and depths of crystallisation and to examine possible ascent paths and varying physical states of magmas in the Criffell pluton.

2. The Criffell Pluton

The ~20 by ~10 km Criffell pluton was emplaced at ~397 Ma (Halliday, et al. 1980) into low-grade wackes and pelites of Llandovery to Wenlock age (433 to 423 Ma), forming part of the Southern Uplands accretionary prism in southern Scotland (Fig. 2.1). Criffell belongs to the Trans-Suture Suite (TSS; Brown et al. 2008), which encompasses several plutons on either side of the Iapetus Suture Zone. The plutons were emplaced after final closure of the Iapetus Ocean (Soper and Woodcock, 2003), so despite displaying a calc-alkaline character their genesis cannot be linked directly to subduction. Instead, independent tectonic evidence suggests that pluton emplacement took place during a phase of extension or transtension, possibly in response to oblique convergence between Avalonia and Laurentia (Brown et al. 2008). Further north in Scotland, others have proposed slab break-off following lithospheric thickening as an alternative cause of tectonic subsidence and extension (Atherton and Ghani, 2002; Oliver et al. 2008; Neilson et al. 2009).

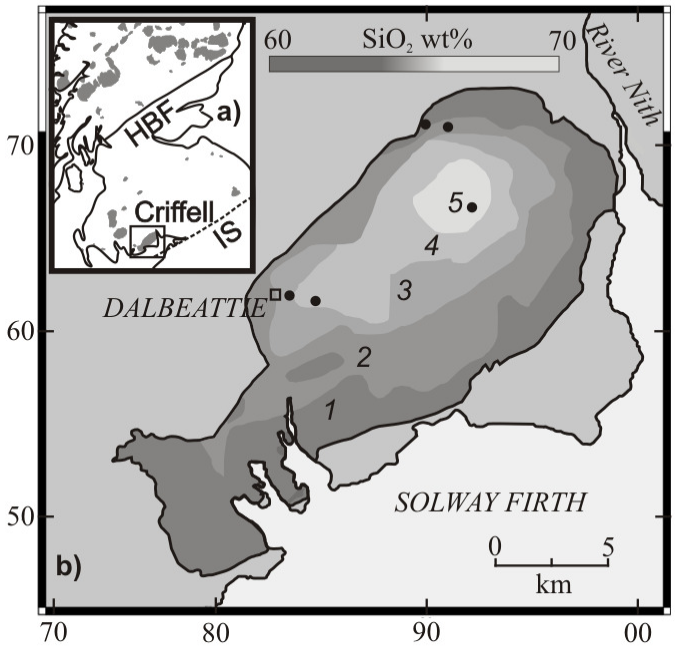

Fig. 2.1 Map of the Criffell pluton. Paler shading reflects increasing WR SiO_2. Zone mineralogy is as follows: 1) clinopyroxene-biotite-hornblende granodiorite; 2) biotite-hornblende granodiorite; 3) biotite granite; 4) biotite-muscovite granite 5) muscovite-biotite granite. Minerals listed in order of increasing modal abundance (Stephens et al. 1985). Black points denote sample sites. Inset: Regional map of major Scottish plutons. Abbreviations are as follows: HBF – Highland Boundary Fault, IS – Iapetus Suture.

Criffell is a normally zoned pluton, with five broadly concentric zones recognised on the basis of changing mineralogical and geochemical character (Stephens, et al. 1985). The three outermost zones (zones 1, 2 and 3) are granodiorite, containing primary hornblende (with occasional cores of clinopyroxene), biotite, plagioclase, potassium feldspar, quartz and accessory allanite, sphene, zircon, apatite and opaque minerals (Fig. 2.2). Accessory minerals occur mainly as inclusions in all major phases, with apatite also found as inclusions in zircon. The zones become progressively more silicic towards the centre of the intrusion (Stephens and Halliday, 1980), and the two innermost zones (zones 4 and 5) are granite containing primary muscovite and monazite but lacking hornblende, sphene and the abundant zircon and magnetite that characterise the granodiorite. WR SiO_2 ranges from ~58 wt% in Zone 1 to ~72 wt% in Zone 5. Zones 1 and 2 are metaluminous while zones 3, 4 and 5 are mildly peraluminous. The transition from outer to inner zones is also associated with increasing initial $^{87}Sr/^{86}Sr$ (0.7052 to 0.7073), $\delta^{18}O$ (8.5 to 11.9 ‰) and decreasing εNd (-0.6 to -3.1) compositions (Halliday, 1984; Halliday et al. 1980; Stephens et al. 1985). Geochemical modelling of these isotope ratios (Stephens et al. 1985) indicates that such trends may reflect the effects of assimilation of local Southern Uplands sediments and the fractional crystallisation of a crystal assemblage similar to that of mafic enclaves found within the granodiorite. However, $^{207}Pb/^{204}Pb$ isotopes have since shown that the local Southern Uplands sediments into which the pluton is emplaced are unlikely to have contributed to the crustal signature of the Criffell pluton (Fig. 2.3) (Thirlwall, 1989). Similarities in the $^{207}Pb/^{204}Pb$ compositions of Lake District plutons and those situated north of the Iapetus suture, including Criffell, have been used to suggest they share a common source, the composition of which compares closely with the $^{207}Pb/^{204}Pb$ composition of the Skiddaw Group sediments found in the English Lake District to the south (Fig. 2.3) (Thirlwall, 1989). These conclusions are consistent with seismic evidence for underthrusting of Avalonia beneath the Laurentian margin during the Caledonian Orogeny, potentially as far north as the Midland Valley (Hall, 1984; Beamish and Smythe, 1986; Klemperer and Matthews, 1987; Freeman et al. 1988; Klemperer et al. 1991).

The origins of the configuration of mineralogical and geochemical zones in Criffell remain uncertain. In the outer granodiorites, the alignment of plagioclase, amphibole and biotite crystals gives these rocks a prominent foliation. At a mineral scale, this foliation has been shown to accompany protoclastic textures where small quartz crystals have a mortar texture about larger, kinked plagioclase crystals (Stephens, 1999). Furthermore, the kinking of biotite crystals provides further evidence that strain occurred in the solid state and was not magmatic in origin (Stephens, 1999). Corrioux (1987) suggested that the formation of a foliation in the outer zone of the pluton resulted from the later intrusion of the inner zones, providing evidence for at least two stages of emplacement. WR isotopic variations and discontinuous compositional zones (Stephens et al. 1985; Stephens, 1992) provide further evidence for multiple sources and emplacement episodes. Mafic enclaves are a conspicuous feature of zones 1, 2 and 3; they are isotopically distinct from their host rocks, indicating that they are not the product of crystal settling but instead represent different magmas whose relationship to the WR compositions of the granitic rocks remains unclear (Holden et al. 1987; Holden, 1991).

Apatite is the dominant accessory mineral in all five zones of the Criffell pluton. It forms as euhedral, prismatic crystals between 30 μm and >1 mm in length and occurs mainly as inclusions in other minerals, including zircon. Sphene occurs only in zones 1 and 2 as large (up to 2mm) euhedral crystals making up nearly 2 modal % of the WR (Fig. 2.2). Euhedral morphology and the scarcity of impingement textures and mineral inclusions indicate that it was an early crystallising phase (Stephens et al. 1985). Allanite and monazite were not observed in thin section, but are present in very small quantities in mineral separates from metaluminous (Zones 1 and 2) and peraluminous (Zone 5) samples respectively. Zircon in zones 1 to 4 is seen to occur mainly as solitary, euhedral inclusions up to 200 μm long in all major mineral phases and may also occur as a free crystal phase. Only a very small number of heavily cracked zircon crystals were found in Zone 5. Importantly, the Criffell pluton along with other TSS plutons in Southern Scotland and Northern England lack inherited zircon. This was shown by an extensive investigation of zircon U-Pb ages, including 17 analyses from four of the TSS (Pidgeon and Aftallion, 1978). These findings have

since been confirmed by U-Pb dating using Secondary Ionisation Mass Spectrometry (SIMS) on > 100 zircon crystals from the Criffell, Fleet and Shap plutons (Miles et al., in review). SEM imaging also shows no evidence of internal resorption (Fig. 2.2c and 2.2d), suggesting that most zircons are not xenocrystic. In this respect, the Criffell pluton (along with other TSS plutons) differs from the numerous Caledonian granite plutons that crop out to the north of the Highland Boundary Fault in Scotland, reflecting either substantial differences in source regions or mineral resorption prior to emplacement (or both).

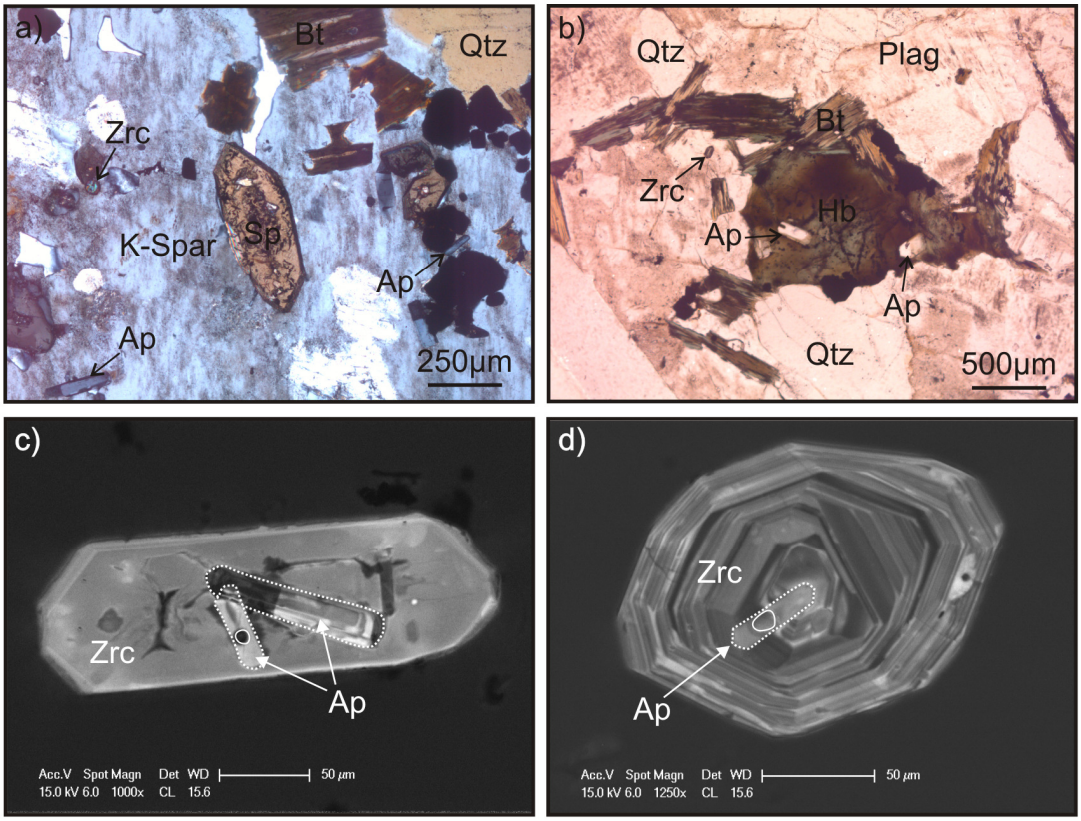

Fig. 2.2 a) Petrographic relations between phases in the outer zones of the Criffell pluton. b) Petrographic relations in Zone 4. Images *a* and *b* show the euhedral nature of apatite inclusions in different host phases. c) Cathodoluminescence (CL) image of a zoned zircon with apatite inclusion from Zone 1. d) CL image of a zoned zircon crystal with apatite inclusion from Zone 3. Abbreviations: Ap – apatite, Bt – biotite, Hb – hornblende, K-Spar – potassium feldspar, Plag – plagioclase feldspar, Qtz – quartz, Sp – sphene, Zrc – zircon.

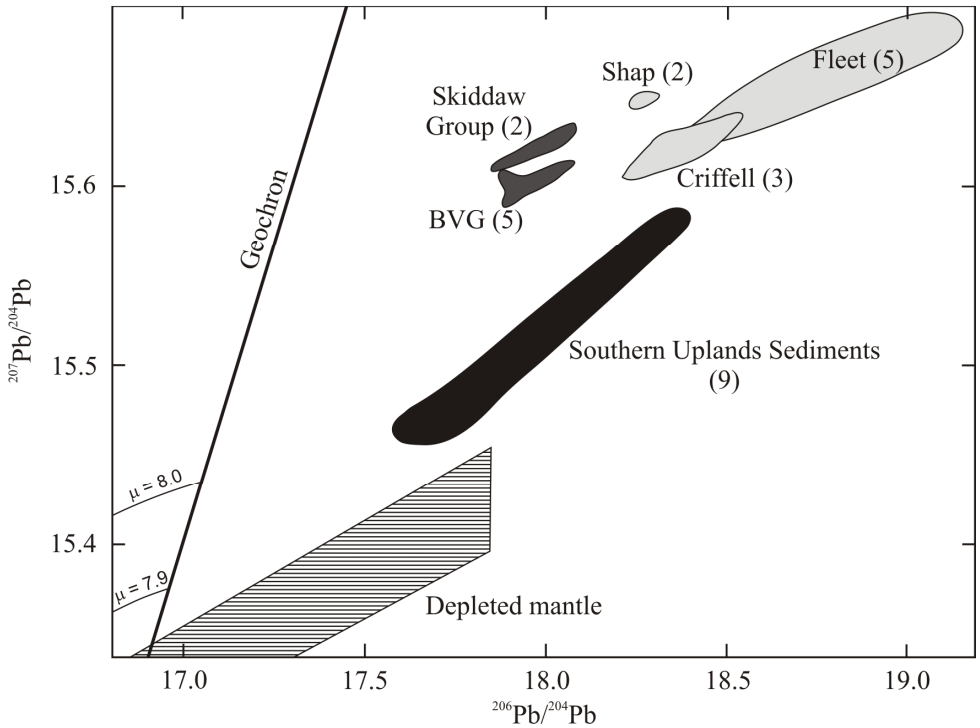

Fig. 2.3 Pb-Pb diagram modified from Thirlwall (1989) showing the Pb isotope compositions of the TSS plutons, Skiddaw Group sediments (Thomas 1985; Stone and Evans 1997), Southern Uplands sediments (Stone and Evans 1995), Borrowdale Volcanic Group (BVG) (Thirlwall, 1986) and depleted mantle (Zindler and Hart, 1986). All plutons extend to more radiogenic $^{207}Pb/^{204}Pb$ compositions than the Southern Uplands sediments into which they are intruded. Numbers in brackets refer to the number of available analyses.

3. Methodology

Samples were collected from each zone of the Criffell pluton. WR major and trace element concentrations were determined using a PANalytical PW2404 wavelength-dispersive sequential X-ray fluorescence spectrometer at the University of Edinburgh.

Apatite compositions were determined primarily by a Cameca SX-100 electron probe supported for comparative purposes by ion microprobe analyses using a Cameca ims 4f at the University of Edinburgh Ion Microprobe Facility (EIMF). Good agreement was observed between the two methods. Zircon-hosted apatite was analysed in zircons mounted in epoxy blocks following standard zircon separation techniques (see Appleby et al. 2008). Back-scattered electron (BSE) and cathodoluminescence (CL) images were taken on polished surfaces using a Philips XL30P Scanning Electron Microscope (SEM) at the University of Edinburgh. Apatite hosted by other phases was analysed directly in polished thin sections.

A wavelength dispersive method (WDS) was used for electron probe analysis of apatite using PC0, LTAP, LPET and LIF dispersion crystals. Beam conditions were 20 kV and 60 nA for trace and most major elements, with a 10 nA defocused beam used to minimise loss of alkalis during analysis.

Apatite inclusions were analysed using the Cameca ims4f ion microprobe, with a 5 nA $^{16}O^-$ primary ion beam with 15 keV net impact energy and a spot size of approximately 15 µm. Only high energy secondary ions (100-140 eV) were measured in order to reduce molecular ion overlap. F/Ca ion yields were determined using Durango and Wilberforce apatite standards. The very small size of some apatite inclusions in zircon resulted in the need to test for beam overlap with zircon. The very low concentration of Zr in apatite relative to zircon means the magnitude of any overlap can be estimated by taking the ratio of an average zircon Zr concentration (~420,000 ppm) and that of the apatite analysed. Grains that showed evidence for overlap were discounted. Data obtained by both analytical methods (ion probe and electron probe) are similar.

Amphiboles in Zone 1 were analysed in polished thin sections using a wavelength dispersive method (WDS) using a Cameca SX-100 electron probe using LTAP, TAP and PET dispersion crystals. Beam conditions were 25 kV and 10 nA for Na, Mg, Al, Si, K, Ca and Fe, and 15 kV and 100 nA for Ti and Mn.

4. Result

4.1 Whole-rock compositions

WR data are from Stephens and Halliday (1980), Stephens et al. (1985) and this study (Fig. 2.4; Appendix D). The transition from zones 1 to 5 is associated with decreasing MgO, MnO, Sr, La, Ce, Y, Zr, Ni (Fig. 2.4) together with TiO_2, Al_2O_3, Fe_2O_3, CaO, P_2O_5, Nb, Y, Cr, V, Ba, Sc and Nd, and increasing SiO_2, K_2O, Rb, U and Pb (Appendix D).

WR REE profiles (Stephens et al. 1985) are smooth across all zones with little or no Eu anomaly evident in any zone. WR Ce decreases from 104 ppm to 22 ppm while Y decreases from 26 ppm to 3 ppm with increasing SiO_2 across the entire WR suite (Figs. 2.4 and 2.5). LREE/HREE ratios increase with increasing SiO_2 in metaluminous zones, and Ce/Yb ratios increase from 62 to 98. However, in peraluminous zones, Ce/Yb ratios decrease from 97 to 53 with increasing SiO_2. The Ce-Y array in the WR is steeper than in apatite crystals (Fig. 2.5), implying different controls on their Ce and Y contents. The progressive decrease in the total abundance of REE with increasing SiO_2 has been attributed to the removal of small amounts of accessory minerals by fractional crystallisation (Stephens et al. 1985). In our preferred model the Ce-Y array for the WR samples is attributed to fractional crystallisation of an assemblage of plagioclase (40%), amphibole (35%), biotite (20%), sphene (2.5%), apatite (2%) and zircon (0.5%) together with assimilation of Skiddaw Group sediments assuming an assimilation to mass crystallised ratio of 0.3 (Fig. 2.5).

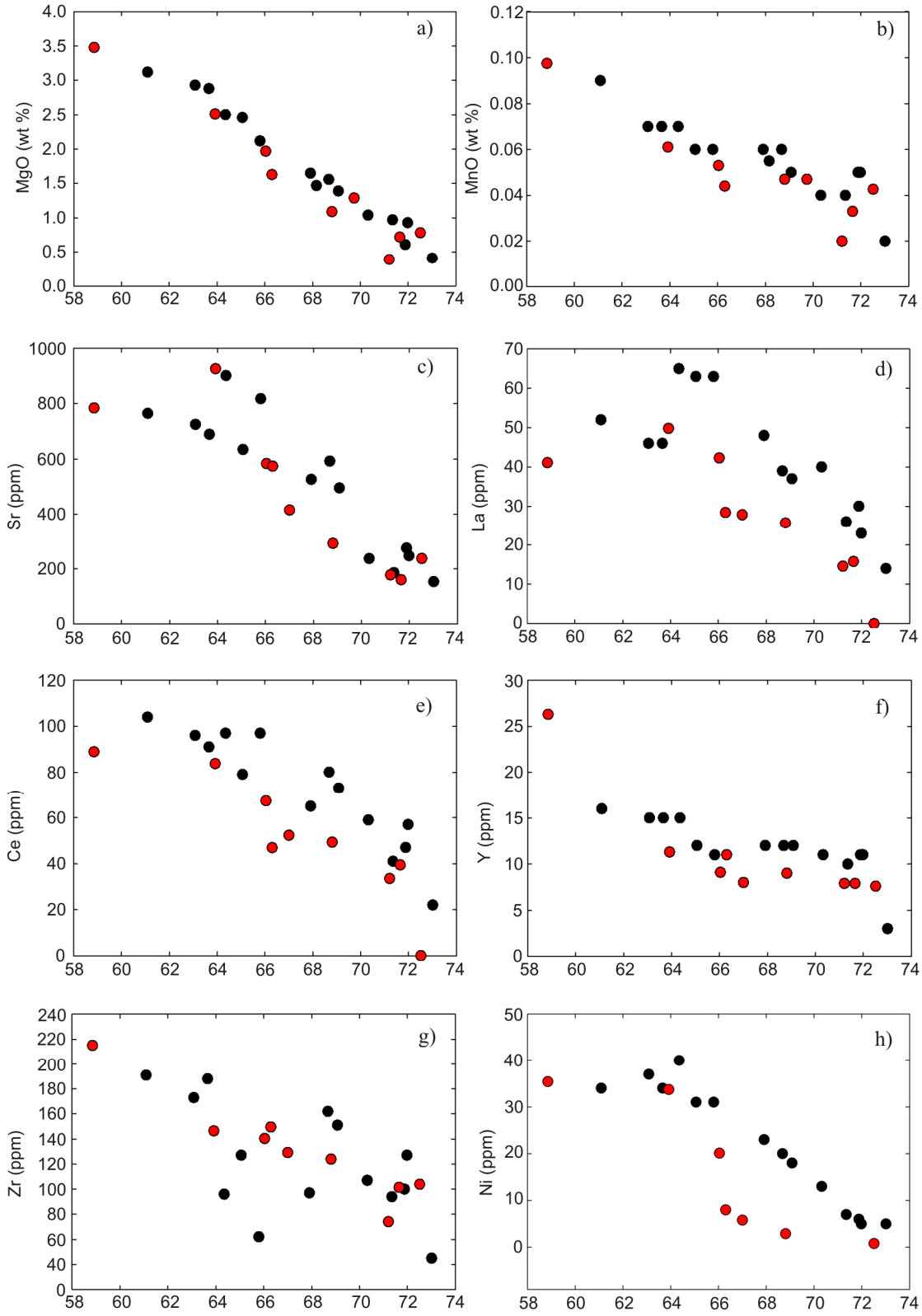

Fig. 2.4 Harker plots showing a selection of major and trace elements vs. SiO_2 for whole-rock samples from the Criffell pluton. Major element data are presented as oxide wt %; trace elements are presented as ppm. Dark data points are from this study; red data point are from Stephens and Halliday (1980).

4.2 Apatite trace element compositions

Average chondrite-normalised apatite REE profiles (Fig. 2.6; Appendix E) and Ce vs Y plots (Fig. 2.7) for apatite show that crystals from different parts of the pluton yield different Ce-Y trends. Apatites from metaluminous zones (1 and 2) display linearly correlated Y and Ce compositions (Ce: 521 - 3979 ppm; Y <662 ppm) and lack significant Eu anomalies (trend 1) (Fig. 2.6).

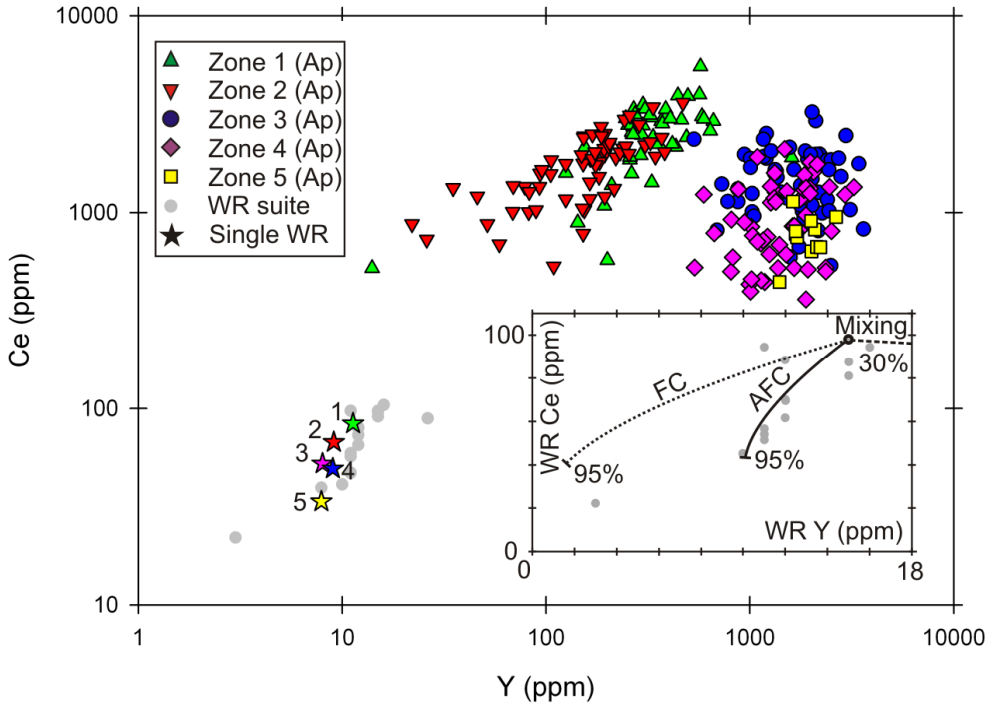

Fig. 2.5 Ce-Y data for the WR suite and apatite crystals from single samples (see figure key). The WR compositions of samples used for apatite analyses are plotted using stars labeled with their zone number. Substantial variability is seen in the compositions of apatite crystals from single samples, similar in percentage terms to that of the entire WR suite. Inset figure shows WR data and three petrological models: assimilation and fractional crystallisation (AFC), fractional crystallisation (FC) and simple mass balance mixing. In all models, granodiorite sample 244 from Stephens et al. (1985) has been used as a starting composition (Ce = 98 ppm, Y = 13 ppm). For AFC modeling, Skiddaw Group sedimentary rocks have been used as a crustal contaminant (Ce = 35 ppm, Y = 86 ppm, from Cooper et al. 1988) and assimilation to fractional crystallisation ratio of 0.3 assumed based on a similar study by Stephens et al. (1985). A crystal assemblage similar to that of mafic enclaves found in granodiorites has been used with modal proportions of: plagioclase = 40%, amphibole = 35%, biotite = 20%, sphene = 2.5%, apatite = 2% and zircon = 0.5%). Partition coefficients have been taken or estimated from Fujimaki et al. (1984), Ewart and Griffin (1994), Sisson (1994), Schnetzler and Philpott (1970), Tiepolo et al. (2002), Sano et al. (2002), Thomas et al. (2002), Fujimaki et al. (1986) and Prowatke and Klemme (2006). Mass balance has been used to model simple mixing between granodiorite sample 244 and Skiddaw Group sedimentary rock. AFC models provide the closest match with WR analyses.

By contrast, apatites from peraluminous zones (4 and 5) are relatively depleted in LREE (Ce mostly < 2000 ppm), show larger absolute variations in Y and HREE (Y: 383 - 3054 ppm) (trend 2, Fig. 2.7) and have prominent negative Eu anomalies (Fig. 2.6). In Zone 3, a small number of mainly apatite crystals fall on trend 1 and have weak Eu anomalies; they are therefore compositionally similar to apatite crystals in zones 1 and 2. The majority of apatites in Zone 3 fall on trend 2 and are therefore similar to those in zones 4 and 5 (Fig. 2.7).

In order to compare WR and apatite trace element and REE trends, the Ce and Yb contents of the magmas from which apatites crystallised have been calculated using apatite-melt partition coefficients from Fujimaki et al. (1986) (Fig. 2.8). Yb has been used in place of Y due to the availability of published Yb partition coefficient data. Like Y in apatite, the Yb concentrations of the melts from which apatites crystallised in individual metaluminous samples are limited in absolute terms relative to Ce (Ce: 90 to 20 ppm; Yb: < 7 ppm) and occupy a similar region of compositional space to that of the WR suite (Fig. 2.8). In peraluminous zones, calculated Ce-Yb concentrations in the melts in equilibrium with the apatites follow similar trends to those of Ce-Y in apatite (Ce <70 ppm; Yb: 9 to 2 ppm) and contrast markedly with the trend followed by the WR suite (Fig. 2.8). Yb concentrations in apatite were determined by ion microprobe.

Th and U in apatite decrease from Zone 1 (260-20 and 150-30 ppm, respectively) to Zone 5 (< 10 ppm and < 20 ppm, respectively) (Fig. 2.9; Appendix E). In general, the Th and U contents of zircon-hosted apatites are higher than for apatite hosted by other phases in each zone (Appendix E). However, beam overlap with enclosing zircon may have affected some analyses, and only data from apatite crystals hosted by Th- and U-poor minerals (all hosts except for zircon) are plotted in figure 9 and used to infer general trends. Th/U ratios decrease in tandem with Ce in metaluminous zones, but there is little evidence of any correlation in peraluminous zones. Only in intermediate zones (Zones 2 and 3) is there evidence that Th/U ratios correlate with Y (Fig. 2.9).

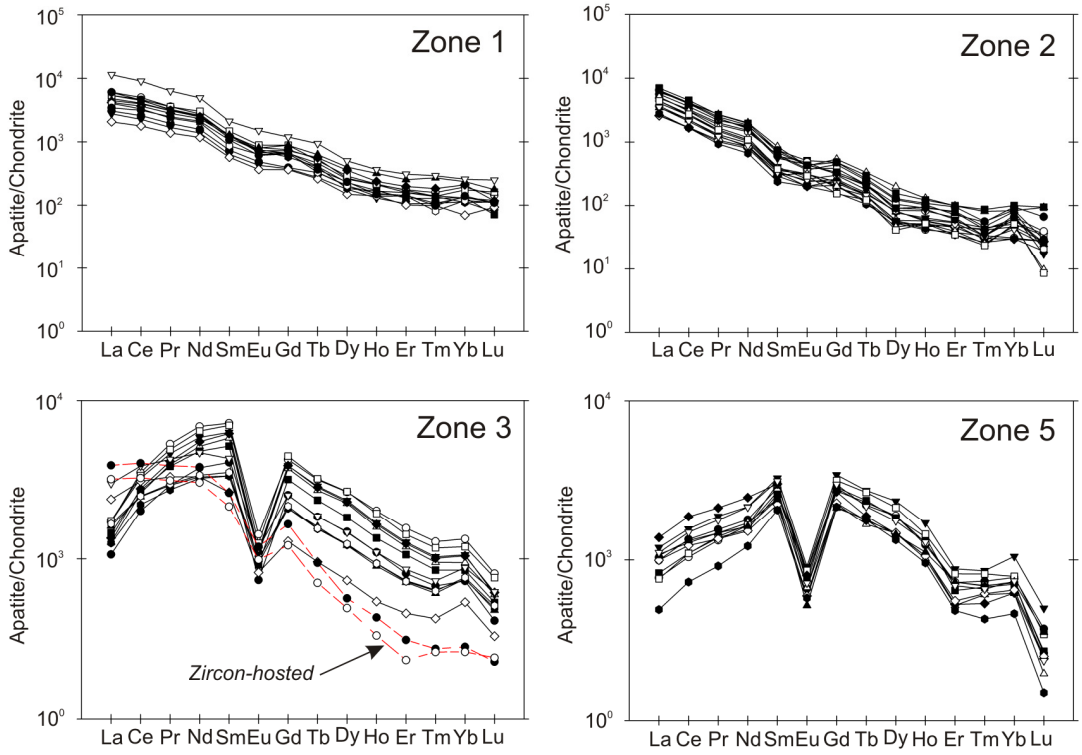

Fig. 2.6 Chondrite-normalised REE patterns for apatites in different zones of the Criffell pluton. Apatite hosted by zircon in Zone 3 is distinguished (red, dashed lines) from that hosted by other phases and shares more characteristics with those in zones 1 and 2. Apatite hosted by other phases in Zone 3 is similar to that in Zone 5.

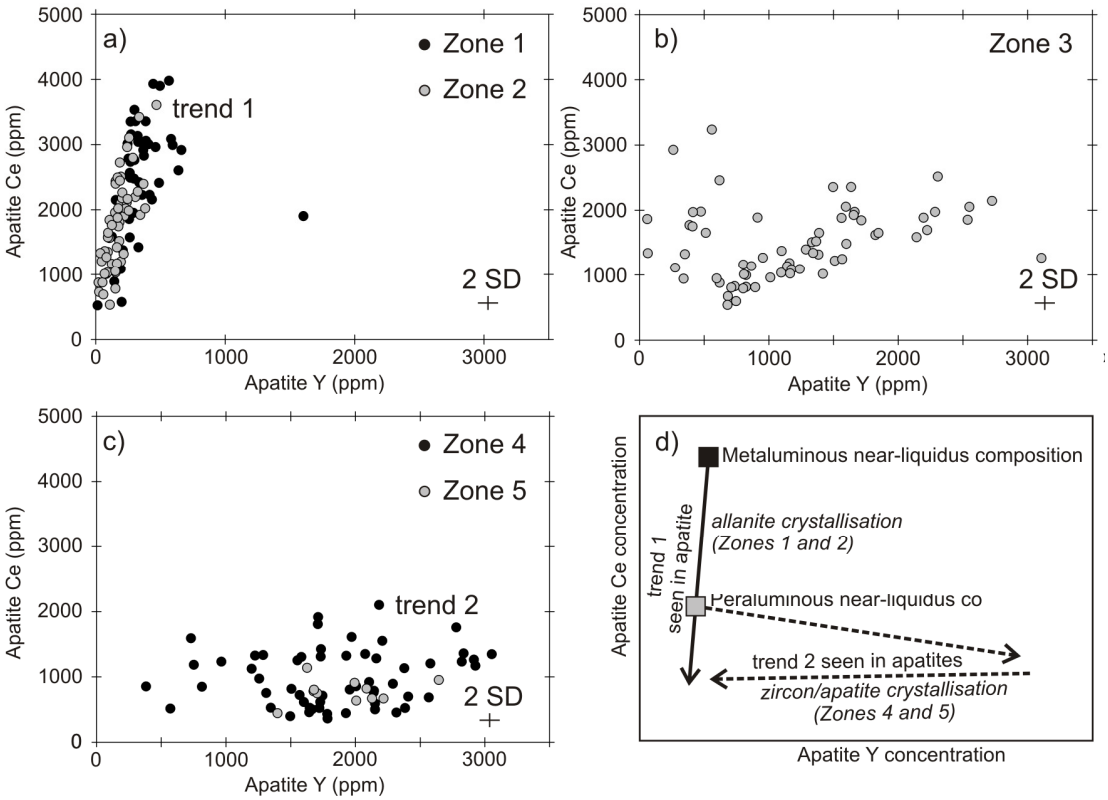

Fig. 2.7 Ce (ppm) vs. Y (ppm) in apatites from zones 1 to 5 of the Criffell pluton. Apatite from zones 1 and 2 (a) define near vertical trends characterised by Ce depletion. Apatite from zones 4 and 5 (c) define a near-horizontal trend of Y depletion and consistently low Ce. The compositions of a small number of apatite crystals from Zone 3 (b) resemble those of apatite crystals from metaluminous zones 1 and 2. The majority of apatite in Zone 3 resemble those in zones 4 and 5, but shows a more pronounced trend of Ce depletion. 2 SD analytical error bars are shown for EPMA analyses. Ion probe analyses are subject to smaller errors (~ 10%). (d) is a schematic illustration of compositional trends in metaluminous and peraluminous samples. The former is controlled primarily by allanite extraction, the latter is inferred to reflect initial LREE depletion and HREE enrichment caused by early monazite crystallisation. Later-crystallised apatite follows a trend of HREE depletion.

5. Discussion

Crustal hot zone models propose that magma compositions are initially determined by open system processes occurring in the deep crust and upper mantle, and that crystallisation and textural evolution occur later in shallow crustal reservoirs (Annen and Sparks, 2002; Annen et al. 2006a; Annen et al. 2006b). The trace element compositions of the earliest accessory minerals to crystallise are therefore likely to reflect those of the bulk magma. However, if accessory minerals crystallise largely in shallow reservoirs, the evolution and subsequent distribution of elements between accessory minerals may be determined by processes that are independent of those that determined the bulk magma composition. Here we examine the extent to which accessory mineral and WR compositions document different stages of magma history.

5.1 Bulk magma variations at depth: whole-rock chemistry

Despite evidence for crustal involvement in the generation of the Criffell magmas (Halliday et al. 1980; Harmon and Halliday, 1980; Halliday, 1984; Stephens and Halliday, 1984; Harmon et al. 1984; Stephens, 1988; Stone and Evans, 1997; Highton, 1999), subsequent $^{207}Pb/^{204}Pb$ data (Thirlwall, 1989) have shown that the substantial thickness of Southern Uplands sediments (~11 km; Stephens, 1999) into which the pluton is emplaced cannot have contributed significantly to the crustal signature of these magmas (Fig. 2.3). Instead, their $^{207}Pb/^{204}Pb$ compositions are more similar to those of the Skiddaw Group sedimentary rocks which crop out south of the Iapetus Suture on Avalonian crust (Thirlwall, 1989). Seismic imaging indicates that this Avalonian crust can be traced beneath the southern margin of Laurentia and is present at depths of > 11km beneath the Criffell pluton due to tectonic underthrusting that occurred during final closure of the Iapetus Ocean (Hall, 1984; Beamish and Smythe, 1986; Klemperer and Matthews, 1987; Freeman et al. 1988; Klemperer et al. 1991). The open system magmatic processes responsible for generating the range of WR compositions therefore appear to have originated at depths of 11 km or more. It follows that petrological models assuming the local

Southern Upland sedimentary rocks are a major crustal contaminant in the Criffell magmas (Stephens et al. 1985) should be re-evaluated.

Petrological modelling of the WR evolution requires knowledge of the crystallising mineral assemblage at depth, in addition to constraints on the composition of potential assimilants. Redox conditions in the amphibole-bearing granodiorites have been shown to lie close to the hematite-magnetite buffer (Stephens et al. 1985) and contain the buffering assemblage necessary for using Al-in-hornblende barometers (Johnson and Rutherford, 1989). The crystallisation of most granitic systems is typically eutectic and most of the buffering assemblage required for hornblende barometry is likely to have crystallised largely simultaneously with amphibole. The results of the Johnson and Rutherford Al-in-hornblende barometer when applied to Zone 1 (Appendix K) reveal that the present mineral assemblage formed at 4 – 6 km (0.8 – 1.5 kbars) depth, within the Southern Uplands accretionary prism. Anderson and Smith (1995) suggest that temperature should also be considered when calculating crystallisation depths using Al-in-hornblende barometers. Crystallisation temperatures have been calculated using the amphibole-plagioclase geothermometer of Blundy and Holland (1990) (albite components are estimated at ~ 75% using optical methods), revealing crystallisation temperatures between 674^{o}C and 692^{o}C. Using temperature as a further variable and applying the barometer of Anderson and Smith (1995) suggest crystallisation pressures of 2 to 2.4 kbar which equates to ~7 – 9 km depth. Both barometers therefore indicate that the granodiorite mineral assemblage is unlikely to represent the mineral assemblage that was present at the time when most WR compositions were determined at depths > 11 km. Despite strong evidence for significant crustal contamination at depth, the absence of inherited zircons in the Criffell magmas (Pidgeon and Aftalion, 1978) indicates that the current assemblage of accessory phases may also have formed during later stage crystallisation at shallow depths. Their modal proportions and compositions cannot therefore be used to model the evolution of WR compositions at depth.

By contrast, magmatic mafic enclaves that show isotopic disequilibrium with their host granodiorites (Holden et al. 1987; Holden, 1991) in the outer zones of the pluton

have been suggested to represent cognate material that may ultimately have been entrained by ascending magmas, providing potential insights into the process of magma differentiation at depth. Following the approach of Stephens et al. (1985), new AFC, mixing and fractional crystallisation models have been calculated using a mineral assemblage similar to that of the mafic enclaves (40% plagioclase, 35% amphibole, 20% biotite, 2.5% sphene, 2% apatite and 0.5% zircon) and Skiddaw Group sedimentary rocks as a crustal contaminant (Ce = 35 ppm, Y = 86 ppm; Cooper et al. 1988). Granodiorite sample 244 (Stephens et al. 1985) has been used as a starting composition (Ce = 98 ppm, Y = 13 ppm). Despite uncertainties regarding the origin of the mafic enclaves, AFC processes involving an assemblage identical or similar to that of the mafic enclaves coupled with assimilation of Skiddaw Group (or similar) materials with an assimilation to fractional crystallisation ratio of 0.3 provides the best fit to the trend of decreasing Ce and Y exhibited by the WR suite (Fig. 2.5). Further uncertainties may result from inferences and estimates of some partition coefficients due to an absence of published data.

5.2 Late-stage crystallisation history at shallow levels: apatite mineral compositions

While WR compositions appear to reflect open system differentiation at depth, it is unclear whether or not shallow level crystallisation processes involved further changes to the WR compositions. The trace element compositions of apatite have previously been shown to archive the petrogenetic history of granitic magmas (Nash, 1984; Shnukov et al. 1989; Sha and Chappell, 1999; Hoskin et al. 2000; Belousova et al. 2001; 2002; Chu et al. 2009). If, like zircon and hornblende, apatite formed during crystallisation at shallower levels and saturated from the bulk magma, then apatite compositions provide a way of determining the crystallisation history of the Criffell magmas that may not always be recorded by WR compositions. Ce-Y trends reveal that apatites from single samples would appear to have crystallised from melts with up to two orders of magnitude variability in Ce and Y contents (Fig. 2.5). Here we examine the processes by which such compositional diversity is attained and the extent to which apatite retains evidence of magma processes that are distinct from – and independent of - those recorded by WR compositions.

5.3 Apatite saturation

Apatite crystals occur almost exclusively as inclusions in different host minerals and it is possible that they crystallised at the crystal-melt interface during phenocryst growth under locally saturated conditions or in late-stage interstitial melt pools (Bacon, 1989; Hoskin et al. 2000). Local saturation of apatite may prevent crystals from documenting compositions that reflect the bulk magma. This is because local concentration gradients may occur adjacent to growing phenocrysts while the highly evolved compositions of late-stage interstitial melts may bear little resemblance to bulk magma composition. Furthermore, interstitial melts may crystallise under lower temperatures, thereby changing the way some trace elements partition into accessory phases (Hoskin et al. 2000). It is therefore important to determine if apatite became saturated in, and crystallised from, the bulk magma or from local pockets of magma that were isolated from the bulk magma or adjacent to growing phenocrysts. Crystal morphology alone is not enough to distinguish crystals formed in these two settings (Bacon, 1989). In isolated interstitial melt pockets, melt compositions are likely to be more variable and a range of accessory minerals would be expected to saturate sequentially. However, in the Criffell pluton the overwhelming majority of apatite inclusions are found in isolation from other accessory minerals, consistent with crystallisation from the bulk magma. Furthermore, the existence of distinctive and continuous trends as opposed to more random distributions of apatite compositions supports the maintenance of chemical connectivity between apatites and the bulk magma rather than growth at phenocryst interfaces. We therefore favour bulk saturation in all zones of the Criffell pluton.

5.4 Causes of compositional diversity in apatites in metaluminous granites

In order to model the range of Ce-Y compositions exhibited by apatites from single metaluminous samples (Fig. 2.5), it is first necessary to investigate how their concentrations vary in response to crystallisation. WR compositions, which are considered to be representative of magma compositions at the time of emplacement, are similar to those from which only the most Ce-rich apatites crystallised in zones 1

and 2 (Fig. 2.8). Crystallisation therefore appears to have induced a trend from high to low Ce concentrations in apatites within these zones, consistent with the common occurrence of decreasing REE concentrations with increasing crystallisation found in other granites that result from the fractionation of REE by accessory minerals (Stephens et al. 1985; Sha and Chappell, 1999; Hoskin et al. 2000; Belousova et al. 2001; Chu et al. 2009).

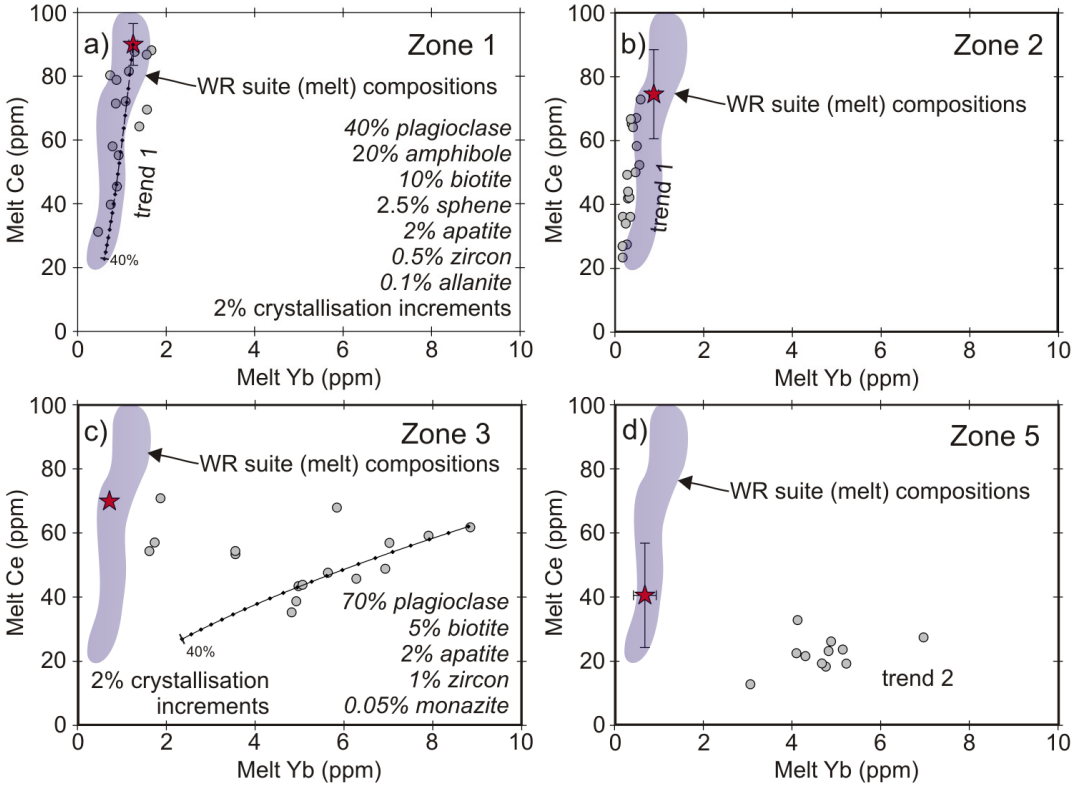

Fig. 2.8 Calculated melt compositions. Ce and Yb melt compositions calculated from apatite compositions (small circles) using published apatite-melt partition coefficients (Fujimaki 1986). Yb data are only available for ion probe analyses. Average whole-rock (WR) compositions for each zone were calculated using data from Stephens and Halliday (1980) and Stephens et al. (1985) with 1SD error bars shown for each population (zone). (a) and (c) also show calculated crystallisation models assuming a starting composition similar to average WR for Zone 1. The minerals used and their modal proportions are listed in the figure. Peraluminous crystallisation models assume a starting composition that post-dates monazite saturation (Yb = 9 ppm, Ce = 50 ppm). Shaded fields show the Ce-Yb compositions of the entire WR suite.

Other studies have shown that REE diversity in apatites may also result from an increase in partition coefficients between apatite and silicate melts with increasing differentiation, SiO_2 and polymerisation (Prowatke and Klemme, 2006). In this model, increased differentiation in the absence of other accessory minerals should lead to an *increase* in the REE content of apatite. However, the observed trend is one of *depletion* in REE with increasing crystallisation (Figs. 2.7 and 2.8). Furthermore,

the change from metaluminous to peraluminous zones is associated with only small variations in SiO_2 (<3 wt %) despite large changes in the REE patterns of apatite crystals. Any effect of increasing SiO_2 on the partitioning of REE in apatites from single samples is therefore considered to be of secondary importance.

Having concluded that the observed trends in apatite compositions may also reflect the crystallisation of other accessory phases, the range of compositions observed within single samples may be modelled in terms of the re-distribution of REE amongst competing accessory phases during crystallisation.

Assuming a starting composition similar to that of the WR, no reasonable combination of petrographically observed minerals is capable of reproducing the observed trend of Ce depletion seen in the calculated melt compositions from which apatites in single metaluminous samples crystallised. For example, assuming modal proportions of 40% plagioclase, 20% amphibole, 2.5% sphene, 2% apatite and 0.5% zircon (using the published partition coefficient data of Fujimaki et al. 1984; Fujimaki, 1986; Sisson, 1994; Tiepolo et al. 2002; Sano et al. 2002), only around half the observed decrease in Ce concentration is predicted after 95% crystallisation.

Another accessory mineral found only in magnetic heavy mineral separates from zones 1 and 2 that is also commonly stabilised in metaluminous magmas is allanite (Montel, 1986). Allanite is highly effective at removing LREE, with mineral-melt partition coefficients as high as ~ 2800 (Mahood and Hildreth, 1983). By contrast, there is a minimal difference in the efficiency of HREE removal by allanite relative to apatite. Allanite crystallisation is also consistent with the overall decrease in the Th content and Th/U ratios of apatite in these zones (positive correlations between Ce and Th in apatites have R^2 values of ~ 0.7 to 0.9) (Fig. 2.9). The latter decrease in Th/U is likely to reflect increased partitioning of Th relative to U in allanite (Hoskin et al. 2000). Crystallisation models indicate that the observed trend in Ce depletion seen in calculated melt compositions can be replicated after ~ 40% crystallisation by the additional crystallisation of only 0.1% allanite (Fig. 2.7) and demonstrates the

ability of allanite to generate cryptic signatures of its presence in the Ce and Y contents of apatite.

Experimental studies suggest that even for relatively modest concentrations of LREE, allanite is easily saturated in silicate rocks at relatively low temperatures (~700^{o}C) (Klimm et al. 2008). Furthermore, Janots et al. (2007) calculated that allanite is stable at temperatures as low as 250^{o}C in pelites with 0.88 wt % CaO and 700 ppm LREE. At higher CaO contents such as those of the Criffell magmas, allanite stability should be even greater. Monazite crystallisation may also effectively reduce the concentration of LREE in granitic magmas, but is seldom saturated in metaluminous magmas (Montel, 1986). Furthermore, the preferential uptake of Nd relative to other REE by monazite commonly results in negative Nd anomalies in other crystallising phases (Sha and Chappell, 1999; Chu et al. 2009). No significant negative WR-normalised Nd anomalies are observed in metaluminous apatites (Fig. 2.6 and 2.10). We therefore consider allanite the more likely LREE-controlling co-existing phase in metaluminous zones.

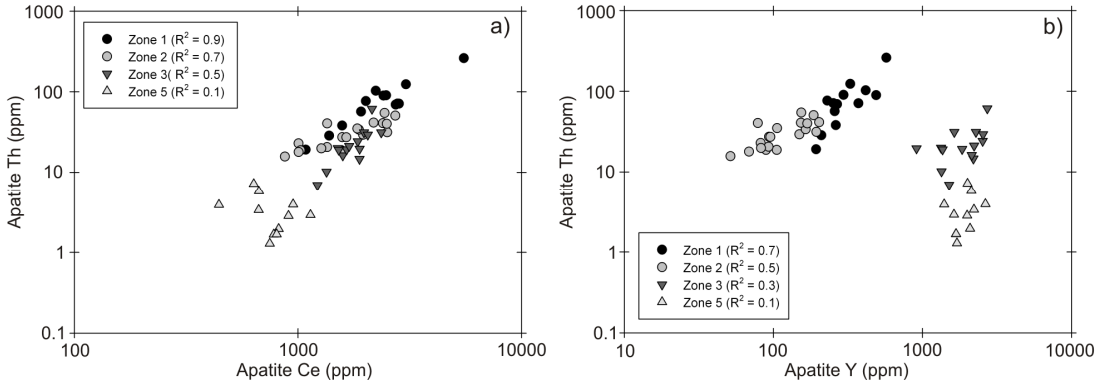

Fig. 2.9 a) Apatite Ce vs. Th (ppm) for all zones of the Criffell pluton. R^2 values are listed in the key and reflect the extent to which Th and Ce correlate. Positive correlations are observed in metaluminous zones only and relate to simultaneous crystallisation of allanite. Low concentrations of Th in peraluminous zones reflect earlier monazite crystallisation, while low R^2 values indicate little further depletion of Th with Ce and monazite crystallisation. b) Apatite Y vs. Th showing similar results to the previous plot. R^2 values for Y-Th correlations for each zone are given in the key.

5.5 Might the WR and accessory mineral compositions have been determined together in the metaluminous magmas?

The suggestion that allanite was part of the crystallisation assemblage at shallow levels encourages us to look again at whether it was also present during the development of the WR compositions.

AFC models that assume a crystallisation assemblage similar to that of mafic enclaves coupled with assimilation of Skiddaw Group sedimentary rocks are capable of generating the observed range of WR compositions without allanite crystallisation (Fig. 2.5). Furthermore, the preference exhibited by allanite for LREE relative to HREE means that if allanite crystallisation was a dominant control on WR differentiation, as is apparently the case during the crystallisation of apatite, more evolved metaluminous WRs (with higher SiO_2) would have *lower* LREE/HREE ratios. LREE/HREE ratios in the metaluminous WR suite *increase* with progressive differentiation and have been interpreted by Stephens et al. (1985) to reflect a dominant amphibole control rather than allanite, but may also reflect zircon crystallisation. It therefore seems likely that independent processes determined both WR and apatite trace element compositions in distinct regions of the magmatic system, consistent with other evidence suggesting that WR Pb isotope compositions (Fig. 2.3) were determined at significantly greater depths than those at which crystallisation of amphibole and zircon occurred in the granodiorites.

5.6 Causes of compositional diversity in apatites in peraluminous granites

Apatite crystals from peraluminous zones (zones 4 and 5) define a second trend of variable Y (and Yb) and low Ce relative to those in metaluminous zones (trend 2, Fig. 2.7) but have indistinguishable textural relations with their host phases. This trend is distinct from that defined by the entire WR suite (Figs. 2.4, 2.5 and 2.8) and indicates that independent magmatic processes have determined the evolutionary trends of WR and crystal compositions in these zones. Apatites in other peraluminous plutons have been shown to define similar compositional trends (Sha

and Chappell, 1999; Hoskin et al. 2000; Belousova et al. 2001; 2002; Chu et al. 2009) reflecting the crystallisation of LREE-rich monazite. Monazite is known to saturate readily in peraluminous, two-mica granites. This is supported here by evidence that WR compositions in Zones 4 and 5 fall within the experimentally constrained field for monazite saturation (Montel, 1986). Furthermore, small amounts of monazite were recovered in mineral separates from Zone 5. Apatites in zones 4 and 5 commonly display more negative WR-normalised Nd anomalies than those from metaluminous zones (Fig. 2.10), implying that monazite crystallisation may have imposed compositional controls over the REE compositions of apatite and other co-existing phases. The consistent absence of such Nd anomalies in the WR suite, including in the most evolved and peraluminous WR, indicates that such signatures were not inherited from the WR and that monazite has not influenced WR compositions during AFC processes at depth. The consistently low concentrations of Ce and Th in apatite (Fig. 2.9) and the absence of further depletion of these elements during apatite crystallisation in zones 4 and 5 suggest that most monazite crystallisation preceded that of apatite in these magmas. Crystallisation of monazite and apatite at different stages of crystallisation may seem contrary to most eutectic systems. However, perlaluminous WR compositions in these zones favour early saturation of monazite (Montel, 1986) while the low abundance of CaO (often < 1 wt %) in the most peraluminous zones is likely to have delayed apatite crystallisation. London (1992) suggested that monazite crystallisation may slow or cease completely once P is accommodated in additional apatite and plagioclase during later stages of crystallisation.

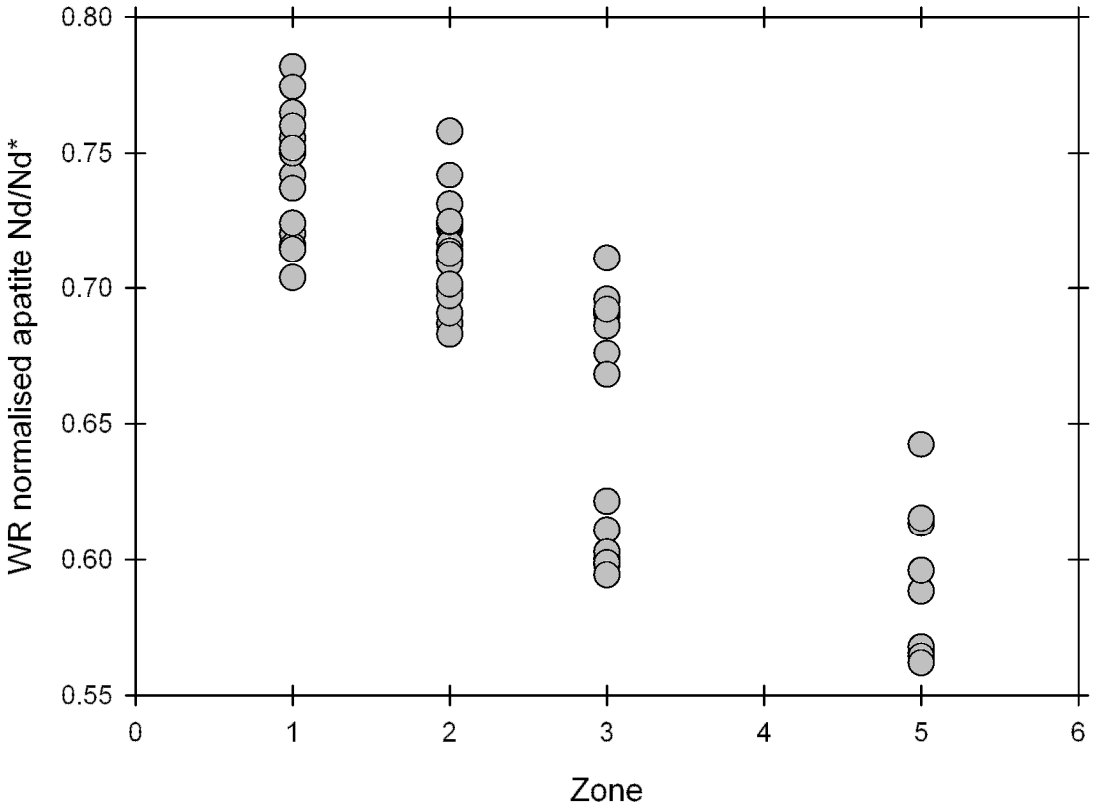

Fig. 2.10 Calculated apatite Nd anomalies normalised to average WR Nd anomalies for different zones [Nd/Nd* = Nd/(Ce×Sm)^{½}]. WR REE data from Stephens et al. (1985). A general decrease from zones 1 to 5 is apparent in WR-normalised Nd anomalies in apatites from progressively more evolved zones and cannot have been inherited from the WR. Negative Nd anomalies reflect saturation of monazite.

In addition to having crystallised from Ce-depleted melts, apatites from peraluminous magmas commonly have higher HREE contents than are consistent with the HREE contents of the WR. This effect is difficult to explain but may to some extent reflect the absence of major phases such as amphibole (in which HREE are also compatible). Crystallisation of apatite and zircon in Zone 4 is likely to have resulted in Y (and Yb) depletion. Crystallisation alone is therefore likely to induce a progression from high to low Y and Yb concentrations in apatite (Fig. 2.7 and Fig. 2.8).

In summary, the similarity in the textural relationship between apatite and host phases in all zones of the pluton, the absence of monazite control in determining WR compositions in peraluminous zones, and the absence of inherited zircon are

consistent with a model where WR and accessory mineral compositions are largely determined separately during different stages of magma history.

5.7 Causes of compositional diversity in apatites from a transitional zone (Zone 3)

The compositions of most of the apatites analysed from Zone 3 resemble those of zones 4 and 5, and presumably also reflect the effects of monazite crystallisation. However, the compositions of a small number of apatite grains, mainly those hosted by zircon, resemble those in zones 1 and 2 (Figs. 2.7 and 2.8). The WR suite indicates that the transition from metaluminous to peraluminous compositions is associated with progressive differentiation. The presence of apatite compositions in Zone 3 on both trends shows that in this zone, early crystallisation is likely to have been dominated by allanite, while apatites that crystallised later were subject to the effects of monazite crystallisation. This is consistent with the stabilisation of monazite relative to allanite in more peraluminous magmas (Montel, 1986).

6. Magma generation, ascent and pluton emplacement

The production of chemically diverse WR compositions within deep-seated regions of the crust followed by crystallisation of the observed mineral phases at shallower depths is consistent with the crustal hot zone model (Annen and Sparks, 2002; Annen et al. 2006a; Annen et al. 2006b). In this model, magmas of silicic and intermediate composition are generated through the repeated intrusion of sills formed from mantle melts that differentiate that causes partial melting of pre-existing and hydrous host rocks and sills. A wide range of WR trace element concentrations, isotopic compositions and water contents can then be generated through the mixing of residual hydrous mafic melts and crustal partial melts. The volumes and rates of melt production depend largely on the volumes of intruded mantle-derived material and how readily the crust fuses, which are in turn broadly dependent on the depths of sill emplacement, temperatures, crustal composition and water activity. Hydrous mafic sills act primarily as a heat and water source for subsequent melt generation, and as such may not necessarily be a dominant component in the newly formed silicic magmas.

Pidgeon and Aftalion (1978) found no geochronological evidence of zircon xenocrysts in any of the post-Caledonian plutons emplaced south of the Highland Boundary Fault (a total of 17 analyses). These findings have since been confirmed by recent U-Pb dating of > 100 zircon crystals from three TSS granites, including the Criffell pluton (Chapter 5). Though not unique, and with the possible exception of the mafic enclaves, the granitic rocks of the Criffell pluton and other plutons south of the Highland Boundary Fault are relatively unusual amongst the Caledonian granite plutons of northern Britain in lacking inherited crystals from the source regions and the hot zone in which differentiation is likely to have taken place. The paradox is further reinforced by evidence that the Criffell magmas satisfy many of the conditions used to identify low temperature silicic magmas that usually contain a significant inherited component, such as the continued decrease in WR Zr with increasing SiO_2 (Fig. 2.4) used by Chappell et al. (2004) to identify low temperature granites and persistent zircon saturation. The absence of chemical evidence for either

monazite or allanite having affected WR compositions despite their likely involvement in controlling REE distributions amongst accessory minerals during final crystallisation also alludes to an absence of inherited crystals. Furthermore, amphibole-plagioclase thermometry (Blundy and Holland, 1990) applied to granodiorites in Zone 1 (Appendix K) indicates temperatures of ~ 680 ± 5°C (error quoted as 1 SD for the analysed population; thermometer uncertainty is ± 75°C). These results suggest that inherited zircon grains (along with other accessory minerals) should form a considerable proportion of the crystal population in the Criffell pluton given WR isotopic evidence for supracrustal contamination (Halliday et al. 1980; Harmon and Halliday, 1980; Halliday, 1984; Harmon et al. 1984; Stephens and Halliday, 1984; Stephens, 1988; Thirlwall, 1989; Stone and Evans, 1997; Highton, 1999).

In the absence of inherited zircon, zircon saturation temperatures (Watson and Harrison, 1983) of ~ 745 °C (± 29°C, 1SD for data set population) (Appendix D) should provide a minimum estimate of magma temperatures upon emplacement and are similar to the temperatures reported by Miller et al. (2003) for 'cold' and usually inheritance-rich granites. However, most studies indicate that granitoids should carry crystal fractions of ~ 5 – 25 % from their source at temperatures of ~ 750°C (e.g. Miller et al. 1986; Patiño Douce and Beard, 1995; Patiño Douce and Harris, 1998; Miller, 2003). Harrison et al. (2007) suggested that zircon saturation temperatures may underestimate zircon crystallisation temperatures by up to 100°C, and may overestimate the proportions of inherited crystals transported from depth. However, Annen et al. (2006a) have demonstrated that water activity may also play an important role in determining the crystal cargoes of ascending magmas. Calc-alkaline magmas generated in crustal hot zones are H_2O-rich, with higher pressures enabling large amounts of H_2O to remain dissolved. At ~ 750°C and moderate crustal depths of ~ 25 km, large volumes of granitic melt require ~ 6 wt% H_2O (Holtz and Johannes, 1994; Miller et al. 2003). Hot zone silicic magmas are therefore buoyant and have relatively low densities and viscosities even at low temperatures (Annen et al. 2006a). In consequence, such silicic magmas may readily segregate on timescales of 10^4 to 10^6 years by compaction (McKenzie, 1984; Jackson et al. 2003) or more

rapidly under conditions of deformation (Brown, 1994; Petford, 2003). Subsequent silicic magma ascent from the hot zone may be rapid and adiabatic on timescales of hours or days (Clemens and Mawer, 1992; Petford, et al. 1993; Annen et al 2006a; Annen, et al. 2006b). During adiabatic ascent, granitic magmas may enter a super-liquidus state (Clemens et al. 1997; Annen et al. 2006a; Blundy and Cashman, 2001; Blundy et al. 2006;) due to the slightly steeper slope of the adiabat relative to the water-rich liquidus, resulting in the resorption of most or all entrained crystals (Fig. 2.11).

The abundance of hornblende in calc-alkaline magmas like those of the Criffell pluton suggests water saturated conditions (e.g. Berndt et al. 2005). Phase relations in silicic calc-alkaline dacites show that amphibole crystallisation requires water contents of ~ 4 – 6 wt % (Scaillet and Evans, 1999; Scaillet and MacDonald, 2001). These estimates further support the need for water contents of ~ 6wt % for sufficient granitic melt generation at temperatures of ~ 750^{o}C (Holtz and Johannes, 1994; Miller et al. 2003). Assuming an H_2O content of ~ 6wt %, magmas that ascend along a 4^{o}C/kbar adiabatic gradient (Holtz and Johannes, 1994) intersect the water-saturated liquidus at pressures of ~ 1kbar (~ 4 km) (Fig. 2.11). Crystallisation is likely to occur only after ascending magmas intersect the H_2O-saturated liquidus, leading to stalling, rapid loss of volatiles, increased viscosity and potentially rapid crystallisation (e.g. Blundy and Cashman, 2001; Blundy et al. 2006). Crystallisation depths of ~ 4 - 6 km indicated by amphibole barometry are therefore consistent with the stalling and crystallisation of magmas of granitic composition with ~ 6wt% H_2O at these depths due to intersection of the H_2O-saturated liquidus. In light of this, the absence of inherited zircons in cold granites (with temperatures of ~ 760^{o}C) may need re-evaluation in terms of temperature (Miller et al. 2003) in addition to water contents and the potential effects of super-liquidus magmas.

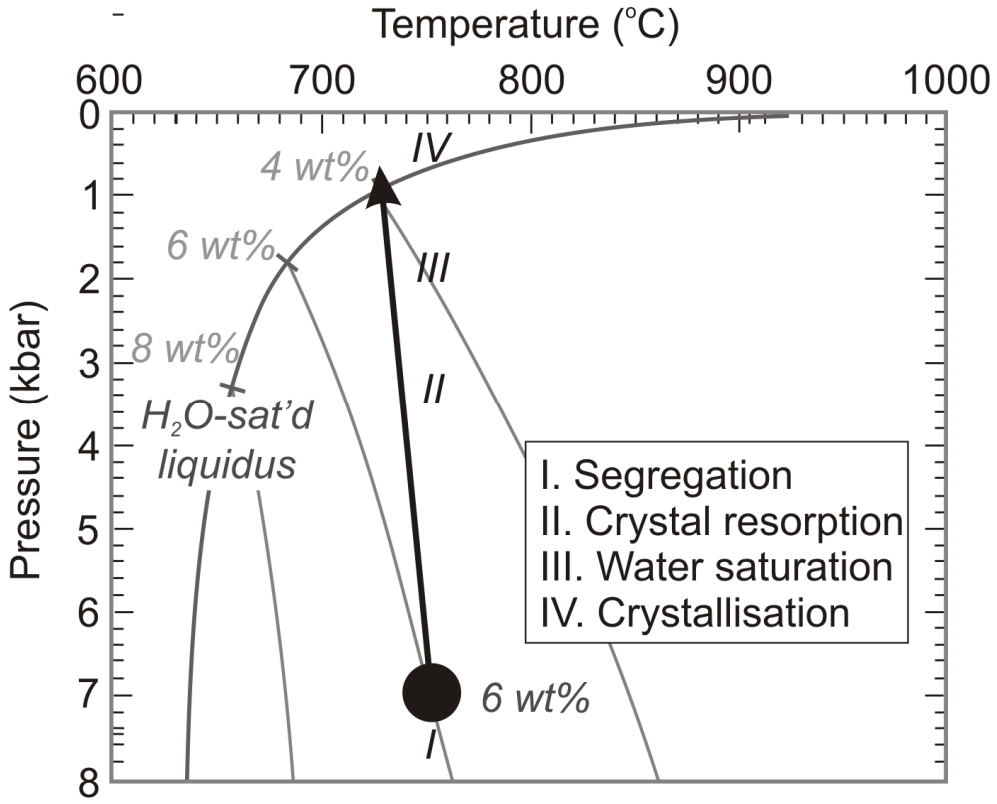

Fig. 2.11 Pressure-temperature diagram showing the adiabatic ascent of a granitic magma generated at ~ 7 kbar and ~ 750°C with a water content of ~ 6 wt % (stage I). Small ticks indicate intersection points between liquidi with different water contents and the water-saturated liquidus. Different processes are shown to take place at different stages of ascent (after Annen et al. 2006a). The positions of water-rich and water-saturated granitic liquidi are taken from Holtz et al. (2001). The melt is assumed to ascend adiabatically with a cooling of 4°C/kbar (Holtz and Johannes, 1994) (stage II). Following segregation from the melt zone, the melt temperature exceeds that of the liquidus, leading to a super-liquidus state (Clemens et al. 1997) and the likely resorption of entrained crystals. Water saturation is reached at ~ 2 kbars at a temperature that is higher than that of the liquidus (stage III). Crystallisation and degassing are thought to occur upon intersection with the water saturated liquidus (stage IV) at ~ 1kbar and ~730°C.

It is thought that, due to the potentially small volumes of single magma batches, the rapid water loss on intersecting the water-saturated liquidus and the subsequently large increases in viscosity, crystallisation is likely to occur under nearly closed system conditions (Annen et al. 1986). This would be consistent with the preservation of near-liquidus compositions by some apatites (the most Ce-rich apatites) and the WR in metaluminous zones of the Criffell pluton (Fig. 2.8). Under such circumstances, mineral compositions, and particularly those of REE-rich accessory phases crystallising at shallow depths, will become highly susceptible to

the competitive crystallisation of other co-existing accessory phases, as noted here. The resulting patterns of trace element concentrations in apatites and their host rocks may thus provide evidence of the ascent and crystallisation processes of magmas and the possible attainment of transient super-liquidus conditions during adiabatic ascent, prior to stalling and crystallisation. The passage of melts through a super-liquidus state ensures that open system deep crustal processes recorded by the WR remain distinct from closed system crystallisation processes recorded by the accessory and major minerals.

Confirmation of the processes associated with crustal hot zones and the assembly of multiple magma batches following melt separation and ascent to shallower levels indicate that pluton assembly is likely to have been incremental. Such assembly is consistent with a growing consensus that large plutonic bodies grow incrementally (Wiebe and Collins, 1998; Glazner et al. 2004; Coleman et al. 2004; Glazner and Bartley, 2006; Kemp et al. 2006b; Lipman, 2007; Miller, 2008; Appleby et al. 2008) and may explain how textural diversity occurs, often on short lengths scales, within large plutons such as Criffell.

Despite providing robust insights into magmatic processes, the trace element compositions of accessory minerals are in many situations likely to reflect processes that occur at shallow levels only. An integrated WR *and* accessory mineral approach is therefore needed to fully model the petrological history of silicic magmas that have likely followed protracted histories in lower and upper regions of the lithosphere. By contrast, the isotopic compositions of accessory minerals should retain evidence of processes that occurred prior to magma emplacement.

7. Concluding remarks

1. WR compositions in the Criffell pluton record the effects of open system differentiation (Stephens et al. 1985) in the deep crust. High WR $^{207}Pb/^{204}Pb$ isotope compositions (Thirlwall, 1989) indicate that the local Southern Uplands sedimentary rocks into which the Criffell pluton is emplaced were not the source of crustal contamination. More likely sources are found in Avalonian crust south of the Iapetus Suture, which is thought to extend to depths > 11 km beneath the Southern Uplands. Decreasing concentrations of Ce and Y in the WR can be modelled by assimilation of Avalonian sedimentary rocks and the fractional crystallisation of a mineral assemblage similar to that of mafic enclaves found in Criffell granodiorite.

2. Al-in-hornblende barometry and plagioclase-hornblende thermometry suggest that crystallisation of the present granodiorite crystal assemblage occurred at 0.8 - 1.5 kbars (~ 4 - 6 km depth) and ~ 680ºC. Despite evidence for zircon saturation (progressively decreasing Zr with SiO_2 in the WR) and supracrustal contamination, the absence of inherited zircon indicates that the observed zircon assemblage crystallised on emplacement at shallower depths.

3. Accessory apatite inclusions in a range of host phases crystallised through bulk saturation of the magma. Variations of up to two orders-of-magnitude in the Ce and Y (trend 1) contents of apatites from single metaluminous samples result from the crystallisation of co-existing allanite. Despite the importance of allanite in determining the composition of apatite in metaluminous samples, increasing LREE/HREE ratios with SiO_2 in the metaluminous WR suite suggest that, during WR differentiation, amphibole or zircon crystallisation (rather than allanite) was the dominant control on compositional evolution.

4. Apatites in peraluminous zones define a second trend of low Ce and Th together with elevated Y (and Yb) and have more negative WR-normalised Nd anomalies than those from metaluminous zones that are consistent with prior crystallisation of

monazite. Evidence for monazite crystallisation is absent at the scale of even the most evolved WR samples, providing good evidence that the trace element trends defined by the WR suite and their apatite crystal cargoes were determined independently.

5. These results are consistent with the crustal hot zone model proposed by Annen and Sparks (2002) and Annen et al. (2006a), where WR compositions are determined by potentially large-scale, open system processes within nested sill complexes in the lower crust.

6. Small batches of water-rich (~ 6wt % H_2O), low-viscosity magma ascend from a deep crustal hot zone adiabatically and achieve a super-liquidus state, resorbing most or all of their crystal cargo, until they stall and crystallise at shallower depths of 4 to 6 km upon intersecting the water-saturated liquidus. It is at these shallower emplacement depths that crystallisation and textural maturation of the pluton occurs. The passage of melts through a super-liquidus state ensures that open system deep crustal processes recorded by the WR remain distinct from closed system crystallisation processes recorded by the accessory and major minerals.

7. Mainly closed system crystallisation within small melt volumes means that accessory apatite trace element compositions largely reflect the saturation of other, competing accessory minerals and that WR compositions are close to initial liquid compositions. Assembly of the Criffell pluton therefore appears to have been incremental.

8. Together, WR and accessory mineral data enable petrogenetic models to be developed at two very different scales and at high enough spatial and temporal resolution to enable processes of pluton assembly to be better assessed. The isotopic compositions retained by accessory minerals may faithfully record the effects of magma differentiation, despite not having crystallised in regions where such compositions are determined. However, the trace element compositions of accessory minerals mainly reflect the crystallisation history at shallower levels. These physical

and geochemical processes identified in the Criffell Pluton should be common to many metaluminous and peraluminous granitic plutons, and may be indicative of transient super-liquidus states of ascending silicic magmas.

Chapter 3

The Timing of accessory mineral crystallisation in granitic rocks constrained by apatite compositions: a case study[†]

Abstract

Zircon archives unrivaled information about the evolution of silicic magmas and the continental crust. However, it remains uncertain as to what stages during the protracted histories of magma evolution its isotopic and elemental record is preserved, and how that record is best constrained. Apatite is a ubiquitous phase that formed as inclusions in other minerals throughout the crystallisation of granitic magmas in the zoned Criffell pluton (Southern Scotland). The rare earth element (REE) contents of apatite inclusions exhibit compositional variations that relate to the co-existence of different accessory phases in different zones. Ce concentrations in apatites (~ 5500 to 500 ppm) co-vary with Y (~ 660 to 0 ppm) from high to low concentrations in metaluminous zones that result from the crystallisation of allanite. The range in Ce concentration is similar in apatites hosted in all mineral phases and there is no evidence of a relative crystallisation sequence in metaluminous magmas. Decreasing Sr concentrations in apatite reflect crystallisation at later stages relative to feldspar and show little evidence of host dependence. In peraluminous zones, apatites have higher concentrations of Y (up to ~3000 ppm) and generally lower concentrations of Ce (<2500 ppm) than would be expected from their respective whole-rocks and reflects the earlier crystallisation of monazite. Apatites formed during later stages of crystallisation in these zones have lower Y concentrations due to removal of Y by zircon and earlier-formed apatite. The most Y-rich and earliest-

[†] Co-authors: Colin Graham – *University of Edinburgh*; Chris Hawkesworth – *University of St Andrews*; Martin Gillespie – *British Geological Survey*; Richard Hinton – *University of Edinburgh*; EIMF

formed apatites in peraluminous zones are hosted exclusively by zircon and suggest that the majority of zircon crystallisation occurred before that of other minerals that host apatite. The abundance of zircons with apparently more primitive oxygen isotopic compositions in large S-type and peraluminous plutons may reflect the earlier crystallisation of zircon in such magmas. The greater ease with which zircon crystallises in less evolved, Zr-rich granodiorites may further bias isotopic records in magmas generated from the mixing of both less and more evolved magmas.

1. Introduction

Zircon has proved a valuable archive of crustal evolution and of the processes that control the differentiation of silicic magmas (e.g. Eiler, 2007; Kemp et al. 2006, 2007; Hawkesworth et al. 2010; Claiborne et al. 2010; Bradley, 2011; Roberts, 2012). However, interpretations of this detailed isotopic and trace element record (e.g. Kemp et al. 2005, 2006, 2007; Appleby et al. 2008, 2010; Hawkesworth and Kemp 2006; Shaw and Flood, 2009; Yang et al. 2007) and of zircon crystallisation temperature spectra (Harrison et al. 2007) have typically been hindered by uncertainties about the timing of zircon crystallisation relative to other minerals during magma evolution. In addition to zircon, apatite has also been shown to document prolonged compositional changes in silicic magmas (Nash, 1984; Sawka, 1988; Shnukov et al. 1989; Sha and Chappell, 1999; Hoskin et al. 2000; Belousova et al. 2001;2002; Chu et al. 2009; Chapter 2). Hoskin et al. (2000) proposed that where accessory minerals record compositional changes in response to magma differentiation, changes to the REE chemistry of accessory minerals like apatite record the effects that other, co-existing, accessory minerals have on the REE characteristics of the magma. We explore how the compositional sensitivity of apatite can be used in conjunction with its inclusion in different hosts, including zircon, to establish the relative crystallisation order of different accessory phases in metaluminous and peraluminous magmas. Relative to other crystallising phases, the chemical archive preserved in zircon is shown to be biased towards earlier stages of crystallisation in the peraluminous magmas of the zoned Criffell pluton in southern Scotland. We examine the implications for whether the stable and radiogenic isotopic compositions preserved in zircon reflect the early, prolonged or final stages of magma evolution in magmas of metaluminous and peraluminous compositions.

2. The Criffell pluton

Stephens et al. (1985) showed that five discrete and broadly concentric zones can be recognised in the Criffell pluton based on the distribution of key minerals (Figure 3.1). WR compositions vary systematically from the outermost zone (Zone 1), which is metaluminous with WR SiO_2 as low as 58 wt %, to the innermost 'core' zone (Zone 5), which is peraluminous and has SiO_2 values approaching 72 wt %. The ~20 by 10 km pluton intrudes weakly metamorphosed Silurian wackes and mudstones of the Southern Uplands accretionary prism, and was intruded at ~397 Ma (Halliday et al. 1980), post-dating final closure of the Iapetus Ocean and collision of Avalonia and Laurentia (Brown et al. 2008 and references therein). Zones 1and 2 are composed of metaluminous granodiorites and include: primary clinopyroxene, hornblende, biotite, plagioclase, potassium feldspar and quartz, with accessory titanite, zircon, apatite, allanite and magnetite occurring predominantly as inclusions. By contrast zones 4 and 5 consist of weakly peraluminous granites, containing primary muscovite, biotite and monazite but lack the clinopyroxene, hornblende, titanite and the abundance of zircon and magnetite that characterise zones 1 and 2. Zone 3 is very mildly peraluminous (molar proportion of Al_2O_3 are approximately equal to that of CaO, K_2O and Na_2O combined) but lacks primary muscovite. Owing to the scarcity of zircon in the most silicic zone (Zone 5), we focus our study on zones 1 to 4 where SiO_2 values range between 58 wt % and 68 wt %. The locations of rock samples collected for this study are shown in Figure 3.1.

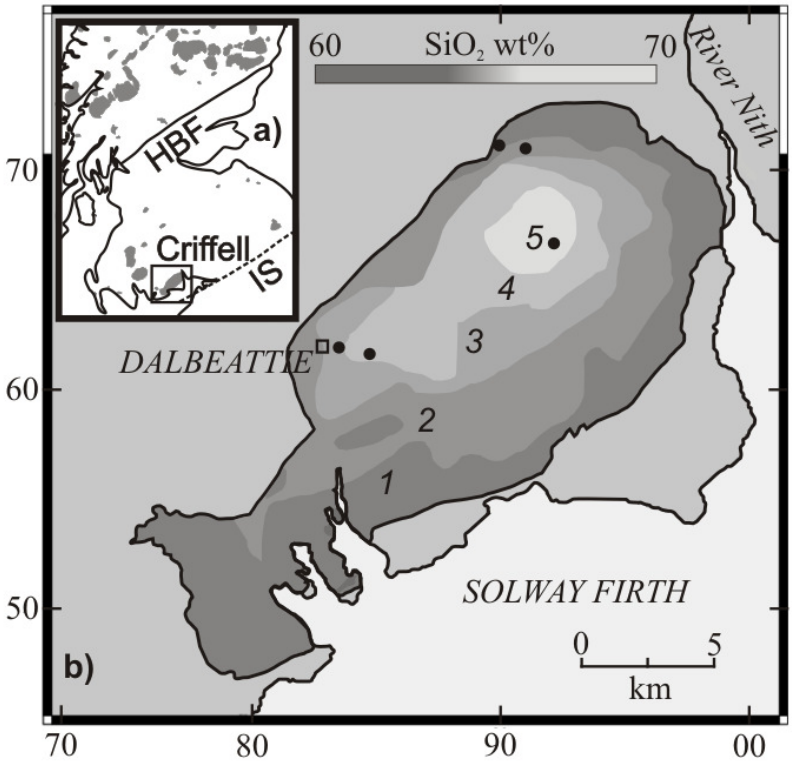

Figure 3.1 Map of the Criffell pluton and inset regional map of Scottish granites. Paler shading reflects increasing WR SiO_2. Zone mineralogy is as follows: 1) clinopyroxene-biotite-hornblende granodiorite; 2) biotite-hornblende granodiorite; 3) biotite granite; 4) biotite-muscovite granite 5) muscovite-biotite granite. Minerals listed in order of increasing modal abundance (Stephens et al. 1985). Black points denote sample sites. Inset: Regional map of major Scottish plutons. Abbreviations are as follows: HBF – Highland Boundary Fault, IS – Iapetus Suture.

Currently unpublished new zircon U-Pb ages obtained as part of this study support the published results of Pidgeon and Aftalion (1978) in showing that there is no detectable inherited zircon component in the Criffell pluton. The absence of inherited zircons is common to several other granitic plutons in the Southern Uplands region of Scotland, and distinguishes them from Caledonian granites north of the Highland Boundary Fault. Simple concentric zoning and a lack of significant resorption boundaries in cathodoluminescence (CL) images indicate that zircon is predominantly the product of direct crystallisation within the Criffell magmas, with no detectable inheritance from source rocks or antecrysts from other magmas. Continued zircon saturation is implied by decreasing concentrations of Zr with increasing SiO_2 (Stephens and Halliday, 1984; Chappell et al. 2004; Chapter 2) in the WR suite. Together with evidence for significant volumes of S-type and peraluminous granites and isotope evidence for significant supracrustal and

sedimentary contamination and/or assimilation (Halliday 1984; Harmon and Halliday, 1980b; Harmon, et al. 1984; Highton, 1999; Stephens, 1988; Stephens and Halliday, 1984; Stone, et al. 1997; Thirlwall, 1989), the absence of inherited zircon in the Criffell pluton and other local plutons is unusual. Pb isotopes (Thirlwall 1989) have confirmed that WR compositions were determined at depths of > 11 km during open system differentiation involving Avalonian-derived sedimentary components within mid to lower crustal hot zones (Chapter 2). Calc-alkaline compositions and the abundance of amphibole in granodiorites together with evidence of low magmatic temperatures (estimated at ~ 750^{o}C from zircon saturation thermometry, Watson and Harrison, 1983) have been used to infer high water contents in the Criffell magmas (~ 6wt %, Chapter 2). Such high water contents are thought to result in low viscosity magmas that can ascend rapidly, and potentially acquiring a super-liquidus state (Annen et al. 2006a; Blundy and Cashman, 2001; Blundy et al. 2006; Clemens et al. 1997; Chapter 2) that results in resorption of entrained minerals, including inherited accessory zircon. Final emplacement is thought to results from the stalling of ascending magmas upon intersection of the water-saturated liquidus at ~ 4-6 km depth, in agreement with the results of amphibole barometry (Chapter 2). It is suggested that the entire assemblage of minerals observed in the Criffell pluton is the result of crystallisation at the level of final emplacement.

Apatite is the most abundant accessory mineral in all five mineralogical zones of the Criffell pluton, and forms euhedral, prismatic inclusions of between 30 μm and >1 mm in length in several host minerals. Apatite is found predominantly as inclusions and not interstitially, and is the only visible inclusion phase found in the ~ 500 Criffell zircons studied. In this respect, the textures of accessory minerals in Criffell differ from those reported by Jennings et al. (2011) in which a large variety of inclusion phases were found in zircons from the Dronning Maud Land pluton, Antarctica (SiO_2 = 53 to 72 wt %). Sphene constitutes up to 2 modal % in the outer zones (zones 1 and 2) and occurs as euhedral crystals that are often > 1mm in size. There is little evidence of impingement textures around any of the sphene crystals suggesting that they represent an early crystallised phase relative to other minerals in these zones (Stephens et al. 1985). The low abundance of zircon together with its

heavily cracked appearance in the most silicic zone (Zone 5) is likely to reflect low Zr abundances in the initial magmas and radiation damage respectively. Allanite has been found in small amounts in magnetic mineral separates (Appendix L) from zones 1 and 2 (metaluminous samples). Monazite has been found amongst heavy mineral separates from Zone 5 but not petrographically.

3. Analytical Methods

Apatite was analysed *in situ* from polished thin sections made from samples collected from each zone of the Criffell pluton. Apatites hosted by zircon were analysed following standard heavy mineral separation of zircon and mounting in epoxy blocks prior to polishing.

Apatite was analysed by electron and ion microprobes using a Cameca SX-100 and ims 4f respectively at the University of Edinburgh Ion Microprobe Facility (EIMF). Electron probe microanalysis (EPMA) was carried out using a wavelength dispersive method (WDS) using PC0, LTAP, LPET and LIF dispersion crystals. Beam conditions were set at 20 kV and 60 nA for trace and most major elements, with a 10 nA defocused beam used for alkali elements.

Apatite inclusions were analysed using the Cameca ims 4f ion microprobe, using a 15 µm, 5 nA $^{16}O^-$ primary ion beam with 15 keV net impact energy. Only high energy secondary ions (100-140 eV) were measured in order to reduce molecular ion overlap. F/Ca ion yields were determined using Durango and Wilberforce apatite standards. Due to the small size of some zircon-hosted apatite, any beam overlap with zircon was assessed by comparing the minimal Zr content of apatite (< ~ 10 ppm) with that in an average zircon (420,000 ppm). Analyses that showed evidence of overlap were discounted.

4. Results

The Ce and Y contents of apatites from all zones define two compositional trends (Fig. 3.2). Apatites in metaluminous zones (zones 1 and 2) are generally more Ce-rich (up to ~ 5500 ppm) and Y poor (Y < ~ 660 ppm) than those in peraluminous zones, with little evidence to indicate that their compositions relate in any way to their host phase. Apatites in the most peraluminous zone studied (Zone 4) are relatively depleted in Ce (mostly < 2000 ppm) and relatively enriched in Y (up to ~ 3000 ppm), with the most Y-rich apatites hosted in zircon. Zircon-hosted apatites in Zone 3 (transitional between metaluminous and peraluminous in composition) display REE compositions that are similar to those in zones 1 and 2. Apatites hosted by other minerals in this zone resemble apatites in zones 4 and 5. This may indicate that during apatite saturation, a change occurred in the identity of the accessory minerals crystallising and/or that the relative timing of zircon crystallisation changed relative to other phases in response to the change in magma composition.

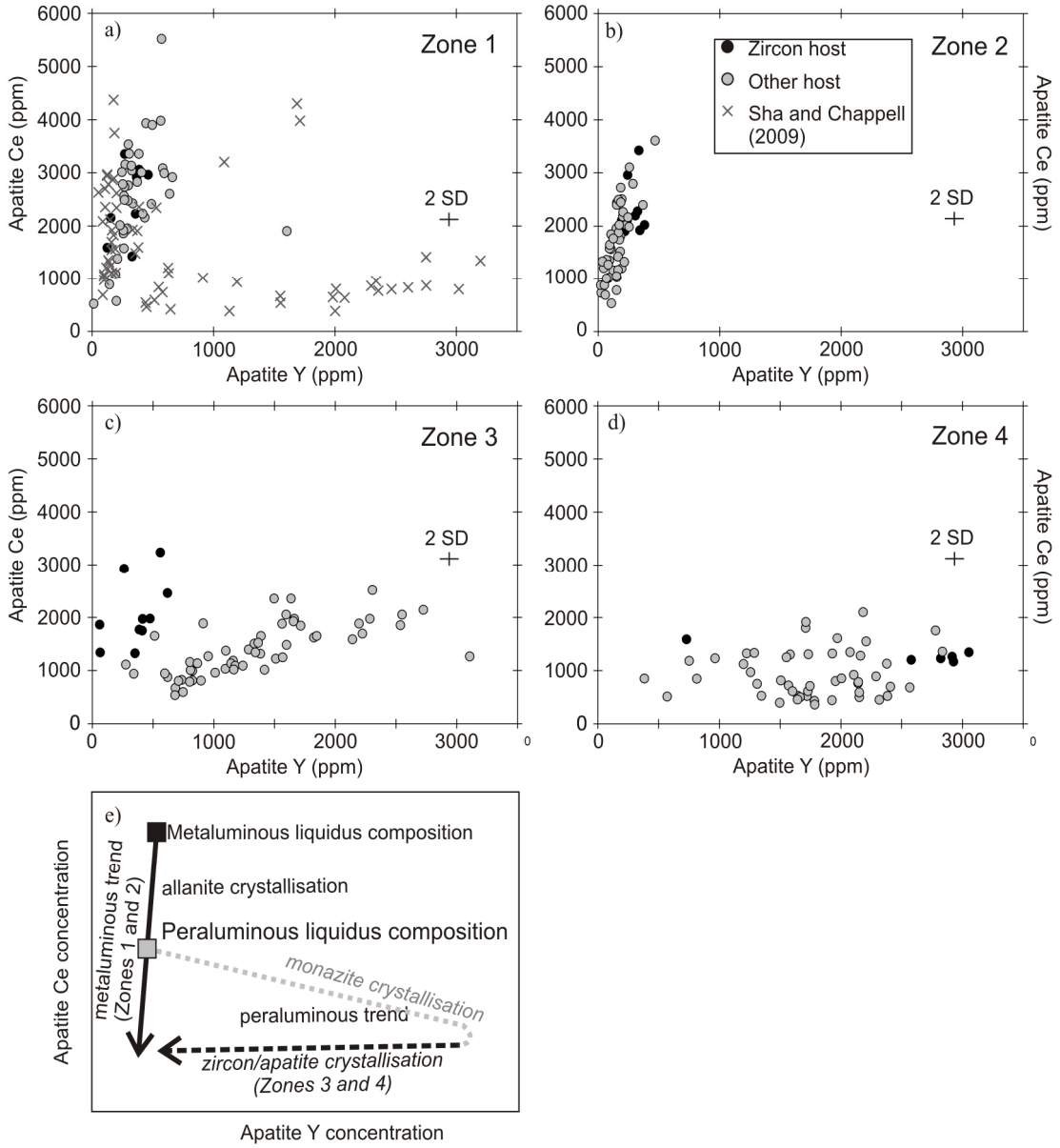

Figure 3.2 Apatite Ce (ppm) vs. Y (ppm) for the outer four zones of the Criffell pluton. Host phases are distingusihed using symbols shown in the figure key. Apatite from zones 1 (a) and 2 (b) plot along a trend of Ce depeletion, where the earlierst apatite is the most Ce-rich. Apatite compositions show little relation to their host phases in these zones. Apatite from Zone 4 (d) plot along a horizontal trend, where monazite that crystallised before apatite resulted in Ce depletion and Y enrichment in apatite. Zircon (and apatite) crystallisation depleted later-formed apatite in Y and the trend is from high to low Y. Zircon-hosted apatite is the more Y-rich, indicative of earlier crystallisation than that hosted by other phases. Zone 3 (c) is transitional between metaluminous and peraluminous. Zircon-hosted apatite pre-dated most monazite crystallisation and plots along a similar trend to apatite in zones 1 and 2. Most apatite hosted by other phases post-dates monazite saturation and follows a trend similar to that of Zone 4. Apatite data from Chu et al. (2009) and Sha and Chappell (1999) are included in figure (a) as grey crosses for comparative purposes and to illustrate the occurrence of similar trends in other granitic plutons.

The highest Sr concentrations in apatite inclusions are found in Zone 1 (~200 - 700 ppm) and the lowest in Zone 4 (below detection limit and up to ~ 400 ppm), consistent with an overall trend of decreasing Sr in the WR from zones 1 to 4 (Appendix E; Fig. 3.3). The Sr content of apatites in Zone 3 mostly resemble those in Zone 4 (< 400 ppm). However, a small number of zircon-hosted apatites in Zone 3 have Sr concentrations > 500 ppm and are therefore similar to apatites in zones 1 and 2 (Fig. 3.3). Peak Sr concentrations in apatites hosted by different phases in individual samples lie mostly within analytical error of each other; however zircon can be seen to host the most Sr-rich apatite in each of the zones (Fig. 3.3).

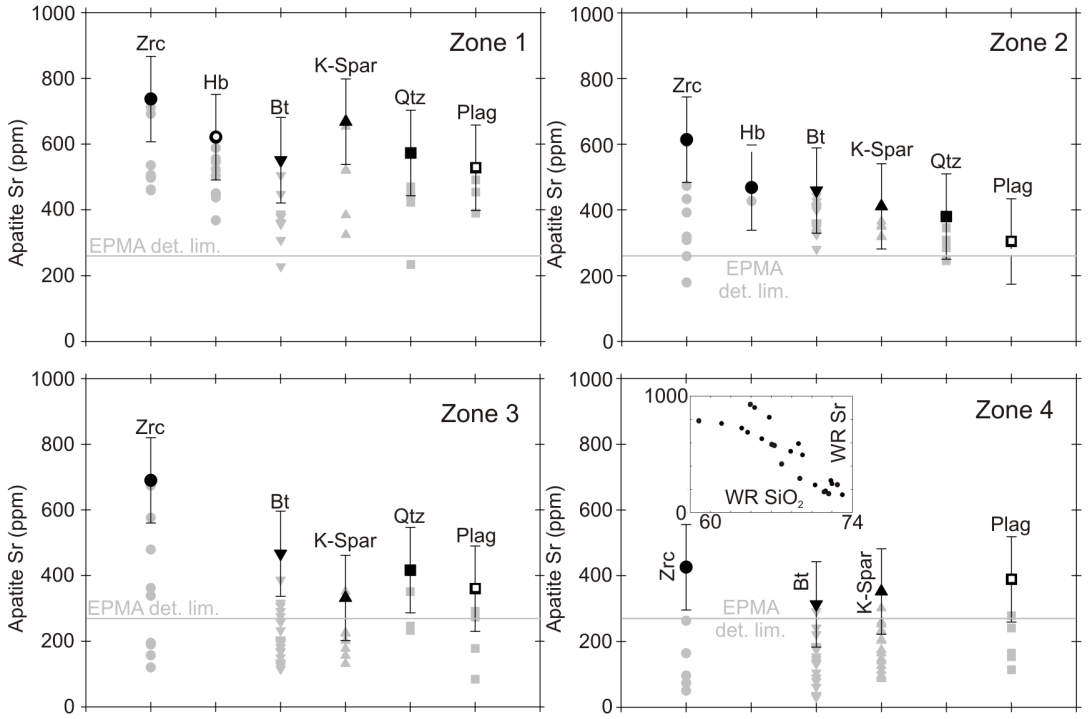

Figure 3.3 Strontium (Sr) concentrations of apatite crystals hosted by different phases from four increasingly silicic zones of the Criffell pluton. More Sr-depleted apatite is inferred to have crystallised at relatively later stages of crystallisation relative to plagioclase. Significant overlap in the composition of apatite hosted in different phases indicates simultaneous crystallisation. Peak Sr concentrations are shown in bold together with analytical errors. Peak measurements reflect the onset of host crystallisation relative to plagioclase and are mostly within error for all phases, except in Zone 3 where zircon is host to the most Sr-rich apatites. There is subtle evidence for more elevated peak Sr concentrations in apatites hosted by zircon in all zones. Inset figure shows variations in WR Sr against an index of magma differentiation (SiO_2). A decrease in WR Sr with magma differentiation and increasing SiO_2 is mirrored by the overall decrease in Sr concentrations in apatites in zones 1 to 4. WR data from this study and Stephens and Halliday (1980). Error bars represent 1 SD analytical errors for Sr analyses using an EPMA, with the 3 SD detection limit shown in (d).

5. Discussion

The inclusion of apatite in all major minerals is a unique feature amongst the accessory mineral assemblage studied in the Criffell pluton. This prevalent textural characteristic together with compositional sensitivity to the crystallisation of other mineral phases (Nash, 1984; Sawka, 1988; Shnukov et al. 1989; Sha and Chappell, 1999; Hoskin et al. 2000; Belousova et al. 2001; 2002; Chu et al. 2009; Chapter 2) indicates that it may be used as a reliable proxy to examine the extended crystallisation history of silicic magmas.

In order to reliably identify changes to the bulk composition of crystallising magmas, it must first be established that apatite saturation occurred in response to bulk saturation of the magmas and not within melt inclusions that remained chemically isolated from the bulk magma. Consistently smooth chondrite-normalised trace element patterns in apatites such as those from the Criffell pluton have been used by Hoskin et al. (2000) to indicate bulk saturation of apatite. By contrast, apatites saturated from small melt inclusions within different host phases have been shown to exhibit more varied chondrite-normalised REE patterns. A case for bulk saturation may also be made from the textural isolation of apatite inclusions from other accessory minerals; local saturation in small melt inclusions would be expected to result in the sequential crystallisation of other accessory minerals, leading to close spatial associations. Bulk saturation indicates that chemical connectivity was maintained between accessory phases and the bulk magma during crystallisation and therefore enables compositional changes in apatite to be interpreted in the context of changes to the bulk magmatic environment.

At temperatures below 600^{o}C, apatite is likely to retain REE zonation on scales of ~ 100 μm for ~ 10^7 years (Cherniak, 2000). Most granites cool to below 600^{o}C on timescales that are significantly less than 10^7 years meaning that in the absence of subsequent high temperature and prolonged thermal events, apatite should retain REE compositions that reflect original magmatic processes.

5.1 Early saturation of apatite

Bulk saturation supports the use of apatite saturation thermometers (Harrison and Watson, 1984) that constrain the temperature at which apatite has the potential to begin crystallising in magmas of a given composition. The calculation requires both an estimate of the Si and P concentrations of the magma at the time of apatite saturation and evidence that apatite was a liquidus or near-liquidus phase (Piccoli and Candela, 1994; Coulson et al. 2001). Plutonic WR compositions are increasingly thought to represent solidified melts rather than crystal cumulates (Reubi and Blundy, 2009; Glazner, 2007; Ulmer, 2007). Even distributions of minerals (as opposed to clusters of similar minerals) in all zones of the Criffell pluton also favour such interpretations. Evidence suggests that the most Ce-rich apatites found in individual samples crystallised from magmas with compositions similar to their respective WR in metaluminous zones of the Criffell pluton (Chapter 2). These results indicate that WR compositions therefore remain a useful proxy for magma compositions and that apatite is likely to have been a near-liquidus phase in these samples. In magmas of a similar composition to the WR suite, apatite saturation would commence at temperature of between 910^{o}C and 990^{o}C. These temperatures are significantly higher than the 660^{o}C 'wet' granite solidus estimated by Tuttle and Bowen (1958) and are also significantly higher than previously calculated temperatures of < 700^{o}C using Ti-in-zircon (Ferry and Watson, 2007) and amphibole-plagioclase thermometry (Blundy and Holland, 1990) in these samples. It is therefore likely that apatite began crystallising early relative to other phases in the Criffell magmas. These results are consistent with the evidence of Hoskin et al. (2000) that apatite is an early crystallising phase across the entire spectrum of magmas compositions (~ 50 to 75 wt % SiO_2) found in the Boggy Plain zoned pluton of eastern Australia.

5.2 Constraints on the relative timing of accessory mineral saturation using apatite

The striking differences seen in the Ce-Y composition trends in apatite inclusions from different zones of the Criffell pluton are mirrored by apatites from a number of other plutons and have been shown to reflect the effects of other competing accessory minerals (Sha and Chappell, 1999; Hoskin et al. 2000; Belousova et al. 2001; Chu et al. 2009). No attempt has however been made to investigate the extent to which different host minerals record different stages of chemical change during the crystallisation of silicic magmas. Apatite inclusions provide a means of identifying changes in the crystallising assemblage of minerals and estimating the relative crystallisation orders amongst their host mineral in metaluminous and peraluminous silicic magmas.

5.2.1 Metaluminous zones

REE concentrations in granitic magmas often decrease in response to crystallisation due to the removal of REEs by REE-rich accessory phases (Hoskin et al. 2000; Stephens et al. 1985). This same trend is also apparent in minerals that crystallise progressively and continuously through to later stages of crystallisation, including in apatite (Hoskin et al. 2000; Chapter 2). Crystallisation models that assume a mineral assemblage similar to that seen petrographically in the Criffell granodiorites are unable to reproduce the full range in Ce compositions indicated by apatite Ce concentrations (Chapter 2). Other studies that report similar levels of compositional diversity in apatites from metaluminous magmas together with marked decreases in their concentration of Th suggest that small modal proportions (~0.1%) of additional allanite are required in order to fully model decreasing concentrations of Ce in apatite (Chu et al. 2009; Sha and Chappell, 1999) and is consistent with the discovery of small amounts of allanite in magnetic heavy mineral separates.

There is little evidence in zones 1 and 2 that apatite hosted by any particular phase, including zircon, records a distinct stage of Ce depletion induced primarily by allanite crystallisation (Fig. 3.2). Zircon-hosted apatites occupy similar regions of Ce-Y space to those hosted by other phases and indicate that all phases, including apatite and zircon, may have crystallised largely simultaneously throughout the final crystallisation history of the metaluminous zones.

The Sr contents of apatites have previously been used as a proxy for constraining the onset of apatite saturation relative to other Sr-rich phases, and in particular that of plagioclase (Belousova et al. 2001; Jennings et al. 2011). More Sr-depleted apatite is likely to have grown after of the onset of plagioclase crystallisation while the opposite is true of apatite that is relatively more enriched in Sr. Similarly, the peak Sr concentration of apatites included in different phases offer the potential to constrain the relative onset of host crystallisation in relation to plagioclase crystallisation. The observed range in Sr seen in apatites from single samples suggests that apatite crystallised together with plagioclase rather than before or after, when compositional diversity may be more limited. The Sr concentration of apatites hosted by different phases, like those of Ce and Y, appear similar and suggest that crystallisation of all phases occurred over a similar period of magma history. Although the highest concentrations of Sr in apatites within different hosts lie mostly within analytical error, the slightly elevated peak concentrations seen in zircon-hosted apatites is consistent with the earlier onset of zircon crystallisation relative to other host phases, including plagioclase in these zones.

5.2.2 Peraluminous zones

The Ce-Y trends exhibited by apatite from peraluminous zones show little relation to those in metaluminous zones or those of the WR suite (Fig. 3.2). Apatites from these zones show a marked increase in Y together with generally lower concentrations of Ce than would be expected from WR compositions. They are also characterised by more negative WR-normalised Nd anomalies than apatites in metaluminous zones, a feature commonly attributed to the co-existence of monazite in many other peraluminous granites (Wark and Miller, 1993; Sha and Chappell, 1999; Hoskin et

al. 2000; Belousova et al. 2001; Chu et al. 2009; Chapter 2). Monazite crystallisation in the more silicic zones is consistent with its discovery in small amounts in heavy mineral separates in the most peraluminous zone (Zone 5) and it is commonly stabilised in peraluminous magmas (Montel, 1986). The relative enrichment in HREE seen in apatites from peraluminous zones relative to metaluminous zones has proven difficult to explain, but to some extent may result from the absence of HREE-rich phases such as amphiboles and pyroxenes in peraluminous magmas. Despite having lower concentrations of Ce than would be expected from WR compositions, apatites from zones 4 and 5 show little evidence of further depletion in Ce (Fig. 3.2). This may indicate that the diagnostic chemical fingerprints used to identify monazite saturation were determined prior to apatite saturation in these zones. However, the stark contrasts between apatite and WR compositional trends together with the persistence of negative Nd anomalies in WR-normalised apatite REE patterns (Chapter 2) suggest that monazite crystallisation post-dates the evolution and determination of WR compositions. These characteristics are, however, likely to pre-date the crystallisation of apatite during crystallisation at the level of emplacement because of the lack of further depletion in Ce. Early monazite crystallisation in peraluminous magmas is consistent with experimental evidence (Montel, 1986) while the low abundance of CaO (often < 1 wt %) in the most peraluminous zones would likely have delayed apatite crystallisation. Furthermore, monazite crystallisation may slow or cease completely once P is accommodated in additional apatite and plagioclase during later stages of crystallisation (London, 1992). Following monazite saturation, the subsequent crystallisation of zircon and apatite has been shown to induce depletion in the Y concentration of later apatites. Throughout apatite saturation, increasing crystallisation is therefore associated with a trend from high to low Y in apatite.

In contrast to metaluminous zones, there is strong evidence that zircon-hosted apatite is compositionally distinct from that hosted by other phases. Zircon-hosted apatites are in general more Y-rich than those hosted by other phases (Fig. 3.2). Assuming that apatite compositions become progressively more depleted in Y with increasing crystallisation, zircon growth capable of encapsulating apatite crystals appears to

have occurred at an earlier stage of crystallisation relative to other host minerals during the final crystallisation of these zones. Subsequent zircon growth may well have occurred, as indicated by continued decreases in the Y content of later formed apatites, but at a rate that was not able to encapsulate mineral inclusions. Later growth of zircon is likely to have been as mineral overgrowths on previously nucleated crystals. Extensive amounts of overlap in the compositions of apatites hosted by all phases other than zircon suggest that they crystallised largely simultaneously.

All but the very highest Sr measurements made by EPMA on peraluminous apatite inclusions fall below analytical detection limits, limiting any comparative evaluation. The overall general decrease in Sr from zones 1 to 4 is, however, maintained.

5.2.3 Transitional zone

Zone 3 has a composition that is transitional between metaluminous and peraluminous. Despite being more SiO_2-rich than Zone 4, it is mildly less peraluminous (Appendix E). A small number of apatite inclusions resemble those from more metaluminous zones (zones 1 and 2) in being more Ce-rich and Y-poor than other apatite crystals, including those in zones 4 and 5. This small number of metaluminous apatites is hosted exclusively by zircon (Fig. 3.2). Noting that the transition from metaluminous to peraluminous magmas coincides largely with increasing SiO_2 and magma differentiation, the interpretation in Zone 3 is that zircon and zircon-hosted apatites reflect a stage of magma crystallisation that mainly pre-dates the saturation of monazite. In contrast to Zone 4, apatites hosted by other phases show some evidence of decreasing Ce and Y that may reflect simultaneous crystallisation of monazite with other host phases and their encapsulated apatite crystals. This zone therefore preserves evidence for the first appearance of monazite in progressively more peraluminous magmas and also indicates that most zircon crystallised at an earlier stage of magma evolution relative to other minerals in more peraluminous and silicic magmas (Fig. 3.4).

In Zone 3, zircon-hosted apatites are found to have the highest Sr concentrations. Assuming that Sr concentrations are primarily governed by the proportion of feldspar crystallisation (Belousova et al. 2001; Jennings et al. 2011), the most Sr-rich apatites represent some of the earliest formed crystals. Their restriction of such apatites within zircon supports REE evidence for the early saturation of zircon in these magmas relative to other phases during final crystallisation. Unlike REE patterns, there is also more compositional overlap between the Sr contents of zircon-hosted apatites and those hosted by other major phases. This may reflect the independent controls on Sr and REE budgets (the former controlled mainly by feldspar, the latter by accessory phases).

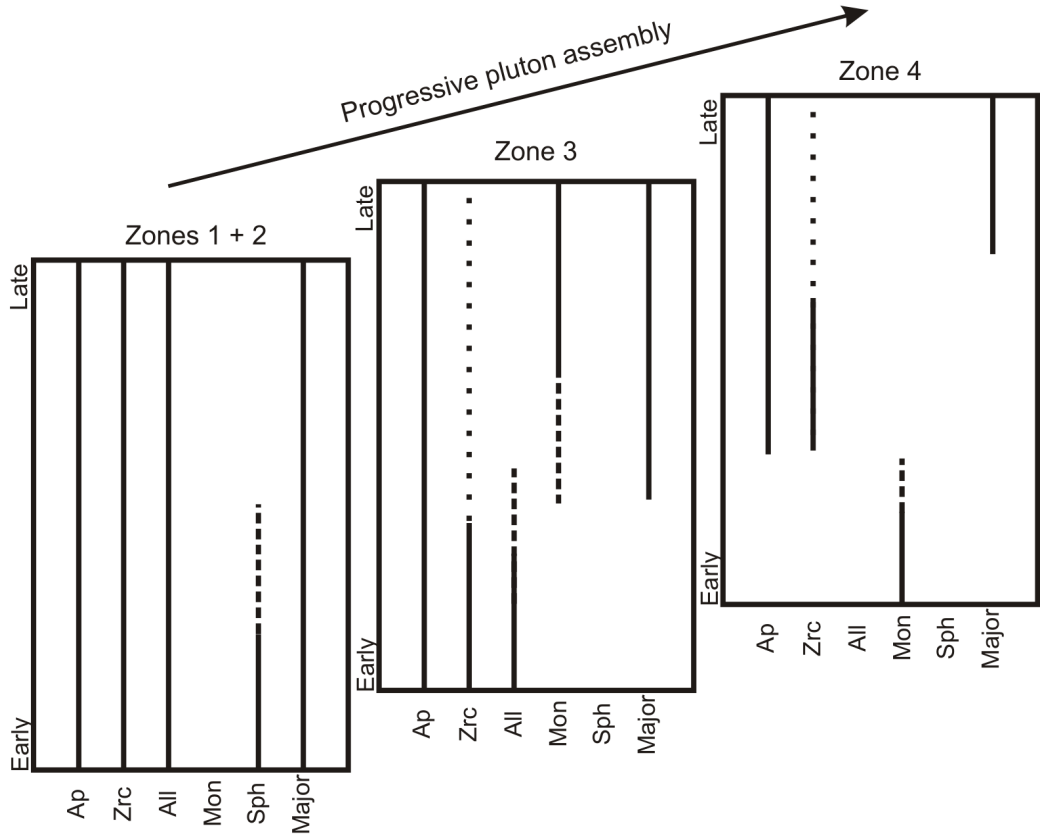

Figure 3.4 Schematic illustration of the crystallisation orders of minerals in different zones of the Criffell pluton. Time increases vertically while it is assumed that zones 1 to 4 were emplaced at progressively later staged of pluton assembly (Stephens et al. 1985). Solid lines represent high certainties of crystallisation, long dashes represent greater uncertainty and small dashes represent mineral overgrowths. Abbreviations are as follows: Ap = apatite, Zrc = zircon, All = allanite, Mon = monazite, Sph = sphene, Major = all observed major mineral phases (hornblende, biotite, feldspars and quartz).

5.3 Wider implications

Constraining the relative timing of accessory mineral crystallisation, and in particular that of zircon, enables both their stable and radiogenic isotope compositions to be better placed in the context of often protracted magmatic histories. Whereas many I-type granites have been shown to represent the products of multiple magmas derived from different sources and varying degrees of magma mixing (e.g. John and Wooden, 1990; Ferreira et al. 2003; Gerdes et al. 2002; Kemp et al. 2007; Kemp and Hawkesworth, 2003; Lackey et al. 2005, 2006; Miller et al. 1990), S-type granites were once attributed solely to the melting of sedimentary material (Chappell and White, 1974). However, recent oxygen isotope studies have revealed that the zircons of some S-type granites have mantle-like $\delta^{18}O$ compositions, indicative of more primitive magmas not detected in WR compositions (Kemp et al. 2008; Appleby et al. 2010). Zircons from individual samples of some S-type granites from the East Scottish Highlands (Appleby et al. 2010) and the Lachlan Fold Belt of Australia (Kemp et al. 2006a) exhibit considerable inter-grain isotopic variability. This variability has been attributed to mixing between newly emplaced magmas from a crustal hot zone and silicic magmas resident at the level of pluton emplacement. Where isotopic variability is evident, the preservation of more primitive isotopic compositions may simply be a consequence of magma mixing (Appleby et al. 2010). However, this study demonstrates that in peraluminous magmas these compositions may to some extent also reflect crystallisation during earlier stages of magma differentiation. Although the mineral assemblage of the Criffell pluton represents only the final crystallisation of magmas with compositions pre-determined at much deeper crustal levels (Chapter 2), these conclusions are applicable to all magmas of a similar composition and to situations where WR chemistry may continue to evolve in conjunction with crystallisation of the observed mineral assemblage. The small numbers of zircon crystals found in the most silicic zones of the Criffell pluton reflect the difficulties of crystallising zircon from Zr-depleted magmas. Despite evidence from zircon for the involvement of more primitive magmas in the formation of large S-type plutons (Appleby et al. 2010; Kemp et al. 2006a), WR compositions show that the volumes of more primitive magmas are likely to be small relative to

those of more evolved and silicic components. However, the difficulties of crystallising zircon in highly silicic (SiO_2 > ~ 70 wt %) and often Zr-depleted magmas relative to the ease with which zircon appears to crystallise in more Zr-rich, granodiorites may also explain a probable bias in the isotope compositions preserved by zircon in S-type plutons. Most zircon isotope compositions in granodiorites therefore record a more prolonged history of magma evolution relative to those from peraluminous magmas.

In contrast to the results of this study, textural evidence in other studies suggests that in many rock types, particularly those with more primitive (SiO_2-poor) compositions and formed at higher temperatures, zircon crystallised at later stages of crystallisation (Maas et al. 1992; Hoskin et al 2000; Cavosie et al. 2004; Hopkins et al. 2008; Darling et al. 2009; Nutman and Hiess, 2009; Jennings et al. 2011). Zircon in magmas of different compositions therefore document different stages and durations of magma history. Caution is therefore required when making direct comparisons between zircon compositions extracted from magmas of varying peraluminous composition. Comparative studies of apatite inclusions in different hosts provide a potentially powerful means of interpreting the isotopic compositions of zircons in the context of the protracted and complex evolutionary histories in silicic magmas.

6. Conclusions

1. Apatite crystallised in response to bulk saturation in the Criffell pluton and is present as inclusions in all major mineral phases including zircon. Calculated apatite saturation temperatures are ~ 900^{o}C and are in excess of the wet granite solidus and crystallisation temperatures of <700^{o}C estimated from Ti-in-zircon and amphibole-plagioclase mineral thermometers. These temperatures suggest early saturation of apatite in the Criffell magmas, ensuring their capacity to record the crystallisation history of the magmas.
2. In metaluminous zones, Ce concentration decreases primarily in response to allanite crystallisation. Apatites that crystallised at progressively later stages of crystallisation inherit lower concentrations of Ce. All host minerals encapsulate apatites that span a similar range of Ce concentrations and show no host dependence. There is no evidence to suggest that different host minerals crystallised at distinctly different stages of crystallisation in these zones.
3. Decreasing Sr concentration in apatite is used to track increasing degrees of plagioclase crystallisation. Peak Sr concentrations in apatites hosted by different phases reflect the onset of host crystallisation relative to plagioclase. Most peak Sr concentrations from different hosts from the same metaluminous samples lie within analytical error of each other. However, apatites with the highest peak Sr concentration are found in zircon in all zones of the pluton, indicating that zircon saturated at an early stage of crystallisation in all zones of the pluton.
4. Apatites in the most peraluminous magmas are displaced to lower Ce and higher Y values relative to those in metaluminous zones. The absence of monazite-induced negative Nd anomalies in the WR and the lack of further depletion in Ce seen during apatite crystallisation suggest that it crystallised after WR compositions were determined but before apatite saturation during final crystallisation. Of the zones where monazite crystallisation is evident, only in a transitional zone (Zone 3) between metaluminous and peraluminous compositions did zircon and apatite saturation occur before that of monazite.

Peak Sr concentrations are found in zircon-hosted apatites in Zone 3, supporting earlier crystallisation of zircon relative to feldspar in the transitional zone (Zone 3). Apatites that formed at later stages of crystallisation are likely to have lower concentrations of Y that reflect the crystallisation of zircon and apatite.

5. Zircon-hosted apatites may be distinguished from those hosted by other phases in peraluminous zones and are characterised by more Y-rich compositions. Assuming a general trend of Y depletion in response to increasing degrees of accessory mineral crystallisation, zircon-hosted apatites formed at relatively earlier stages of crystallisation relative to those in other host phases. Overlap in the compositions of apatites hosted by most phases other than zircon suggests simultaneous crystallisation of these phases.
6. The earlier crystallisation of zircon relative to other mineral phases in peraluminous magmas may help to explain why there is an apparent bias towards more primitive isotope compositions in zircons found in some large S-type plutons. Additionally, the low abundance of zircon in highly silicic magmas (SiO_2 > ~ 70 wt%) in the Criffell pluton reflects low concentrations of Zr in these magmas. Despite the likelihood of only small volumes of more primitive magmas in the formation of S-type plutons, the elevated Zr concentrations of granodiorite magmas like those of the outer zones of Criffell may enable easier and more abundant crystallisation of zircon, thereby also biasing the zircon isotopic record in heterogeneous magmas.

Chapter 4

Mn in apatite: A new redox proxy for silicic magmas[†]

Abstract

The oxidation states of magmas provide valuable information about the valency state and speciation of redox sensitive elements, the release and speciation of volatile elements during volcanic eruptions, source rock compositions, open system magmatic processes and tectonic settings. Increased Mn concentrations in apatite in granitic rocks from the zoned Criffell granitic pluton (southern Scotland) correlate with decreasing Fe_2O_3 (Fe^{3+}) and Mn in the whole-rock (WR) and reflect increased Mn^{2+}/Mn^{3+} and greater compatibility of Mn under reduced conditions. A transition from oxidised outer zones to reduced inner zones is supported by oxygen fugacities (fO_2) calculated using redox sensitive Ce anomalies in magmatic zircons. Median fO_2 values show that zircon in the outer zones (metaluminous granodiorite) crystallised from magmas that were ~ 2.5 log units above the fayalite-magnetite-quartz (FMQ) buffer. By contrast, zircons from inner zones (peraluminous granite) crystallised from reduced magmas that were ~ 2 log units below the FMQ buffer. Apatite Mn concentrations provide a new and independent means of constraining relative redox changes in a wide spectrum of magma compositions that may be experimentally calibrated. The method may be applied to lunar magmas, silicic volcanic rocks and potentially detrital studies.

[†] Co-authors: Colin Graham – *University of Edinburgh*; Chris Hawkesworth – *University of St Andrews*; Martin Gillespie – *British Geological Survey*; Richard Hinton – *University of Edinburgh*; EIMF

1. Introduction

Constraining the redox state of magmas is important for understanding the molecular speciation of volcanic gases containing sulphur, carbon and hydrogen exsolved on eruption, and is thus a key link in constraining the composition of the early Earth atmosphere (Trail et al. 2011; Scaillet and Gaillard, 2011; Binder and Keppler, 2011). Sulphur emissions from explosive and oxidised silicic magmas may significantly exceed those from reduced magmas (Scaillett et al. 1998) and may thus have a significantly greater climatic impact (Robock, 2000). Redox conditions and their variations also provide important constraints on magma sources and evolution. It is widely accepted that calc-alkaline magmas are more oxidised than their tholeiitic counterparts (Gill, 1981; Arculus, 2003; Carmichael, 1991; Kelly and Cottrell, 2009; Lee et al. 2010). This is reflected in Fe depletion during differentiation of calc-alkaline magmas that results from the stabilisation of Fe^{3+}-bearing oxide minerals under more oxidising conditions (Gill, 1981). Quantitative estimates of redox conditions are calculated using oxygen fugacity (fO_2) – a measure of the availability and capacity of oxygen to participate in reactions of minerals and fluids. However, it remains unclear to what extent the higher oxygen fugacities of calc-alkaline magmas are inherited from source regions or develop through differentiation and assimilation (see Lee et al. 2010) or redox reactions during degassing (Holloway et al. 2004). Irrespective of why calc-alkaline magmas are more oxidised, their association with subduction processes (e.g. Ishihara, 2004) may enable better constraints to be placed on the tectonic environments in which igneous materials formed.

Estimating the fO_2 conditions of magmas has traditionally relied on the measured Fe^{2+}/Fe^{3+} ratios of magmatic glasses and mineral phases (Carmichael and Ghiorso 1990). These methods are undermined by the effects of subsequent alteration, but these can to some extent be overcome by examining heterovalent transition elements such as V and Cr that are generally immobile during alteration, but whose partitioning is redox-sensitive (Canil, 1997). The concentration of redox sensitive elements such as Fe, Mn, Ce and Eu in robust accessory minerals offers great

potential in obtaining reliable estimates of redox conditions. Ce anomalies in zircon have recently been calibrated experimentally by Trail et al. (2011) to determine the oxidation state of Hadean magmas. The Mn content of apatite has also been shown to be redox sensitive in silicic rocks (Sha and Chappell, 1999; Hoskin et al. 2000; Belousova et al. 2001; 2002; Chu et al. 2009). We have adapted and developed the use of accessory minerals to determine redox conditions (fO_2) in silicic magmatic rocks, using the post-Caledonian granitic Criffell pluton in southern Scotland as a case study. We examine the extent to which Ce anomalies in zircon and the redox state of Mn in apatite are correlated. Apatite Mn compositions may permit robust estimates of redox conditions in a wide spectrum of magma compositions and may also be applied to detrital minerals, and to terrestrial and lunar magmas.

2. The Criffell pluton

The Criffell pluton is one of a large number of post-Caledonian granitic plutons in northern parts of the United Kingdom. The pluton was emplaced at ~397 Ma (Halliday et al. 1980) into low-grade wackes and pelites of Llandovery to Wenlock (444 to 423 Ma) age that form part of the Southern Uplands accretionary prism in southern Scotland (Fig. 4.1). The pluton is normally zoned (Stephens et al. 1980, 1985), with outer zones (1 and 2) of metaluminous granodiorite (~ 58 wt % SiO_2), a transition Zone (3), and inner zones (4 and 5) of peraluminous granite (~ 72 wt % SiO_2). Granodiorite samples contain primary hornblende (with occasional cores of clinopyroxene), biotite, plagioclase, potassium feldspar, quartz and accessory sphene, zircon, apatite, allanite and magnetite (with very minor haematite). Granite samples contain primary muscovite and small amounts of monazite but lack hornblende, sphene and the abundant zircon and magnetite that characterise the granodiorite. The small amounts of magnetite in the most silicic zone containing zircon (Zone 4) have ilmenite (and potentially rutile) trellis exsolution lamellae (Fig. 4.2).

A general trend of decreasing Fe_2O_3 with indices of differentiation (e.g. SiO_2) in the whole-rock (WR) suite, together with independent estimates of oxygen fugacity from

Fe compositions in biotite have been attributed to a gradual transition from more oxidising conditions in outer zones (close to the haematite-magnetite buffer) to less oxidising conditions in the inner zones (close to the nickel-nickel oxide buffer) (Stephens et al. 1985). Abundant early crystallised sphene and magnetite in the granodiorite is consistent with more oxidising conditions (Wones, 1966). A gradual decrease in the modal abundance of these minerals and the presence of minor ilmenite trellis exsolution textures (Fig. 4.2) in magnetite indicate that more granitic magmas became progressively more reduced (Pinto and Hartmann, 2011).

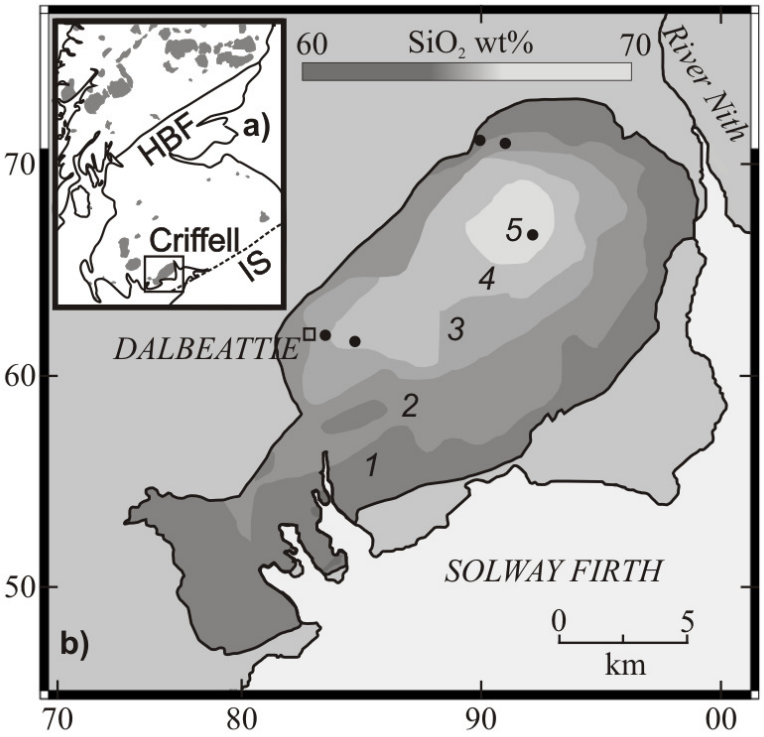

Fig. 4.1 a) Regional map of major Scottish plutons. Abbreviations: HBF – Highland Boundary Fault, IS – Iapetus Suture. b) Map of the Criffell pluton. Paler shading reflects increasing WR SiO_2. Compositional contour are plotted from Stephens and Halliday (1980). Zone mineralogy is as follows: 1) clinopyroxene-biotite-hornblende granodiorite; 2) biotite-hornblende granodiorite; 3) biotite granite; 4) biotite-muscovite granite 5) muscovite-biotite granite. Minerals listed in order of increasing modal abundance (Stephens et al.. 1985). Black points denote sample sites.

Apatite crystals up to 1mm long are prevalent in all zones of the pluton, typically occurring as inclusions in most minerals including zircon. Apatite compositions have been shown to reflect bulk compositional changes in the magma (Chapter 2). Zircon

occurs in all zones, although the presence of only rare and highly fractured crystals in Zone 5 (innermost granite) probably reflects low Zr concentrations in the melt and possible radiation damage. Unpublished U-Pb ages obtained as part of this study reveal no inherited zircon in any part of the pluton, consistent with the conclusions of an earlier study (Pidgeon and Aftalion, 1978). The general absence of resorption surfaces within concentrically zoned zircon crystals indicates that most are primary and do not represent antecrysts.

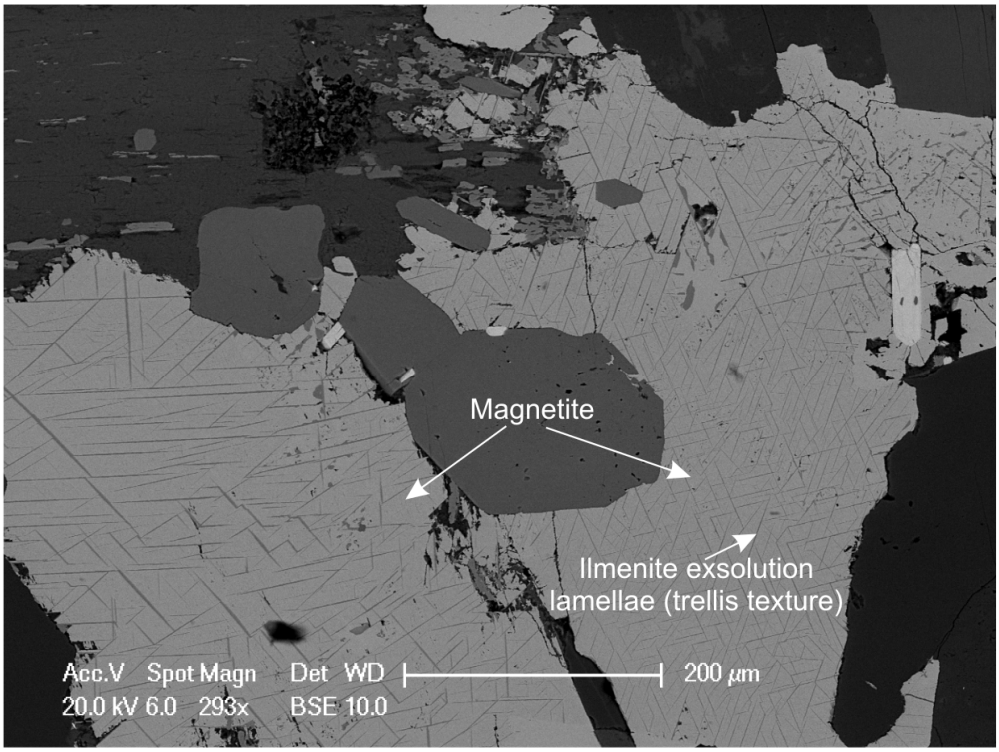

Fig. 4.2 Back-scatter Scanning Electron Microscope (SEM) image of ilmenite (and potentially rutile) trellis-like oxidation-related exsolution lamellae in a magnetite host from Zone 4 of the Criffell pluton. Exsolution lamellae are not seen in magnetite from other zones.

3. Methodology

WR major oxide compositions were determined by Stephens and Halliday (1980) using 'rapid wet' methods and the two-solution method of Riley (1958). SiO_2 and Al_2O_3 were analysed by automatic spectrophotometric methods; Na_2O and K_2O by atomic emission; total FeO, MnO, MgO and CaO by atomic absorption; TiO_2 and P_2O_5 by automatic colorimetry; and ferrous iron by titration with potassium dichromate.

Apatites from the outer four zone of the pluton were analysed in thin section to provide textural context. Zircon-hosted apatite was analysed following standard heavy liquid and magnetic separation of zircon and mounting in epoxy blocks. Mn abundances were measured using a Cameca SX-100 at the University of Edinburgh and converted from weight % concentrations to ppm. Analyses were carried out using PC0, LTAP, LPET and LIF dispersion crystals and a wavelength dispersive method (WDS). A ~1 μm beam was used with 20 kV and 60 nA beam conditions used for trace and most major elements, with a 10 nA defocused beam used for alkalis to minimise loss during analysis. The quality of analysis spots was determined using back-scattered electron (BSE) and cathodoluminescence (CL) images of polished surfaces obtained with a Philips XL30P Scanning Electron Microscope (SEM) at the University of Edinburgh.

Approximately 100 zircon crystals per sample were separated, with ~ 10 crystals per sample analysed by ion microprobe at the University of Edinburgh using a Cameca ims-4f ion microprobe. Zircon trace elements were analysed at 15 keV net impact energy using a ~ 15 μm diameter primary O^- beam at ~5 nA with 4.5 keV secondary positive ions measured at ~ 120 keV offset following the method of Hinton and Upton (1991). Ten cycles were carried out due to the low abundance of some REE in zircon. All analyses were standardised using a NIST SRM-610 glass standard (trace element concentrations based on Pearce et al. 1997) and referenced against Si. 91500 (Weidenbeck et al. 2004) was used as a secondary zircon standard. Count rates

measured at mass 134 were used to correct overlap of $ZrSiO^+$ with $^{138}Ba^+$,$^{139}Ba^+$, $^{140}Ce^+$and $^{141}Pr^+$and light REE-oxide overlap onto HREE. Measurements of zircon standard 91500 were also used to correct for interference of LREE on HREE and Hf^{2+} on Y.

4. Results

4.1 Mn and Fe contents in apatites and whole-rocks

Total Mn concentrations in apatite increase systematically by up to a factor of ~ 27 between Zone 1 (190 – 582 ppm) and Zone 4 (1713 - 5076 ppm) (Fig. 4.3c; Appendix E). Mn in the WR decreases by a factor of ~ 2 with increasing SiO_2 (Fig. 4.3a, c; Appendix E), suggesting that Mn is more easily partitioned into apatite in more silicic zones. There is no evidence to suggest that the Mn concentration of apatite inclusions is dependent on the host mineral (Appendix E). Total Fe concentrations do not appear to vary between zones, and lie mostly between ~100 and 4600 ppm with similar degrees of variability within and between zones (Fig. 4.3d). However, unlike Mn, Fe concentrations show marked increases in apatites hosted by Fe-rich minerals such as hornblende and biotite, implying some degree of Fe exchange between apatite inclusions and their Fe-rich hosts. Fe concentrations in apatites hosted by Fe-poor minerals such as zircon, quartz and feldspars mirror the trends shown by Mn and increase from between ~ 100 - 300 ppm in zones 1 and 2, 140 - 840 ppm in Zone 3 and 260 – 1700 ppm in Zone 4 (Fig. 4.3c). WR Fe_2O_3 (Fe^{3+}) varies from 0.28 wt% to 2.61 wt% and shows a general decrease with increasing SiO_2 (Fig. 4.3b). Mn/Fe ratios in apatites (excluding those hosted in hornblende and biotite due to Fe exchange) show an increase in their maximum values from Zone 1 (all < 3) to Zone 4 (all < 12). There is also an increase in MnO/FeO_{Total} (where total refers to Fe_2O_3 + FeO) ratios in the WR suite from 0.017 to 0.035 with increasing SiO_2.

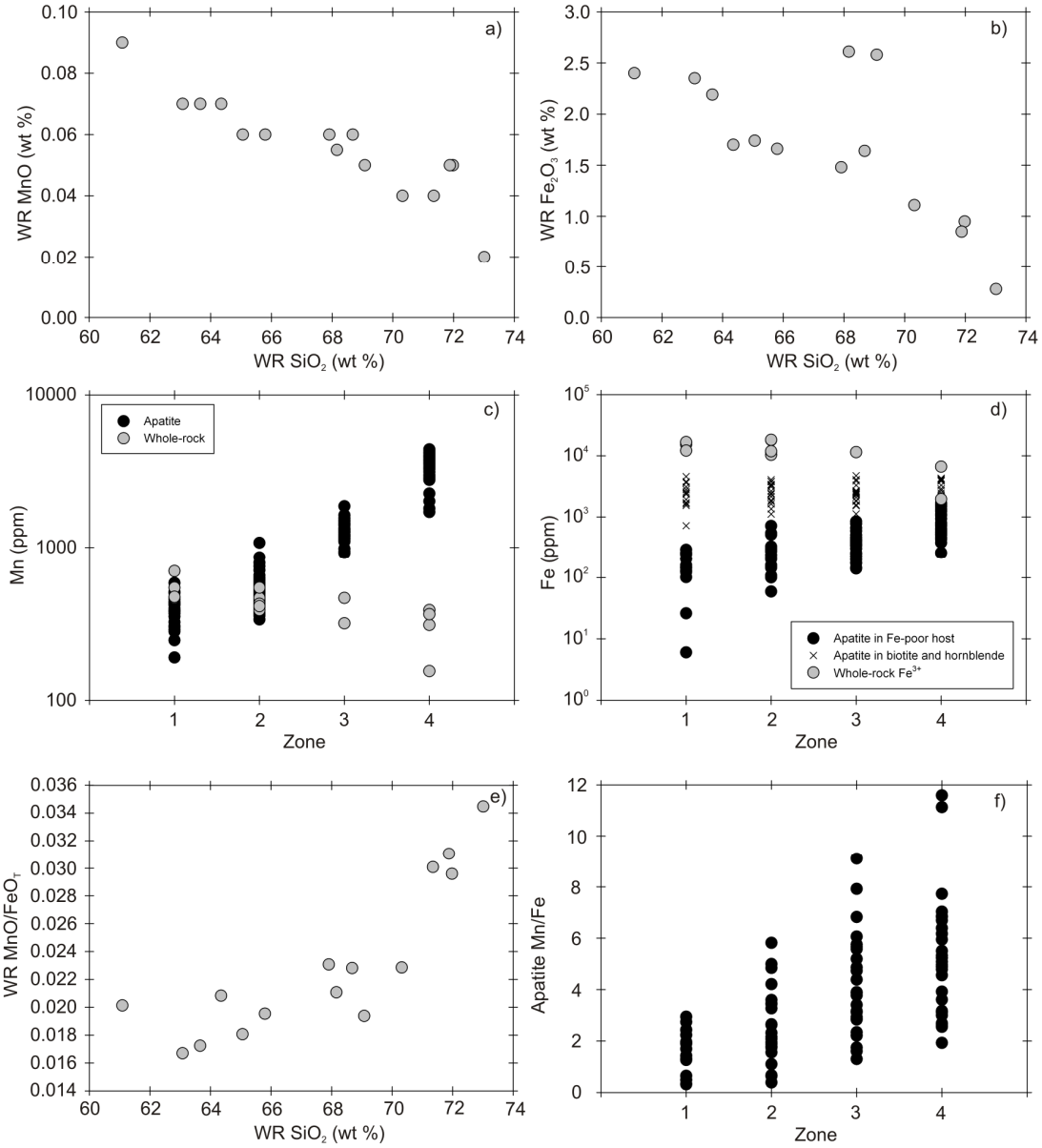

Fig. 4.3 a) WR MnO vs. SiO_2 for all zones; b) WR Fe_2O_3 vs. SiO_2 for all zones; c) WR (grey) and apatite (black) Mn concentrations (re-calculated as ppm) for different zones of the pluton. Mn concentrations decrease from outer (Zone 1) to inner (Zone 4) zones while apatite concentrations increase, reflecting increasingly compatible substitution of Mn into apatite. d) WR (grey) Fe_2O_3 in different zones of the pluton, apatite hosted in Fe-poor minerals (zircon, feldspars, quartz) (black) and apatite hosted by Fe-rich biotite and hornblende (crosses) plotted for different zones of the pluton. The general decrease in Fe_2O_3 in the WR is evident along with a general increase in apatite Fe concentrations for those hosted by Fe-poor minerals. Apatite hosted by Fe-rich minerals has higher Fe concentrations and appears to have undergone Fe-exchange with their hosts. Data from apatites hosted by Fe-poor minerals excludes 4 anomalously high data points. e) Increasing WR MnO/FeO_{Total} vs.SiO_2; f) Increasing Mn/Fe in apatites hosted in Fe-poor minerals only and excluding the same anomalous data points as in (d). EPMA 2σ analytical error on Mn concentrations in apatite is ~ ±150 ppm.

4.2 Ce in zircon and crystallisation temperatures

Positive Ce anomalies are a common feature of igneous zircon (Fig. 4.4; Appendix J), reflecting the ability of Ce to exist as both Ce^{3+} and Ce^{4+} under oxidising conditions (Hinton and Upton, 1991; Ballard et al. 2002; Hoskin and Schaletgger, 2003; Trail et al. 2011). At magmatic temperatures, homogenisation of REE concentrations at a 10 μm scale in zircon only occurs on timescales greater than the age of the Earth (Cherniak and Watson, 2003). Unlike Eu anomalies, Ce anomalies are not influenced by feldspar crystallisation. Evidence suggests that the large Ce anomalies in zircon reflect a ~ 4 to 6 orders of magnitude increase in the compatibility of Ce^{4+} relative to Ce^{3+} (the latter represents 99.0% - 99.7% of the total Ce in most melts) rather than large increases in the abundance of Ce^{4+} (Colombini et al. 2011). The increased solubility of Ce^{4+} is likely to result from similarities in its size and charge relative to Zr^{4+} with which it substitutes. Ce anomalies are conventionally calculated using the expression $Ce/Ce^* = Ce_N/(La_N \times Pr_N)^{1/2}$ where element abundances are normalised (N) to the Chondritic Uniform Reservoir (CHUR). Median Ce/Ce* values for apatite in zones 1 to 3 of the Criffell pluton are similar and range from 52 to 63, while the median value for Zone 4 is much lower at 28. Every zone is characterised by significant scatter in Ce/Ce* values, the three outermost zones having interquartile ranges (within which 50 % of the data reside) of ~ 18 to 34 while the innermost analysed zone (Zone 4) has an interquartile range of ~ 107.

Zircon crystallisation temperatures have been calculated (Appendix I) using the modified Ti-in-zircon thermometer of Ferry and Watson (2007), allowing for variations in the activity of Si and Ti. The inherent problems of assessing these activities at the time of zircon crystallisation mean that the thermometer provides only semi-quantitative estimates of crystallisation temperatures. However, overestimates or underestimates of silica and titanium activities result in offsetting errors in crystallisation temperatures (Ferry and Watson, 2007). The abundance of quartz in all zones makes it likely that silica activity was close to unity during zircon saturation, so estimated crystallisation temperatures will be towards the top of the

range. A lack of rutile in analysed samples indicates that titanium activity was below unity; however the presence of other Ti-rich phases such as sphene in the outer zones of the pluton indicate that it was not very low (an observation made in other plutons, e.g. Hayden and Watson, 2007; Claiborne et al. 2010). We therefore assume a titanium activity value of 0.7 following a similar study by Claiborne et al. (2010). Average zircon crystallisation temperatures and standard deviations are 680 (± 32) ^{o}C 669 (± 24) ^{o}C, 681 (± 38) ^{o}C and 634 (± 32) ^{o}C in zones 1 to 4 respectively.

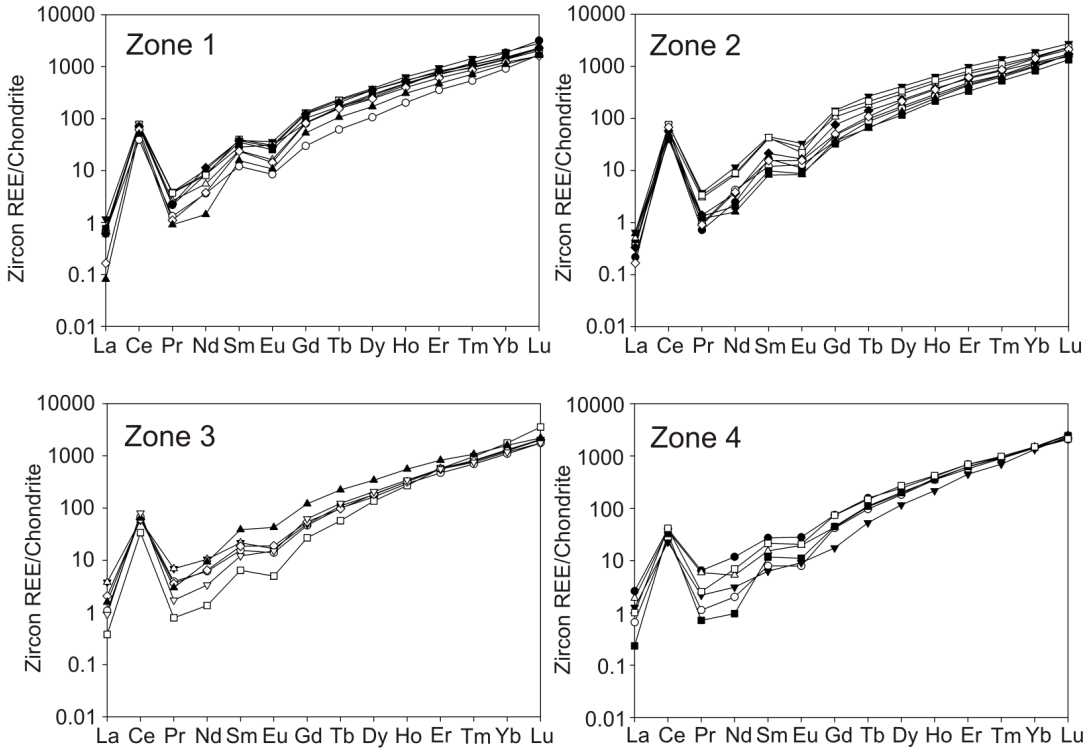

Fig. 4.4 Chondrite-normalised zircon REE profiles for different zones of the Criffell pluton. Compositions determined using a Cameca 4f ion microprobe at the University of Edinburgh.

5. Discussion

The decoupling of apatite and WR Mn compositions in a range of plutons (Sha and Chappell, 1999; Belousova et al. 2001; 2002; Chu et al. 2009) indicates that Mn concentrations in apatite are largely independent of the major element composition of the original melts. These studies have developed the use of apatite as a provenance indicator based on the different concentrations of Mn and other elements in apatites from different granite sources. Although links have been drawn between the abundance of Mn in apatites and the redox states of different granitic magmas (e.g. Belousova et al. 2001), no attempt has yet been made to determine fO_2 values and to evaluate the extent to which redox proxies in magmatic apatite and zircon are complementary to each other and to independent redox proxies.

5.1 Redox controls on apatite compositions

As the most abundant group of phosphate minerals, apatites are a common constituent of igneous rocks. The apatite structure consists of rigid PO_4 tetrahedra, a 9-fold Ca1 site and a Ca2 site bonded to six oxygen atoms and one anion (Cl, F, OH). Despite having the general formula $Ca_{10}(PO_4)_6(OH,F,Cl,Br)_2$, the apatite structure is highly tolerant to structural distortion and chemical substitutions and can therefore display a wide variety of compositions (Pan and Fleet, 2002). A large number of cation species are able to substitute into apatite as a result of its structural tolerance, including redox sensitive elements like Mn, Fe and the REEs. The maximum Mn content in natural fluorapatite is 1.37 Mn per formula unit, with Mn^{2+} substituting preferentially onto Ca1 sites (Pan and Fleet, 2002). Despite the absence of speciation curves and only some spectroscopic data to support Mn^{5+} substitution for P^{5+} (Hughes et al. 2004), the ability of apatite to incorporate REEs strongly implies that Mn^{3+} might also be present in the apatite structure under appropriate redox conditions.

In the Criffell pluton the Mn content of apatite increases in tandem with decreasing ferric iron (Fe^{3+}) in the WR (Fig. 4.3), which is in turn strongly controlled by the redox state of the magma (Lee et al. 2010 and references therein). Higher concentrations of Fe^{3+} (Stephens et al. 1985) and an absence of ilmenite exsolution in magnetite in the granodiorite of zones 1 and 2 result from more oxidising conditions, which should also result in higher Mn^{3+}/Mn^{2+} in these magmas. By contrast, the innermost granites (zones 4 and 5) are characterised by lower WR Fe^{3+} and show exsolution lamellae of ilmenite within magnetite hosts, reflecting more reducing conditions (Pinto and Hartmann, 2011). The increased compatibility of Mn in apatites from reduced zones of the pluton is likely to result from increased Mn^{2+} relative to Mn^{3+} in these zones. Mn^{2+} exhibits similarities in ionic radius when in 7- (0.9Å) and 9-fold (1.0Å) coordination with that of Ca^{2+} (1.14Å) with which substitution occurs. By comparison, Mn^{3+} has an ionic radius of 0.62Å to 0.67Å depending on the degree of distortion, and requires the substitution of additional charge balancing ions.

Despite its theoretical potential, it is necessary to evaluate the extent to which the observed variations in Mn reflect magmatic conditions at the time of crystallisation and not later modifications. Silicic magmas generally crystallise at temperatures of ~750^{o}C, consistent with the results of Ti-in-zircon thermometry in the Criffell pluton (Appendix I). At these temperatures, diffusive loss of Mn will occur in apatite crystals with an effective radius of 0.5 mm on timescales of ~10^5 to 10^6 years (Cherniak, 2005). However, silicic plutonic rocks are unlikely to be held at such temperatures for extended periods of time and particularly when they are assembled incrementally by the emplacement of small melt batches, as is thought to have occurred during development of the Criffell pluton (Chapter 2). Once cooled to below 600^{o}C, apatites will only incur diffusive loss on timescales of ~10^8 years (Cherniak, 2005). Furthermore, a number of the apatite crystals analysed as part of this study are significantly greater than 0.5mm in size. It is therefore reasonable to assume that apatite retains Mn concentrations from the time of crystallisation providing subsequently prolonged and extreme thermal events can be ruled out.

Published partition coefficient data for Mn in apatite are rare and it remains difficult to fully assess the effects of changing temperature on Mn partitioning. However, calculated zircon crystallisation temperatures (Appendix I) indicate little change in the temperatures at which crystallisation occurred in different zones of the pluton. Nonetheless, some effect on Mn partitioning caused by changes of temperature during crystallisation cannot at present be ruled out.

Fe can constitute up to ~ 1wt % in apatite while Mössbauer spectroscopy suggest that Fe^{2+} is readily substituted onto both Ca sites (Pan and Fleet, 2002). Despite a lack of published evidence for Fe^{3+} incorporation in apatite, it would appear plausible from crystal chemistry arguments in a similar manner to Mn^{3+} discussed previously. Fe concentrations in apatite are expected to follow similar patterns to Mn, with increasing substitution of more compatible Fe^{2+} relative to Fe^{3+} under reduced conditions. However, our data reveal substantial scatter in the concentration of Fe in apatites that appears to be related to exchange with nearby Fe-rich phases such as hornblende and biotite (Fig. 4.3d). This scatter is not evident in the Mn concentrations of apatite, which do not show any relation to their host phase. Fe analyses in apatites hosted by Fe-poor minerals like quartz and feldspars appear to follow the expected trend, with increased concentrations of Fe in apatites from more reduced zones (Fig. 4.3d). Diffusion data for Fe in apatite are not available; however, the ability of Fe to exchange between apatite and other minerals limits its use in developing a redox proxy, particularly in detrital studies where original textural context is not available.

In primitive, mantle-derived rocks, where Mn and Fe are present almost exclusively as Mn^{2+} and Fe^{2+} respectively (Canil et al. 1994), Mn/Fe ratios have been shown not to vary in response to different degrees of partial melting or fractional crystallisation (Ruzika et al. 2001). This is thought to reflect the similar partitioning behaviour of both elements (Qin and Humayun, 2008). In support of this, many studies indicate near constant values of Mn/Fe in mantle-derived rocks within individual planetary

bodies (Laul et al. 1972; McDonough and Sun, 1995; Ruzicka et al. 2001). However, in this study and others (Cerny et al. 1985; London et al. 2001), granitic suites of rocks show increases in MnO/FeO_{Total} ratios with indices of differentiation like SiO_2. This effect is likely to result from the ability of biotite to preferentially fractionate Fe ($Kd_{Bt/melt} \approx 25$) from Mn ($Kd_{Bt/melt} \approx 5$) in silicic rocks. It is therefore difficult to assess the degree to which the increases in Mn/Fe seen in apatites from more silicic zones reflects redox and/or crystallisation effects.

Unlike other redox sensitive elements and element ratios in apatite, Mn concentrations have the potential to provide a relatively unambiguous and reliable indicator of redox states in the magmas from which apatites crystallised.

5.2 Redox states determined from zircon

The positive Ce anomaly commonly seen in igneous zircon has long been considered to reflect redox conditions in the melt at the time of crystallisation (Hinton and Upton, 1991; Ballard et al. 2002; Trail et al. 2011). In a recent experimental study, Trail et al. (2011) calibrated the magnitude of the Ce anomaly against fO_2 at 900-1300ºC, and applied their method to natural Hadean zircons from Jack Hills (W Australia) in order to examine the oxidation state of their original host magmas.

The Ce/Ce* values of zircons from zones 1 to 4 and their crystallisation temperatures have been used to calculate fO_2 using the experimentally calibrated expression of Trail et al. (2011). These values are reported relative to the fayalite-magnetite-quartz (FMQ) buffer (at standard pressure conditions of 1 bar) for each calculated crystallisation temperature in log units (ΔFMQ). Each unit represents one log unit deviation in fO_2 from the FMQ buffer, where positive values signify more oxidised conditions and negative values more reduced conditions than those of the buffer. Median ΔFMQ values decrease steadily from +2.5 to +2 to -0.8 to -2 log unit deviations from the FMQ buffer in zones 1 to 4 respectively (Fig. 4.5). However, there is also significant intra-sample scatter, with interquartile ranges up to ~ 10 log units in Zone 4, similar to those reported by Trail et al. (2011).

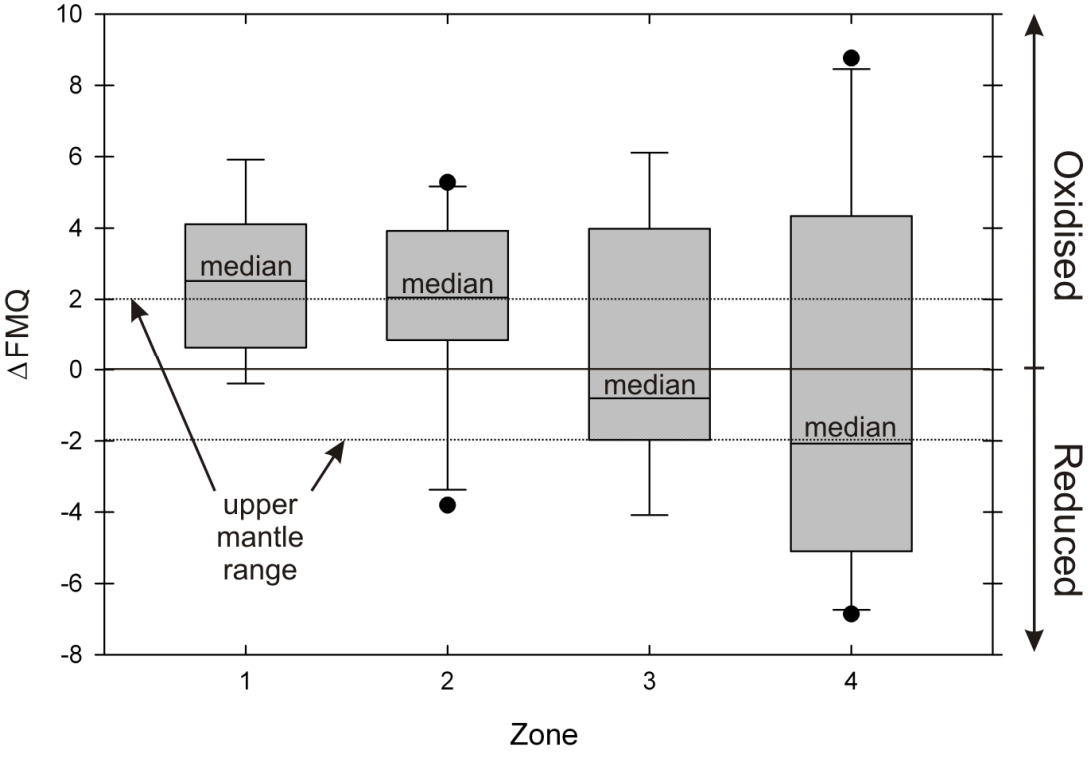

Fig. 4.5 Oxygen fugacity values calculated using the expression of Trail et al. (2011) plotted as log unit deviations from the fayalite-magnetite-quartz (FMQ) buffer (Frost 1991) (ΔFMQ). Horizontal lines represent median values and the upper and lower box boundaries represent interquartile ranges. Error bars represent 1.5 times the interquartile range and data points outside of these regions are considered outliers. Upper mantle oxygen fugacities are from Delano 2001; Mallmann and O'Neill 2009 and Frost and McCammon 2008.

Most of the variability in the calculated values of fO_2 appears to result from the estimation of Ce/Ce*, which is strongly dependent on La and Pr abundances in zircon since $Ce/Ce^* = Ce_N/(La_N \times Pr_N)^{1/2}$. The measured concentrations of LREE in natural zircons vary significantly (Hanchar and van Westrenen, 2007). Such variability may in part reflect possible inclusions of LREE-rich phases like allanite and monazite in zircon crystals (Nagasawa, 1970). Inclusion concentrations as low as 0.01 to 0.001 volume % may have a significant effect on the measured LREE content of zircon (Jain et al. 2001). Small amounts of monazite found in heavy mineral separates from Zone 5 support the possibility that small inclusions may be present in more peraluminous zones, and may in part account for the larger scatter in fO_2 values in these zones. Ion microprobe analyses of LREE concentrations in zircon are close

to background levels (analytical errors for La are ~14% in this study). The variability in measured LREE concentrations has a significant effect on the predicted Ce* value, which in turn has a larger effect on estimated Ce/Ce* ratios and calculated fO_2 values. Conventional methods of calculating Ce/Ce* may permit general trends to be inferred when using median values; however, large ranges in calculated fO_2 values such as those reported by Trail et al. (2011) should be considered carefully in light of these effects.

6. Wider implications and concluding remarks

Despite significant uncertainties related to the interpretation of Ce anomalies in zircon, it remains necessary to use an integrated zircon-apatite approach to obtain quantitative estimates of fO_2 from apatite Mn concentrations (Fig. 4.6). The relatively large variance shown by zircon relative to apatite in Fig. 4.6 alludes to the potential that may lie in using apatite as a more robust proxy for determining redox conditions. Once calibrated, the presence of apatite in a wide spectrum of magma compositions means the method can be deployed beyond the realm of zircon-rich silicic magmas and to a wide range of geologically relevant fields of research.

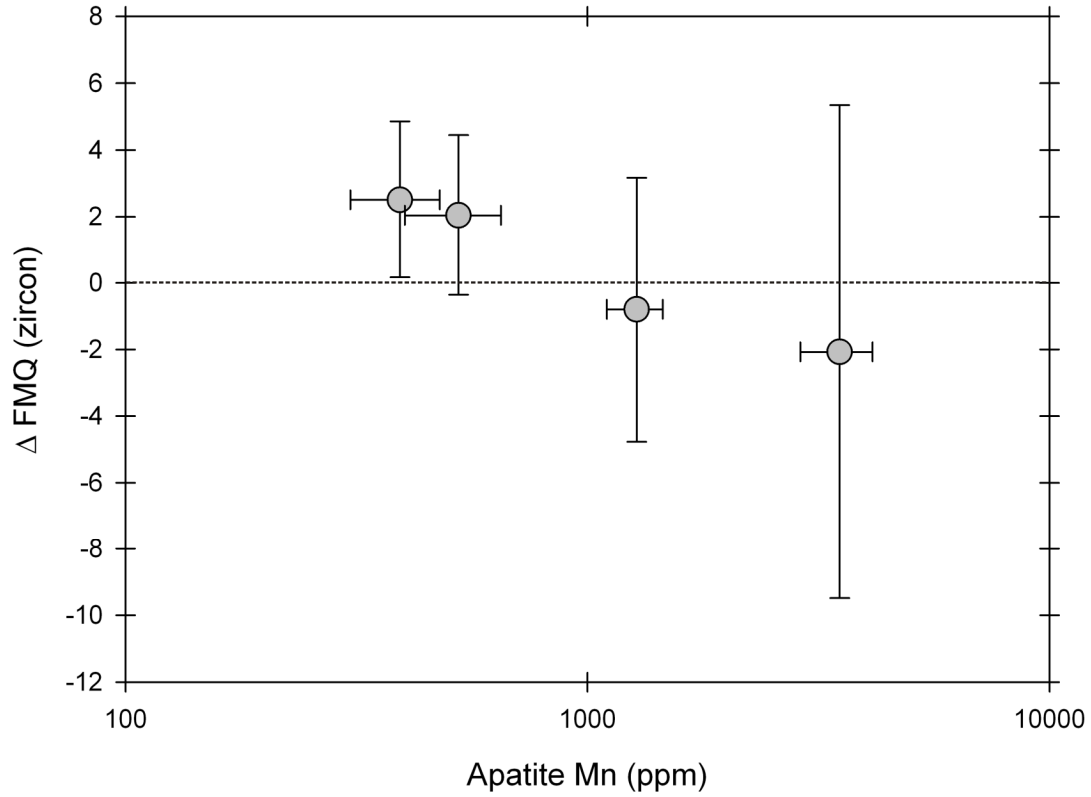

Fig. 4.6 Average Mn concentrations with 1SD population error bars for the four zones of the Criffell pluton plotted against median ΔFMQ values calculated from Ce anomalies (using the method of Trail et al. 2011) in co-existing zircon. Vertical error bars represent interquartile ranges in calculated values of ΔFMQ.

The isotopic record of detrital accessory minerals has already proved central to many studies of early continental crust evolution (e.g. Eiler, 2007; Kemp et al. 2006b, 2007; Hawkesworth et al. 2010; Wilde et al. 2001). Detrital accessory minerals may also offer insights into the redox states of magmas lost from the geological record, such as those of the Archaean eon (Lee et al. 2010; Trail et al. 2011). Like zircon, apatite is a prevalent and robust accessory phase in the detrital record (Morton and Yaxley, 2007; Corfu and Easton, 2001; Chamberlain and Bowring, 2001), and is commonly preserved as an inclusion phase in a range of host minerals in even the most re-worked sediments.

Apatite is also becoming an increasingly valuable tool in the evaluation of lunar magmatism and particularly in relation to estimates of the water content of lunar basalts (e.g. McCubbin et al. 2010).

Volcanic emissions such as sulphur are highly susceptible to the redox states of erupting magmas and are known to have significant climatic impacts (Robock, 2000). Apatite may provide a new, robust and important proxy for examining the redox conditions and by association the volatile contents of recent and historically important volcanic events.

Variations in apatite Mn are here shown to be largely insensitive to WR composition, suggesting redox conditions exert a greater control than melt compositions. The absence of constraints on the composition of the melt from which detrital apatite crystallised may not therefore significantly affect estimates of its redox condition. Apatite may therefore potentially provide valuable and more reliable estimates of redox conditions than zircon.

Chapter 5

Using zircon isotope compositions to constrain crustal structure and pluton evolution in a complex lithotectonic terrane: The Iapetus Suture Zone in northern Britain[†]

Abstract

The Trans-Suture Suite (TSS) of I- and S-type granite plutons in Northern Britain was emplaced during the early Devonian and post-dates subduction of the Iapetus Ocean. New zircon U-Pb ages indicate emplacement at 410 ± 6 Ma for the Criffell pluton, 416 ± 5 Ma for the Shap pluton and 410 ± 3 Ma for the outer zone of the Fleet pluton. These emplacement ages are older than previously reported, coincident with the intrusion of the regionally prolific lamprophyre dykes, and consistent with emplacement within transtensional tectonic environments. Resolvable age differences between the outer (410 ± 3 Ma) and inner two zones of the Fleet pluton (387 ± 5 Ma) suggest two distinct stages of emplacement. Zircon oxygen isotope compositions from the TSS range from ~ 5.0 ‰ up to ~9.0 ‰ with similar intra-pluton variability between zones in the Criffell and Fleet plutons that reflect additions from supracrustal and sedimentary sources. Zircon populations from the least evolved (lowest SiO_2) outer zones of Criffell and Fleet show limited $\delta^{18}O$ heterogeneity. Larger degrees of $\delta^{18}O$ heterogeneity are seen between zircons from inner, more silicic zones and reflect the preservation of magma heterogeneity during magma ascent from deep crustal hot zones. Up to ~ 30% of zircons from S-type granites have mantle-like $\delta^{18}O$, indicating the involvement of more mafic magmas in

[†] Co-authors: Colin Graham – *University of Edinburgh*; Chris Hawkesworth – *University of St Andrews*; Martin Gillespie – *British Geological Survey*; Richard Hinton – *University of Edinburgh*; EIMF; Bruno Dhuime – *University of Bristol*

their formation. Magmatic zircons from dioritic enclaves have U-Pb ages that are up to ~ 9 Ma older than their host granodiorites and may represent entrained, cognate material derived from crustal hot zones. Initial εHf values from the three plutons are distinctive from each other, show little or no variation within plutons and differ substantially from mantle values, reflecting significant crustal re-working. Zircon Hf model ages are consistent with geophysical evidence for underlying Avalonian crust beneath the Iapetus Suture. Zircon O-Hf isotope arrays display two-stages of mixing. The first array, defined at an inter-pluton scale, is thought to reflect mixing between re-melted juvenile crust or depleted mantle and Avalonian crust, with maximum crustal contributions in the Shap pluton and least in the Criffell pluton. The second set of arrays, at an intra-pluton scale, is defined by variations in zircon $\delta^{18}O$ and is consistent with further mixing with up to 50% of a sedimentary component derived from underthrust Avalonian crust. The integration of zircon isotopic compositions with geological and geophysical evidence of crustal structure permits the sources and evolution of the granites to be constrained. Calc-alkaline compositions are attributed to partial melting during lithospheric transtension of mantle hydrated by earlier dehydration of subducting Iapetus ocean crust.

1. Introduction

Manifested in large granitic plutons are the processes responsible for partial melting and magmatic differentiation that ultimately determine the evolution of a large proportion of the continental crust (Campbell and Taylor, 1983; Kemp et al. 2007). The different isotopic compositions of granitic rocks and the mantle (Appleby et al. 2008; DePaolo 1981; Gray 1984; Hamilton et al. 1980; Jahn et al. 2000; Keay et al. 1997; Kemp et al. 2007; McCulloch and Chappell, 1982) often reflect the involvement of reworked (remelted) crustal material in the formation of granites that is additional to – or exclusive of - the effects of direct fractionation of mantle-derived magmas. The isotopic compositions of granitic rocks and their variations therefore also serve as windows into the chemical evolution, crustal residence time and structural and lithological configuration of their source regions, and have traditionally been categorised as either I–type (infracrustal igneous rocks formed at depth) or S-type (supracrustal and derived from rocks originating at the Earth's surface) (Chappell and White, 1974). However, the petrogenesis of both I-type (Clayburn et al. 1983; Ferreira et al. 2003; Gerdes et al. 2002; Halliday 1984; Halliday et al. 1980; Harmon and Halliday, 1980a; John, 1990; Lackey et al. 2005, 2006; Miller et al. 1990) and more recently S-type (Appleby et al. 2010; Kemp et al. 2006a) granites has been shown to involve multiple sources, including mantle, lower and upper crustal components, indicating that isotopic heterogeneity in granites may to a large extent reflect magma mixing and assimilation, in addition to differences in their source rock compositions (see Kemp and Hawkesworth, 2003).

WR compositions provide cumulative evidence for the processes that ultimately determine magma compositions but are also subject to later, post-solidus alteration. Many of these problems have been circumvented by studying robust accessory minerals such as zircon that preserve chemical evidence for the stable and radiogenic isotope compositions of their host magmas at the time of crystallisation. These crystals can now be analysed to reveal different magmatic processes at high temporal and spatial resolution (e.g. Appleby et al. 2008, 2010; Bradley, 2011; Griffin 2002;

Hawkesworth and Kemp, 2006; Kemp et al. 2007; Kinny and Maas, 2003; Roberts 2012; Valley et al. 2005). Improvements in the micro-analysis of accessory minerals now enable high precision, high spatial resolution *in situ* analyses of zircon isotope compositions to be integrated with U-Pb dating (Ireland, 2003; Parrish, 2003) to reveal a detailed record of magma sources and evolution.

The Devonian post-Caledonian granites of northern Britain have proved particularly enigmatic. Despite their calc-alkaline compositions, these granites have been shown largely to post-date closure and subduction of the Iapetus Ocean (Soper, 1986; Soper and Woodcock, 2003; Thirlwall, 1981). Their compositions and widespread occurrence (Fig.1) have revealed valuable information about the lower crustal structure of Britain at the time of their emplacement and have helped to delineate distinct crustal terranes throughout Scotland (Frost and O'Nions, 1985; Halliday et al. 1980; Hamilton et al. 1980; Harmon and Halliday, 1980a; Pidgeon and Aftalion, 1978). The Trans-Suture Suite (TSS) represents a particularly unusual sub-set of Devonian granites found throughout Southern Scotland and Northern England (Brown et al. 2008), straddling both sides of the Iapetus Suture Zone and thus precluding a direct subduction origin (Soper, 1986; Thirlwall, 1981). Furthermore, their mutual compositional similarities raise the possibility of a common source region on both sides of the suture zone beneath the English Lake District and Scottish Southern Uplands (Halliday, 1984; Harmon and Halliday, 1980b; Harmon et al. 1984; Highton, 1999; Stephens, 1988; Thirlwall, 1989). A further unusual feature of the granites is the absence of inherited zircons despite the occurrence of large volumes of granitic rocks with S-type and peraluminous characteristics (Pidgeon and Aftalion, 1978) that require a major input from sedimentary sources. High precision and spatial resolution micro-analytical isotope techniques are applied to provide a revised geochronological framework to investigate the chronology and synchronicity of the plutons in relation to the regional geological and tectonic evolution. The oxygen and hafnium isotope compositions of magmatic zircons reveal contrasting degrees of magma heterogeneity in I- and S-type components of the TSS. Zircon Hf model ages are used to identify substantial reworking of Avalonian crust during the

formation of the TSS on both sides of the Iapetus Suture. These results therefore support independent geochemical and geophysical evidence for the existence of underlying Avalonian crust beneath the Iapetus Suture and for its direct involvement in the genesis and evolution of the TSS granites. In this paper we attempt to characterise the different source components identified in the lower crust and upper mantle beneath the suture.

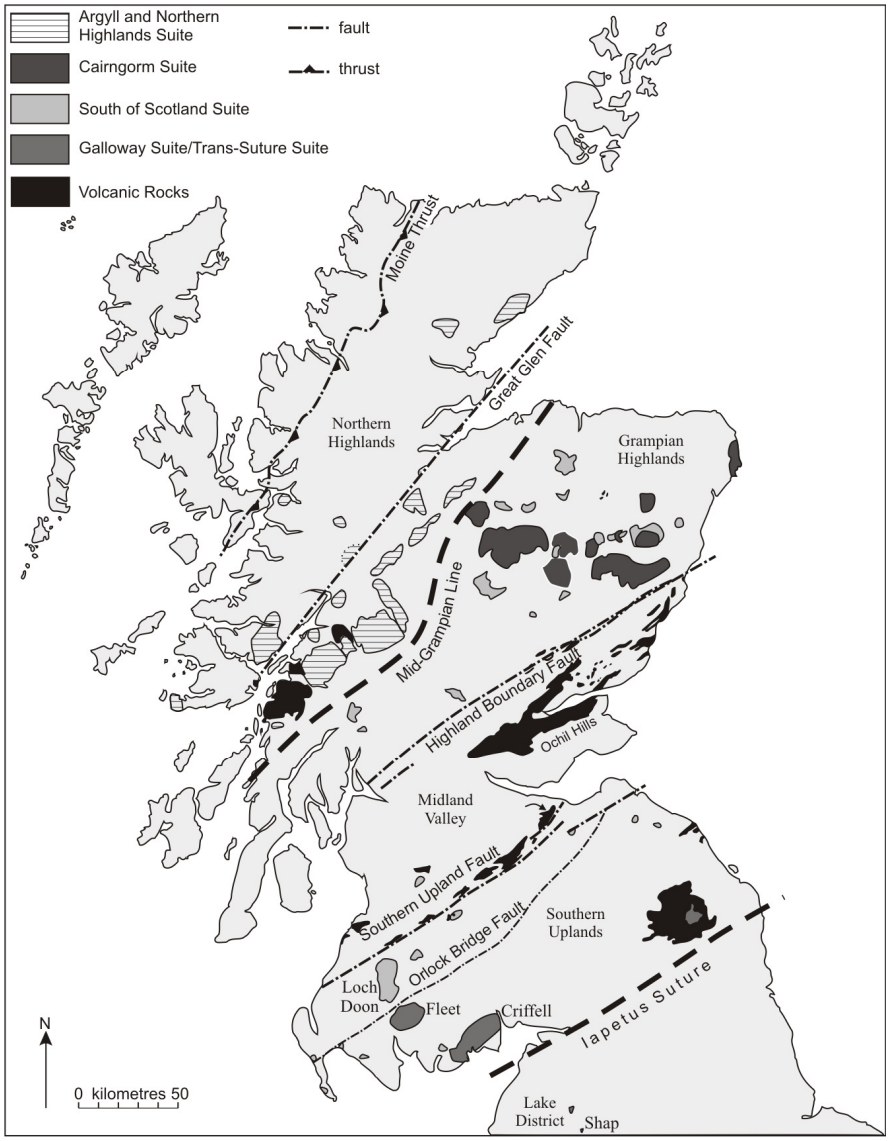

Fig. 5.1 Modified map of late Caledonian plutonic and volcanic rocks (black) in the northern United Kingdom, modified from Highton (1999). Plutons are classified according to the geochemical parameters outlined by Read (1961), Stephens and Halliday (1980) and Stone (1997).

2. Geological Background

2.1 Tectonic evolution of the Iapetus Suture Zone

The Caledonian Orogeny followed a protracted history throughout the early Paleozoic from the Ordovician and into the early Devonian. The earliest orogenic events in Scotland were associated with closure of a back-arc basin and collision of the continent-facing Midland Valley arc (Bluck, 1983) with the Laurentian margin to the north during the Grampian Orogeny (470-460 Ma). Southward subduction of Iapetus Ocean crust ceased following arc collision, and subsequent northward-directed subduction beneath the accreted arc marked the beginning of closure of the Iapetus Ocean beneath Laurentia (Leggett et al. 1983). Northward subduction was associated with propagation of the Southern Uplands–Longford Down accretionary prism in the hanging wall of the suture zone (Barnes et al. 1989). On the adjacent Avalonian margin, final closure of the Iapetus Ocean was signalled by deposition of the Windermere Supergroup (late Ordovician to end Silurian in age) within an associated flexural basin (Kneller, 1991). Reduced accretionary deformation in the Southern Uplands accretionary prism is evident during the late Wenlock period (422 - 428 Ma), signalling a slowing of Iapetus subduction (Kemp, 1987). Iapetus subduction is thought to have completely ceased by *c.* 420 Ma (Kemp, 1987; Soper and Woodcock, 2003; Brown et al. 2008). Further constraint on the cessation of convergence has been presented using the K-Ar ages of unfoliated lamprophyre dykes within the Southern Uplands accretionary prism (Rock et al. 1986). These ages suggest that convergence and deformation had stopped by 418 Ma. Together, biostratigraphic and geochronological evidence suggest that convergence ceased between 424 Ma and 418 Ma (Soper and Woodcock, 2003). Subsequent deformation during the Early Devonian is inferred to have resulted predominantly from sinistral transtension (Dewey and Strachan, 2003; Soper and Woodcock, 2003) during oblique convergence of Laurentia and Avalonia. Later regional folding, faulting and cleavage formation are evident, particularly in the Lake District, towards the early Devonian, with broader folding identified north of the Iapetus Suture. The coeval nature of this deformation with the Acadian Orogeny in the Canadian Appalachians

led Soper (1987) to refer to this as the Acadian Event in Britain, which has been linked to further compression of Eastern Avalonia and Laurentia caused by collision of the Armorica microcontinent (Soper 1986; Soper et al. 1992)

2.2. Post-Caledonian magmatism across northern Britain

Despite the above biostratigraphical and geochronological evidence that subduction of the Iapetus Ocean had ceased by ~ 420 Ma, plutonic and volcanic calc-alkaline magmatism with subduction-like geochemical characteristics became prevalent at this time, particularly on the Laurentian terrane, and continued until the early Devonian. The volcanic rocks have particularly high K_2O, Mg, Ni, Cr and V contents, are mainly silica saturated and have been attributed to the mixing of primitive mantle melts with sediments thought to be subducted lower Palaeozoic greywackes (Thirlwall, 1982, 1983, 1986). Broad, systematic variations in the compositions of volcanic rocks were found perpendicular to the main Caledonian structural trends (Thirlwall, 1981) that were later found to be mirrored by plutonic rocks of a similar age (Stephens and Halliday, 1984). These variations were considered to be consistent with a WNW-dipping subduction zone beneath Scotland, where the depth of melting increased away from the Iapetus Suture Zone (Thirlwall, 1982), but is difficult to reconcile with geological evidence that Iapetus subduction had ceased by ~ 420 Ma (Brown et al. 2008).

A number of alternative tectonic models have been proposed to reconcile apparently conflicting evidence. These include volatile loss from a stationary slab (similar to the Cascades of California and Oregon; Thirlwall, 1981) and fluxing of the overlying mantle wedge by active subduction followed by later shearing, extension and mantle melting (Hutton and Reavy, 1992). Freeman et al. (1988) suggested that the Avalonian subcontinental mantle became detached from its overlying crust and continued to subduct despite the crust having ceased subducting, while Neilson et al. (2009) and Oliver et al. (2008) proposed slab break-off following orogenic

thickening to account for voluminous I-type magmatism and rapid uplift. The latter authors suggested that slab break-off resulted in asthenospheric upwelling and melting of the subcontinental lithosphere to form lamprophyric underplate that subsequently led to the remelting of the lower crust through thermal advection and conduction. These models invoke a genetic link between the regional occurrence of lamprophyric magmas and apparently much larger volumes of calc-alkaline plutonic and volcanic material.

The plutonic and volcanic rocks that straddle the Iapetus Suture have proved particularly difficult to reconcile with regional tectonic models at the end of the Caledonian Orogeny, primarily because of their proximity to the suture (Fig. 5.1). It also remains unclear whether at a regional scale the small degrees of mantle melting required for the formation of lamprophyric magmas are consistent with the much larger volumes of magma represented by broadly contemporaneous plutonism and volcanism. Brown et al. (2008) proposed a transtensional model for the formation of the TSS, drawing particular attention to the coeval deposition of the Old Red Sandstone sediments in apparently transtensional basins during the early Devonian on both sides of the suture zone. Their deposition has been shown to require tectonic subsidence linked to enhanced geothermal gradients in the Welsh slate belts due to extension and passive mantle upwelling (Soper and Woodcock, 2003). Extension or transtension is also consistent with the concurrent intrusion of the regional K-lamprophyre dykes formed following small amounts of lithospheric thinning and adiabatic mantle melting between 420 Ma and 400 Ma (Brown et al. 2008; Dewey and Strachan, 2003; Rock et al. 1986). However, Brown et al. (2008) acknowledge that published U-Pb ages suggest emplacement during periods of transpression.

2.3 The Trans-Suture Suite (TSS) granites

The predominantly I-type, post-Caledonian Devonian Scottish granites were distinguished from the older S-type granites found in northern Scotland by Read (1961). Further subdivision by Stephens and Halliday (1984) into the Argyll,

Cairngorm and South of Scotland suites followed from compositional distinctions relating to different source compositions in different tectonic terranes (Fig. 5.1). The South of Scotland Suite was subdivided into granites with low initial $^{87}Sr/^{86}Sr$ north of the Orlock Bridge Fault (e.g. the Loch Doon pluton; Fig. 5.1) and those with high initial $^{87}Sr/^{86}Sr$ compositions south of the fault, including the TSS (Stone et al. 1997), that are likely to reflect increased contamination by a sedimentary component. The southern subdivision of the South of Scotland plutons (e.g. the Criffell and Fleet plutons) shares many compositional characteristics with plutons of similar age in the English Lake District (e.g. Shap pluton), emplaced within Avalonian crust to the south (Harmon and Halliday, 1980b; Harmon et al. 1984; Highton, 1999; Stephens 1988; Thirlwall, 1989).

In the absence of inherited detrital zircon (Pidgeon and Aftalion, 1978), U-Pb dating of magmatic zircons from plutons south of the Highland Boundary Fault constrain emplacement ages only. By contrast, plutons north of the Highland Boundary Fault commonly contain a significant proportion of inherited zircons, many with Archean ages consistent with underlying basement of a similar age. Pidgeon and Aftalion (1978) attributed these differences to an absence of older basement material south of the Highland Boundary Fault. However, the absence of inherited zircon in general may also be attributed to resorption during magma ascent, particularly in low viscosity and water-rich magmas that may attain super-liquidus states (Chapter 2).

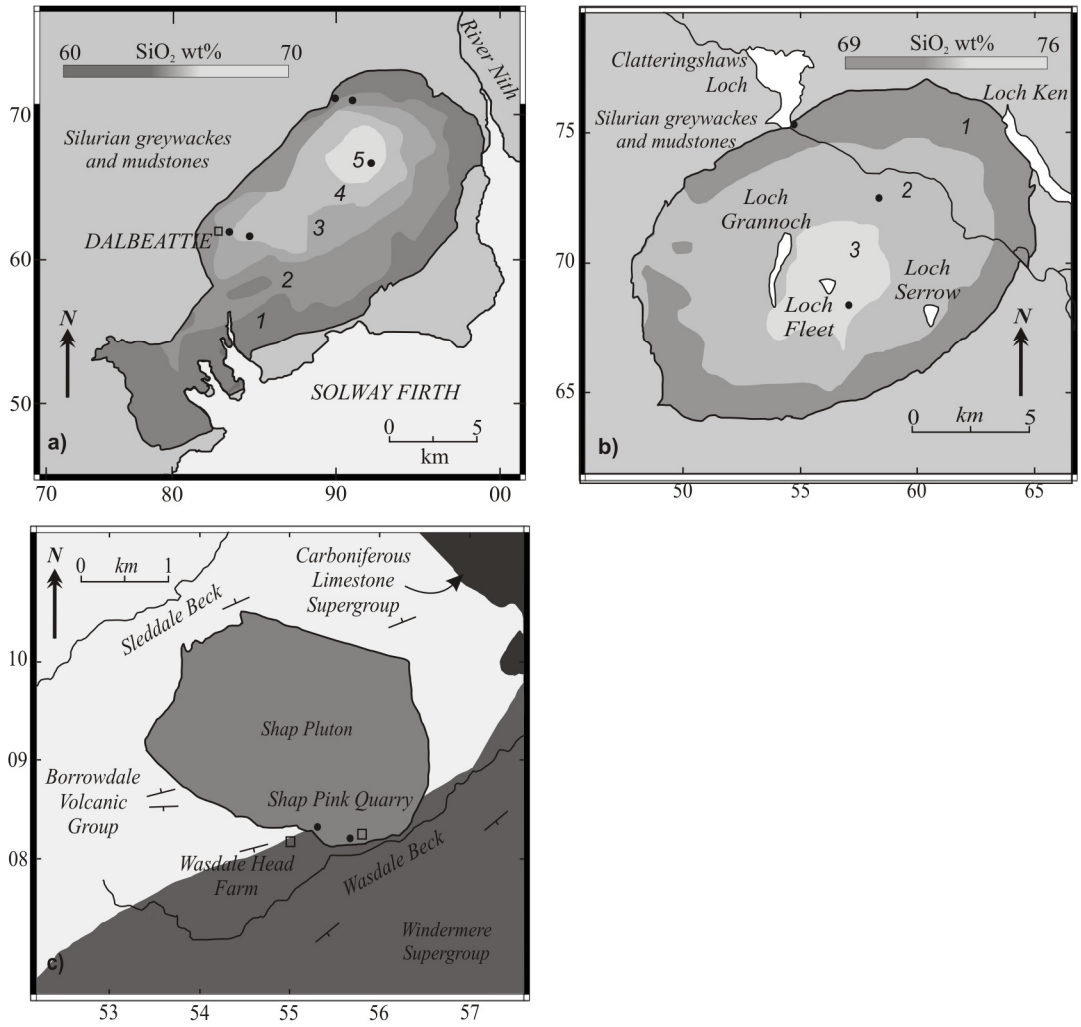

Fig. 5.2 Simplified geological maps of the Criffell (a), Fleet (b) and Shap (c) plutons. Zone colouration reflects approximate silica content, with darker colours indicative of lower SiO_2. Zone mineralogy in the Criffell pluton is as follows: 1) clinopyroxene-biotite-hornblende granodiorite; 2) biotite-hornblende granodiorite; 3) biotite granite; 4) biotite-muscovite granite 5) muscovite-biotite granite. Zone mineralogy in the Fleet pluton is as follows: 1) coarse grained biotite granite; 2) coarse-grained biotite-muscovite granite; 3) fine-grained biotite-muscovite granite. Minerals listed in order of increasing modal abundance. Black points denote sample sites.

2.3.1 The Criffell Pluton

A Rb-Sr age suggests that the Criffell pluton was emplaced at ~397 ± 2 Ma (Halliday et al. 1980) into low-grade wackes and pelites of Llandovery to Wenlock age (444 to 423 Ma) that form part of the Southern Uplands accretionary prism in southern Scotland (Fig. 5.2a). The pluton is of global significance as a classic example of a normally zoned pluton (Stephens and Halliday 1980; Stephens et al. 1985). Outer zones (1 and 2) are of metaluminous granodiorite (~ 59 to 69 wt % SiO_2) containing primary hornblende (with occasional cores of clinopyroxene), biotite, zoned plagioclase, potassium feldspar, quartz and accessory sphene, zircon, apatite, allanite and magnetite (with very minor hematite) (Figs. 3 and 4). Inner zones (4 and 5) are of peraluminous granite (~ 69 to 73 wt % SiO_2) that contains primary muscovite and small amounts of monazite but lack hornblende, sphene and the abundant zircon and magnetite that characterise the granodiorites. Only in samples from zones 1 to 4 was zircon found in great enough abundance for statistically meaningful analyses to be conducted.

Mineralogical zoning is accompanied by isotopic zoning, with outer granodiorites having initial $^{87}Sr/^{86}Sr$ ratios of 0.7052, εNd values of -0.6 and $\delta^{18}O$ values of 8.5 ‰ (Halliday, 1984; Halliday et al. 1980). Inner granites have initial $^{87}Sr/^{86}Sr$ ratios up to 0.7073, εNd values of -3.1 and $\delta^{18}O$ values of 11.9 ‰. Simultaneous variations in isotope and Rare Earth Element (REE) compositions were interpreted by Stephens et al. (1985) to result from assimilation and fractional crystallisation (AFC) involving both mafic lower crustal/mantle and sedimentary components. The absence of local melting in surrounding country rocks indicates that immediately adjacent sediments were not a major source of contamination, while the Pb isotope compositions of the TSS are markedly different from that of the Southern Uplands sediments (Thirlwall, 1989). Pluton assembly occurred via incremental assembly of multiple batches of magma. This is supported by the alignment of minerals and mafic enclaves in the outer zones of the pluton interpreted to result from the later intrusion of the more evolved central zones (Stephens et al. 1985).

Mafic enclaves are a common feature in the outer three zones of the pluton. Oscillatory zoned plagioclase within the enclaves provides evidence for a magmatic origin (Holden et al. 1987). The enclaves have been variously interpreted to represent residual components following partial melting of the crust, restite from a basic precursor, cognate material, congealed syn-plutonic injections of basic magmas or segregated immiscible liquids (see Holden et al. 1987).

2.3.2 The Fleet Pluton

The ~ 10 km by 12 km Fleet pluton intrudes the Llandovery sediments (428 to 444 Ma) of the Central Belt of the Southern Uplands (Fig. 5.2b) and is situated south of the Orlock Bridge fault (Fig. 5.1). Pidgeon and Aftalion (1978) reported a zircon U-Pb age of 396 ± 6 Ma from near the margin of the granite, consistent with a Rb-Sr mineral-whole-rock age of 392 ± 2 Ma that lies within analytical error (Halliday et al. 1980). A fabric related to ductile deformation that wraps around cordierite porphyroblasts in the aureole and is cut by the granite contact is thought to reflect syn-tectonic emplacement of the pluton during reactivation of the Moniaive Shear Zone caused by Acadian deformation (Lintern et al. 1992; Phillips et al. 1995; Barnes et al. 1995; Brown et al. 2008; Stone et al. 1997). Gravity anomalies indicate that the pluton extends to a depth of ~ 11 km beneath the current surface (Parslow, 1973). SiO_2 contents vary from 69 to 76 wt% and are on average more evolved than other TSS granites. Their typical S-type compositions are reflected in their petrology. The pluton has two main granite facies, including an outer biotite granite and inner biotite-muscovite granite (Figs. 2 and 3). The latter facies has subsequently been subdivided into fine and coarse grained units (Parslow, 1968).

Elevated initial $^{87}Sr/^{86}Sr$ ratios of 0.7062 to 0.7083 and low εNd values of -3.0 to -3.4 (Stephens and Halliday, 1984) also reflect the predominantly S-type characteristics of the Fleet pluton, with evolved $\delta^{18}O$ (WR) values of ~11‰ indicative of a large sedimentary component (Halliday, 1984; Halliday et al. 1980; Stephens and

Halliday, 1984). The Fleet pluton has been shown to share many geochemical similarities with the Lake District plutons (Stephens and Halliday, 1984; Thirlwall, 1989), post-dating closure of the Iapetus Ocean.

2.3.3 The Shap Pluton

The Shap pluton was emplaced into Caradoc (~ 455Ma) volcanics of the Borrowdale Volcanic Group (BVG) in the English Lake District (Figs. 1 and 2c). Pidgeon and Aftalion (1978) reported a zircon U-Pb age of 390 ± 6 Ma, while Wadge (1978) reported an age of 394 ± 3 Ma based on a whole-rock-feldspar isochron, similar to the 397 ± 7 Ma age estimated from K-Ar biotite dating. Davidson et al. (2005) reported an older single mineral Sr isochron age of 405 ± 2 Ma.

Stephenson (1999) noted three distinct stages of pluton growth based primarily on the modal abundance of large K-feldspar megacrysts now thought to be igneous in origin (Lee and Parsons, 1997). Stage 1 (~10% volume of the pluton) is represented by the outer margins of the pluton with 15% pink, Carlsbad-twinned orthoclase-perthite megacrysts up to 5 cm in size. The groundmass consists of orthoclase, plagioclase (zoned from andesine to albite), quartz and biotite (Fig. 5.3). Accessory minerals include sphene, apatite, magnetite, zircon, fluorite, monazite, allanite, amphibole and pyrite. The dominant stage 2 granite (90% of the pluton) is broadly similar to the stage 1 granite but contains 30% orthoclase and reduced proportions of biotite. This trend continues into the final (stage 3) granitic veins with up to 60% orthoclase megacrysts.

Significant assimilation of sediments is indicated by elevated ^{18}O compositions, with $\delta^{18}O$ values of ~11‰, initial $^{87}Sr/^{86}Sr$ values (0.707) and low εNd (-2.0) (Wadge et 1978; Harmon and Halliday, 1980; Halliday, 1984). However, the predominantly I-type mineralogy of the Shap granite raises the possibility that crustal fluids have significantly altered the isotopic composition of the pluton either during or post

emplacement (Halliday, 1984). Hydrothermal processes are also implied by the presence of fluorite and pyrite in this pluton.

Abundant megacryst-bearing microdioritic inclusions up to 2m in size occur in addition to country rock xenoliths in the Shap pluton. Many authors have suggested that such features represent injections of mafic magma, possibly related to the intrusion of a regional K-lamprophyre dyke swarm (Granthem, 1928; Stephenson, 1999; Cox et al. 1996), although a widely-accepted interpretation is still lacking.

In summary, published data indicate that the three plutons discussed were intruded at similar times between 397 Ma and 390 Ma, a period dominated by transpression (Brown et al. 2008), and share many common chemical characteristics, including elevated initial $^{87}Sr/^{86}Sr$ and similar ^{207}Pb isotope compositions. The Criffell and Fleet plutons both show textural evidence for incremental assembly and are chemically and mineralogically zoned. The plutons differ mainly in their major element compositions and in the scale of chemical zoning. The Criffell pluton is zoned from an I-type outer region to a more S-type inner region, while the Fleet pluton is considered S-type, and becomes increasingly S-type towards its inner zones.

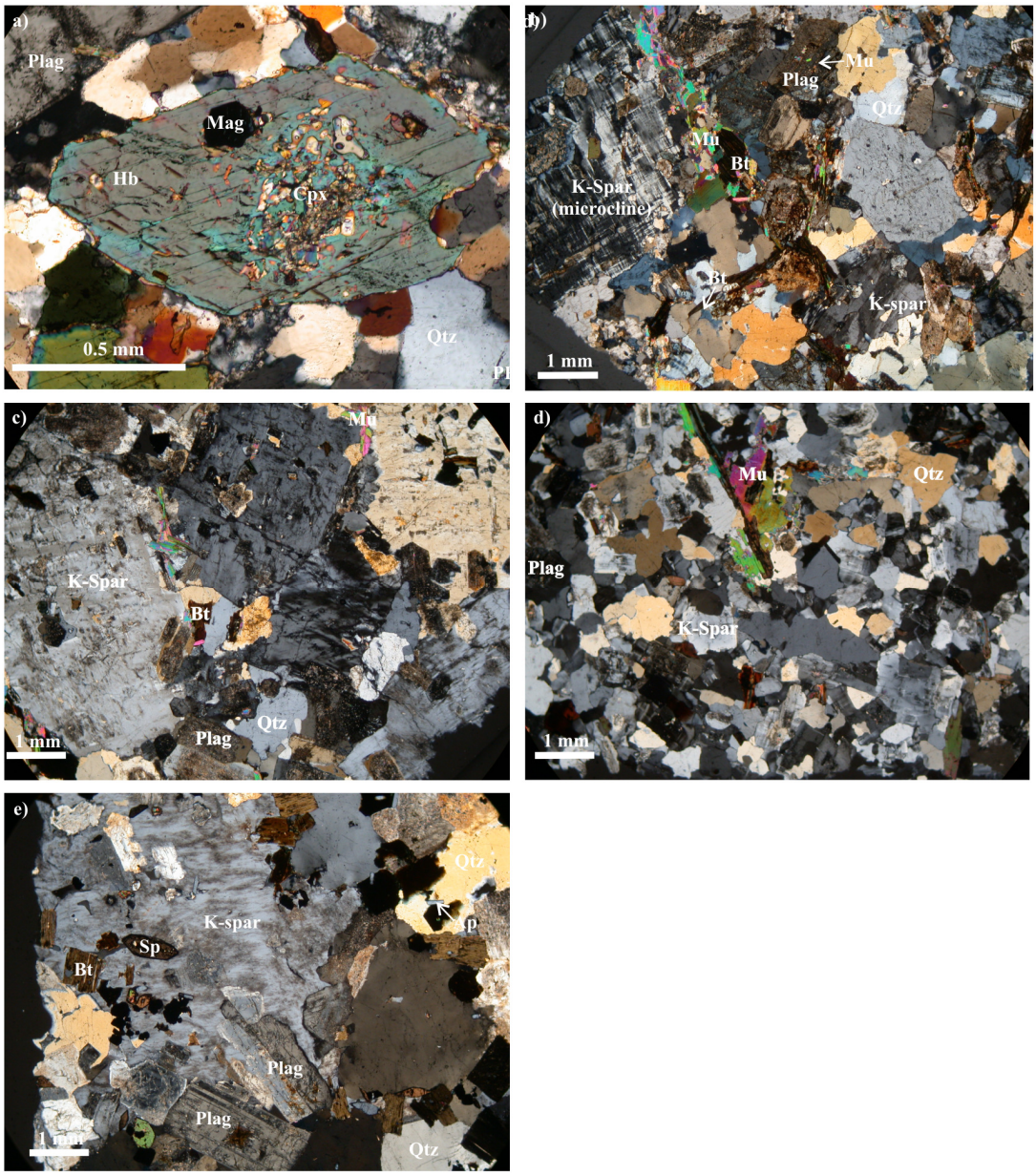

Fig. 5.3 Representative petrological micrographs of the Criffell, Fleet and Shap ganitoids. a) Zone 1 granodiorite (Criffell); b) Zone 5 granite (Criffell); c) Zone 2 granite (Fleet); d) Zone 3 granite (Fleet); e) Stage 2 granite (Shap). Abbreviations are as follows: Ap – apatite, Bt – biotite, Cpx – clinopyroxene, Hb – hornblende, K-Spar – Potassium feldspar, Mag – magnetite, Mu – muscovite, Plag – plagioclase, Qtz – quartz, Sp – sphene.

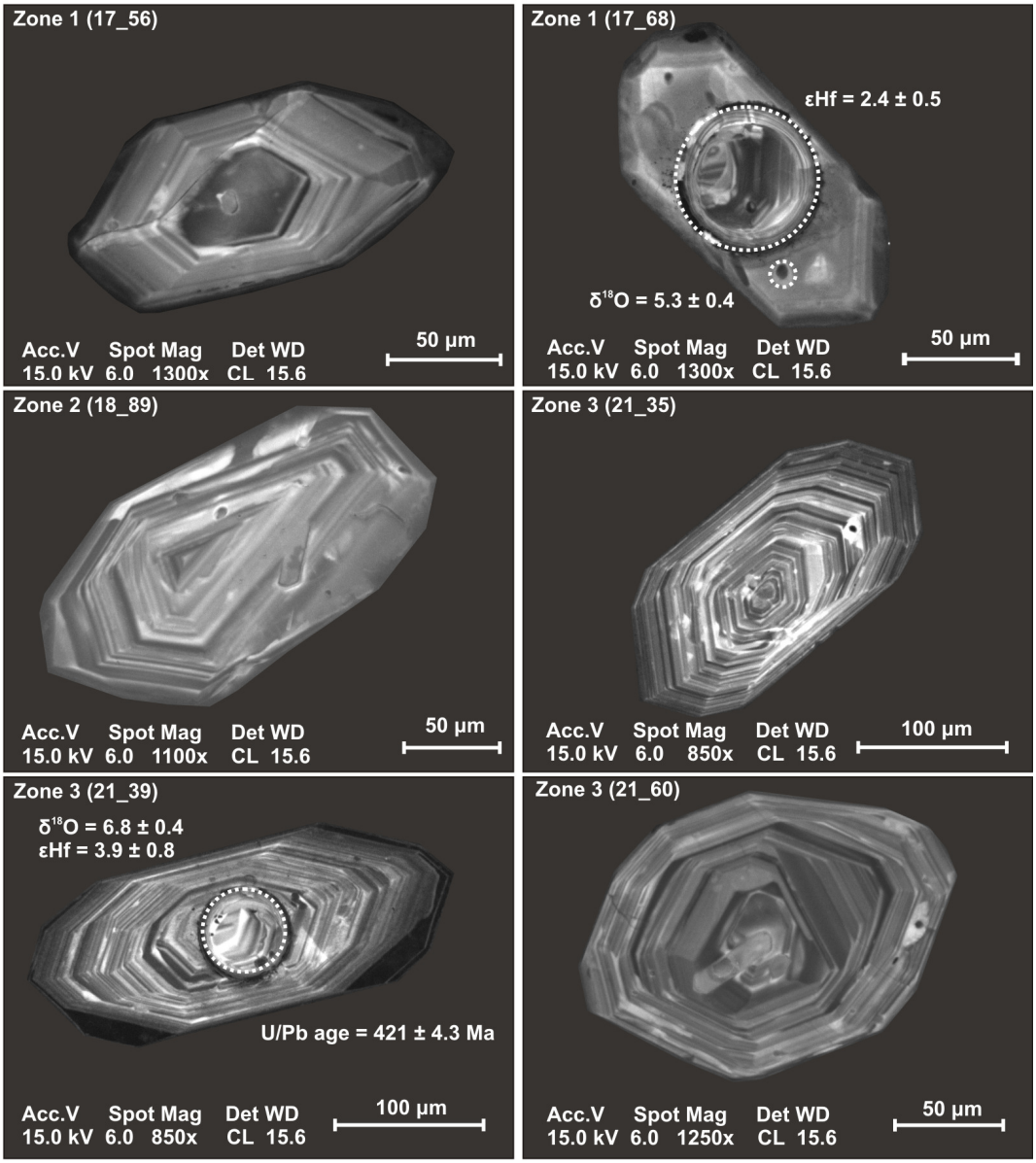

Fig. 5.4 CL images of a representative selection of zircon crystals from the Criffell pluton. Concentric zoning is evident in most crystals. Two crystals show laser and SIMS analysis pits with their analytical results.

2.4. Present-day structure of the Iapetus Suture

Evidence from seismic profiles constrains crustal structure and lithological components across the Iapetus Suture and northwards through the Caledonian fold belts of northern Britain. Northwest-southeast seismic profiles from the BIRPS seismic survey imaged a north-dipping (~ 20^{o}) zone of reflectivity in the middle and lower crust traced over 900 km from the Atlantic margin west of Ireland to the North Sea (Beamish and Smythe, 1986; Freeman et al. 1988; Hall, 1984; Klemperer and Matthews, 1987; Klemperer et al. 1991). This reflection is interpreted to represent Avalonian crust underthrust beneath the Laurentian margin. Brown et al. (2008) suggest that flattening of subducting Iapetus oceanic lithosphere occurred in response to the subduction of progressively younger and more buoyant lithosphere up to 420 Ma. The geometry of the suture zone close to the Moho is less certain, but it appears to flatten and merge with a set of strong sub-horizontal reflections in the lower crust beneath the Midland Valley, interpreted as Iapetus oceanic crust or imbricated basement and sedimentary cover from the continent-ocean margin of Avalonia (Soper et al. 1992). These reflectors indicate that underthrust Avalonian crust extends at least as far north as the Midland Valley. Similar reflections have been imaged along the approximately north-south WIRE reflection profiles offshore from western Ireland (Klemperer et al. 1991). The occurrence of Avalonian sediments beneath the Southern Uplands is consistent with the high $^{207}Pb/^{204}Pb$ ratios of the Southern Uplands granites (Fig. 5.5) and has been attributed to the presence of Ordovician Skiddaw Group sediments found south of the Iapetus Suture on the Avalonian terrane (Thirlwall, 1989). Here we use the U-Pb, O and Hf isotope compositions of zircons from the TSS and an understanding of the structural and lithological make-up of the crust to identify the source lithologies that contributed to TSS granite magma genesis and evolution. Furthermore, we provide a more refined geochronological timeframe for the emplacement of the TSS.

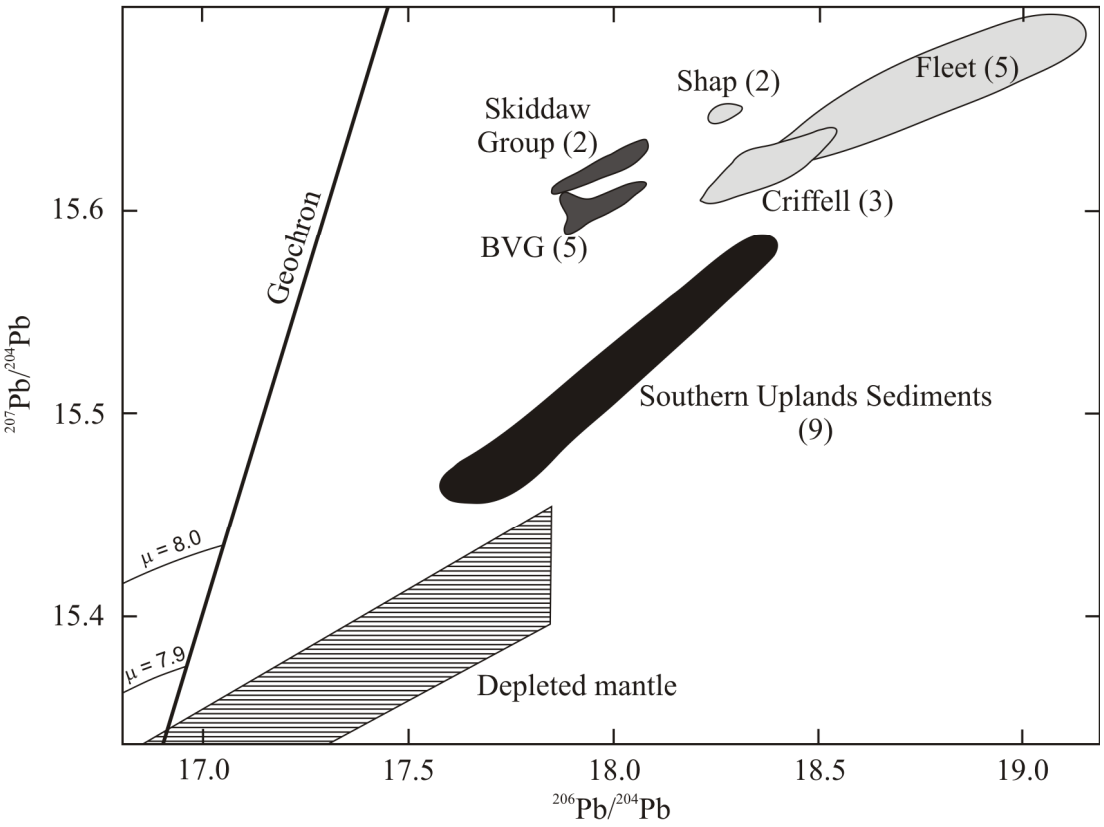

Fig. 5.5 Pb-Pb diagram modified from Thirlwall (1989) showing the Pb isotope compositions of the TSS plutons, Skiddaw Group sediments (Thomas 1985; Stone and Evans 1997), Southern Uplands sediments (Stone and Evans 1995), Borrowdale Volcanic Group (BVG) (Thirlwall, 1986) and depleted mantle (Zindler and Hart, 1986). All plutons extend to more radiogenic $^{207}Pb/^{204}Pb$ compositions than the Southern Uplands sediments into which they are intruded. The Fleet pluton in particular also extend to more radiogenic compositions than the Skiddaw sediments, and implies that a further upper crustal component was involved, potentially unexposed Avalonian basement. Numbers in brackets refer to the number of available analyses.

3. Methodology

3.1 Zircon preparation

Rock samples of approximately 5 kg from different zones of the Criffell, Fleet and Shap plutons were crushed and sieved to < 500 μm prior to density separation using a Wilfley Table at the University of St Andrews separation facility. Heavy liquids, including Tetrabromoethane (TBE) and methylene iodide were used for further mineral separation. Non-magnetic fractions were separated by Frantz magnetic separators at the Universities of St Andrews and Edinburgh. Approximately 100 zircon crystals were picked from each sample and mounted in epoxy (Araldite/Epothin) blocks with fragments of 91500 zircon standard positioned at the centre of each block. Polished mounts were imaged by back-scattered electrons and cathodoluminescence (CL) using a Phillips XL30CP Scanning Electron Microscope (SEM) at the University of Edinburgh to establish the positions of inclusions, cracks and internal compositional zoning (Fig. 5.5).

3.2 Zircon U-Th-Pb analysis

U-Th-Pb dating was carried out following oxygen isotope analysis using a Cameca ims 1270 ion microprobe at the University of Edinburgh. A 4 to 5 nA primary O^{2-} beam was used for zircon analysis with 22.5 keV impact energy following the method of Kelly et al. (2008). Resulting analytical pits were ~ 25 μm and ellipsoidal in shape following beam focusing and alignment under Köhler illumination, with further spatial resolution achieved using a field aperture. U, Th and Pb were analysed at a mass resolution (M/ΔM) of > 4000R using a peak switching routine. No energy centring was carried out and an energy window of 60 eV was used throughout. Pb ion yields were increased by a factor of ~ 2 by flooding the sample surface with oxygen. Any effects from surface contamination were minimised by pre-rastering a ~ 15 μm surface area for 120 seconds prior to analysis. Pb/U ratios were calibrated using a slope factor of 2.6 between ln (Pb/U) vs. ln (UO_2/U). U/Pb ratios were calibrated against measured ratios of zircon standard 91500 with an age of ~1062.5

Ma and assuming a $^{206}Pb/^{238}U$ ratio of 0.17917 (Wiedenbeck et al. 1995). Standard analyses were carried out after every 3 to 4 unknown analyses. Calculated Th/U ratios in all unknown samples were obtained by comparison with measured Th/U ratios (Th/U = 0.362) and $^{206}Pb/^{238}U$ in zircon standard 91500 assuming closed system behaviour. U and Hf concentrations of 81.2 ppm and 5880 ppm respectively in the standard were assumed and elemental concentrations determined based on the observed oxide ratios of the standard (UO_2/Zr_2O_2 and HfO/Zr_2O_2).

Corrections for dead time (51 ns), detector background (~ 0.01-0.03 counts per second) and common Pb were carried out. Measurements with $^{204}Pb > 10$ ppb were discarded because of large common Pb corrections. Uncertainties in the U/Pb ratio of 91500 are approximately 0.8 % greater than those expected from counting statistics alone and are assumed to be random errors (Ireland, 2003). These random errors have been propagated in the standards and unknowns together with the observed variations in Pb/U ratios for each analysis (typically close to the counting errors). Measurements carried out on zircon standard 91500 are typically between 0.7 and 1.0 % per analysis. Observed variations in $^{207}Pb/^{206}Pb$ ratios from cycle to cycle during each analysis approach those expected from counting statistics. Quoted uncertainties on individual ages are 1 SD while those on calculated group ages are quoted as 2 SD.

ISOPLOT (version 3) was used for plots and age calculation (Ludwig, 2003), with mean and weighted mean $^{206}Pb/^{238}U$ concordant ages used for magmatic zircons. BSE and SE imaging of analytical pits were subsequently used to assess pit quality, cracks and the presence of inclusions.

3.3 Zircon oxygen isotope analysis

Oxygen isotope analysis of zircons was carried out using a Cameca ims 1270 ion microprobe at the University of Edinburgh following the methods described by Cavosie et al. (2005) and Kemp et al. (2006b) with data reported as per mil (‰)

values relative to Vienna Standard Mean Ocean Water (VSMOW). A primary $^{133}Cs^{+}$ ion beam of approximately 20 μm diameter was used at 6 nA. A normal-incidence electron flood gun was used for charge neutralisation, with secondary ions extracted at 10 kV. Both $^{18}O^{-}$ and $^{16}O^{-}$ ions were monitored simultaneously on dual Faraday cups. Total acquisition times of ~ 200 seconds included secondary ion beam centring, pre-sputtering for 50 seconds and data collection over 10 cycles, each lasting 4 seconds. Instrumental drift was corrected daily by normalising all unknown samples to zircon standard 91500 ($\delta^{18}O$ = 9.86 ‰) (Wiedenbeck et al. 2004). Bracketing analyses of 91500 were used to obtain linearly interpolated values of $^{18}O/^{16}O$ that were subsequently used to normalise the $^{18}O/^{16}O$ ratios of unknown samples. Analyses of 91500 in groups of 5 to 10 were carried out after every 10 to 15 analyses of unknowns. Following corrections for instrument drift, unknown zircon analyses were normalised to an average daily $^{18}O/^{16}O$ value for zircon standard 91500.

HfO_2 concentrations in unknown zircon samples were determined using Cameca SX100 electron microprobes at the Universities of Edinburgh and Bristol. Variations in the instrumental mass fractionation (IMF) during $^{18}O/^{16}O$ analysis by ion microprobe have been shown to reflect variations in HfO_2, particularly analyses at high energy offset using a Cameca ims 4f (Peck et al. 2001). IMF corrections were not required in this study due to the use of a Cameca ims 1270 (which does not require high energy offset) and the small measured variations in HfO_2 (generally < 0.5 wt%). Zircon oxygen isotope data are presented as histograms with bin widths determined from 1 SD precision in the $\delta^{18}O$ composition of 91500. Cumulative probability curves are fitted by summing the probability distributions of a suite of data with normally distributed errors (Isoplot ver. 3.00; Ludwig, 2003). Grain-scale variation plots illustrate the extent to which data lie within analytical error (2 SD) of the mean.

Following the approach of Appleby et al. (2008), zircon standard 91500 is assumed to have a homogenous isotopic composition. Variations greater than 2σ about the

mean $\delta^{18}O$ of 91500 are considered to be real. Analytical precision from session to session was generally between 0.3 and 0.6 ‰.

3.4 Zircon Hf isotope analysis

Zircon Lu-Hf isotope compositions were obtained using a ThermoFinnigan Neptune multicollector inductively-coupled plasma mass spectrometer (MC-ICP-MS) coupled with a New Wave Research UP193HE laser at the University of Bristol. Similar sites to those used for oxygen isotope analyses were chosen using a spot size of 40 or 50 μm. Ablation was carried out in helium and later mixed with argon and nitrogen using a pulsed laser at 4 Hz with an energy density of ~ 6 J/cm^2 over 60s. Total analysis times were ~ 90s, including 30s of background measurements. Corrections for interferences and mass bias followed the University of Bristol procedure outlined by Hawkesworth and Kemp (2006) and Kemp (2009). Mass bias effects with interference-free ^{171}Yb were corrected using an exponential law and $^{173}Yb/^{171}Yb$ = 1.130172 (Segal et al. 2003). A $^{176}Yb/^{171}Yb$ value of 0.897145 was used to calculate the ^{176}Yb interference on ^{176}Hf (Segal et al. 2003) with mass bias-corrected ^{171}Yb monitored during the run. Mass bias effects on interference-free ^{175}Lu were conducted assuming $\beta Lu = \beta Yb$ and using an exponential law. Mass bias-corrected ^{176}Lu was monitored during the run and the magnitude of the ^{176}Lu interference on ^{176}Hf was calculated using $^{176}Lu/^{175}Lu$ = 0.02655 (Vervoort et al. 2004). An exponential law was used to correct for mass bias on interference corrected $^{176}Hf/^{177}Hf$ values before normalising to Hf standard JMC-475 = 0.282160. The accuracy and long term reproducibility of the measurements was estimated by analysing two zircon reference standards, including Plesovice ($^{176}Hf/^{177}Hf$ = 0.282476 (25), *n = 29* with a 40μm beam; $^{176}Hf/^{177}Hf$ = 0.282474 (17), *n = 36* with a 50 μm beam) and Mud Tank ($^{176}Hf/^{177}Hf$ = 0.282503 (27), *n = 27* with a 40μm beam; $^{176}Hf/^{177}Hf$ = 0.282501 (18), *n = 30* with a 50μm beam) (errors are reported at 2 SD). Initial εHf values for all samples were calculated using the mean $^{206}Pb/^{238}U$ ages for each zone. Epsilon values are reported relative to initial Chondritic Uniform Reservoir (CHUR) values calculated from present day values of $^{176}Lu/^{177}Hf$ =

0.0336 and $^{176}Hf/^{177}Hf = 0.282785$ (Bouvier et al. 2008). A ^{176}Lu decay constant of $\lambda = 1.867 \times 10^{-11}$ yr^{-1} (Scherer et al. 2001) was used.

4. Results

A summary of zircon O-Hf-U-Pb isotope compositions for each zone of the Criffell, Fleet and Shap plutons together with associated enclaves is provided in Table 1. Variations in O, Hf and U-Pb isotope values are generally limited within single zones and are presented as mean values. Small crystals, cracks and inclusions limited multiple analyses on single grains. Errors represent 2 SD variations about the mean values.

Table 5.1. Summary results for zircon oxygen, Hf and U-Pb analyses

Pluton	Sample	SiO_2 (wt%)	$\delta^{18}O$(Zrc) ‰*	±2σ	n	εHf_t(Zrc)†	±2σ	n	$^{206}Pb/^{238}U$ (Ma)	±2σ	n
Criffell	Zone 1 (0917)	63.9	5.8	0.8	13	+2.9	0.7	10	408	14	9
	Zone 2 (0918)	66.0	5.8	1.1	15	+3.8	0.6	10	409	14	9
	Zone 3 (0921)	69.5	6.5	1.0	21	+3.7	0.8	10	414	10	7
	Zone 4 (0922)	68.8	7.2	1.5	22	+3.1	0.5	10	412	5	4
	Enc. Zone 1 (0917E)		6.3	0.5	15	+3.1	0.7	10	411	6	10
	Enc. Zone 2 (0918E)		6.2	0.4	15	+3.9	0.7	10	420	8	6
Fleet	Zone 1 (0933)	68.8	6.8	0.8	15	+0.7	1.2	10	410	6	4
	Zone 2 (0934)	71.2	7.1	1.5	15	+0.1	1.7	10	386	8	7
	Zone 3 (0935)	73.8	6.4	1.7	10	+1.2	2.1	5	391	8	3
Shap	Zone 1 (0923)	67.0	7.9	0.5	25	-0.2	0.7	10	417	13	7
	Zone 2 (0932)	69.1	7.6	0.4	20	-0.4	1.2	10	414	3	4
	Enc. Zone1 (0925)		7.7	0.6	24	-0.2	0.7	10	418	8	7
	Enc. Zone 2 (0926)	59.7	7.8	0.8	25				417	6	5

Enc. = enclave. * = 2 SD analytical errors vary from session to session but are generally between 0.3‰ and 0.6‰. † = 2 SD analytical error of ±0.8εHf units

4.1 The Criffell Pluton

Zircons from all zones have a mean $^{206}Pb/^{238}U$ age of 410 ± 6 Ma (n = 29) (Table 1). A large number of zircons from all zones have crystallisation ages that lie within analytical error of each other, although the youngest zircons occur in the outer two zones despite reported field evidence for the later intrusion of the inner zones (Stephens et al. 1985).

Mean zircon oxygen isotope compositions (Fig. 5.6) and heterogeneity amongst populations increase from Zone 1 (5.8 ± 0.8 ‰ (2SD; n = 13) to Zone 4 (7.2 ± 1.5 ‰

(2SD; n = 22). In zones 1, 2 and 3, 70%, 80% and 90% respectively of grains lie within analytical error of their population means (calculated independently for each session). By comparison, only 64% of analyses in zone 4 lie within analytical error of the population mean.

Zircon εHf_t compositions show limited variation and range between + 2.4 and + 4.4. Mean εHf_t values for each zone largely lie within analytical error of each other and indicate that all magmas had similarly homogenous Hf isotope compositions.

4.2 The Fleet Pluton

Zircon ages yielded a weighted mean $^{206}Pb/^{238}U$ age of 394 ± 11 Ma (n = 14) for the entire pluton (Table 1). However, the outermost biotite granite zone gives a mean $^{206}Pb/^{238}U$ age of 410 ± 3 Ma (n = 4) that is distinct from that of the two inner muscovite-bearing zones, which lie within analytical error of each other and have a mean $^{206}Pb/^{238}U$ age of 387 ± 5 Ma (n = 11).

Zircons from the outer two zones of the Fleet pluton yielded mean oxygen isotope compositions of 6.8 ± 0.8 ‰ (2 SD; n = 15) and 7.1 ± 1.5 ‰ (2 SD; n = 15) respectively (Fig. 5.6). Zircons from the inner fine-grained biotite-muscovite granite yielded a mean value of 6.4 ± 1.7 ‰ (2 SD; n = 10). In the outer zone, 73% of analyses fall within analytical error of the mean, while 53% and 40% of analyses in the middle and inner-most zones respectively fall within analytical error of their mean population values.

Mean εHf_t values for each zone of the Fleet pluton lie largely within analytical error (0.8 εHf units) of each other (excluding two points with εHf <-10) but are lower than those of the Criffell pluton, with mean εHf_t values for each zone of: Zone 1 0.7 ± 0.6, Zone 2 = 0.7 ± 0.9 and Zone 3 = 1.7 ± 1.1 (1 SD group error).

4.3 The Shap Pluton

Zircon $^{206}Pb/^{238}U$ ages (Table 1) for the granitic samples lie within analytical error of each other and yielded a mean $^{206}Pb/^{238}U$ age of 416 ± 5 Ma (n = 11).

Mean zircon oxygen isotope compositions for both stage 1 and 2 granites of the Shap pluton lie within analytical precision of each other, with mean oxygen isotope compositions between 7.6‰ and 7.9‰ (Table 1; Fig. 5.7). 85% of analyses in the stage 1 population fall within analytical error of the population mean while 76% of analyses in the stage 2 population fall within analytical error of the population mean.

Mean Hf compositions lie within analytical error of each other, with group means of: Outer zone granite = -0.3 ± 3, Inner zone granite = -0.4 ± 0.6 (1 SD group error). These values are more negative than those from the Criffell and Fleet plutons.

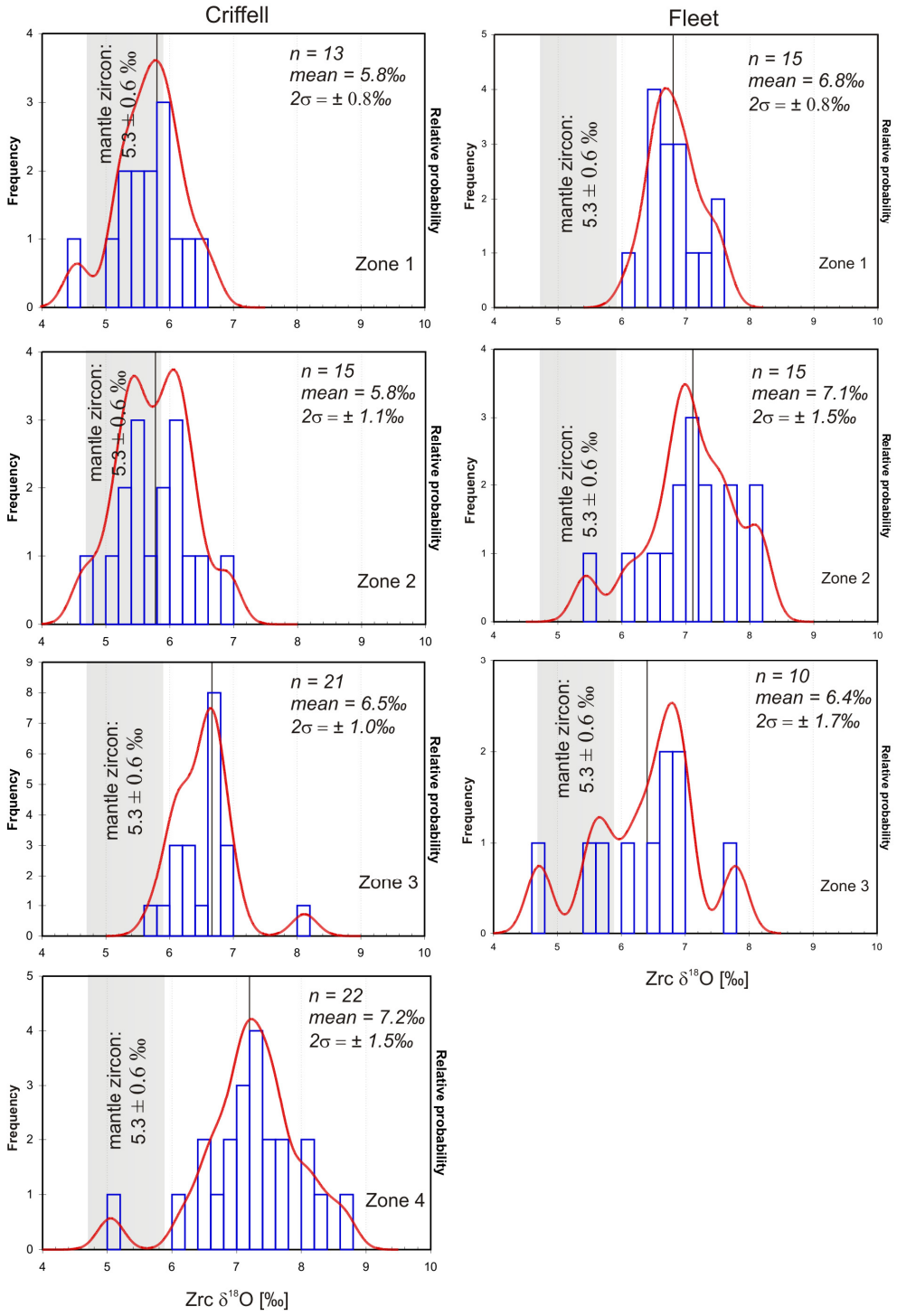

Fig. 5.6 Cumulative $\delta^{18}O$(Zrc) probability-histograms for zircon crystals from zones 1 to 4 of the Criffell pluton and zones 1 to 3 of the Fleet pluton. Outer zones of both plutons show more homogeneity in composition than inner, more silicic zones. Bin widths of histograms determined by 1 SD analytical errors; error bars are for 2 SD analytical errors.

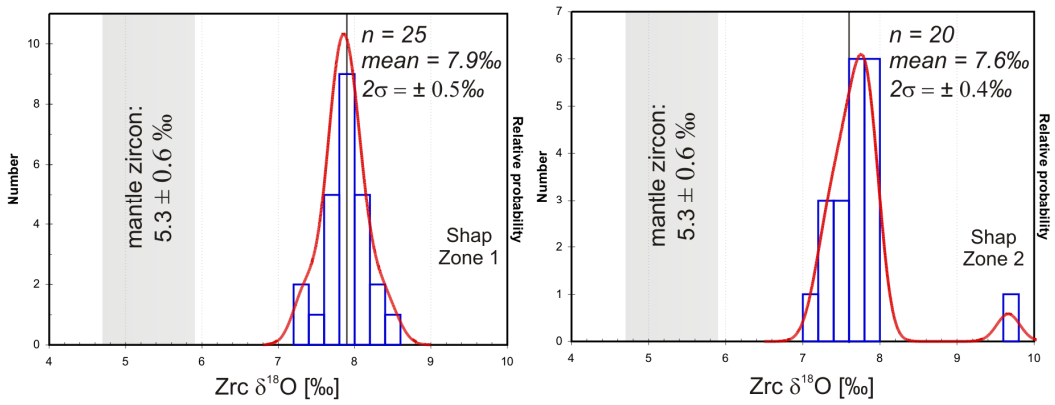

Fig. 5.7 Cumulative $\delta^{18}O$(Zrc) probability-histograms for the Shap granite. Both granitic zones show unimodal distributions of oxygen isotopes. Bin widths of histograms are 1 SD; error bars are for 2 SD analytical errors.

4.4 Dioritic enclaves

Diorite enclaves from the Criffell and Shap plutons have been studied. Zircons from a diorite enclave in Zone 1 of the Criffell pluton have a mean $^{206}Pb/^{238}U$ age of 411 ± 3 Ma (n = 10), which is within analytical error of the mean age of its host granodiorite (408 ± 7 Ma (n = 9)) (Table 1). A second enclave from Zone 2 of the Criffell pluton yielded a mean $^{206}Pb/^{238}U$ age of 420 ± 4 Ma (n = 6), which is distinctly different in age from its granodiorite host (mean age of 409 ± 7 Ma (n = 9)). Dioritic enclaves from the Shap pluton have a mean $^{206}Pb/^{238}U$ age of 418 ± 4 Ma (n = 11) and are within analytical error of the granite hosts (Table 1).

Oxygen isotope compositions for the two Criffell enclaves have mean and 2 SD population values of 6.3 ± 0.5 ‰ (2SD; n = 15) and 6.2 ± 0.4 ‰ (2SD; n = 15) respectively and differ from their host granodiorites (Fig. 5.8; Table 1). Mean oxygen isotope compositions for the Shap enclaves are indistinguishable from their host granites.

The mean εHf_t values of zircons extracted from all mafic enclaves lie within analytical error of their respective host granitoids.

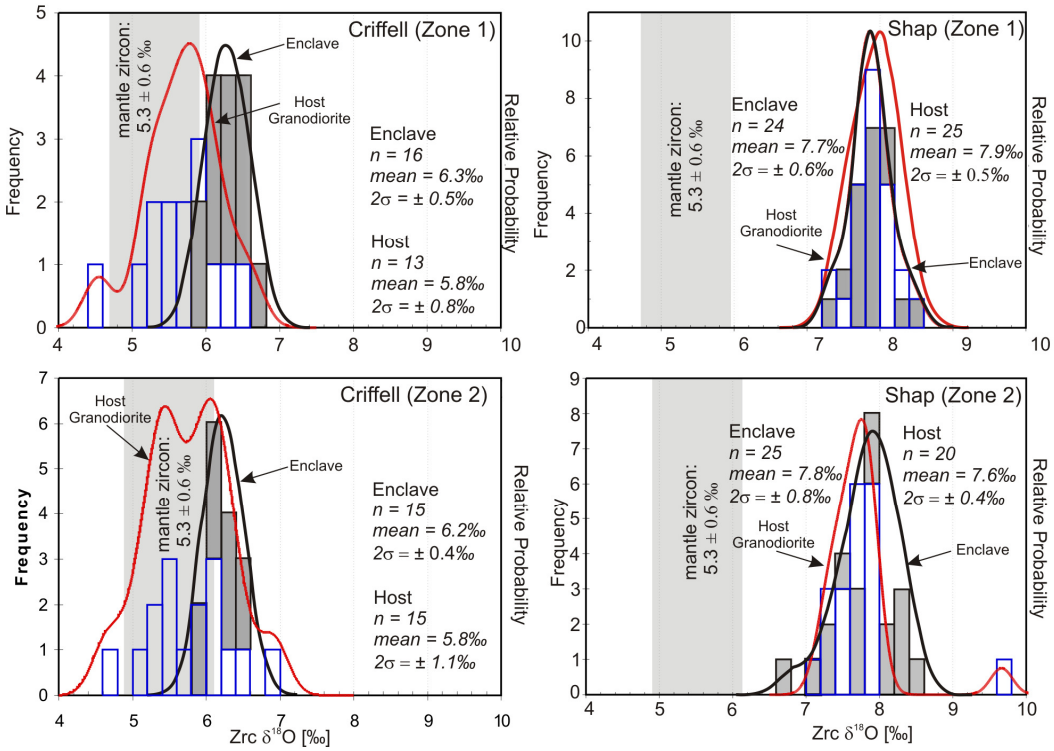

Fig. 5.8 Cumulative $\delta^{18}O$(Zrc) probability-histograms for enclaves and their host granitoids from the Criffell (a and b) and Shap (c and d) plutons. Enclaves from the Criffell pluton have tighter distributions and are generally more ^{18}O enriched than their hosts, while probability distributions for enclaves from the Shap pluton are largely similar to their hosts. Bin widths are for 1 SD analytical errors. The mean and 2 SD values for enclave and host populations are quoted in the figure.

5. Discussion

Previous age estimates for the TSS suggest that the plutons were emplaced during a phase of transpression and were often determined using poorly constrained discordia-concordia (e.g. Pidgeon and Aftalion, 1978) or whole-rock Rb-Sr methods susceptible to alteration (see Brown et al. 2008 and references therein). Our new geochronological results indicate earlier emplacement during transtensional tectonic environments. Within this time framework, the increasing heterogeneity in zircon oxygen isotope compositions in more silicic zones of the TSS plutons is discussed with reference to the involvement of mafic magmas in the formation of the S-type granites. Model ages are used to investigate the possibility that underthrust Avalonian basement was involved in the evolution of the TSS. These new findings are used to examine the interrelated magmatic and tectonic processes that have led to the distinguishing characteristics of the TSS relative to other post-Caledonian Devonian granites. These include their proximity to the Iapetus Suture at a time when subduction had ceased precluding a subduction related origin despite calc-alkaline compositions, the absence of inherited zircons despite strong chemical evidence for the partial melting and assimilation of sedimentary components, and the similar ^{207}Pb isotope compositions of all the TSS plutons (Thirlwall, 1989).

5.1 New constraints on the emplacement history of the TSS

The published age estimates for the TSS plutons range between ~ 400 and 390 Ma and are co-incident with a phase of transpression, possibly associated with Acadian deformation (Brown et al. 2008). A mean $^{206}Pb/^{238}U$ age of 410 ± 6 Ma for the Criffell pluton in this study is significantly older than the 397 ± 2 Ma Rb-Sr age reported by Halliday et al. (1980). The latter authors recognise the possibility of Rb and/or Sr redistribution caused by post-solidus alteration which may to some extent explain the difference in age observed between the two methods.

Previous age estimates for the Shap pluton are mostly < 400 Ma (Pidgeon and Aftalion, 1978; Wadge, 1978) while we have obtained a significantly older mean $^{206}Pb/^{238}U$ age of 416 ± 5 Ma for granitic samples. Contact metamorphic minerals related to intrusion of the Shap pluton have been shown to overgrow metamorphic cleavage in the surrounding country rocks (Boulter and Soper 1973). Additionally, some granitic dykes associated with the Shap granite are themselves cleaved, suggesting that cleavage formation and pluton emplacement occurred simultaneously (Soper and Kneller, 1990). New U-Pb ages reported here indicate that cleavage in the surrounding country rocks formed earlier than previously thought in Northern England and prior to Acadian transpression. Cleavage in Northern England may therefore be more closely related to cleavage forming events in the Southern Uplands (*c*. 420 Ma, Barnes et al 1989).

A mean $^{206}Pb/^{238}U$ age of 387 ± 5 Ma for the two inner zones of the Fleet pluton is broadly consistent with the previous estimates of Pidgeon and Aftalion (1978) and Halliday et al. (1980). However, a resolvable age difference is evident between intrusion of these zones and that of the older and outer-most biotite zone which has a mean age of 410 ± 3 Ma. New age determinations reported here firmly place the Criffell and Shap plutons together with the outer-most zone of the Fleet pluton within a predominantly extensional or transtensional regime constrained by independent geochronological, sedimentary and tectonic evidence (Brown et al. 2008) (Fig. 5.9). These ages are also co-incident with intrusion of the regionally prolific lamprophyre dyke swarm (Rock et al. 1986) and enhanced geothermal gradients identified in the Welsh slate belts at this time (Soper and Woodcock, 2003). Emplacement of the TSS is therefore likely to have been aided by regional extension (or transtension).

Conversely, the inner two zones of the Fleet pluton were emplaced immediately following a supposedly transpressional regime associated with a brief phase of Acadian compression (Fig. 5.9). The end-Acadian deformation has been difficult to constrain in Britain, but is thought to have ended by 390 Ma (Brown et al. 2008). Renewed extension is suggested following Acadian compression in the late

Devonian by renewed deposition in the Strathmore Basin (Armstrong and Patterson, 1970) and this may also be associated with the second phase of magmatism seen in the Fleet pluton. Deformation of cordierite in the thermal aureole of the Fleet pluton together with biotite overgrowths of local cleavage has previously been used to suggest coeval activity on the Moniaive Shear Zone and pluton emplacement (Lintern et al. 1992; Barnes et al. 1995; Phillips et al. 1995). New evidence for earlier emplacement of the outer zone of the Fleet pluton (410 Ma) presented here suggests that deformed minerals may be associated with the earlier intrusive phase while later biotite overgrowth of local cleavage may be associated with the second and later phase of emplacement (387 Ma). Reactivation of the Moniaive Shear Zone may therefore have occurred between the two intrusive phases (410 to 387 Ma).

In summary and in contrast to previous studies (see Brown et al. 2008 and references therein), new U-Pb ages in all zones of the three TSS plutons studied show that pluton emplacement occurred within predominantly extensional or transtensional tectonic environments between 420 and 400 Ma (Soper and Woodcock, 2003; Brown et al. 2008). Low grade metamorphism in the Southern Uplands sediments (Kemp, 1987) indicates that significant crustal thickening did not occur and that extension in response to crustal delamination is unlikely. Furthermore, the occurrence of granites on both sides of the suture is difficult to reconcile with slab break-off (c.f. Neilsen et al. (2009); Oliver et al. (2008)). Oblique convergence between the former continents of Avalonia and Laurentia (Brown et al. 2008) is therefore favoured as the cause of transtension and passive mantle melting.

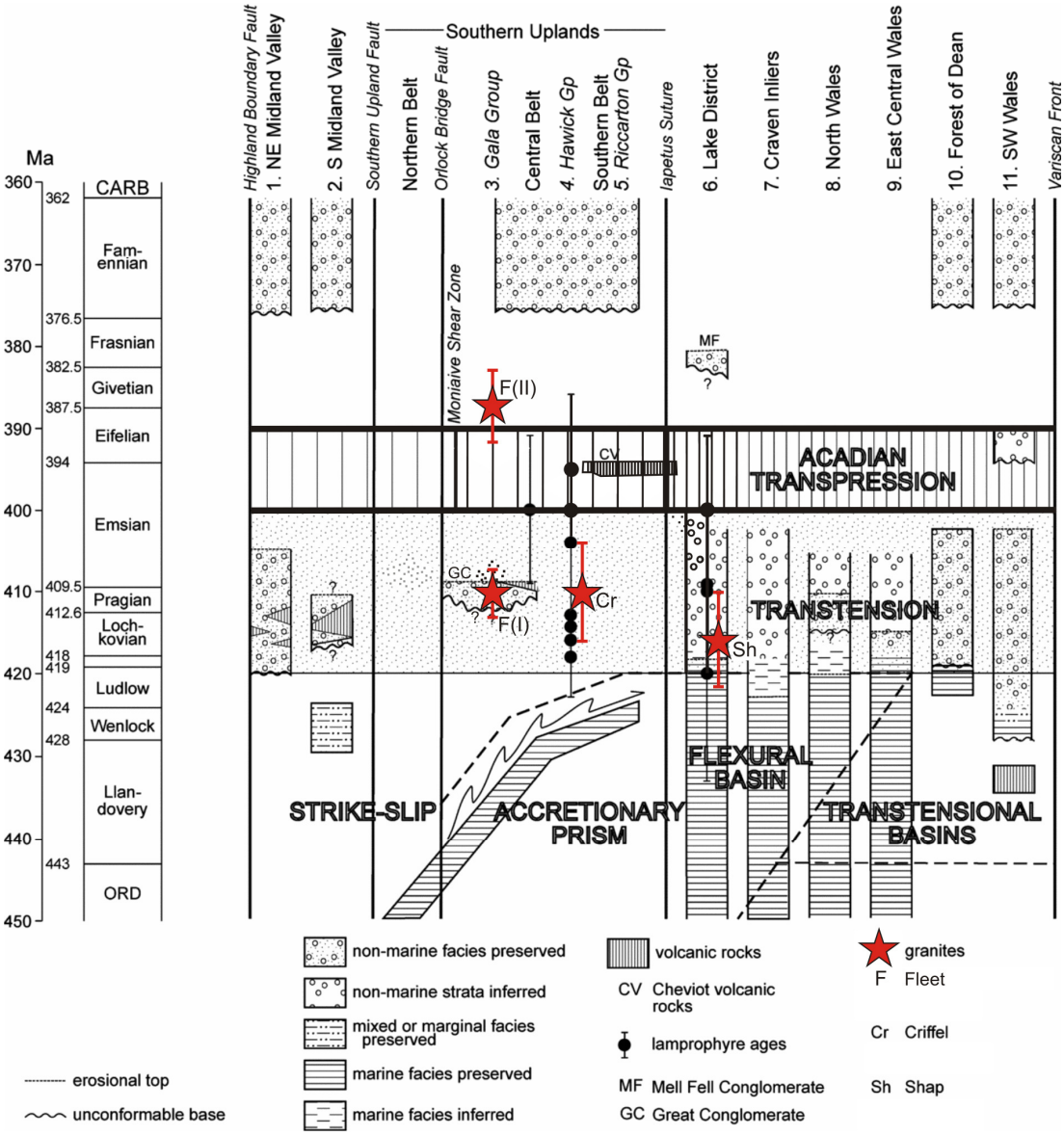

Fig. 5.9 Tectono-stratigraphic framework for Britain during the Siluro-Devonian time (after Soper and Woodcock, 2003 and Brown et al. 2008). New zircon U-Pb ages are used to re-position the TSS plutons into an independently inferred transtensional tectonic regime, co-incident with the deposition of sediments in transtensional basins and the intrusion of the regional swarm of lamprophyre dykes. F(I) and F(II) refer to the two stages of pluton emplacement seen in the Fleet pluton.

5.2 Isotopic constraints on the evolution of magma compositions

5.2.1 Zircon Oxygen Isotopes

In addition to providing new time frames for TSS pluton emplacement, zircons have yielded oxygen isotope compositions that have enabled a number of magmatic sources to be identified and distinguished. Under closed system conditions where magma differentiation is controlled by crystallisation alone, all minerals should remain in isotopic equilibrium and melt-zircon fractionation factors (Δ(melt-Zrc)) increase with increasing SiO_2 (Valley et al. 1994). It follows that compositional variability larger than analytical error (~ 0.6 ‰) can only result from the addition of isotopically distinct materials.

The total range in zircon $\delta^{18}O$ is up to ~ 4 ‰ in the Criffell pluton, ~ 3.5 ‰ in the Fleet pluton and ~ 1.3‰ in Shap (Figs. 6 and 7). The range of values observed in the former two plutons requires the assimilation (or mixing) of material from compositionally distinct sources, consistent with the variations in $^{87}Sr/^{86}Sr$ and εNd reported by Halliday (1984) and Halliday et al. (1980) in the WR suites. Zircon populations in individual samples from the outer zones of the Criffell and Fleet plutons have unimodal $\delta^{18}O$ distributions that lie mainly within analytical error of their means (2 SD in the populations of between 0.6 and 0.8 ‰). However, with increasing WR SiO_2, mean $\delta^{18}O$(Zrc) compositions in magmatic zircons generally increase in tandem with $\delta^{18}O$ heterogeneity within sample populations (Fig. 5.6). These observations imply that there was a range in magma compositions at the time of zircon crystallisation, and that in some cases zircons from different magma batches may have been preserved within the same whole rock sample. Similarly cryptic evidence of magma heterogeneities and mixing has also been reported from zircon $\delta^{18}O$ compositions in the Devonian Lochnagar pluton in the Scottish Highlands (Appleby et al. 2008).

The existence of primary magmatic zircons with more primitive isotope compositions than would otherwise be predicted from WR compositions has been noted from other S-type granites (e.g. Appleby et al. 2010; Kemp et al. 2006a; 2009) and this evidence contradicts some previous models for the origin of S-type plutons by melting of only sedimentary material (Chappell and White, 1974). The cryptic evidence for the involvement of mafic magmas in the genesis of S-type granites signals a potentially important role for such granites in the formation of stable new continental crust (see Hawkesowrth et al. 2010).

5.2.2 Mafic enclaves

Differences between the Nd isotope compositions of host granodiorites and mafic, dioritic enclaves in the Criffell pluton have previously been used to argue that they do not originate from restite separation or cumulate formation from their host rocks (Holden, et al. 1987; Holden, 1991). New U-Pb ages obtained using zircons separated from one such enclave from Zone 2 reveal a mean age of 420 ± 4 Ma. This age is significantly older than that of another mineralogically similar enclave (411 ± 4 Ma) in Zone 1, and its host granodiorite (409 ± 4 Ma) (Table 1). This confirms that both enclaves and their host granitoids have different magmatic histories, even if they now appear as part of the same overall magmatic episode. The oxygen isotope compositions of zircons from both enclaves in the Criffell pluton show unimodal distributions, with all grains falling within analytical error of their means (Fig. 5.8). Mean zircon $\delta^{18}O$ for both enclaves is ~ 0.5 ‰ higher than the mean $\delta^{18}O$ of their host granodiorites and both the enclaves studied have more limited $\delta^{18}O$ distributions (± 0.4 - 0.5 ‰ 2SD), providing further evidence of discrete origins. The mineral assemblage of mafic enclaves has been successfully used to model the evolution of WR compositions assuming fractional crystallisation and assimilation of Avalonian sediments (Stephens et al. 1985; Chapter 2). The older ages reported from zircons separated from some of the enclaves together with different WR isotope compositions may support the interpretation that mafic enclaves in the Criffell pluton represent entrained assemblages from the crustal hot zone located at depths of > 11

km beneath the pluton. U-Pb ages together with zircon oxygen isotope compositions from mafic enclaves in the Shap pluton lie largely within error of their hosts and therefore do not offer any further evidence of their formation (Fig. 5.8).

5.3 Isotope evidence for crustal reworking

The WR compositions of late- and post-Caledonian Devonian granites throughout Scotland have provided valuable information about the large-scale divisions of lower crustal domains (Frost and O'Nions, 1985; Halliday et al. 1980; Hamilton et al. 1980; Harmon and Halliday, 1980b; Pidgeon and Aftalion, 1978). However, the characteristics of individual sources remain ambiguous and it is unclear whether the TSS is the product of mantle-derived magmas contaminated by crustal components, reflecting net additions to the continental crust, or results entirely from crustal reworking (Clayburn et al. 1983; Halliday 1984; Halliday et al. 1980; Harmon and Halliday 1980b; Frost and O'Nions 1985). The O-Hf isotopic compositions of magmatic zircons have recently provided a further means of distinguishing different source contributions and relative proportions of crustal growth and reworking (e.g. Appleby et al. 2010; Hawkesworth and Kemp, 2006; Kemp et al. 2007; Marschall et al. 2010).

Between ~ 50% and 62% of zircon crystals from the more mafic outer two zones of Criffell have oxygen isotope compositions that fall within the accepted range of mantle-like compositions (5.3 ± 0.6 ‰; Valley et al. 1998). Such compositions may reflect magmas derived directly from the mantle or from juvenile lower crust, potentially representing net additions to the crust. By contrast, more evolved zones of Criffell contain only ~ 5% mantle-like zircons, compared to up to 30% in the inner and most evolved zone of the Fleet pluton (Fig. 5.6). In these zones, the majority of zircons therefore have $\delta^{18}O$ compositions that exceed those in equilibrium with mantle or juvenile lower crust and instead reflect reworking of ^{18}O-rich upper crustal material. No zircons from the Shap pluton exhibit mantle-like compositions (Fig. 5.7).

In contrast to oxygen isotopes, the initial εHf_t values of all zircons from all three plutons are lower than those of contemporaneous depleted mantle (~ +16 ± 3; Vervoort and Blichert-Toft, 1999), where the variability of ± 3 εHf units is estimated from present-day variations in MORB (Griffin et al. 2000; Fig. 5.10). However, enriched mantle compositions may be similar to zircon compositions in the Criffell pluton. Characterising Devonian mantle compositions in the Iapetus Suture region is therefore crucial for estimating relative mantle and crustal contributions in the TSS.

Enriched mantle compositions have been identified from the εNd compositions of mantle-derived mafic magmas of upper Silurian to Lower Devonian (~ 416 Ma) age across Scotland (Thirlwall, 1982). In detail, enriched mantle components with εNd values between +1.1 and -3.6 (estimated εHf = +3.6 to -2.9) have been found *north* of the Highland Boundary Fault. However, upper Silurian to Lower Devonian (~ 416 Ma) age calc-alkaline lavas *south* of the Highland Boundary fault, close to the TSS, have εNd values up to +6.4 (estimated εHf_t values of +11.4) that are more characteristic of depleted mantle. Some offset to more radiogenic Sr relative to the Sr-Nd mantle array is thought to reflect earlier subduction-related modification of a predominantly depleted mantle (Thirlwall, 1982). It is therefore more likely that any mantle contributions to the TSS were sourced within depleted and not enriched mantle.

Variability in zircon εHf_t compositions is limited among zircons from individual plutons, but they vary between plutons by ~ 5 εHf units. The most positive and mantle-like zircon εHf_t compositions are found in the Criffell pluton (+3.4 ± 0.3), while the most negative and crust-like values are found in the Shap pluton (-0.4 ± 0.5) with intermediate values from the Fleet pluton (+1.0 ± 0.8). εHf_t data therefore suggest that all zircon compositions, including those with apparently mantle-like $\delta^{18}O$ values formed from either non-mantle sources or by the hybridisation of mantle and crustal components.

5.4 Granite sources in the Iapetus Suture Zone

The identity of crustal sources in each of the TSS plutons is difficult to constrain due mainly to the absence of basement exposure. Zircon O-Hf arrays reveal two apparent trends (Fig. 5.10), one defined at an inter-pluton scale, extending from radiogenic (Shap) to less radiogenic (Criffell) εHf_t compositions, and the second at an intra-pluton scale, ranging from low to high ^{18}O compositions with little variation in εHf_t.

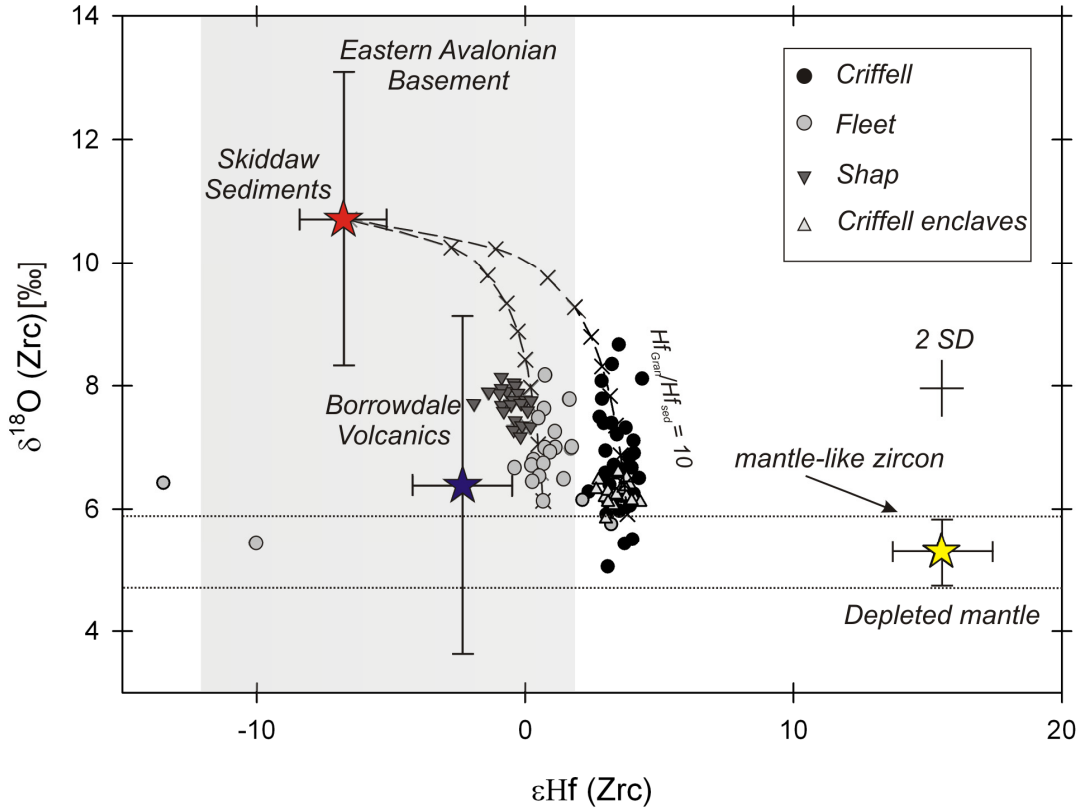

Fig. 5.10 εHf_t vs. $\delta^{18}O$ of zircons from the Criffell, Fleet and Shap plutons, with the estimated average compositions (with 1 SD) of potential endmembers. The composition of Eastern Avalonian basement is estimated from recalculated Nd isotope compositions (using the Nd-Hf correlation from Vervoort and Blichert-Toft, 1999) using data from Murphy et al. (2000). No oxygen isotope data for Avalonian basement is available. Similar Pb isotope compositions in all three plutons support a common source for all three plutons, consistent with similar Hf compositions between estimated Avalonian basement and the TSS. Slightly more radiogenic Hf compositions in the Criffell pluton may reflect minor contributions from depleted mantle or a further juvenile source. Further mixing with Skiddaw Group (or similar) sediments is proposed to generate the vertical arrays of compositions, marked with 10% increments of sedimentary contaminant. Other source rock compositions are from: Depleted mantle: Vervoort and Blichert-Toft (1999); Avalonian basement: Murphy et al. (2000); Skiddaw Group sediments: Stone and Evans (1997); Thomas (1985). Oxygen compositions for the Skiddaw Group have been re-calculated as equilibrium zircon compositions using the whole-rock-zircon equilibrium relationship outlined by Lackey et al. (2005).

5.4.1 Inter-pluton $\delta^{18}O$-εHf_t trend

Differences in zircon εHf_t between different plutons may indicate discrete sources for each of the three plutons, or that each lies at a different position along a single mixing curve between primitive and evolved source regions. A source or sources common to all three plutons is favoured by the persistent occurrence of high $^{207}Pb/^{204}Pb$ compositions in all plutons (Thirlwall, 1989) (Fig. 5.5). Pb isotope compositions also imply no involvement of Southern Uplands sediments in the genesis of the TSS (Thirlwall, 1989; Chapter 2) and mean that all potential sources reside at depths that exceed the thickness of the sediment pile. Stephenson (1999) suggests that the Southern Uplands sediments extend to depths equivalent to the Iapetus Suture itself, indicating that all potential sources must therefore lie within or below the Avalonian terrane that underlies the suture. Elevated Pb isotope compositions have been linked to Avalonian sediments with a similar composition to those found in the English Lake District (Thirlwall et al. 1989; Chapter 2). However, Pb isotope compositions in the Fleet pluton extend to more radiogenic compositions than the Skiddaw Group sediments (Fig. 5.5) and suggest that an underlying crustal component within the Avalonian terrane may also be involved.

Model ages provide a potential means of identifying and characterising the magmatic sources involved in the formation of the TSS. Dhuime et al. (2011) point out that juvenile crust generated in modern arcs does not resemble the Hf isotope composition of depleted mantle and as such, model ages should be calculated using the 'new crust' reference line and not depleted mantle. Only zircons with mantle-like oxygen isotope compositions can be considered to provide Hf model ages that reliably date crustal extraction from the mantle (Dhuime et al. 2012). Those with more ^{18}O-enriched isotope compositions than mantle values reflect crustal reworking and provide only hybrid model ages with little geological significance. However, zircons from the three TSS suite plutons studied show limited variation in Hf despite larger intra-pluton variations in ^{18}O. In the case of the three plutons studied and when calculating Hf model ages, there is therefore no need to limit the selection of crystals to mantle-like zircons only. Model ages using zircons from the Criffell pluton,

calculated using the 'new crust' reference curve, suggest ages of ~ 0.9 to 1.0 Ga (Fig. 5.11).

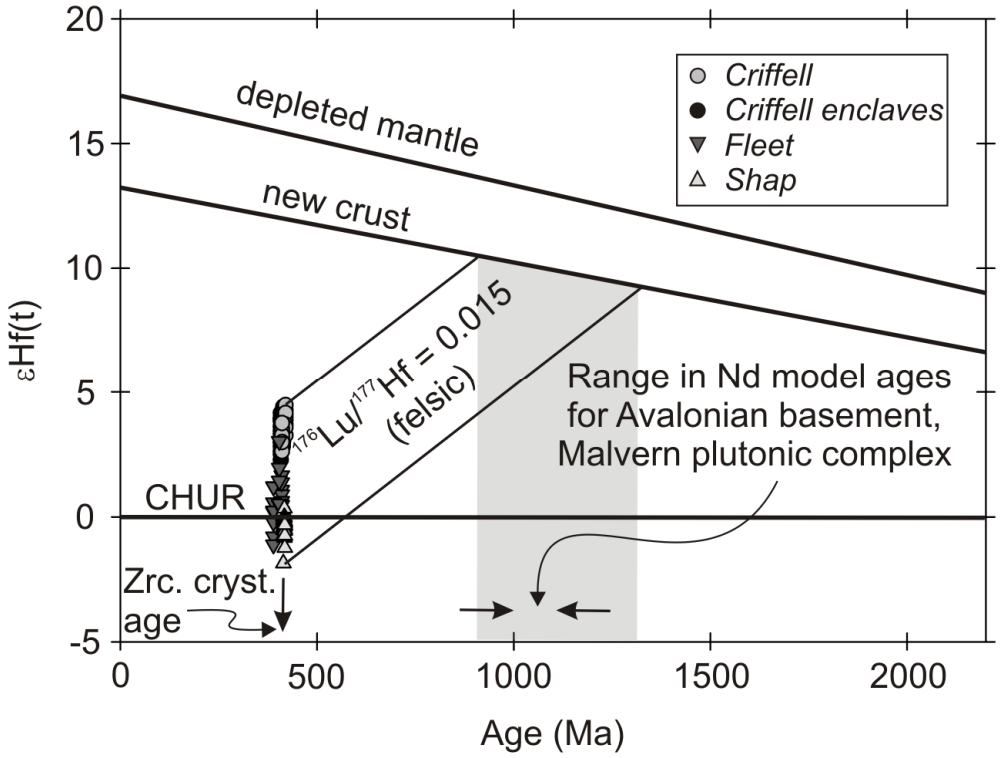

Fig. 5.11 Model age calculations for the TSS plutons calculated using the 'new crust' reference line of Dhuime et al. (2011). A Lu/Hf ratio of 0.015 has been used assuming silicic crust. Model age estimates are youngest for the Criffell pluton and increase in the Fleet and Shap plutons and lie within the range of model ages estimated for Avalonian basment (between horizontal arrows) (Murphy et al. 2000) re-calculated using a 'new crust' Nd reference line (see text). Zircon crystallization ages (Zrc. cryst. age) are shown by a vertical arrow.

Due to a lack of exposure, model ages for the Avalonian basement have relied on Sm-Nd analyses from Neoproterozoic to Early Silurian igneous rocks thought to be derived almost exclusively from remelting of Avalonian basement (e.g. Ayuso, 1986; Murphy et al. 2000; Nance et al. 2008; Nance, 1996). Confirmation of basement isotopic compositions has come from close similarities in the calculated Nd model ages of arc-related igneous rocks formed across a range of different periods throughout the Avalonian terrane. Most studies suggest that the Avalonian basement was generated in a series of ocean island arcs between 1.2 and 1.0 Ga (Murphy et al. 2000). In the UK, the Malvern Plutonic Complex (~ 677 Ma) is thought to provide one of the only opportunities to examine the Avalonian basement, yielding model ages of between 1.2 and 1.0 Ga (Thorogood, 1990), similar to estimates from other

regions of Avalonia (Murphy et al. 2000). However, these model ages assume that new crust resembles the Nd compositions of depleted mantle. In order to enable more reliable comparisons between the Hf model ages calculated in this study and published data on Avalonian basement, a new crustal reference line for Nd isotopes has been estimated. This uses the εHf_t composition of 'new crust' (εHf = +13.2, Dhuime et al. 2011) together with a Nd-Hf relationship of $\varepsilon Hf = 1.40\varepsilon Nd + 2.1$ (Vervoort and Blichert-Toft, 1999). Model ages for Avalonian basement calculated using a 'new crust' curve for Nd range between ~ 1.0 and 1.1 Ga.

The similarities observed between the model ages of proposed Avalonian basement and those of the TSS of plutons suggests that a significant proportion of Avalonian re-working was involved in the formation of this granite suite. The slightly younger model ages estimated using zircons from the Criffell pluton relative to Avalonian basement model ages may reflect small contributions from depleted mantle or an additional juvenile source. In general, Hf isotope compositions support independent seismic evidence for the underthrusting of Avalonian crust beneath the Laurentian margin (Beamish and Smythe, 1986; Freeman et al. 1988; Hall 1984; Klemperer and Matthews, 1987; Klemperer et al. 1991).

5.4.2 Intra-pluton $\delta^{18}O$-εHf_t trends

Intra-pluton trends are characterised by variations in the degree of ^{18}O enrichment (Fig. 5.10) and are highly indicative of supracrustal contributions. Pb isotope compositions in the WR suite (Thirlwall, 1989) indicate that the sediments are likely to be similar in composition to the Skiddaw Group (Fig. 5.5). Average $\delta^{18}O$ (12.7 ± 1.6 ‰ 1SD) and εHf (-6.5 ± 2.4 1SD) compositions for the Skiddaw Group sediments have been estimated using published data from Thomas (1985) and Stone and Evans (1997), with oxygen compositions recalculated to give equilibrium zircon oxygen isotope compositions. Best-fit mixing curves between the most primitive ^{18}O components in each pluton and the Skiddaw Group suggest sediment contributions of

up to ~ 50% in the most S-type zones of the Criffell pluton. Equivalent calculations for the Fleet pluton also indicate sedimentary contribution of up to ~50%.

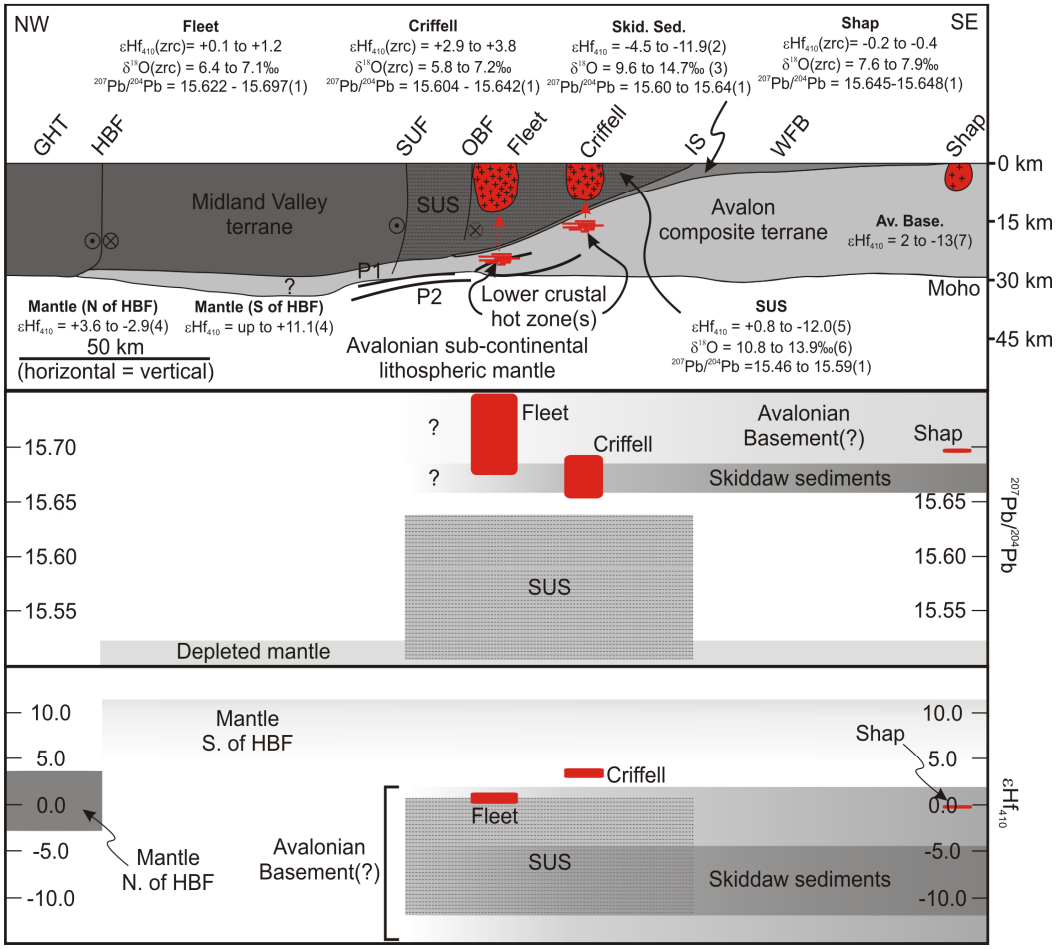

Fig. 5.12 Cross-section of the Iapetus Suture based on the construction of Brown *et al.* (2008) along the UK Geotraverse North line at the present day showing proposed Hf, O and Pb isotope compositions of granitoids and possible magma sources. Horizontal scale is the same in all plots. Avalonian crust is shown underthrusting the Laurentian margin with proposed hot zones at depths of > 11 km within the underthrust Avalonian crust (positions beneath the suture are unconstrained). P1 and P2 represent prominent seismic reflectors interpreted as either Iapetus oceanic crust or imbricated basement and sedimentary cover (see text). Pale shading within the lithospheric mantle, beneath the suture zone crust, represents mantle melting and lamprophyric magma genesis. Curved arrows represent ascent of these melts into the crust and their possible role as contributing melts and heat sources in the genesis of the TSS. Abbreviations are: GHT – Grampian Highland Terrane; HBF – Highland Boundary Fault; SUF – Southern Uplands Fault; OBF – Orlock Bridge Fault; SUS – Southern Uplands Sediments; IS – Iapetus Suture; WFB – Windermere Flexural Basin; Skid. – Skiddaw Group sediments; Av. – Avalonia; zrc – zircon compositions. Granitoid O and Hf (recalculated at 410 Ma) isotope compositions are those measured in this study in zircons from the Criffell, Fleet and Shap plutons. Pb isotope data is from Thirlwall (1989). Depleted mantle Pb isotope compositions around the Iapetus Suture at 410 Ma are from Frost & O'Nions (1985). Hf compositions (recalculated at 410 Ma) are estimated from published Nd data using the Nd-Hf relationship of Vervoort & Blichert-Toft (1999). Mantle oxygen isotope compositions are from Valley *et al.* (1998). Other data sources include: Stone & Evans (1997), Thomas *et al.* (1985), Thirlwall (1986), O'Nions *et al.* (1983), Halliday *et al.* (1980), Murphy *et al.* (2000).

Although many uncertainties remain regarding the nature of the source rocks beneath the Iapetus Suture, the common source or sources suggested by WR isotopes (Thirlwall, 1989) are consistent with zircon O-Hf isotopic data from the three TSS plutons examined here. These results are also consistent with crustal models based on seismic evidence for the underthrusting of Avalonian material beneath the Laurentian margin (Freeman et al. 1988; Hall, 1984; Klemperer and Matthews, 1987; Klemperer et al. 1991; Soper et al. 1992). Using the lithospheric cross-section constructed by Brown et al. (2008) from seismic and geological constraints, crustal hot zones in which magma compositions were predominantly determined would be located at depths of > 20 km beneath the Fleet pluton and > 11 km beneath the Criffell pluton (Fig. 5.12).

5.5 Tectonic controls on pluton formation and emplacement

The calc-alkaline compositions of the TSS together with their proximity to the former Iapetus subduction zone have presented a significant challenge to understanding the tectonic-magmatic evolution of the region. Despite evidence for periods of transtension following closure of the Iapetus at ~ 420 Ma, previous age estimates suggest that the TSS plutons were emplaced during periods of transpression at ~ 400 to 390 Ma (see Brown et al. 2008 and references therein). Reconciling the formation of granite plutons with tectonic evidence of transpression has led to the recent suggestion of 'incipient delamination' linked to changes in the distribution of vertical stresses following lithospheric shortening (O'Reilly et al. 2012). The new U-Pb ages reported here show that all three TSS plutons studied were emplaced during phases of transtension before ~ 400 Ma and after ~ 390 Ma (Fig. 5.9). It is therefore unnecessary to appeal to mechanisms such as 'incipient delamination' and it is likely that the simultaneous intrusion of mafic lamprophyre dykes (Rock et al. 1986) and the TSS of granite plutons resulted primarily from passive melting and heat transfer into the crust during lithospheric transtension constrained by independent geochronological, sedimentary and tectonic evidence (see Brown et al. 2008).

Transtension is a characteristic tectonic feature of arcs as well as regions of oblique continental convergence, and is increasingly being recognised as an important factor in the formation and preservation of granitic plutons (e.g. Tikoff and Teyssier, 1992; Grocott et al. 1994; Teyssier et al. 1995; Dewey, 2002; Hanson and Glazner, 1995; Paterson and Fowler, 1993; Weinberg et al. 2004; Kemp et al. 2009; Kirsch et al. 2012; Hawkesworth et al. 2010). Granites in the Lachlan Fold Belt (SE Australia) have been shown to represent changing net additions to the local continental crust that reflects the interplay of transtension and transpression, albeit during active subduction (Kemp et al. 2009). I-type granites, similar in compositions to I-type components of the TSS have been shown to represent 70% new crustal growth, confirming the importance of extensional tectonic regimes in creating new crustal material. Furthermore, zircon O-Hf isotope compositions from the S-type granites of the Lachlan Fold Belt generated during phases of crustal thickening were shown to contain up to ~30% mantle material. These results mirror the discovery of cryptic signatures of mafic magma involvement in S-type plutons found here and in other recent micro-analytical studies that suggest that S-type granites may also represent net additions to the continental crust in some areas (Appleby et al. 2010).

Transtension and extension are also likely to aid pluton emplacement. On the basis of numerical modelling and using viscosities of 10^6 Pa·s and density contrasts of ~ 200 kgm^{-3} considered representative of calc-alkaline granitoids, Petford et al. (1993) suggest that dyke ascent is a viable mechanism for the transport of large volumes of granitoid melt through the crust, particularly in areas of extension or transtension. It was proposed that the critical dyke width required in order to prevent melts from freezing is between 2m and 7m. Calculated batholith-filling times are therefore orders of magnitude greater than mean cavity-opening rates, estimated at ~ 0.7cm a^{-1} from fault slippage rates (Tikoff and Teyssier, 1992). It is therefore likely that many, if not most, plutons form incrementally, reflecting decreasing volumes of available melts for extraction from deeper source regions (Petford et al. 1993) and potentially crustal hot zones (Annen and Sparks 2002; Annen et al. 2006). Such findings are supported by zircon U-Pb ages, including those from the Fleet pluton that indicate

assembly over ~ 23 Ma. It is highly implausible that plutons could have been maintained in fully molten states in the upper crust over tens of millions of years, with similar conclusions from other studies used to infer incremental assembly over protracted time periods (Coleman, 2004; Glazner et al. 2004; Lipman, 2007).

The absence of inherited zircons in the TSS has also been used to distinguish them from other Devonian granites throughout Scotland (Pidegon and Aftalion, 1978). However, with strong evidence for the involvement of supracrustal components in the formation of the TSS together with continued zircon saturation throughout magma evolution (Chapter 2), the absence of inherited zircon is unlikely to reflect source characteristics or dissolution in zircon-undersaturated melts. Instead, it is more likely to reflect distinct magmatic processes in the TSS relative to other Devonian granites. The calc-alkaline compositions and low magmatic temperatures (~650 ^{o}C to 750 ^{o}C) of the TSS are considered to result from elevated water contents (Chapter 2) and the absence of inherited zircons to reflect resorption during wet magma ascent under super-liquidus conditions. Elevated water contents in the TSS relative to Devonian plutons further north in Scotland is consistent with their proximity to the former Iapetus Suture, where prolonged dehydration of Iapetus oceanic crust is likely to have occurred, analogous to the early Basin and Range suites in the western United States (Humphreys et al. 2003). Significant hydration of the underlying mantle lithosphere is also evident from the regionally prolific occurrence of lamprophyre dykes in and around the Iapetus Suture (Rock et al. 1986).

There is therefore good evidence that the unusual characteristics of the TSS plutons reflect the unique tectonic and crustal setting in which their genesis and emplacement took place.

6. Conclusions

New zircon U-Pb ages confirm that the Criffell and Shap plutons were emplaced earlier than previously thought, with mean ages of 410 ± 6 Ma and 416 ± 5 Ma for the Criffell and Shap plutons respectively. An age of 410 ± 3 Ma for the outer zone of the Fleet pluton is also considerably older than previous estimates; however, the two inner zones reveal a mean age of 387 ± 5 Ma and demonstrate a protracted history of pluton growth. These new ages confirm that pluton emplacement occurred during an inferred stage of transtension, coinciding with the regional intrusion of a lamprophyric dyke swarm. The emplacement of the inner zones of the Fleet pluton may coincide with post-Acadian extension.

Zircon oxygen isotope compositions in different zones of the Criffell, Fleet and Shap plutons show intra-zone variability at the pluton scale consistent with open system differentiation. At an intra-sample scale, zircons in more primitive granodiorites are isotopically homogeneous, while greater isotopic variation is evident amongst zircon crystals in more silicic zones, reflecting the preservation of compositionally diverse magmas prior to crystallisation. The occurrence of more primitive zircon oxygen isotope compositions in the more silicic zones also reflects the involvement of more mafic magmas in the formation of large S-type plutons such as Fleet.

Mafic enclaves in the Criffell pluton are shown to contain zircons with different oxygen isotope compositions and in one example mean U-Pb ages are ~9 Ma older than their hosts. They are considered to represent entrained cognate material in segregated magma batches, derived potentially from regions of magma generation and differentiation in lower crustal hot zones.

Zircon εHf_t values are distinct and show little variation in each of the Criffell, Fleet and Shap plutons. Zircon εHf_t compositions in all plutons reveal model ages consistent with the involvement of Avalonian basement in magma genesis. Previous

Pb isotope studies (Thirlwall, 1989) have confirmed the absence of local Southern Uplands sediments in the origin and evolution of the TSS plutons and instead point to the involvement of sedimentary components found in the underthrust Avalonian terrane. Hf model ages in all TSS plutons calculated using the most mantle-like zircons are similar to estimated model ages for Avalonian basement. Further mixing with up to 50% of a sedimentary component similar to the Skiddaw Group found on the Avalonian terrane is capable of reproducing intra-pluton trends of ^{18}O enrichment in zircons from the Criffell and Fleet plutons.

Evidence for high water contents in these granites linked to the adiabatic ascent of transiently super-liquidus melts and resorption of all entrained crystals (Chapter 2) reflects the importance of hydrated lithosphere in magma genesis. This may in turn have resulted from earlier dehydration of the subducting Iapetus oceanic crust and is consistent with the extensive occurrence of lamprophyric dykes and calc-alkaline granitoids of the same age around the suture zone. Many of the unusual chemical and physical characteristics that distinguish these calc-alkaline granites from other late and post-Caledonian granites can therefore be linked to their emplacement and formation during crustal transtension within the Iapetus suture zone.

Chapter 6

The hydrothermal history of British Devonian granites: Insights from zircon, quartz and whole-rock oxygen isotope compositions[†]

Abstract

Zircon $\delta^{18}O$ compositions in two Devonian calc-alkaline Trans-Suture Suite (TSS) granites in Scotland preserve magmatic $\delta^{18}O$ compositions that are mostly out of isotopic equilibrium with the $\delta^{18}O$ compositions of their whole-rocks and co-existing quartz. The latter two archives have elevated $\delta^{18}O$ compositions that suggest hydrothermal alteration and exchange related to the circulation of ^{18}O-rich magmatic fluids with no detectable input from ^{18}O-depleted meteoric water. Larger degrees of disequilibrium in the outer zones of the two plutons reflect additional fluid exchange with local ^{18}O-rich sedimentary rocks. By contrast, the hydrothermal history of the mostly tholeiitic British Tertiary Igneous Province (BTIP) is characterised by low $\delta^{18}O$ compositions (<5.3‰) related to circulation of meteoric water and assimilation of local ^{18}O-depleted rocks. These differences result from fundamentally different hydrothermal histories that reflect different tectonic environments, mantle conditions and emplacement depths. Meteoric water circulation (if any) around the TSS plutons is likely to have been limited or excluded by deeper emplacement (4 to 6 km; BTIP: 1 to 2 km), emplacement into metasediments with low permeability and reduced thermal potential related to protracted and incremental pluton assembly. The water-rich magmas of the TSS, that determine their calc-alkaline compositions, reflect derivation in part from previously hydrated mantle.

[†] Co-authors: Colin Graham – *University of Edinburgh*; Chris Hawkesworth – *University of St Andrews*; Martin Gillespie – *British Geological Survey*; Richard Hinton – *University of Edinburgh*; EIMF

1. Introduction

The oxygen isotope composition ($\delta^{18}O$) of magmas and their resultant rocks may be controlled by a variety of processes including the compositions of source rocks, fractional crystallisation, water contents, exchange with magmatic fluids and post-solidus hydrothermal alteration (e.g. Taylor, 1986; Eiler, 2001; Valley et al. 2005). Whole-rock compositions provide evidence for the cumulative effects of some or all of these processes and it has proved difficult to distinguish their individual actions. Zircon provides a robust and reliable archive of magmatic compositions at the time of crystallisation and is largely immune from the effects of post-solidus exchange that modify whole-rock (WR) analyses and those of less robust minerals such as feldspar (Valley 2003). Integrated studies that combine the $\delta^{18}O$ compositions of zircon, WR and coexisting minerals therefore provide a valuable means of examining magmatic equilibration, re-equilibration and post-magmatic alteration. Zircon has also been successfully used to determine crustal structure and magmatic evolution in a number of igneous and metamorphic rocks from a wide range of tectonic provinces (King et al. 1998; 2002; 2004; Bindeman and Valley, 2000, 2003, Peck et al. 2000; 2001; King and Valley, 2001; Valley et al. 2002, Valley, 2003; Appleby et al. 2008; 2010). The magmatic and hydrothermal histories of granites from the Devonian Trans-Suture Suite (TSS) are examined and compared to those from the British Tertiary Igneous Province (BTIP) using the $\delta^{18}O$ compositions of zircon, quartz and their respective WR. Their compositions are used to reveal fundamentally different hydrothermal histories and processes that reflect contrasting tectonic environments, mantle compositions, emplacement depths and assembly times.

1.1 The Devonian Trans-Suture Suite Plutons

The Criffell and Fleet plutons are situated in the Southern Uplands of Scotland (Fig. 6.1). The plutons form part of a sub-set of Devonian granites situated adjacent to the Iapetus Suture and are referred to as the Trans-Suture Suite (TSS) (Brown et al. 2008). The plutons have calc-alkaline compositions despite post-dating Iapetus

subduction and closure. Further uncertainty regarding the origins of these plutons has arisen from U-Pb ages that suggest emplacement during times of regional transpression (see Brown et al. 2008 for a review). New emplacement ages determined using high precision Secondary Ionisation Mass Spectrometry (SIMS) of zircons from three of the TSS (Criffell, Fleet and Shap) now confirm that all plutons were emplaced during pre- and pos-Acadian stages of transtension (Chapter 5; Brown et al. 2008).

The Criffell pluton was emplaced at 410 ± 6 Ma (Chapter 5) into low-grade wackes and pelites of Llandovery to Wenlock (444 to 423 Ma) age that form part of the Southern Uplands accretionary prism in southern Scotland (Fig. 6.1b). The pluton is normally zoned (Stephens et al. 1980, 1985), with outer zones (1 and 2) of metaluminous granodiorite (~ 58 wt % SiO_2), a transition Zone (3), and inner zones (4 and 5) of peraluminous granite (~ 72 wt % SiO_2). Granodiorite samples contain primary hornblende (with occasional cores of clinopyroxene), biotite, plagioclase, potassium feldspar, quartz and accessory sphene, zircon, apatite, allanite and magnetite (with very minor haematite). Granite samples contain primary muscovite and small amounts of monazite but lack hornblende, sphene and the abundant zircon and magnetite that characterise the granodiorite. Only in zones 1 to 4 was zircon found in great enough abundance for analysis. Mineralogical evidence for hydrothermal alteration is limited to moderate sericitisation of some feldspar crystals and minor chloritisation of ferromagnesian minerals, mainly biotite.

The ~ 10 km by 12 km Fleet pluton intrudes the Llandovery sediments (428 to 444 Ma) of the Central Belt of the Southern Uplands (Fig. 6.1c) and is situated south of the Orlock Bridge fault (Fig 6.1a). New zircon ages suggest an emplacement age of 410 ± 3 Ma for the outer zone of Fleet and 387 ± 5 Ma for the two inner zones (Chapter 5). SiO_2 contents vary from 69 to 76 wt% and are on average more evolved than other TSS granites. Their typical S-type compositions are reflected in their petrology. The pluton has two main granite facies, including an outer biotite granite and inner biotite-muscovite granite (Fig 6.1c). The latter facies has subsequently been subdivided into fine and coarse grained units (Parslow, 1968). A contact

metamorphic aureole within the Lower Palaeozoic greywackes has a maximum width of 1.5 km from the granite contact (Parslow, 1968). Evidence for hydrothermal alteration is limited to some sericitisation of feldspars and chloritisation of biotite.

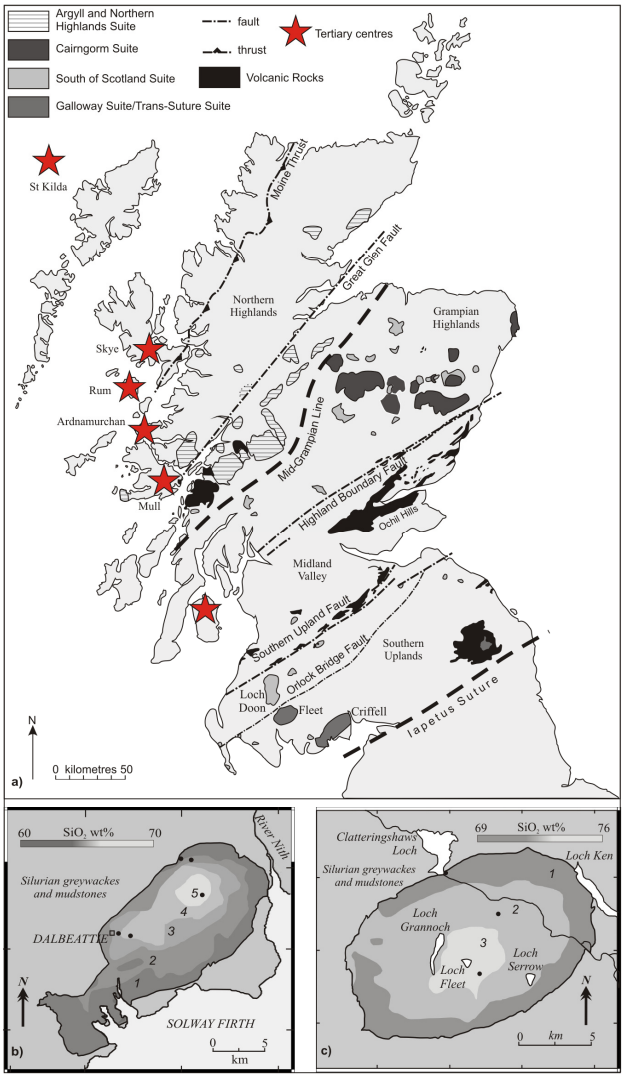

Fig. 6.1 a) Modified regional geological map of Devonian and post-Caledonian plutonic and volcanic rocks (black) in the northern United Kingdom together with Tertiary igneous centres (stars), modified from Highton (1999). Plutons are classified according to the geochemical parameters outlined by Read (1961), Stephens and Halliday (1980) and Stone (1997). b) and c) Simplified geological maps of the Criffell (b) and Fleet (c) plutons. Zone colouration reflects approximate silica content, with darker colours indicative of lower SiO_2 and more primitive compositions. Zone mineralogy in the Criffell pluton is as follows: 1) clinopyroxene-biotite-hornblende granodiorite; 2) biotite-hornblende granodiorite; 3) biotite granite; 4) biotite-muscovite granite 5) muscovite-biotite granite. Zone mineralogy in the Fleet pluton is as follows: 1) coarse grained biotite granite; 2) coarse-grained biotite-muscovite granite; 3) fine-grained biotite-muscovite granite. Minerals listed in order of increasing modal abundance. Black points denote sample sites.

2. Methodology

2.1 Whole-rock oxygen isotope compositions

Oxygen isotope analyses of whole-rock samples were carried out at the Scottish Universities Environmental Research Centre (SUERC) at East Kilbride. The method followed the Macaulay et al. (2000) modification of the laser fluorination method of Sharp (1990). 1mg of powdered sample was reacted with ClF_3 using a CO_2 laser. Resultant oxygen was purified and converted to CO_2 on platinised graphite, and the yield measured with a capacitance manometer. A Micromass PRISM 3 duel inlet, triple collector mass spectrometer was used to analyse the oxygen isotope composition of the CO_2, with a working standard gas calibrated against international reference standard NBS28. The accuracy and precision were ±0.4‰ (2σ), and NBS28 gave a value of 9.56‰.

2.2 Zircon oxygen isotope analysis: SIMS

Zircon crystals set in epoxy blocks and up to 200 μm in size with concentric magmatic zoning (Fig. 6.2) were analysed for oxygen isotope compositions using a Cameca ims 1270 ion microprobe at the University of Edinburgh following the methods of Cavosie et al. (2005) and Kemp et al. (2006b) with data reported as per mil (‰) values relative to Vienna Standard Mean Ocean Water (VSMOW). A primary $^{133}Cs^+$ ion beam of approximately 20 μm was used at 6 nA. A normal-incidence electron flood gun was used for charge neutralisation, with secondary ions extracted at 10 kV. Both $^{18}O^-$ and $^{16}O^-$ ions were monitored simultaneously on dual Faraday cups. Total acquisition times of ~ 200 seconds included secondary ion beam centring, pre-sputtering for 50 seconds and data collection over 10 cycles, each lasting 4 seconds. Instrumental drift was corrected daily by normalising all unknown samples to zircon standard 91500 ($\delta^{18}O$ = 9.86 ‰) (Wiedenbeck et al. 2004). Bracketing analyses of 91500 were used to obtain linearly interpolated values of $^{18}O/^{16}O$ that were subsequently used to normalise the $^{18}O/^{16}O$ ratios of unknown samples. Analyses of 91500 in groups of 5 to 10 were carried out after every 10 to 15 analyses of unknowns. Following corrections for instrument drift, unknown zircon

analyses were normalised to an average daily $^{18}O/^{16}O$ value for zircon standard 91500.

HfO_2 concentrations in unknown zircon samples were determined using a Cameca SX100 electron microprobes at the Universities of Bristol and Edinburgh. Variations in the instrumental mass fractionation (IMF) during $^{18}O/^{16}O$ analysis by ion microprobe have been shown to reflect variations in HfO_2, particularly analyses at high energy offset using a Cameca ims 4f (Peck et al. 2001). IMF corrections were not required in this study due to the use of a Cameca ims 1270 (which does not require high energy offset) and the small measured variations in HfO_2 (generally < 0.5 wt%). Analytical precision from session to session was generally between 0.3 and 0.6 ‰ (2σ).

2.3 Quartz oxygen isotope analysis: SIMS

The oxygen isotope compositions of quartz grains were determined in polished thin sections with a Cameca ims 1270 ion microprobe, using the same instrument set-up as that used for zircon oxygen isotope analyses. Unknown quartz analyses were normalised to grains of Bogola quartz standard ($\delta^{18}O$ = 12.3 ± 0.3 ‰; Elsenheimer and Valley, 1993), which were analysed after every 5 to 10 unknowns. Internal precision (~ 0.2 ‰) was calculated from the Bogola quartz standard. External precision varies between 0.2‰ and 0.4‰ (2σ) from session to session. In general, heterogeneity within and between quartz crystals exceeded the external analytical precision (intra grain 2σ variations are between ~ 0.6 and 2.1 ‰). Where possible, multiple analyses were made on single crystals in order to identify oxygen isotope zonation caused by exchange around crystal edges or due to changing magmatic compositions.

3. Results

3.1 Whole-rock oxygen isotopes

All WR oxygen isotope compositions are reported in Table 6.1. In the Criffell pluton, WR $\delta^{18}O$ compositions range from 9.2 ‰ in Zones 1 and 2, to 9.8 ‰ in Zone 3, 9.6 ‰ in Zone 4 and up to 11.1 ‰ in the inner-most granite, Zone 5. In the Fleet pluton, WR values increase from 10.4 ‰ in the outermost zone (Zone 1), to 10.5 ‰ in Zone 2 and up to 11.2‰ in the inner-most Zone 3.

3.2 Zircon oxygen isotope compositions

Mean zircon oxygen isotope compositions for each zone of the Criffell pluton are: Zone 1 = 5.8 ± 0.8 ‰ (2 SD; *n* = 13), Zone 2 = 5.8 ± 1.1 ‰ (2 SD; *n* = 16), Zone 3 = 6.5 ± 1.0 ‰ (2 SD; *n* = 21) and Zone 4 = 7.2 ± 1.5 ‰ (2 SD; *n* = 22). 2 SD are for individual population from each zone (Table 6.1). In zones 1, 2 and 3, 70%, 80% and 90% respectively of grains lie within analytical error of their population means (calculated independently for each session). By comparison, only 64% of analyses lie within analytical error of the population mean in Zone 4 (Fig. 6.3).

In the Fleet pluton, zircons from the inner fine-grained biotite-muscovite granite yielded a mean $\delta^{18}O$ value of 6.4 ± 1.7 ‰ (2 SD; *n* = 10). Zircons from the outer two zones yielded mean oxygen isotope compositions of 6.8 ± 0.8 ‰ (2 SD; *n* = 15) and 7.1 ± 1.5 ‰ (2 SD; *n* = 15) respectively. In the outer zone, 73% of analyses fall within analytical error of the mean, while 53% and 40% of analyses in the middle and inner-most zones respectively fall within analytical error of their mean population values (Fig. 6.4).

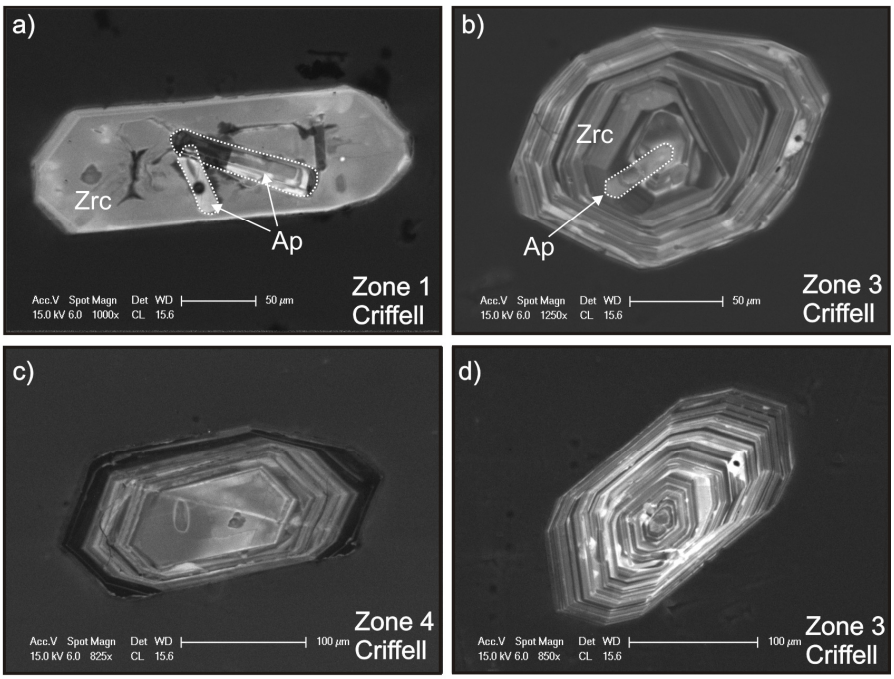

Fig. 6.2 Cathodoluminescence (CL) images of zoned zircons from the Criffell pluton. (a) and (b) also show apatite inclusions. Abbreviations: Ap – apatite, Zrc – zircon.

3.3 Quartz Oxygen Isotope Data

The $\delta^{18}O$ compositions of quartz grains were analysed in polished thin sections of samples from zones 1 and 3 of the Criffell pluton and zones 1 and 2 of the Fleet pluton. In both plutons, quartz crystals range in size from tens of microns to over 1mm and often have annealed and open cracks (Fig. 6.5). Some quartz grains show concentric zoning with varying luminescence (Fig. 6.5a) while others show subtle differences in luminescence between different sectors (Fig. 6.5b). Luminescence is generally lower in cracks than within quartz grains. In the Criffell pluton, the range of $\delta^{18}O$ (Qtz) away from obvious cracks and inclusions is 8.7 to 10.1 ‰ in Zone 1 and 9.9 to 10.2 ‰ in Zone 3 (Fig. 6.6). In the Fleet pluton, $\delta^{18}O$ (Qtz) compositions range from 10.4 ‰ to 12.8 ‰ in Zone 1 and from 9.2 ‰ to 13.5 ‰ in Zone 2. Some traverses show evidence for isotopic gradients across grains (Figs. 6.5 and 6.6), most of which show a tendency for higher $\delta^{18}O$ compositions around crystal margins relative to crystal cores. The $\delta^{18}O$ composition of re-precipitated quartz within less luminescent cracks is generally higher than in surrounding crystals of quartz (Fig. 6.5c).

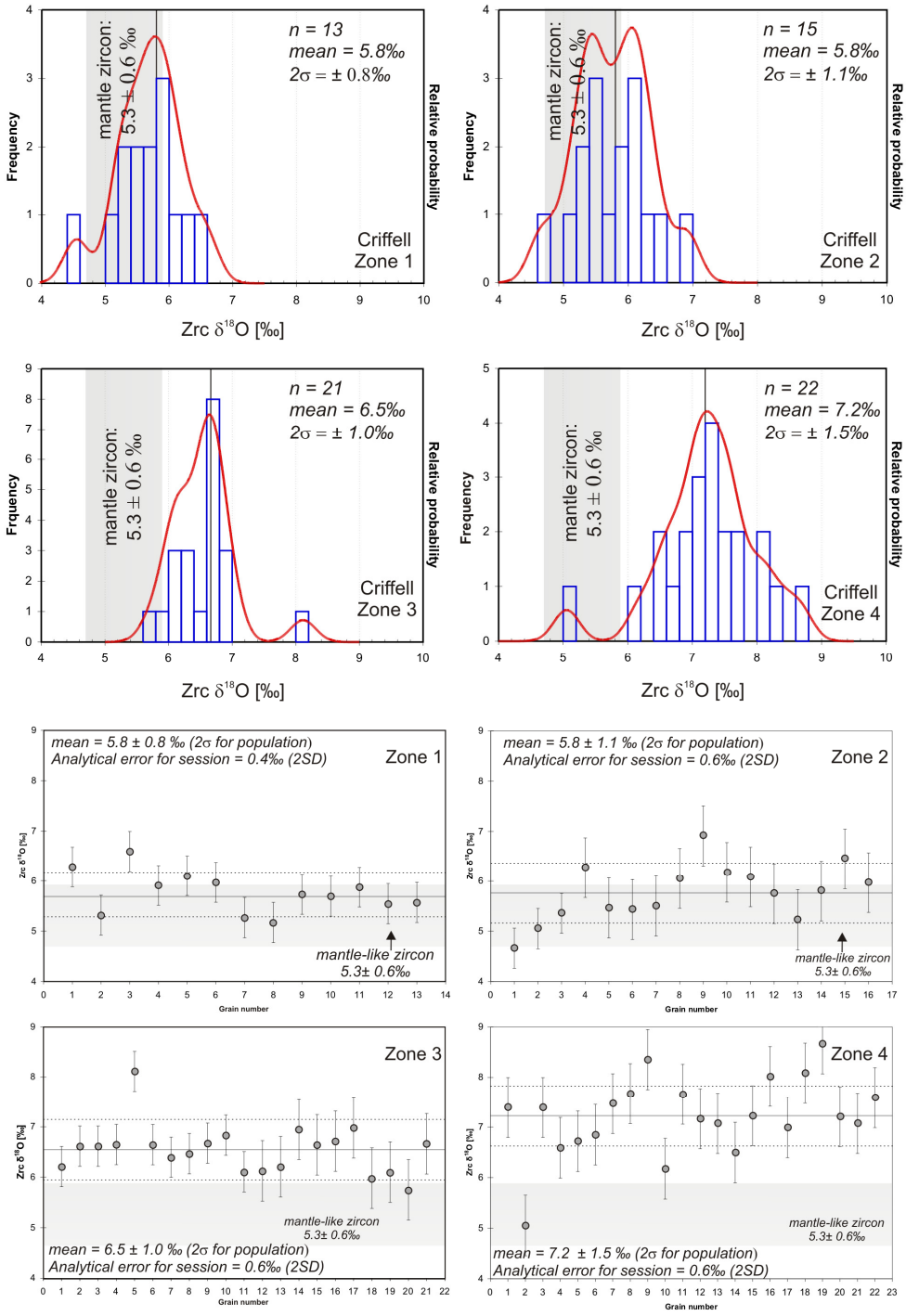

Fig. 6.3 Cumulative probability-histograms and grain-scale variation plots of $\delta^{18}O$ of zircon crystals from zones 1 to 4 of the Criffell pluton. For grain-scale variation plots, 2 SD analytical errors are plotted about calculated mean oxygen isotope compositions for each zone. Grains that fall within error are assumed equivalent. Outer zones (zones 1 to 3) show more homogeneity in composition than Zone 4. Bin widths of histograms determined by 1 SD analytical errors; error bars are for 2 SD.

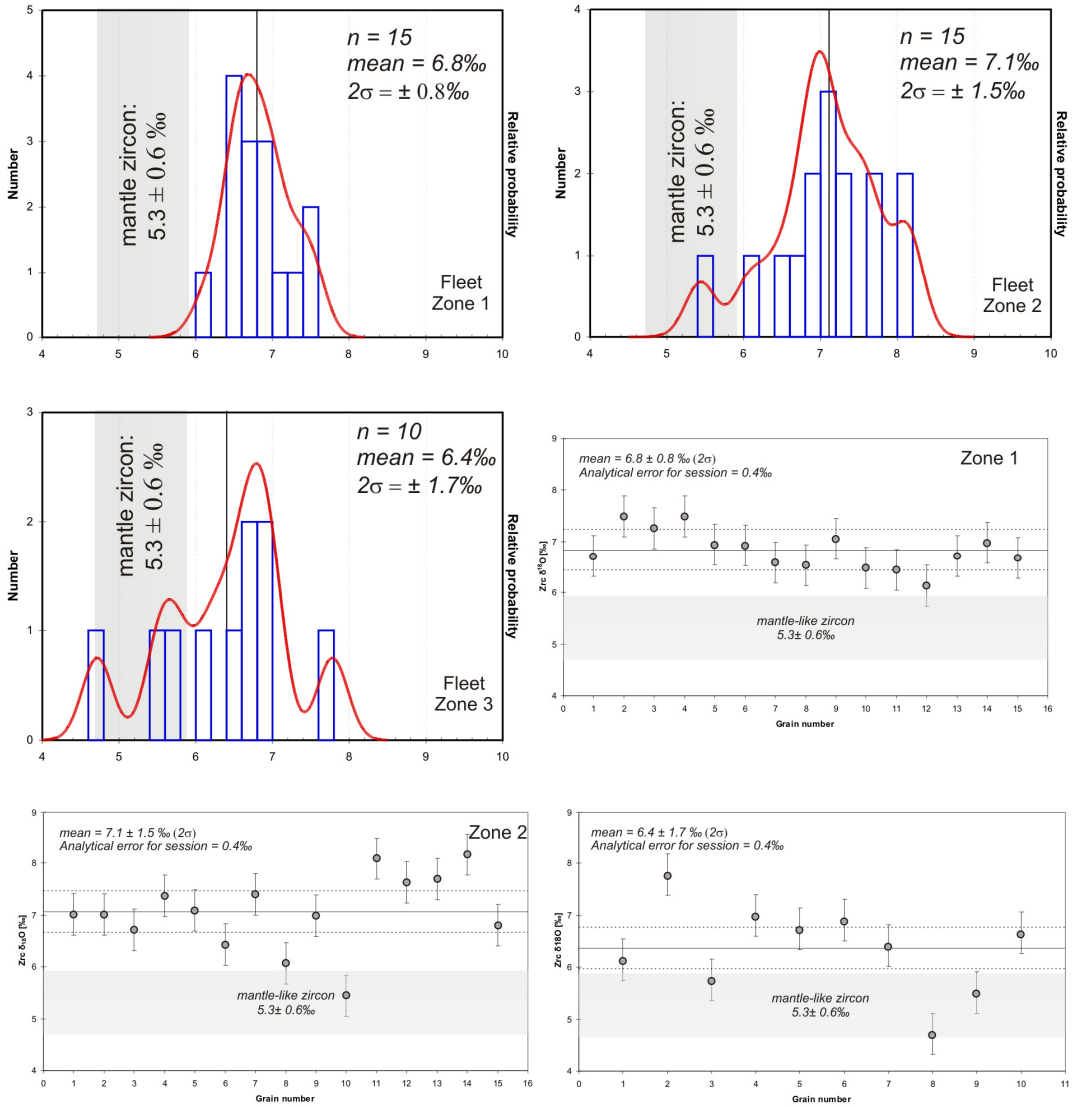

Fig. 6.4 Cumulative probability-histograms and grain-scale variation plots of $\delta^{18}O$ of zircon crystals from Zones 1 to 3 of the Fleet pluton. Zones 1 and 2 show unimodal distributions of oxygen isotopes. For grain-scale variation plots, 2SD analytical errors are plotted about calculated mean oxygen isotope compositions for zones 1 to 3. Bin widths of histograms are 1 SD analytical errors; error bars are for 2 SD

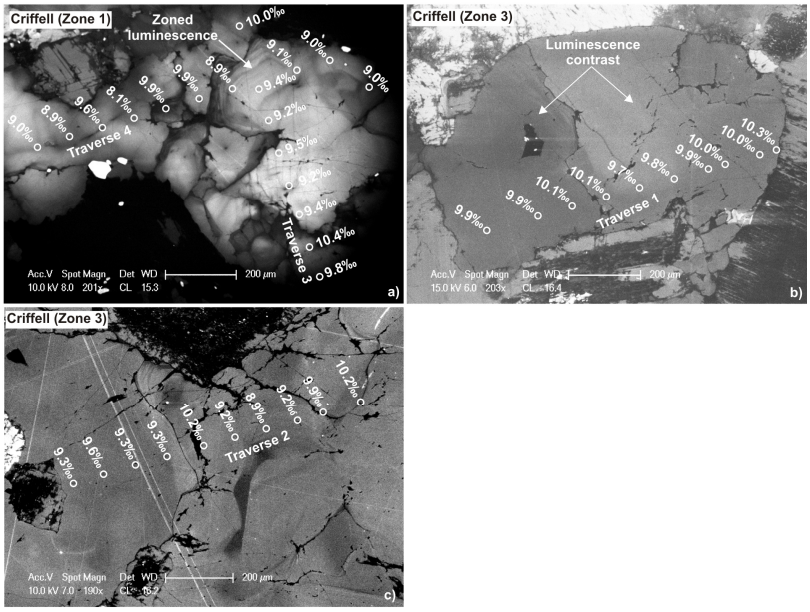

Fig. 6.5 CL images of quartz crystals analysed for $\delta^{18}O$ compositions showing ion probe analytical pits and compositions from the Criffell and Fleet plutons. Traverse numbers correspond to those in Fig. 6.

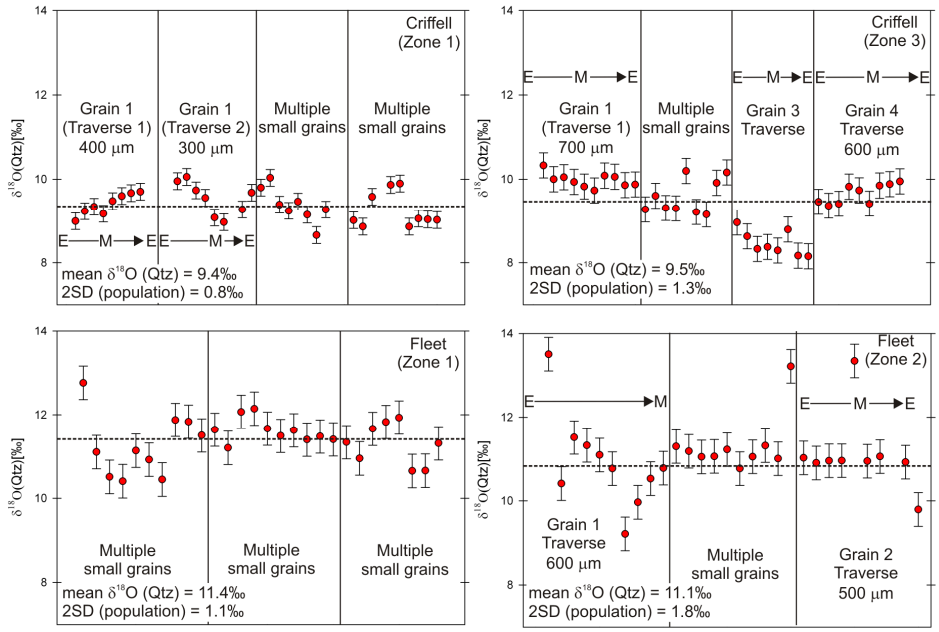

Fig. 6.6 $\delta^{18}O$ compositions of quartz crystals from zones 1 and 3 of the Criffell pluton and zones 1 and 2 of the Fleet pluton. Mean compositions are represented by horizontal dashed lines for each zone, with numerical values for mean compositions and 2SD variations for the populations noted in the figure Single grain traverses are distinguished from traverses carried out across multiple small grains. All traverses are from crystals and collections of crystals from different areas of a single thin section and are not spatially continuous with each other. 'E' and 'M' represent 'edge' and 'middle' analyses in larger grains. Error bars (±0.4‰) have been calculated assuming a homogeneous standard compositions and using 2SD variations from standard compositions. Compositional gradients are evident across some ~ 300 - 600 µm grain traverses.

4. Discussion

Zircon has long been proposed to retain magmatic isotopic compositions (e.g. Valley et al. 1994; Gilliam and Valley, 1997; Monani and Valley 2001; King et al. 1997; Hawkesworth and Kemp, 2006). However, the extent to which zircon crystals and their respective WR remain in oxygen isotope equilibrium provides a means of assessing whether zircon crystallised from magmas with compositions similar to those represented by their respective WR. A further internal check can be made from examining oxygen isotope equilibrium between zircon and quartz. However, ion microprobe analyses (Valley and Graham 1996) together with laser studies of $\delta^{18}O$ in quartz grains from individual granites have shown that quartz does not always remain retentive of magmatic compositions (Gilliam and Valley, 1997; King et al. 1997; King, 2001; Monani and Valley, 2001; King et al. 2004; Lackey et al. 2008) and in a similar manner to WR compositions, its $\delta^{18}O$ composition may also reflect later hydrothermal processes. Hydrothermal circulation involving $\delta^{18}O$-depleted meteoric water (with $\delta^{18}O$ composition between - 40 ‰ and 5.3 ‰) may significantly lower $\delta^{18}O$ compositions while fluids derived from $\delta^{18}O$-rich sediments ($\delta^{18}O$ generally > 7‰) may elevate $\delta^{18}O$ compositions (Eiler, 2001; Valley et al. 2005). A comparative and integrative study of $\delta^{18}O$ compositions preserved in zircon, WR and quartz therefore offers an opportunity to identify and distinguish magmatic and hydrothermal processes in different igneous rocks from a range of tectonic environments.

4.1 Magmatic $\delta^{18}O$ compositions in TSS zircons

All zircon from the TSS is thought to be magmatic in origin, confirmed by euhedral crystal morphologies, a lack of resorption boundaries (Fig. 6.2) in cathodoluminescence (CL) and by an absence of inherited U-Pb ages (Pidgeon and Aftalion, 1978; Chapter 5). Furthermore, zircon $\delta^{18}O$ compositions from the outer three zones of the Criffell pluton are also largely homogenous within precision of SIMS analysis and also indicate that $\delta^{18}O$ inheritance is not present in these zones. The lack of grain size $\delta^{18}O$ dependence in all zones of the two TSS plutons provides

further evidence that zircon isotope compositions have not been affected by hydrothermal exchange. Furthermore, oxygen diffusion in zircon occurs only slowly, particularly under dry conditions, where the loss of 10μm zones occurs on timescales of $>10^9$ years at 600°C but may occur on timescales of ~10^5 years under wet conditions at similar temperatures (Watson and Cherniak, 1997). Despite more rapid diffusion under wet conditions, temperatures of >600°C are unlikely to have been maintained for long periods in the TSS plutons given evidence for incremental assembly over time periods of as much as 23 Ma (Stephens et al. 1985; Chapter 2). At 400°C, 10μm zones will only be lost on timescales of $>10^8$ years even under wet conditions (Watson and Cherniak, 1997). It is therefore likely that zircon $\delta^{18}O$ compositions remain retentive of magmatic compositions at the time of crystallisation.

4.2 Do zircon and whole-rocks represent the same magmas in the TSS?

Equilibrium WR-zircon oxygen isotope fractionation factors (ΔZrc-WR = $\delta^{18}O$(Zrc) - $\delta^{18}O$(WR)) vary systematically with SiO_2 and temperature (Valley et al. 1994; Valley et al. 2005). The increased abundance of quartz and feldspar in more evolved magmas together with the enrichment of ^{18}O in these minerals results in increasing WR $\delta^{18}O$ values with crystallisation. Equilibrium oxygen isotope fractionation factors between zircon and WR therefore increase with SiO_2 at all temperatures. The $\delta^{18}O$ record of zircon therefore remains unaffected by crystallisation (Valley et al. 1994). For granites, equilibrium values for Δ(Zrc-WR) are ~ -2.0‰ according to the relationship reported by Lackey et al. (2005); Valley et al. (1994) and Valley et al. (2005):

$$\Delta^{18}\mathrm{O(Zrc - WR)} = \delta^{18}O(Zrc) - \delta^{18}O(WR) \sim -0.0612(wt\%SiO_2) + 2.5 \quad \ldots(1)$$

For comparison, the calculated and measured values of Δ(Zrc-WR) are shown in Table 6.1. In zones 1 and 2 of both the Criffell and Fleet plutons, WR $\delta^{18}O$

compositions are out of isotopic equilibrium with their zircon crystals (Fig. 6.7). In zones 3 and 4 of the Criffell pluton and Zone 3 of the Fleet pluton, only the most ^{18}O-rich zircons are in isotopic equilibrium with the WR. In general, WR compositions are consistently more ^{18}O-enriched than those in equilibrium with most zircons, indicating either crystallisation of zircon from more primitive (lower $\delta^{18}O$) magmas or later alteration of the WR by ^{18}O-enriched fluids.

WR $\delta^{18}O$ values are highly susceptible to post-solidus alteration and exchange (e.g. King et al. 1997) that primarily reflects isotopic exchange of feldspar with hydrothermal fluids by oxygen volume diffusion down to temperatures as low as 300°C to 400°C (Elphick and Graham, 1988; Farver and Yund, 1991) together with chemical and mineralogical alteration (e.g. Ferry, 1985). Feldspar alteration and exchange in the Criffell and Fleet plutons is consistent with the widespread sericitisation of feldspar crystals. The elevated $\delta^{18}O$ of the WR relative to values in equilibrium with zircon indicate that hydrothermal fluids are not meteoric in origin. Instead, late-stage magmatic fluids resulting from the intersection of ascending magmas with the water-saturated liquidus (Chapter 2) are likely to have provided a major source of magmatic hydrothermal fluids. Further increases in the $\delta^{18}O$ of circulating fluids may also have occurred around the margins of the pluton due to fluid interaction with $\delta^{18}O$-rich sedimentary rocks with compositions between 10.8‰ and 13.9‰ (Halliday et al. 1980). This is supported by greater zircon-WR disequilibrium in the outer zones of the Criffell and Fleet plutons (Fig. 6.7).

WR oxygen isotope compositions therefore do not provide a robust method for assessing isotopic equilibrium or constraining magma $\delta^{18}O$, although equilibrium with the outermost rims of zircon crystals in some samples cannot be excluded. Instead, disequilibrium between WR and zircon is likely to reflect late-stage, post-emplacement hydrothermal alteration as a result of the interaction of water exsolved from ascending magmas with $\delta^{18}O$-rich sediments in hydrothermal systems.

Table 6.1 $\delta^{18}O$ values and fractionation factors for the TSS plutons

Pluton	Sample	SiO_2 (wt %)	$\delta^{18}O$ (Zrc) ‰	±2σ	n	$\delta^{18}O$ (WR) ‰	±2σ	$\delta^{18}O$ (Qtz) ‰	±2σ	n	Δ(Zrc-WR)	Δ(Qtz-Zrc)
Criffel	Zone 1 0917	63.9	5.8	0.8	13	9.2	0.4	9.4	0.8	33	-4.0 to -2.6	2.1 to 5.0
	Zone 2 0918	66.0	5.8	1.1	15	9.3	0.4				-4.3 to -2.4	
	Zone 3 0921	69.5	6.5	1.0	21	9.8	0.4	9.5	1.2	36	-4.1 to -1.7	3.0 to 5.5
	Zone 4 0922	68.8	7.2	1.5	22	9.6	0.4				-4.5 to -0.9	
Fleet	Zone 1 0933	68.8	6.8	0.8	15	10.4	0.4	11.4	1.2	28	-4.3 to -2.9	2.9 to 6.7
	Zone 2 0934	71.2	7.1	1.5	15	10.5	0.4	11.1	1.8	29	-5.1 to -2.3	1.0 to 8.1
	Zone 3 0935	73.8	6.4	1.7	10	11.2	0.4				-6.5 to -3.4	
Shap	Zone 1 0923	67.0	7.9	0.5	25	10.9	0.4				-3.6 to -2.4	
	Zone 2 0932	69.1	7.6	0.4	20	9.7	0.4				-2.5 to -1.8	

4.3 Do zircon and quartz represent the same magmas in the TSS?

Quartz has been proposed as a potentially reliable archive of magmatic oxygen isotope compositions (Valley and Graham, 1996; Appleby et al. 2008). However, isotope exchange may occur by rapid solution/re-precipitation along cracks, fractures and crystal boundaries and, given sufficient time, by slow temperature-dependent volume diffusion (Valley and Graham, 1996). Quartz compositions in the Lochnagar pluton in the Scottish Highlands were found not to vary in relation to cracks or between crystals of different sizes (Appleby et al. 2008). It was therefore considered likely that quartz had retained its oxygen isotope composition from the time of crystallisation and was not altered by isotopic exchange with hydrothermal fluids or feldspar (Appleby et al. 2008). By contrast, quartz crystals from the Criffell and Fleet

plutons exhibit compositional heterogeneity that is often concentrated around the margins of quartz crystals and along cracks that is consistent with late or post-magmatic exchange (Fig 6.5).

The extent of zircon-quartz disequilibrium can be estimated using the empirical equation (Valley et al. 2003):

$$\delta^{18}O_{Qtz} - \delta^{18}O_{Zrc} = \Delta_{Qtz-Zrc} \approx 1000\ln(\alpha_{Qtz-Zrc}) = A_{Qtz-Zrc}10^6/T^2 \quad \ldots (2)$$

Where $A_{Qtz\text{-}Zrc}$ = 2.64; T = temperature in Kelvin derived from Ti-in-zircon thermometry (Watson and Harrison, 2005; Watson et al. 2006).

Ti-in-zircon thermometry (Ferry and Watson 2007) yields temperatures of 600°C to 750°C for all zones of the Criffell pluton and 670°C to 870°C for all zones of the Fleet pluton (Appendix I). Quartz $\delta^{18}O$ compositions in equilibrium with zircon have been calculated at these temperatures for zones 1 and 3 in Criffell and zones 1 and 2 in Fleet (Fig. 6.8). Results indicate that the lowest $\delta^{18}O$ quartz analyses, often in the central regions of quartz crystals and away from cracks, are in oxygen isotopic equilibrium with co-existing zircon in all four samples. However, a significant number of quartz analyses (> 50% in some samples) have $\delta^{18}O$ values that are higher than would be expected under equilibrium conditions.

The elevated $\delta^{18}O$ compositions of some quartz crystals relative to that in equilibrium with zircon may reflect later crystal growth from magmas subjected to further assimilation of $\delta^{18}O$-rich sediments during crystallisation. Changes to the $\delta^{18}O$ composition of the remaining magma caused by assimilation have been shown to change isotope fractionations between early- and late-crystallising minerals in other studies (King and Valley, 2001; Lackey et al. 2002). However, WR Pb isotope compositions indicate that the sediments into which the Criffell and Fleet plutons were intruded and crystallisation took place did not contribute to the evolution of their WR compositions (Thirlwall, 1989; Chapter 2). On this basis, assimilation during crystallisation is considered unlikely.

A further means of elevating $\delta^{18}O$(Qtz) compositions relative to zircon is by post-solidus, low-temperature exchange between quartz and other minerals. Quartz (and feldspar) preferentially takes-up ^{18}O relative to coexisting minerals and fluids during mineral exchange, resulting in ^{18}O enrichment (King et al. 2004). Although this is likely, the greater degree of ^{18}O disequilibrium observed between zircon and quartz in the outer zones of the two plutons (Fig. 6.7) is consistent with hydrothermal circulation following interaction of magmatic fluids with local ^{18}O-rich sediments. Further evidence for hydrothermal alteration can be seen in a plot of $\delta^{18}O$(Qtz) vs. $\delta^{18}O$(Zrc) for coexisting quartz and zircon that indicates apparent mean temperatures of ~ 480 ^{o}C to 670^{o}C (Fig. 6.8). For Zone 1 of the Criffell pluton and zones 1 and 2 of the Fleet pluton, these temperatures are significantly lower than zircon crystallisation temperatures of ~ 650^{o}C and 750^{o}C for these zones. Similar evidence for disequilibrium between zircon and quartz has been observed in the Idaho (King, 2001) and central Sierra Nevada batholiths (Lackey et al. 2008) where closed system resetting of $\delta^{18}O$(Qtz) by oxygen exchange was proposed during sub-solidus cooling. These conclusions are supported by evidence of faster oxygen diffusion (Elphick and Graham, 1988; Elphick et al. 1991; Farver and Yund, 1991) and lower closure temperatures for oxygen exchange (Dodson, 1973) in quartz relative to zircon. By comparison, coexisting quartz and zircon in Zone 3 of the Criffell pluton indicate near- 'equilibrium' temperatures of ~ 670^{o}C, and are within error of Ti-in-zircon temperatures of 680^{o}C for this zone. It appears that quartz and zircon in this latter zone suffered less sub-solidus exchange and remain largely in isotopic equilibrium, consistent with varying intensities of hydrothermal circulation in different regions of the pluton, particularly between inner and outer zones.

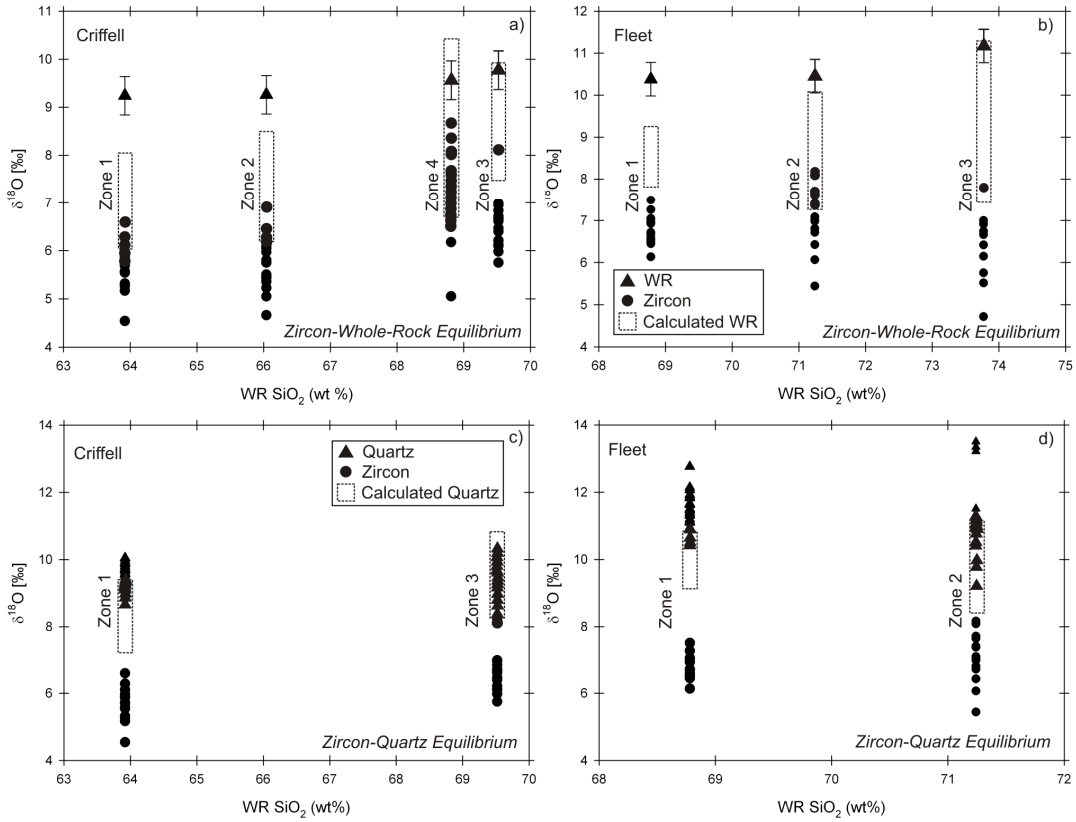

Fig. 6.7 Assessment of oxygen isotopic equilibrium between zircon, whole-rock (WR) and quartz. 'Calculated WR' and 'calculated quartz' compositions have been calculated using equations 1 and 2 respectively (see text). Temperatures calculated from Ti-in-zircon thermometry (Ferry and Watson 2007). Zircon in zones 1 and 2 of the Criffell pluton and zone 1 of the Fleet pluton are out of oxygen isotope equilibrium with the WR, while in zones 3 and 4 of the Criffell pluton and zones 2 and 3 of the Fleet pluton, only the most δ^{18}O-rich zircon compositions are in isotopic equilibrium with their respective WR. Measured WR compositions appear too high to be in equilibrium with their zircons and may reflect alteration and exchange of the WR related to hydrothermal fluids derived from local δ^{18}O-rich sediments. Similar results are noted for quartz, with only the most δ^{18}O-rich zircons in equilibrium with co-existing quartz. While this may reflect crystallization from different magmas, isotopic heterogeneities within quartz crystals indicate that they may also have been affected by hydrothermal exchange related to fluids exchanged with local δ^{18}O-rich sediments.

4.4 A comparison of hydrothermal histories in the Devonian TSS and British Tertiary Igneous Province (BTIP)

The Tertiary magmatic centres situated mainly in the north-western British Isles (Fig. 6.1a) are collectively referred to as the British Tertiary Igneous Province (BTIP). They are the manifestation of intense igneous activity during the Palaeocene and early Eocene (~ 63-52 Ma) which accompanied initiation of the Iceland mantle

plume and opening of the North Atlantic Ocean (White 1988; White and McKenzie, 1989).

In contrast to the Devonian TSS, many of the BTIP tholeiitic and alkaline igneous centres have developed classic bulls-eye patterns of low $\delta^{18}O$ caused by hydrothermal alteration involving large fluxes of heated meteoric water (Taylor and Forester, 1971; Forester and Taylor, 1977). In addition, contact metamorphic aureoles are generally larger than those around the Devonian granites, despite smaller volumes of granite in the Tertiary centres. For example, contact metamorphism around the Tertiary Beinn an Dubhaich granite on Skye extends away from the granite margin by up to 4 km (Hoersch, 1979), while that of the much larger Devonian Fleet pluton extends no more than 1.5 km into the local sediments (Parslow, 1968). Zircon and quartz from many of the granitic Tertiary igneous centres have been shown to have low and sub-mantle-like (<5.3 ± 0.3 ‰, Valley et al. 1998) $\delta^{18}O$ compositions (Valley and Graham, 1996; Gilliam and Valley, 1997; King et al. 1997; Monani and Valley, 2001). Zircon $\delta^{18}O$ compositions from different regions of the same granite bodies on the Isle of Skye were found to be remarkably homogeneous, with an average $\delta^{18}O(Zrc)$ reproducibility of only ±0.2 ‰ (Gilliam and Valley, 1997; Monani and Valley, 2001). Significant heterogeneity was however observed between the $\delta^{18}O$ compositions of zircons from different granite bodies ($\delta^{18}O(Zrc)$ = 0.6 to 5.3 ‰). Crucially, no evidence of zircon inheritance was found from surrounding country rocks and euhedral crystals with consistent magmatic zoning have confirmed their primary magmatic origin. No grain size dependence was found by these studies in the oxygen isotope compositions of zircon crystals and no correlation was observed between $\delta^{18}O(Zrc)$ and Quartz-Zircon fractionation factors ($\Delta_{Qtz\text{-}Zrc} = \delta^{18}O(Qtz) - \delta^{18}O(Zrc)$) that would otherwise indicate hydrothermal exchange in both minerals. Similarly to zircons from the TSS, and in contrast to quartz $\delta^{18}O$ compositions, it is thought unlikely that zircon oxygen isotope compositions have suffered hydrothermal exchange and instead reflect magmatic compositions.

In contrast to the TSS, low zircon $\delta^{18}O$ compositions reflect the existence of $\delta^{18}O$-depleted magmas thought to have resulted from the assimilation and partial melting of ^{18}O-depleted and hydrothermally altered crust (Gilliam and Valley, 1997; Monani and Valley, 2001). Variable lowering of the $\delta^{18}O$ compositions of surrounding country rocks occurred in response to hydrothermal systems established around early mafic intrusions that pre-date granite formation in the BTIP (Monani and Valley, 2001).

Hydrothermal processes in the TSS and BTIP were therefore associated with quite different fluid compositions; the latter dominated by ^{18}O-rich magmatic fluids, the former by ^{18}O-depleted meteoric water. These contrasts are likely to reflect different magmatic and emplacement histories together with mantle and tectonic environments.

The elevated $\delta^{18}O$ compositions of hydrothermal fluids in the TSS are likely to reflect exchange with, and alteration by magmatic fluids that underwent further $\delta^{18}O$ enrichment through interaction with local sedimentary rocks. High magmatic water contents are suggested by calc-alkaline compositions and derivation from mantle variably hydrated by previous subduction of Iapetus oceanic crust. By contrast, the theoliitic and alkaline magmas (e.g. Thompson, 1982) generated by active melting of 'dry' mantle following emplacement of the Iceland plume (White, 1988; 1989) is unlikely to have carried substantial magmatic fluids.

Meteoric circulation around the TSS is also likely to have been limited by emplacement depths of ~ 4 to 6km (Chapter 2) within Southern Uplands greywackes with low permeability. By contrast, igneous centres associated with the BTIP are estimated to have been emplaced at depths of only 1-2 km (Bell and Emeleus, 1988), and were readily accessed by meteoric water. Further limits on the extent of hydrothermal circulation and interaction are also likely to result from the thermal potential around emplaced plutons, with rapidly emplaced plutons having greater potential to drive large circulatory cells.

Tertiary magmatic activity related to the initiation of the Iceland plume is thought to have resulted in rapid assembly of large volumes of mafic and silicic magma caused by active mantle melting (White, 1989). The duration of all Tertiary magmatic activity on the Isle of Mull is considered to be only 2.52 ± 0.36 Ma (1σ) while that on the Isle of Skye is though to have occurred within a single magnetic chron (~ 3 Ma) (Chambers and Pringle, 2001). By contrast, zircon U-Pb ages suggest that the assembly of Devonian TSS granites may have occurred incrementally over time periods of as much as 23 Ma (Chapter 5) resulting from passive mantle melting during transtension (Brown et al. 2008). Heat sources are therefore likely to have been much larger and more concentrated adjacent to the BTIP, allowing for much larger hydrothermal systems to be established with access to meteoric water due to shallower emplacement.

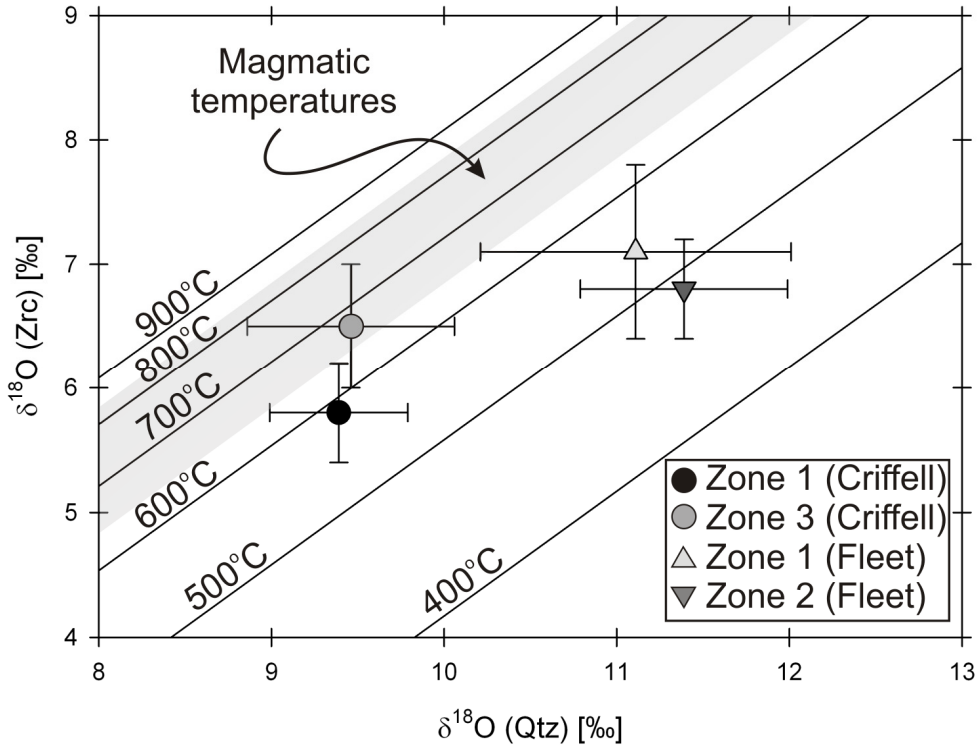

Fig. 6.8 $\delta^{18}O$(zircon) – $\delta^{18}O$(Quartz) plot for zircon and quartz from the TSS plutons. Apparent temperatures are lower than expected for magmatic equilibrium. Magmatic temperatures are calculated using Ti-in-zircon thermometry and isotherms calculated from Valley et al. (2003).

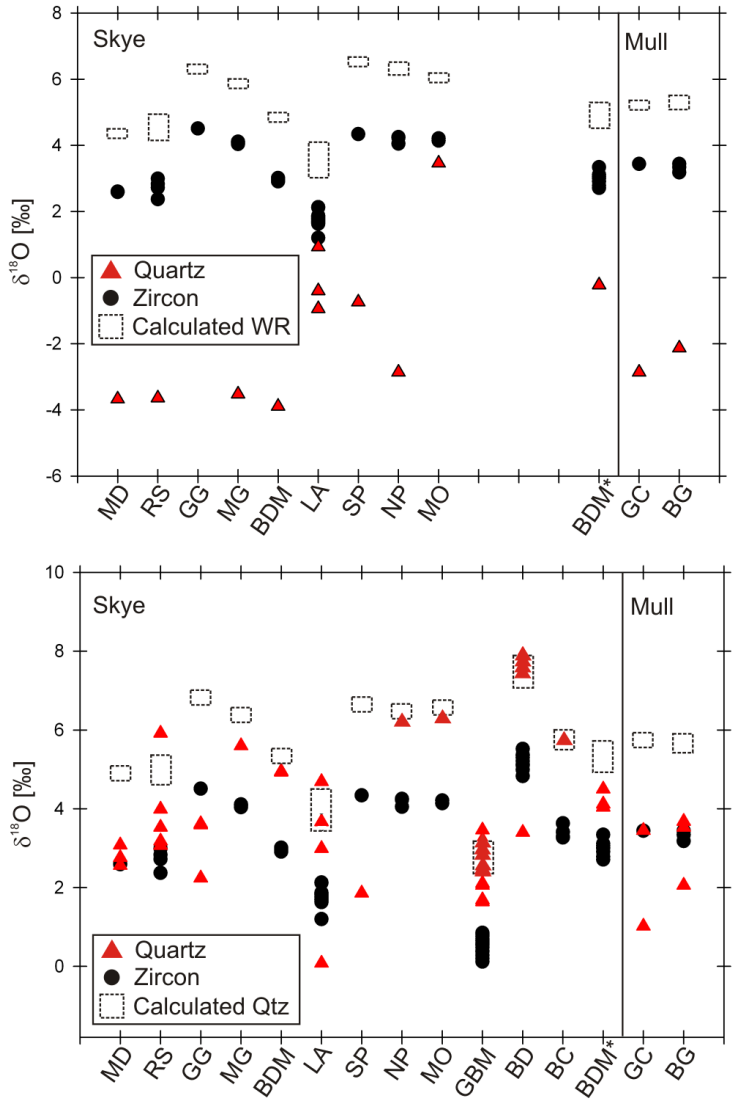

Fig. 6.9 Assessment of oxygen isotopic equilibrium between zircon, whole-rock (WR) and quartz in selected granite bodies from the BTIP on the Isles of Skye and Mull. Data are from Gilliam and Valley (1997) and Monani and Valley (2001). WR SiO_2 compositions are from Thompson (1968) and Kerr et al. (1999). 'Calculated WR' and 'calculated quartz' compositions have been calculated using equations 1 and 2 respectively (see text). Ti-in-zircon data are not available and a temperature of 800°C has been used to calculate the $\delta^{18}O$ compositions of quartz crystals in equilibrium with zircon. Most WR and quartz $\delta^{18}O$ compositions are out of equilibrium with zircon and are lower than is required for equilibrium. Low $\delta^{18}O$ compositions in zircon reflect low magmatic values of $\delta^{18}O$ caused by assimilation of $\delta^{18}O$-depleted country rocks. Disequilibrium between zircon, WR and quartz reflects post-solidus hydrothermal alteration of the latter two records caused by $\delta^{18}O$-depleted meteoric water. Abbreviations are: MD- Meall Dearg, RS- Ruadh Stac, GG- Glamaig, MG- Maol na Gainmhich, BDM- Beinn Dearg Mhor, LA- Loch Ainort, SP- Southern porphyritic, NP- Northern porphyritic, MO- Marsco, GBM- Glas Beinn Mhor, BD- Beinn an Dubhaich, BC- Beinn na Cro, GC- Glen Cannel (Mull), BG- Beinn a Ghraig (Mull). * refers to separate data from Gilliam and Valley for the BDM granite.

5. Conclusions

The $\delta^{18}O$ compositions of zircon, quartz and WR in the TSS and BTIP reveal contrasting hydrothermal histories that reflect fundamentally different tectonic, mantle and emplacement histories. Oxygen isotope disequilibrium between zircon, quartz and whole-rock in the TSS has resulted from hydrothermal exchange and alteration of the former two archives. In the TSS, hydrothermal alteration has elevated oxygen isotope compositions relative to those in equilibrium with zircon. In the BTIP, hydrothermal circulation of oxygen-depleted water has lowered the oxygen isotope compositions of quartz and whole-rock relative to that in equilibrium with zircon. Shallower emplacement (1 to 2 km) of the BTIP granites provided access to meteoric water while their rapid assembly following large amounts of active mantle melting resulted in concentrated heat sources and the formation of large hydrothermal cells. By contrast, the emplacement of the TSS occurred at greater depths (4 to 6 km), in the absence of meteoric water and over more protracted time periods with limited heat available to drive large hydrothermal systems. In the absence of meteoric water, hydrothermal alteration and exchange in the TSS resulted from late ^{18}O-rich magmatic fluids that became further enriched in ^{18}O towards the margins of the plutons due to interaction with ^{18}O-rich local sedimentary rocks. The dominance of magmatic fluids during hydrothermal alteration of the TSS also reflects compositional differences between TSS and BTIP magmas. The former are calc-alkaline and considered 'wet' in composition while the latter are tholeiitic or alkaline and essentially 'dry' in composition. In contrast to the TSS, magmatic $\delta^{18}O$ compositions were lowered in the BTIP by assimilation of ^{18}O-depleted local sediments caused by earlier mafic intrusions. Assimilation of local sediments did not occur in the TSS. This is likely to reflect the reduced heat potential of incrementally assembled plutons and the lack of earlier crustal heating caused by earlier mafic intrusions in the BTIP.

Chapter 7

Conclusions and Further Work

In these concluding remarks, the primary aims of this thesis are reiterated in addition to the main conclusions of each data chapter. Finally, the principal limitations are outlined in addition to any remaining questions and potential for further work.

The broad aims of this thesis concern magmatic processes with applications to granitic rocks in general, and in a regional context, understanding the unusual characteristics of the British Devonian Trans-Suture Suite (TSS) of granite plutons that lie adjacent to the Iapetus Suture Zone. The methods used involve applying an integrated trace element and isotopic approach to accessory minerals from the three TSS plutons of Criffell, Fleet and Shap. This thesis has aimed to:

- Evaluate the magmatic evolution of a suite of enigmatic calc-alkaline Devonian granitic plutons that post-date Iapetus subduction and have previously been shown to lack zircon inheritance despite whole-rock isotopic evidence for significant sedimentary involvement.
- Constrain the timing of zircon crystallisation in I- and S-type magmas in order to determine the stage of magma evolution recorded by zircon and other accessory minerals.
- Compare and contrast the stages of magma history archived by whole-rock and accessory mineral records.
- Compare the compositions and ages of crustal sources sampled by plutons lying north and south of the Iapetus Suture in order to determine their relationship to crustal structure.
- Attempt to quantify the roles of crustal and mantle sources in granite genesis, and establish whether, and to what extent the plutons represent net crustal growth or crustal differentiation.

- Use different scales of isotopic and elemental heterogeneity to test models of incremental pluton assembly and their geological timescales.
- Determine the petrogenetic significance of wide-ranging I-S characteristics in closely related plutons, and any relationship to the synchronous intrusion of mafic lamprophyres.

1. Conclusions

1.1 The whole-rock and accessory mineral record

Whole-rock compositions have traditionally been deployed in order to understand the magmatic history of igneous rocks. In recent decades, accessory minerals have provided further insights at new levels of spatial and temporal resolution. However, the relationship between these archives has remained unclear and each is often considered exclusively of the other. Further uncertainty has arisen due to experimental models that indicate that most calc-alkaline mineral assemblages are the result of shallow-level crystallisation while whole-rock compositions are often thought to reflect much deeper processes (e.g. Ulmer, 2007). These apparently conflicting lines of evidence have been reconciled by the crustal hot zone model of Annen et al. (2006a) in which WR compositions are determined at depth within nested sill complexes prior to magma ascent and emplacement in the upper crust. This model indicates that WR compositions should record a distinct stage of magma history to that of accessory minerals crystallised at shallower depths. Evidence for such distinct stages of magma history has been found in the Criffell pluton.

Whole-rock (WR) compositions in the Criffell pluton have been shown to reflect open system assimilation and fractional crystallisation at depths of > 11km, whereas amphibole barometry and the absence of inherited zircon suggest that the observed mineral assemblages crystallised following emplacement of magmas with little or no crystal cargo at depths of 4 to 6 km.

The crystallisation history is shown to be documented by large trace element variations amongst apatite crystals from within individual samples, where decreasing LREE and Th concentrations in metaluminous zones reflect broadly synchronous crystallisation of allanite. By contrast, low LREE and Th, elevated HREE and negative Nd anomalies in apatites from peraluminous samples are thought to reflect the effects of monazite crystallisation.

WR evolution is likely to have occurred within a deep crustal hot zone where H_2O-rich (~ 6wt %), low viscosity magmas segregated and ascended adiabatically in a super-liquidus state, leading to resorption of most entrained crystals. Stalling, emplacement and crystallisation is likely to have resulted from intersection with the H_2O-saturated liquidus at ~ 4 km, resulting in significant water loss. H_2O contents are suggested to be as important as temperature in the attainment of super-liquidus magmas during ascent. Previously identified distinctions between apparently 'cold' and 'hot' granites based on the presence or absence of inherited zircons respectively (Miller et al. 2003) are therefore blurred by the water contents of different granitic magmas. The trace element contents of most accessory minerals are suggested to be controlled by competitive crystallisation of other accessory minerals in small melt batches and are consistent with the incremental assembly of large granitic plutons like Criffell.

1.2 The timing of zircon crystallisation

Despite the unquestionable value of zircons in providing a robust and reliable window into magma evolution, the silicic magmas from which they are most often derived frequently follow long and complex histories. It is unclear what proportion of magma history is retained by zircon and to what extent this may vary between magmas of different compositions. The Criffell pluton is composed of both I- and S-type granitoid rocks and has provided an ideal opportunity to investigate these issues. Apatite trace elements compositions have been shown to sensitively monitor changing assemblages of other accessory minerals during crystallisation, leading to smooth compositional trends. The compositions of apatite inclusions from different host minerals have been shown to lie along different regions of these trends and suggest that relative crystallisation orders may be identified and distinguished geochemically in some zones. Apatite compositions vary differently depending on their host phase in different zones of the Criffell pluton and reveal changing assemblages of coexisting accessory minerals together with different relative crystallisation orders.

In detail, Ce concentrations in metaluminous apatites (~ 5500 to 500 ppm) have been shown to follow smooth trends from high to low concentrations in Ce-Y space that result from the crystallisation of allanite. The range in Ce concentration is similar in apatites hosted by all phases and no evidence was found for a relative crystallisation sequence in metaluminous magmas. Decreasing Sr concentrations in apatite are thought to reflect crystallisation at later stages relative to plagioclase. In metaluminous zones, there was little evidence of any host dependence in the Sr concentrations of apatite inclusions. Peak Sr concentrations enabled a relative assessment of the onset of host saturation relative to plagioclase. Although subtle, the highest peak Sr concentrations were seen in apatites hosted by zircon in all zones and suggest early zircon saturation relative to other phases. In peraluminous zones, apatites have higher concentrations of Y (up to ~3000 ppm) and generally lower concentrations of Ce (<2500 ppm) than would be expected from their respective whole-rocks and reflect the earlier crystallisation of monazite. Apatites formed during later stages of crystallisation in these zones showed lower Y concentrations due to removal by zircon and earlier-formed apatite. The most Y-rich and earliest-formed apatites in peraluminous zones are hosted exclusively by zircon and reflect the earlier crystallisation of most zircon relative to other apatite hosts. The abundance of zircons with apparently more primitive oxygen isotopic compositions than their host whole-rocks in large S-type and peraluminous plutons may reflect the earlier crystallisation of zircon in such magmas. The low abundance of zircon crystals in the most silicic zones is thought to reflect inherently low concentrations of Zr. The greater ease with which zircon crystallises in more primitive, Zr-rich granodiorites may have further biased the isotopic record in magmas generated from the mixing of more primitive and evolved magmas.

1.3 Apatite as a redox proxy

Redox conditions provide valuable information regarding magmatic sources, with calc-alkaline magmas generally found to be more oxidised due to the addition of water. Furthermore, redox conditions strongly influence volcanic emissions which to a large extent determine atmospheric chemistry. The volcanic rocks found throughout the geological record therefore also provide possible insights into

atmospheric evolution. However, the absence of a direct rock record from the early stages of Earth evolution (the Archean and earlier) has resulted in a reliance on detrital accessory minerals such as zircon and specifically their content of redox sensitive elements such as Ce. Apatite is also a common detrital mineral and is found in great abundance in many silicic rocks. Mn concentrations in apatite show little dependence on host magma compositions and instead correlate with independent redox proxies.

Higher Mn concentrations in apatite in granitic rocks from the zoned Criffell granitic pluton have been shown to correlate with decreasing Fe_2O_3 (Fe^{3+}) and Mn in the whole-rock (WR) and are thought to reflect increased Mn^{2+}/Mn^{3+} and greater compatibility of Mn under reduced conditions. A transition was seen from oxidised outer zones to reduced inner zones and was supported by oxygen fugacities (fO_2) calculated using redox sensitive Ce anomalies in magmatic zircons. Median fO_2 values showed that zircon in the outer zones (metaluminous granodiorite) crystallised from magmas that were ~ 2.5 log units above the fayalite-magnetite-quartz (FMQ) buffer. By contrast, zircons from inner zones (peraluminous granite) crystallised from reduced magmas that were ~ 2 log units below the FMQ buffer. Apatite Mn concentrations therefore provide a new and independent means of constraining relative redox changes in a wide spectrum of magma compositions that may be experimentally calibrated. The method can also be applied to detrital mineral grains in the reconstruction of redox conditions on and in the early Earth, lunar magmas and silicic volcanic rocks.

1.4 Regional constraints on the TSS

The proximity of the TSS to the former Iapetus Suture together with post-subduction granite ages has long precluded a direct relationship to subduction, despite calc-alkaline compositions. New U-Pb dating from the Criffell (410 ± 6 Ma), Shap (416 ± 5 Ma) plutons and the outer (410 ± 3 Ma) and inner (387 ± 5 Ma) regions of the Fleet pluton have revealed distinctly older emplacement ages than previously reported. Taken together with wider geological, sedimentary and tectonic evidence, these ages

demonstrate that all three plutons were emplaced during episodes of pre- and post-Acadian transtension, consistent with the occurrence of temporally related lamprophyre dykes. New ages from the Fleet pluton also demonstrate that pluton assembly occurred over a period of ~ 23 Ma and requires incremental assembly, consistent with textural variations throughout the pluton.

Zircon oxygen isotope compositions in different zones of the Criffell, Fleet and Shap plutons have revealed intra-zone variability at the pluton scale consistent with open system differentiation. At an intra-sample scale, more primitive granodiorites are isotopically homogeneous, while increasing isotopic variability is evident amongst zircon populations in increasingly silicic zones. It is suggested that compositional heterogeneity is likely to be preserved in more viscous and silicic magmas due to less effective magma mixing. There is also strong oxygen isotope evidence to support the involvement of more primitive magmas in the formation of large S-type plutons such as Fleet.

Mafic enclaves in the Criffell pluton were shown to contain zircons with mean U-Pb ages that are up to ~9 Ma older than their hosts. Together with evidence for distinct oxygen isotope distributions amongst their zircon populations relative to their host granitoids, this evidence suggests that they may represent entrained cognate magmatic material within segregated magma batches. Such material may potentially be derived from regions of magma generation and differentiation in crustal hot zones.

Zircon εHf compositions in all plutons provide model ages that are consistent with the involvement of Avalonian basement in magma genesis. Previous Pb isotope studies (Thirlwall, 1989) have confirmed the absence of local Southern Uplands sediments in the generation and evolution of the TSS plutons and instead point to the involvement of components found in the underthrust Avalonian terrane. Zircon O-Hf arrays indicate that the most primitive zircons in each pluton lie on a mixing trend between inferred Avalonian basement and juvenile sources. Further mixing with a sedimentary component similar to the Skiddaw Group found on the Avalonian

terrane is capable of reproducing intra-pluton trends of oxygen enrichment in zircons from the Criffell and Fleet plutons.

The common occurrence of similar isotope compositions in plutons from across the suture zone is consistent with the underthrusting of Avalonian crust beneath the Laurentian margin. Evidence for high water contents in these granites linked to the adiabatic ascent of transiently super-liquidus melts and the resorption of all entrained crystals may reflect the importance of hydrated lithospheric magma sources. This in turn has resulted from earlier dehydration of the subducting Iapetus oceanic crust and is consistent with the extensive occurrence of lamprophyric dykes and calc-alkaline granitoids of the same age around the suture zone. Many of the unusual chemical and physical characteristics that distinguish these calc-alkaline granites from other late- and post-Caledonian granites can therefore be linked to their emplacement and formation during crustal transtension within the Iapetus suture zone.

1.5 Post-emplacement hydrothermal histories

The $\delta^{18}O$ compositions of zircon, quartz and WR in the TSS reveal evidence for hydrothermal exchange and alteration in the former two chemical archives. The $\delta^{18}O$ compositions of quartz and whole-rocks have been elevated relative to those of zircon. These changes reflect the circulation of $\delta^{18}O$-rich magmatic fluids, with further $\delta^{18}O$ enrichment at the margins of the plutons due to fluid interaction with $\delta^{18}O$-rich local sediments. In contrast to granites of the British Tertiary Igneous Province (BTIP), where circulation of meteoric water and assimilation of rocks altered by meteoric water lowered the $\delta^{18}O$ compositions of magmas, there is no evidence that meteoric waters contributed to the hydrothermal evolution of the TSS. These differences reflect markedly different hydrothermal histories that in turn result from different emplacement depths, pre-emplacement histories, tectonic environments and mantle sources. The TSS was emplaced at depths of 4-6 km, significantly deeper than the 1-2 km emplacement depths of BTIP granites, thereby limiting access to meteoric water. Incremental assembly of the TSS, often over time periods of as much as 23 Ma also limited thermal potential for large hydrothermal systems and is in contrast to the rapid emplacement of BTIP magmas. Mantle

sources for the TSS are also likely to have been hydrated by earlier Iapetus subduction, resulting in larger volumes of magmatic fluids. By contrast, BTIP granites generated from active melting of 'dry' mantle would have limited the availability of magmatic fluids. Finally, the earlier emplacement of large mafic bodies during the BTIP is likely to have pre-disposed and hydrothermally altered local crust to assimilation during granite emplacement. No assimilation of local sediments is evident in the TSS and in part reflects an absence of earlier mafic magmatism.

2. Limitations

Some of the limitations of using accessory mineral compositions include:

1. The analytical techniques required are clearly costly and time consuming. Sample sizes are therefore limited and it reasonable to question the extent to which such small sample sets are representative of large magmatic bodies, including granitic plutons.
2. Despite improvements in the spatial resolution of SIMS and laser ablation analyses, their resolutions vary substantially. For example, oxygen isotope analyses generally require a volume of only 20μm^3. By contrast, U-Pb dating requires volumes of ~60 μm^3 (20 μm × 3 μm), REE analyses by SIMS require 100μm^3 (20 μm × 5 μm), while laser ablation requires volumes of up to ~ 1500μm^3 (50 μm × 30 μm). Some of these difficulties have been overcome by developments that allow for multiple analyses on single areas of individual grains. However, when fine-scale compositional zoning is evident, it is impossible to ensure that different isotope compositions are determined from the same compositional zone.
3. Bulk and local saturation of accessory minerals may record markedly different magmatic environments, with locally saturated accessory minerals recording compositions that differ strongly from those of the bulk magma. Crystal morphology alone is insufficient to distinguish bulk and local saturation, as euhedral accessory minerals have been shown to crystallise within existing host minerals (Bacon, 1989; Hoskin et al. 2000). Bulk saturation of apatite is favoured in most zones of the Criffell pluton due to smooth compositional trends amongst crystal populations. Bulk saturation of apatite and zircon is also favoured from their isolated occurrence in all samples from the TSS plutons. Crystallisation from isolated melt pockets would be expected to result in sequential crystallisation of multiple mineral phases, leading to close spatial relations. Despite this, it cannot be guaranteed that all accessory minerals formed in response to bulk saturation.

4. Compositional constraints on potential magma sources are limited, particularly for Avalonian basement with no known exposure. Mantle Hf compositions are also subject to uncertainty due to possible areas of enriched and depleted mantle. It has therefore been difficult to quantify the involvement of different contributing sources.
5. Zircon abundance in the most silicic zones of the Criffell and Fleet plutons is limited due to low Zr concentrations and it has not been possible to obtain statistically meaningful zircon compositions from these zones.
6. The use of Mn in apatite as a potential oxybarameter is currently limited to qualitative assessments and requires experimental calibration.
7. Despite the sensitivity of apatite REE compositions to different magmatic environments, zircon REE patters are notoriously monotonous due to complex substitution mechanisms that depend largely on the availability of elements like P required for coupled substitutions (see Hoskin et al. 2000). Zircon REE compositions are therefore not sensitive to changing magmatic conditions and a comparative study between apatite and zircon REE compositions has not been possible because of these limitations.

3. Further work

Common to all research outcomes is the opening of new potential directions for future research. In this final section, these potential lines of further development are outlined:

- Perhaps one of the most valuable conclusions of this thesis is the discovery that Mn concentrations in apatite may provide a robust means of estimating redox conditions in a wide range of magmatic rocks. With apparently limited dependence on melt compositions, the method may be applied to detrital apatites from the sedimentary record to reveal redox information about magmatic rocks now lost from the geological record. Apatite is also becoming an increasingly useful resource for lunar studies where redox conditions are likely to reveal important information about the water content of the lunar mantle and the processes associated with lunar accretion. At present, only qualitative and relative changes in oxygen fugacity can be made using apatite, while some quantitative estimates are possible from an integrated apatite-zircon approach using the newly calibrated zircon Ce anomaly approach of Trail et al. (2011). Experimental calibration is now required to further investigate the controls on Mn concentrations in apatite which may prove highly valuable to the geological community at large, including lunar studies and those that examine redox controls on volcanic emissions.
- The importance of deep-seated and open system processes in crustal hot zones has been highlighted by whole-rock compositions from the Criffell pluton. However, due to the resoption of most minerals during ascent to the level of emplacement, mineralogical evidence from this stage of magma evolution is limited. Zircon found in mafic enclaves from the Criffell pluton have U-Pb and O isotope compositions that are distinct from their host granodiorites and it has been suggested that these may be the sole remaining archives of deep hot zone processes. Further work is required to examine other minerals in mafic enclaves and in particular the Al content of amphibole that may reveal much deeper crystallisation pressures than those

reported from their host granitoids. Re-equilibration of amphibole compositions during emplacement at shallow depths will need careful consideration.

- The TSS plutons are found at similar erosion levels to small outcrops of intrusion breccias and vent agglomerates in the Southern Uplands (e.g. the Shoulder O'Craig outcrop near Kirkcudbright). New U-Pb ages reported here suggest that the Criffell pluton is mostly contemporaneous with this vent and formed at ~ 410 Ma. Vent agglomerates are considered shallow features and are difficult to reconcile with crystallisation depths of 4-6km for the nearby Criffell pluton. The two feldspar character of both I- and S-type zones of the pluton suggest crystallisation pressures of > ~3 kbar (~ 9km) (Tuttle and Bowen 1958) but this may to some extent be compensated for by increased concentrations of Ca (Fig. 7.1) that raise the feldspar solidus (Parsons et al. 2005). Similar discrepancies between contemporaneous plutonic and volcanic features are seen on a much larger scale near Ben Nevis, where the Glencoe and Ben Nevis calderas are found adjacent to granitic plutons. Further work is required to investigate whether these features represent significant and rapid differential surface movements or whether age constrains require further refinement.

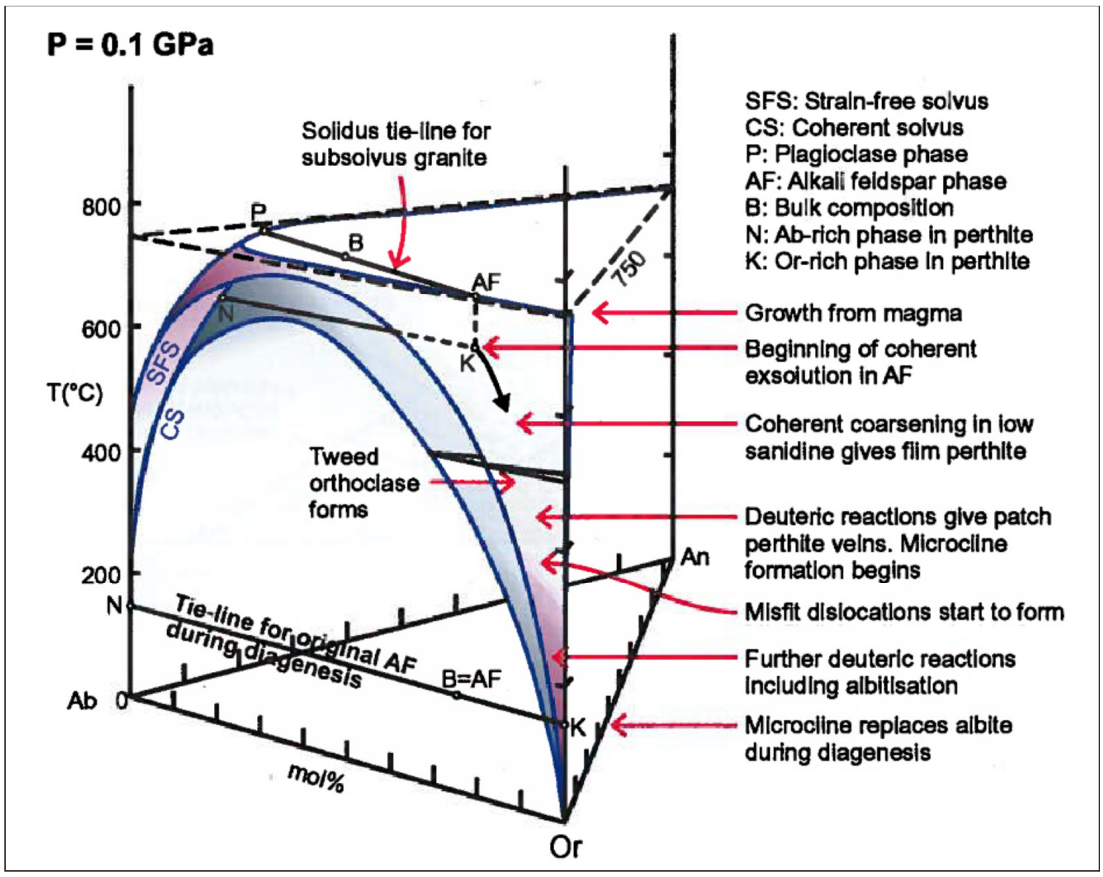

Fig. 7.1 Temperature-composition prism for the ternary feldspar system Albite-Orthoclase-Anorthite from Parsons et al. 2005.

- Significant heterogeneity has been found in zircon oxygen isotope compositions from the most silicic zones of the Criffell and Fleet plutons. The discovery of large degrees of heterogeneity in single hand specimens and at small scales mirrors recent findings at the mafic end of the compositional spectrum, where olivine-hosted melt inclusions were shown to exhibit similar degrees of compositional heterogeneity to that of all MORB (Maclennan, 2008). Both results reflect the importance of microanalyses in revealing cryptic archives of magmatic processes. Textural heterogeneities are often visible over short length-scales in some granitic plutons. A study that focuses on accessory minerals from a small (~ 100m^2) area of a single pluton may place further constrains on the length-scales of compositional heterogeneity.
- Cracks and inclusions within a number of zircon crystals together with the large volumes of material required for Hf isotope analyses have limited the

extent to which intra-crystal compositional variations have been investigated in this study. A detailed study of oxygen isotope variation within zoned crystals, with limited need for large clear surface areas may reveal further evidence of magmatic processes on even smaller scales.

- Zircons with low $\delta^{18}O$ compositions have been found in the S-type Fleet pluton. These results are similar to those reported by Appleby et al. (2010) for S-type granites in NE Scotland, and provide further evidence for the involvement of mafic magmas in the formation of large S-type plutons. Further work is required to investigate the volumes of mafic magmas involved and the role they play in the generation of large volumes of S-type granites.
- The occurrence of both I- and S-type magmas within the TSS is unique amongst the Devonian granites in Northern Britain. The processes that led to contemporaneous emplacement of both granites require evaluation in terms of hot zone processes. Annen et al. (2006) suggest that the distribution of mafic sills within the hot zone may drastically alter the balance between I- and S-type magmas and it will be necessary to investigate whether such changes in sill distributions can account for the formation of large volumes of I- and S-type granites in the Southern Uplands.
- Cleavage around the margins of the Shap and Fleet plutons together with their thermal aureoles is said to show evidence for having been synchronous with pluton emplacement (Soper and Kneller, 1990). The new geochronological data presented here may have significant implication of the timing of cleavage formation in Northern England and Southern Scotland, and may provide better constraints on the regional tectonic evolution of the region.

Bibliography

Allegre, C. J., Hart, S. R. & Minster, J. F. (1983). Chemical structure and evolution of the mantle and continents determined by inversion of Nd and Sr isotopic data, I. Theoretical methods. *Earth and Planetary Science Letters* **66**, 177-190.

Allegre, C. J. & Rousseau, D. (1984). The growth of the continent through geological time studied by Nd isotope analysis of shale. *Earth and Planetary Science Letters* **67**, 19-34.

Andersen, C. A. & Hinthorn.J.R. (1972). U, Th, Pb and REE abundances and^{207}Pb/^{206}Pb ages of individual minerals in returned lunar material by ion microprobe mass analysis. *Earth and Planetary Science Letters* **14**, 195-200.

Anderson, J. L. & Smith, D. R. (1995). The effects of temperature and fO_2 on the Al-in-hornblende barometer. *American Mineralogist* **80**, 549-559.

Annen, C., Blundy, J. D. & Sparks, R. S. J. (2006a). The genesis of intermediate and silicic magmas in deep crustal hot zones. *Journal of Petrology* **47**, 505-539.

Annen, C., Blundy, J. D. & Sparks, R. S. J. (2006b). The sources of granitic melt in Deep Hot Zones. *Transactions of the Royal Society of Edinburgh-Earth Sciences* **97**, 297-309.

Annen, C. & Sparks, R. S. J. (2002). Effects of repetitive emplacement of basaltic intrusions on thermal evolution and melt generation in the crust. *Earth and Planetary Science Letters* **203**, 937-955.

Appleby, S. K., Gillespie, M. R., Graham, C. M., Hinton, R. W., Oliver, G. J. H., Kelly, N. M. & Eimf. (2010). Do S-type granites commonly sample infracrustal

sources? New results from an integrated O, U-Pb and Hf isotope study of zircon. *Contributions to Mineralogy and Petrology* **160**, 115-132.

Appleby, S. K., Graham, C. M., Gillespie, M. R., Hinton, R. W., Oliver, G. J. H. & Eimf. (2008). A cryptic record of magma mixing in diorites revealed by high-precision SIMS oxygen isotope analysis of zircons. *Earth and Planetary Science Letters* **269**, 105-117.

Arculus, R. J. (2003). Use and abuse of the terms calcalkaline and calcalkalic. *Journal of Petrology* **44**, 929-935.

Armstrong, M. & Paterson, I. B. (1970). The Lower Old Red Sandstone of the Strathmore region. *Report of the Institute of Geological Sciences* **70/12**.

Armstrong, H. A. & Owen, A. W. (2001). Tectonic evolution of the paratectonic Caledonides of Northern Britain *Journal of the Geological Society, London* **158**, 475-486.

Armstrong, H. A., Owen, A. W., Scrutton, C. T., Clarkson, E. N. K. & Taylor, C. M. (1996). Evolution of the Northern Belt, Southern Uplands: Implications for the Southern Uplands controversy. *Journal of the Geological Society* **153**, 197-205.

Atherton, M. P. & Petford, N. (1993). Generation of sodium-rich magmas from newly underplated basaltic crust. *Nature* **362**, 144-146.

Kay, R. W. & Kay, S. M. (1993). Delamination and delamination magmatism. *Tectonophysics* **219**, 177-189.

Ayuso, R. A. (1986). Lead-isotopic evidence for distinct sources of granite and for distinct basements in the northern Appalachians, Maine. *Geology* **14**, 322-325.

Bacon, C. R. (1983). Eruptive history of Mount Mazama and Crater Lake Caldera, Cascade Range, USA *Journal of Volcanology and Geothermal Research* **18**, 57-115.

Bacon, C. R. & Druitt, T. H. (1988). Compositional evolution of the zoned calcalkaline magma chamber of Mount-Mazama, Crater Lake, Oregon *Contributions to Mineralogy and Petrology* **98**, 224-256.

Bacon, C. R. (1989). Crystallisation of accessory phases in magmas by local saturation adjacent to phenocrysts. *Geochimica Et Cosmochimica Acta* **53**, 1055-1066.

Ballard, J. R., Palin, J. M. & Campbell, I. H. (2002). Relative oxidation states of magmas inferred from Ce(IV)/Ce(III) in zircon: application to porphyry copper deposits of northern Chile. *Contributions to Mineralogy and Petrology* **144**, 347-364.

Barnes, R. P., Lintern, B. C. & Stone, P. (1989). Timing and regional implications of deformation in the Southern Uplands of Scotland *Journal of the Geological Society* **146**, 905-908.

Barnes, R. P., Phillips, E. R. & Boland, M. P. (1995). The Orlock Bridge Fault in the Southern Uplands of Southwestern Scotland - A terrane boundary *Geological Magazine* **132**, 523-529.

Barnes, R. P. (1999). Geology of the Whithorn, Kirkcowan and Wigtown districts. *Memoir of the Geological Survey of the United Kingdom, Sheets 2, 4W and 4E (Scotland).*

Barnes, R. P. & Stone, P. (1999). Trans-Iapetus contrasts in the geological development of Southern Scotland (Laurentia) and the Lakesman Terrane (Avalonia). In: Woodcock N. H., Q. D. G., Fitches W. R., Barnes R. P. (ed.) *Sight of*

the Suture: the Palaeozoic Geology of the Isle of Man in its Iapetus Ocean Context: Geological Society, London, Special Publications, 307-232.

Beamish, D. & Smythe, D. K. (1986). Geophysical images of the deep crust: the Iapetus suture. *Journal of the Geological Society* **143**, 489-497.

Belousova, E. A., Griffin, W. L., O'Reilly, S. Y. & Fisher, N. I. (2002). Apatite as an indicator mineral for mineral exploration: trace-element compositions and their relationship to host rock type. *Journal of Geochemical Exploration* **76**, 45-69.

Belousova, E. A., Walters, S., Griffin, W. L. & O'Reilly, S. Y. (2001). Trace-element signatures of apatites in granitoids from the Mt Isa Inlier, northwestern Queensland. *Australian Journal of Earth Sciences* **48**, 603-619.

Berndt, J., Koepke, J. & Holtz, F. (2005). An experimental investigation of the influence of water and oxygen fugacity on differentiation of MORB at 200 MPa. *Journal of Petrology* **46**, 135-167.

Bierlein, F. P., Groves, D. I. & Cawood, P. A. (2009). Metallogeny of accretionary orogens - The connection between lithospheric processes and metal endowment. *Ore Geology Reviews* **36**, 282-292.

Binder, B. & Keppler, H. (2011). The oxidation state of sulfur in magmatic fluids. *Earth and Planetary Science Letters* **301**, 190-198.

Blatter, D. L. & Carmichael, I. S. E. (1998). Plagioclase-free andesites from Ziticuaro (Michoacan), Mexico: petrology and experimental constraints. *Contributions to Mineralogy and Petrology* **132**, 121-138.

Bluck, B. (1983). Role of the Midland Valley of Scotland in the Caledonian Orogeny. *Transactions of the Royal Society of Edinburgh-Earth Sciences* **74**, 119-136.

Blundy, J. & Cashman, K. (2001). Ascent-driven crystallisation of dacite magmas at Mount St Helens, 1980-1986. *Contributions to Mineralogy and Petrology* **140**, 631-650.

Blundy, J. & Cashman, K. (2005). Rapid decompression-driven crystallization recorded by melt inclusions from Mount St. Helens volcano. *Geology* **33**, 793-796.

Blundy, J., Cashman, K. & Humphreys, M. (2006). Magma heating by decompression-driven crystallization beneath andesite volcanoes. *Nature* **443**, 76-80.

Blundy, J. D. & Holland, T. J. B. (1990). Calcic amphibole equilibria and a new amphibole-plagioclase geothermometer. *Contributions to Mineralogy and Petrology* **104**, 208-224.

Boulter, C. A. & Soper, N. J. (1973). Structural relationships of the Shap granite. *Proceedings of the Yorkshire Geological Society* **39**, 365-369.

Bouvier, A., Vervoort, J. D. & Patchett, P. J. (2008). The Lu-Hf and Sm-Nd isotopic composition of CHUR: Constraints from unequilibrated chondrites and implications for the bulk composition of terrestrial planets. *Earth and Planetary Science Letters* **273**, 48-57.

Bowen, N. L. (1928). *The evolution of igneous rocks*: Princeton University Press.

Bradley, D. C. (2011). Secular trends in the geologic record and the supercontinent cycle. *Earth-Science Reviews* **108**, 16-33.

Brown, M. (1994). The Generation, Segregation, Ascent and Emplacement of Granite Magma – the Migmatite-to Crustally-Derived- Granite Connection in Thickened Orogens. *Earth-Science Reviews* **36**, 83-130.

Brown, M. (2007). Metamorphic conditions in orogenic belts: A record of secular change. *International Geology Review* **49**, 193-234.

Brown, P. E., Ryan, P. D., Soper, N. J. & Woodcock, N. H. (2008). The Newer Granite problem revisited: a transtensional origin for the Early Devonian Trans-Suture Suite. *Geological Magazine* **145**, 235-256.

Buddington, A. F. (1959). Granite emplacement with special reference to North America. *Geological Society of America Bulletin* **70**, 671-747.

Campbell, I. H. & Allen, C. M. (2008). Formation of supercontinents linked to increases in atmospheric oxygen. *Nature Geoscience* **1**, 554-558.

Campbell, I. H. & Taylor, S. R. (1983a). No water, no granites-no oceans, no continents. *Geophysical Research Letters* **10**, 1061-1064.

Campbell, I. H. & Taylor, S. R. (1983b). No water, no granites - no oceans, no continents *Geophysical Research Letters* **10**, 1061-1064.

Canil, D. (1997). Vanadium partitioning and the oxidation state of Archaean komatiite magmas. *Nature* **389**, 842-845.

Canil, D., Oneill, H. S., Pearson, D. G., Rudnick, R. L., McDonough, W. F. & Carswell, D. A. (1994). Ferric iron in peridotites and mantle oxidation states. *Earth and Planetary Science Letters* **123**, 205-220.

Carmichael, I. S. E. (1991). The redox state of basic and silicic magmas: a reflection of their source regions? *Contributions to Mineralogy and Petrology* **106**, 129-141.

Carmichael, I. S. E. & Ghiorso, M. S. (1990). The effect of oxygen fugacity on the redox state of natural liquids and their crystallising phases: *Reviews in Mineralogy and Geochemistry* **24**, 191-212.

Cavosie, A. J., Valley, J. W. & Wilde, S. A. (2005). Magmatic delta O-18 in 4400-3900 Ma detrital zircons: A record of the alteration and recycling of crust in the Early Archean. *Earth and Planetary Science Letters* **235**, 663-681.

Cavosie, A. J., Wilde, S. A., Liu, D. Y., Weiblen, P. W. & Valley, J. W. (2004). Internal zoning and U-Th-Pb chemistry of Jack Hills detrital zircons: a mineral record of early Archean to Mesoproterozoic (4348-1576 Ma) magmatism. *Precambrian Research* **135**, 251-279.

Cawood, P. A., McCausland, P. J. A. & Dunning, G. R. (2001). Opening Iapetus: Constraints from the Laurentian margin in Newfoundland. *Geological Society of America Bulletin* **113**, 443-453.

Cawood, P. A., Nemchin, A. A., Strachen, R., Prave, T. & Krabbendam, M. (2007). Sedimentary basin and detrital zircon record along East Laurentia and Baltica during assembly and breakup of Rodinia. *Geological Society of London* **164**.

Cerny, P., Meintzer, R. E. & Anderson, A. J. (1985). Extreme fractionation in rare-element granitic pegmatites: selected examples of data and mechanisms. *Canadian Mineralogist* **23**, 381-421.

Chamberlain, K. R. & Bowring, S. A. (2001). Apatite-feldspar U-Pb thermochronometer: a reliable, mid-range (similar to 450 degrees C), diffusion-controlled system. *Chemical Geology* **172**, 173-200.

Chappell, B. W. & White, A. J. R. (1974). Two contrasting granite types. *Pacific Geology* **8**, 173-174.

Chappell, B. W. & White, A. J. R. (1984). I- and S-type granites in the Lachlan Fold Belt, southeastern Australia. In: Kequin, X. & Guangchi, T. (eds.) *Geology of Granites and Their Metallogenic Relations*. Beijing: Sciecne Press, 87-101.

Chappell, B. W. & White, A. J. R. (2001). Two contrasting granite types: 25 years later. *Australian Journal of Earth Sciences* **48**, 489-499.

Chappell, B. W., White, A. J. R., Williams, I. S. & Wyborn, D. (2004). Low- and high-temperature granites. *Transactions of the Royal Society of Edinburgh-Earth Sciences* **95**, 125-140.

Cherniak, D. J. (2000). Rare earth element diffusion in apatite. *Geochimica Et Cosmochimica Acta* **64**, 3871-3885.

Cherniak, D. J. (2005). Uranium and manganese diffusion in apatite. *Chemical Geology* **219**, 297-308.

Cherniak, D. J. & Watson, E. B. (2003). Diffusion in zircon. In: Hanchar, J. M. & Hoskin, P. W. O. (eds.) *Zircon*, 113-143.

Chesner, C. A. (1998). Petrogenesis of the Toba Tuffs, Sumatra, Indonesia. *Journal of Petrology* **39**, 397-438.

Chu, M.-F., Wang, K.-L., Griffin, W. L., Chung, S.-L., O'Reilly, S. Y., Pearson, N. J. & Iizuka, Y. (2009a). Apatite Composition: Tracing Petrogenetic Processes in Transhimalayan Granitoids. *Journal of Petrology* **50**, 1829-1855.

Chu, M. F., Wang, K. L., Griffin, W. L., Chung, S. L., O'Reilly, S. Y., Pearson, N. J. & Iizuka, Y. (2009b). Apatite Composition: Tracing Petrogenetic Processes in Transhimalayan Granitoids. *Journal of Petrology* **50**, 1829-1855.

Claiborne, L. L., Miller, C. F. & Wooden, J. L. (2010). Trace element composition of igneous zircon: a thermal and compositional record of the accumulation and evolution of a large silicic batholith, Spirit Mountain, Nevada. *Contributions to Mineralogy and Petrology* **160**, 511-531.

Clayburn, J. A. P., Harmon, R. S., Pankhurst, R. J. & Brown, J. F. (1983). Sr, O, and Pb isotope evidecne for origin and evolution of Etive igneuos complex, Scotland *Nature* **303**, 492-497.

Clemens, J. D. & Mawer, C. K. (1992). Granitic Magma Transport by Fracture Propagation. *Tectonophysics* **204**, 339-360.

Clemens, J. D., Petford, N. & C.K, M. (1997). Ascent mechanisms of granitic magmas: cause and consequence. In: Holness, M. (ed.) *Deformation-Enhanced Fluid Transport in the Earth's Crust and Mantle*. London: Chapman & Hall, 145-172.

Cloos, M. (1993). Lithospheric buoyancy and collisional orogenesis: Subduction of oceanic plateaus, continental margins, island arcs, spreading ridges, and seamounts *Geological Society of America Bulletin* **105**, 715-737.

Coleman, D. S., Gray, W. & Glazner, A. F. (2004). Rethinking the emplacement and evolution of zoned plutons: Geochronologic evidence for incremental assembly of the Tuolumne Intrusive Suite, California. *Geology* **32**, 433-436.

Collins, W. J. (1998). Evaluation of petrogenetic models for Lachlan Fold Belt granitoids: implications for crustal architecture and tectonic models. *Australian Journal of Earth Sciences* **45**, 483-500.

Collins, W. J. (1999). Evaluation of petrogenetic models for Lachlan Fold Belt granitoids: implications for crustal architecture and tectonic models - Reply. *Australian Journal of Earth Sciences* **46**, 831-836.

Collins, W. J. (2002). Nature of extensional accretionary orogens. *Tectonics* **21**.

Colombini, L. L., Miller, C. F., Gualda, G. A. R., Wooden, J. L. & Miller, J. S. (2011). Sphene and zircon in the Highland Range volcanic sequence (Miocene, southern Nevada, USA): elemental partitioning, phase relations, and influence on evolution of silicic magma. *Mineralogy and Petrology* **102**, 29-50.

Condie, K. C. (1993). Chemical composition and evolution of the upper continental crust: contrasting results from surface samples and shales. *Chemical Geology* **104**, 1-37.

Condie, K. C. (1998). Episodic continental growth and supercontinents: a mantle avalanche connection? *Earth and Planetary Science Letters* **163**, 97-108.

Condie, K. C. (2004). Supercontinents, superplumes and continental growth: the Neoproterozoic record. *Physics of the Earth and Planetary Interiors* **146**, 319-332.

Condie, K. C. (2005). *Earth as an Evolving Planet*. Amsterdam: Elsevier.

Cooper, D. C., Lee, M. K., Fortey, N. J., Cooper, A. H., Rundle, C. C., Webb, B. C. & Allen, P. M. (1988). The Crummock Water aureole: a zone of metasomatism and source of ore metals in the English Lake District. *Journal of the Geological Society* **145**, 523-540.

Corfu, F. & Easton, R. M. (2001). U-Pb evidence for polymetamorphic history of Huronian rocks within the Grenville front tectonic zone east of Sudbury, Ontario, Canada. *Chemical Geology* **172**, 149-171.

Costa, F., Scaillet, B. & Pichavant, M. (2004). Petrological and experimental constraints on the pre-eruption conditions of Holocene dacite from Volcan San Pedro (36 degrees S, Chilean Andes) and the importance of sulphur in silicic subduction-related magmas. *Journal of Petrology* **45**, 855-881.

Couch, S., Harford, C. L., Sparks, R. S. J. & Carroll, M. R. (2003). Experimental constraints on the conditions of formation of highly calcic plagioclase microlites at the Soufrire Hills Volcano, Montserrat. *Journal of Petrology* **44**, 1455-1475.

Coulson, I. M., Dipple, G. M. & Raudsepp, M. (2001). Evolution of HF and HCl activity in magmatic volatiles of the gold-mineralized Emerald Lake pluton, Yukon Territory, Canada. *Mineralium Deposita* **36**, 594-606.

Courrioux, G. (1987a). Oblique diapirism - The Criffel granodiorite granite zoned pluton (Southwest Scotland) *Journal of Structural Geology* **9**, 313-330.

Courrioux, G. (1987b). Oblique diapirism: the criffel granodiorite/granite zoned pluton. *Journal of Structural Geology* **9**, 313-330.

Cox, R. A., Dempster, T. J., Bell, B. R. & Rogers, G. (1996). Crystallization of the Shap granite: Evidence from zoned K-feldspar megacrysts. *Journal of the Geological Society* **153**, 625-635.

Darling, J., Storey, C. & Hawkesworth, C. (2009). Impact melt sheet zircons and their implications for the Hadean crust. *Geology* **37**, 927-930.

Davidson, J., Charlier, B. & Hora, J. M. (2005). Mineral isochrons and isotopic fingerprinting: Pitfalls and promises. *Geology* **33**, 29-32.

Delano, J. W. (2001). Redox history of the Earth's interior since similar to 3900 Ma: Implications for prebiotic molecules. *Origins of Life and Evolution of the Biosphere* **31**, 311-341.

DePaolo, D. J. (1981). Trace element and isotopic effects of combined wallrock assimilation and fractional crystallization. *Earth and Planetary Science Letters* **53**, 189–202.

Detrick, R. S., Mutter, J. C., Buhl, P. & Kim, II. (1990). No evidence from multichannel reflection data for a crustal magma chamber in the MARK area on the Mid-Atlantic Ridge. *Nature* **347**, 61-64.

Dewey, J. F. (2002). Transtension in arcs and orogens. *International Geology Review* **44**, 402-439.

Dewey, J. F. & Strachan, R. A. (2003). Changing Silurian-Devonian relative plate motion in the Caledonides: sinistral transpression to sinistral transtension. *Journal of the Geological Society* **160**, 219-229.

Dhuime, B., Hawkesworth, C. & Cawood, P. (2011). When Continents Formed. *Science* **331**, 154-155.

Dhuime, B., Hawkesworth, C. J., Cawood, P. A. & Storey, C. D. (2012). A Change in the Geodynamics of Continental Growth 3 Billion Years Ago. *Science* **335**, 1334-1336.

Druitt, T. H. & Bacon, C. R. (1989). Petrology of the zoned calcalkaline magma chamber of Mount Mazama, Crater Lake, Oregon. *Contributions to Mineralogy and Petrology* **101**, 245-259.

Eiler, J. M. (2001). Oxygen isotope variations of basaltic lavas and upper mantle rocks. In: Valley, J. W. & Cole, D. R. (eds.) *Stable Isotope Geochemistry*, 319-364.

Eiler, J. M. (2007). Geology - On the origins of granites. *Science* **315**, 951-952.

Elders, C. F. (1987). The provenance of granite boulders in conglomerates of the Northern and Central Belts of the southern Uplands of Scotland *Journal of the Geological Society* **144**, 853-863.

Ewart, A. & Griffin, W. L. (1994). Application of proton-microprobe data to trace-element partitioning in volcanic-rocks. *Chemical Geology* **117**, 251-284.

Faure, G. & Mensing, T. M. (2004). *Isotopes: principles and applications 3rd ed.* New Jersey: John Wiley and Sons, Inc.

Ferreira, V. P., Valley, J. W., Sial, A. N. & Spicuzza, M. J. (2003). Oxygen isotope compositions and magmatic epidote from two contrasting metaluminous granitoids, NE Brazil. *Contributions to Mineralogy and Petrology* **145**, 205-216.

Ferry, J. M. & Watson, E. B. (2007). New thermodynamic models and revised calibrations for the Ti-in-zircon and Zr-in-rutile thermometers. *Contributions to Mineralogy and Petrology* **154**, 429-437.

Fitton, J. G. & Godard, M. (2004). Origin and Evolution of the Ontong Java Plateau. In: Fitton, J. G., Mahoney, J. J., Wallace, P. J. & Saunders, A. D. (eds.) *Geological Society Special Publications*, 151-178.

Fitton, J. G., Saunders, A. D., Larsen, L. M., Hardarson, B. S. & Norry, M. J. (1998). Volcanic rocks from the southeast Greenland margin at 63°N: composition, petrogenesis and mantle sources. *Proceedings of the Ocean Drilling Program, Scientific Results* **152**, 331-350.

Fowler, T. K., Paterson, S. R., Crossland, A. & Yoshinobu, A. (1995). *Pluton emplacement mechanisms: a view from the roof.*

Freeman, B., Klemperer, S. L. & Hobbs, R. W. (1988a). The deep structure of Northern England ans the Iapetus Sure Zone from BIRPS deep seismic reflection profiles *Journal of the Geological Society* **145**, 727-740.

Freeman, B., Klemperer, S. L. & Hobbs, R. W. (1988b). The deep structure of Northern England ans the Iapetus Sure Zone from BIRPS deep seismic reflection profiles *Journal of the Geological Society* **145**, 727-740.

Frost, C. D. & O'Nions, R. K. (1985). Caledonian Magma Genesis and Crustal Recycling. *Journal of Petrology* **26**, 515-544.

Frost, D. J. & McCammon, C. A. (2008). The redox state of Earth's mantle. *Annual Review of Earth and Planetary Sciences*, 389-420.

Frost, R. B. (1991). Introduction to oxygen fugacity and its petrological importance. In: Lindsley, D. H. (ed.) *Oxide minerals: petrologic and magnetic significance: Reviews in Mineralogy*, 1-8.

Fujimaki, H. (1986). Partition-coefficients of Hf, Zr, and REE between zircon, apatite, and liquid. *Contributions to Mineralogy and Petrology* **94**, 42-45.

Fujimaki, H., Tatsumoto, M. & K., A. (1984). Partition coefficients of Hf, Zr, and REE between phenocrysts and groundmasses. *Journal of Geophysical Research* **89**, 662-672.

Fyfe, W. S. (1978). The evolution of the Earth's crust: Modern plate tectonics to ancient hot spot tectonics. *Chemical Geology* **23**, 89-114.

Gardner, J. E., Carey, S., Sigurdsson, H. & Rutherford, M. J. (1995). Influence of magma composition on the eruptive activity of Mount St. Helens, Washington. *Geology* **23**, 523-526.

Garrels, R. M. & Perry, E. A. (1974). *Cycling of carbon, sulfur, and oxygen through geologic time*. New York: Wiley.

Gerdes, A., Montero, P., Bea, F., Fershater, G., Borodina, N., Osipova, T. & Shardakova, G. (2002). Peraluminous granites frequently with mantle-like isotope compositions: the continental-type Murzinka and Dzhabyk batholiths of the eastern Urals. *International Journal of Earth Sciences* **91**, 3-19.

Gill, J. B. (1983). Orogenic Andesites and Plate Tectonics. *American Journal of Science* **283**, 633-634.

Glazner, A. F. & Bartley, J. M. (2006). Is stoping a volumetrically significant pluton emplacement process? *Geological Society of America Bulletin* **118**, 1185-1195.

Glazner, A. F., Bartley, J. M., Coleman, D. S., Gray, W. & Taylor, R. Z. (2004a). Are plutons assembled over millions of years by amalgamation from small magma chambers? *GSA Today* **14**.

Glazner, A. F., Bartley, J. M., Drew, S. C., Gray, W. & Taylor, R. Z. (2004b). Are plutons assembled over millions of years by amalgamation from small magma chambers? *GSA Today* **14**, 4-10.

Glazner, A. F., Bartley, J.M. and Coleman, D.S. (ed.) (2007). *Volcanic/plutonic connections: a view from the Sierra Nevada, California.*

Granthem, D. R. (1928). The petrology of the Shap granite. *Proceedings of the Geologists' Association* **39**, 299-331.

Gray, C. M. (1984). An isotopic mixing model for the origin of granitic-rocks in southeastern Australia. *Earth and Planetary Science Letters* **70**, 47-60.

Griffin, W. L., Pearson, N. J., Belousova, E., Jackson, S. E., van Achterbergh, E., O'Reilly, S. Y. & Shee, S. R. (2000). The Hf isotope composition of cratonic mantle: LAM-MC-ICPMS analysis of zircon megacrysts in kimberlites. *Geochimica Et Cosmochimica Acta* **64**, 133-147.

Griffin, W. L., Wang, X., Jackson, S.E., Pearson, N.J., O'Reilly, S.Y., Xu, X., Zhou, X. (2002). Zircon chemistry and magma mixing, SE China: In-situ analysis of Hf isotopes, Tonglu and Pingtan igneous complexes. *Lithos* **61**, 237-269.

Grocott, J., Brown, M., Dallmeyer, R. D., Taylor, G. K. & Treloar, P. J. (1994). Mechanisms of continental growth in extensional arcs: An example from the Andean plate-boundary zone. *Geology* **22**, 391-394.

Gurnis, M. & Davies, G. F. (1985). Simple parametric models of crustal growth. *Journal of Geodynamics* **3**, 105-135.

Gurnis, M. & Davies, G. F. (1986). Apparent episodic crustal growth arising from a smoothly evolving mantle. *Geology* **14**, 396-399.

Hall, J., Brewer, J.A, Matthews, D.H, Warner, M.R. (1984). Crustal structure across the Caledonides from the 'WINCH seismic reflection profile: Influences on the evolution of the Midland Valley of Scot. *Transactions of the Royal Society of Edinburgh-Earth Sciences* **75**, 97-109.

Halliday, A. N. (1984). Coupled Sm-Nd and U-Pb Systematics in Late Caledonian Granites and the Basement under Northern Britain. *Nature* **307**, 229-233.

Halliday, A. N., Stephens, W. E. & Harmon, R. S. (1980). Rb-Sr and O Isotopic Relationships in 3 Zoned Caledonian Granitic Plutons, Southern Uplands, Scotland - Evidence for Varied Sources and Hybridization of Magmas. *Journal of the Geological Society* **137**, 329-348.

Hamilton, P. J., Onions, R. K. & Pankhurst, R. J. (1980). Isotopic Evidence for the Provenance of Some Caledonian Granites. *Nature* **287**, 279-284.

Hanchar, J. M. & van Westrenen, W. (2007). Rare earth element behavior in zircon-melt systems. *Elements* **3**, 37-42.

Hanson, R. B. & Glazner, A. F. (1995). Thermal requirements for extensional emplacement of granitoids. *Geology* **23**, 213-216.

Harford, C. L., Pringle, M. S., Sparks, R. S. J. & Young, S. R. (2002). The volcanic evolution of Montserrat using 40Ar/39Ar geochronology In: Druitt, T. H. & Kokelaar, B. P. (eds.) *The Eruption of Soufriere Hills Volcano, Montserrat (1995 to 1999)*: Geological Socity, London Memoirs, 93-113.

Harmon, R. S. & Halliday, A. N. (1980). Oxygen and strontium isotope relationships in the British Caledonian granites *Nature* **283**, 21-25.

Harmon, R. S., Halliday, A. N., Clayburn, J. A. P. & Stephens, W. E. (1984). Chemical and isotopic systematics of the Caledonian intrusions of Scotland and Northern England - A guide to magma source regions and magma crust interaction. *Philosophical Transactions of the Royal Society of London Series a-Mathematical Physical and Engineering Sciences* **310**, 709-742.

Harris, N., Vance, D. & Ayres, M. (2000). From sediment to granite: timescales of anatexis in the upper crust. *Chemical Geology* **162**, 155-167.

Harrison, T. M., Watson, E. B. & Aikman, A. B. (2007). Temperature spectra of zircon crystallization in plutonic rocks. *Geology* **35**, 635-638.

Hawkesworth, C., Cawood, P., Kemp, T., Storey, C. & Dhuime, B. (2009). A Matter of Preservation. *Science* **323**, 49-50.

Hawkesworth, C. J., Dhuime, B., Pietranik, A. B., Cawood, P. A., Kemp, A. I. S. & Storey, C. D. (2010). The generation and evolution of the continental crust. *Journal of the Geological Society* **167**, 229-248.

Hawkesworth, C. J. & Kemp, A. I. S. (2006). Using hafnium and oxygen isotopes in zircons to unravel the record of crustal evolution. *Chemical Geology* **226**, 144-162.

Hayden, L. A. & Watson, E. B. (2007). Rutile saturation in hydrous siliceous melts and its bearing on Ti-thermometry of quartz and zircon. *Earth and Planetary Science Letters* **258**, 561-568.

Higgins, M. D. & Roberge, J. (2003). Crystal size distribution of plagioclase and amphibole from Soufrière Hills Volcano, Monserrat: evidence for dynamic crystallization–textural coarsening cycles. *Journal of Petrology* **44**, 1401-1411.

Highton, A. (1999). Late Silurian and Devonian granitic intrusions of Scotland. In: Stephenson, D., Bevins, RE, Millward, D, Highton, AJ, Parsons, I, Stone, P, Wadsworth, WJ (ed.) *Caledonian Igneous Rocks of Britain*, 397-404.

Hinton, R. W. & Long, J. V. P. (1979). High-resolution ion-microprobe measurement of lead isotopes: Variations within single zircons from Lac Seul, northwestern Ontario. *Earth and Planetary Science Letters* **45**, 309-325.

Hinton, R. W. & Upton, B. G. J. (1991). The chemistry of zircon: Variations within and between large crystals from syenite and alkali basalt xenoliths. *Geochimica Et Cosmochimica Acta* **55**, 3287-3302.

Holden, P., Halliday, A. N. & Stephens, W. E. (1987). Neodymium and Strontium Isotope Content of Microdiorite Enclaves Points to Mantle Input to Granitoid Production. *Nature* **330**, 53-56.

Holden, P., Halliday, A. N., Stephens, W. E. & Henney, P. J. (1991). Chemical and isotopic evidence for major mass transfer between mafic enclaves and felsic magma. *Chemical Geology* **92**, 135-152.

Holden, P. H., A. N. ; Stephens., W. E. ; Henny., P. J. . (1991). Chemical and isotopic evidence for major mass transfer between mafic enclaves and felsic magma. *Chemical Geology* **92**, 135-152.

Holloway, J. R. (2004). Redox reactions in seafloor basalts: possible insights into silicic hydrothermal systems. *Chemical Geology* **210**, 225-230.

Holmes, A. (1911). The association of lead with uranium in rock-minerals, and its application to the measuremnt of geologic time. *Proceedings of the Royal Society of London* **85A**, 248-256.

Holtz, F., Becker, A., Freise, M. & Johannes, W. (2001). The water-undersaturated and dry Qz-Ab-Or system revisited. Experimental results at very low water activities and geological implications. *Contributions to Mineralogy and Petrology* **141**, 347-357.

Holtz, F. & Johannes, W. (1994). Maximum and minimum water contents of granitic melts: Implications for chemical and physical properties of ascending magmas. *Lithos* **32**, 149-159.

Hopkins, M., Harrison, T. M. & Manning, C. E. (2008). Low heat flow inferred from > 4 Gyr zircons suggests Hadean plate boundary interactions. *Nature* **456**, 493-496.

Hoskin, P. W. O., Kinny, P. D., Wyborn, D. & Chappell, B. W. (2000). Identifying accessory mineral saturation during differentiation in granitoid magmas: an integrated approach. *Journal of Petrology* **41**, 1365-1396.

Hoskin, P. W. O. & Schaltegger, U. (2003). The composition of zircon and igneous and metamorphic petrogenesis. In: Hanchar, J. M. & Hoskin, P. W. O. (eds.) *Zircon*, 27-62.

Hughes, J. M., Ertl, A., Bernhardt, H. J., Rossman, G. R. & Rakovan, J. (2004). Mn-rich fluorapatite from Austria: Crystal structure, chemical analysis, and spectroscopic investigations. *American Mineralogist* **89**, 629-632.

Humayun, M., Qin, L. P. & Norman, M. D. (2004). Geochemical evidence for excess iron in the mantle beneath Hawaii. *Science* **306**, 91-94.

Humphreys, E., Hessler, E., Dueker, K., Farmer, C. L., Erslev, E. & Atwater, T. (2003). How Laramide-age hydration of North American lithosphere by the Farallon slab controlled subsequent activity in the western United States. *International Geology Review* **45**, 575-595.

Hurley, P. M. & Rand, J. R. (1969). Pre-drift continental nuclei. *Science* **164**, 1229-1242.

Hutton, D. H. W. & Reavy, R. J. (1992). Strike-slip tectonics and granite petrogenesis *Tectonics* **11**, 960-967.

Ireland, T., Williams IS,. (2003). Considerations in zircon geochronology by SIMS. In: Hanchar, J. M. H. P. W. O. (ed.) *Zircon*, 215-241.

Ishihara, S. (1977). The magnetite-series and ilmenite-series granitic rocks. *Mining Geology* **27**, 293-305.

Ishihara, S. (2004). The redox state of granitoids relative to tectonic setting and earth history: The magnetite-ilmenite series 30 years later. *Transactions of the Royal Society of Edinburgh-Earth Sciences* **95**, 23-33.

Jackson, M. D., Cheadle, M. J. & Atherton, M. P. (2003). Quantitative modeling of granitic melt generation and segregation in the continental crust. *Journal of Geophysical Research-Solid Earth* **108**.

Jacobsen, S. B. & Wasserburg, G. J. (1979). The mean age of mantle and crustal reservoirs. *Journal of Geophysical Research* **84**, 7411-7427.

Jahn, B. M., Wu, F. Y. & Chen, B. (2000). Granitoids of the Central Asian Orogenic Belt and continental growth in the Phanerozoic. *Transactions of the Royal Society of Edinburgh-Earth Sciences* **91**, 181-193.

Jain, J. C., Neal, C. R. & Hanchar, J. M. (2001). Problems associated with the determination of rare earth elements of a "Gem" quality zircon by inductively coupled plasma-mass spectrometry. *Geostandards Newsletter-the Journal of Geostandards and Geoanalysis* **25**, 229-237.

Janots, E., Brunet, F., Goffe, B., Poinssot, C., Burchard, M. & Cemic, L. (2007). Thermochemistry of monazite-(La) and dissakisite-(La): Implications for monazite and allanite stability in metapelites. *Contributions to Mineralogy and Petrology* **154**, 1-14.

Jennings, E. S., Marschall, H. R., Hawkesworth, C. J. & Storey, C. D. (2011).

Characterization of magma from inclusions in zircon: Apatite and biotite work well, feldspar less so. *Geology* **39**, 863-866.

John, B. E. W. J. (ed.) (1990). *Petrology and geochemistry of the metaluminous to peraluminous Chemehuevi Mountains Plutonic suite, northeastern California*: Geological Society of America, Memoir

Johnson, M. C. & Rutherford, M. J. (1989). Experimental calibration of the aluminum-in-hornblende geobarometer with application to Long Valley caldera (California) volcanic rocks *Geology* **17**, 837-841.

Joly, J. (1909). *Radioactivity and Geology*. London: Archibald Constable & Co.

Jull, M. & Kelemen, P. B. (2001). On the conditions for lower crustal convective instability. *Journal of Geophysical Research-Solid Earth* **106**, 6423-6446.

Kay, R. W. & Kay, S. M. (1993). Delamination and delamination magmatism. *Tectonophysics* **219**, 177-189.

Keay, S., Collins, W. J. & McCulloch, M. T. (1997). A three-component Sr-Nd isotopic mixing model for granitoid genesis, Lachlan fold belt, eastern Australia. *Geology* **25**, 307-310.

Kelley, S. & Bluck, B. J. (1989). Detrital mica ages from the Southern Uplands using Ar-Ar laser probe *Journal of the Geological Society, London* **146**, 401-403.

Kelley, K. A. & Cottrell, E. (2009). Water and the Oxidation State of Subduction Zone Magmas. *Science* **325**, 605-607.

Kelly, N. M., Hinton, R. W., Harley, S. L. & Appleby, S. K. (2008). New SIMS U-Pb zircon ages from the Langavat Belt, South Harris, NW Scotland: implications for the Lewisian terrane model. *Journal of the Geological Society* **165**, 967-981.

Kemp, A., Hawkesworth, CJ (ed.) (2003). *Granitic perspectives on the generation and secular evolution of the continental crust*. Oxford: Elsevier

Kemp, A. E. S. (1987). Tectonic Development of the Southern Belt of the Southern Uplands Accretionary Complex. *Journal of the Geological Society* **144**, 827-838.

Kemp, A. E. S. & Hawkesworth, C. J. (2003). Granitic perspectives on the generation and secular evolution of the continental crust. In: Rudnick, R. (ed.) *Treatise On Geochemistry*. Oxford: Elsevier, 349-410.

Kemp, A. I. S., Hawkesworth, C. J., Collins, W. J., Gray, C. M., Blevin, P. L. & Eimf. (2009). Isotopic evidence for rapid continental growth in an extensional accretionary orogen: The Tasmanides, eastern Australia. *Earth and Planetary Science Letters* **284**, 455-466.

Kemp, A. I. S., Hawkesworth, C. J., Foster, G. L., Paterson, B. A., Woodhead, J. D., Hergt, J. M., Gray, C. M. & Whitehouse, M. J. (2007). Magmatic and crustal differentiation history of granitic rocks from Hf-O isotopes in zircon. *Science* **315**, 980-983.

Kemp, A. I. S., Hawkesworth, C. J., Paterson, B. A., Foster, G. L., Kinny, P. D., Whitehouse, M. J., Maas, R. & Eimf. (2006a). Exploring the plutonic-volcanic link: a zircon U-Pb, Lu-Hf and O isotope study of paired volcanic and granitic units from southeastern Australia. *Transactions of the Royal Society of Edinburgh-Earth Sciences* **97**, 337-355.

Kemp, A. I. S., Hawkesworth, C. J., Paterson, B. A. & Kinny, P. D. (2006b). Episodic growth of the Gondwana supercontinent from hafnium and oxygen isotopes in zircon. *Nature* **439**, 580-583.

Kemp, A. I. S., Hawkesworth, C.J., Collins, W.J., Gray, C.M., Blevin, P.L., EIMF. (2009). Isotopic evidence for rapid continentalgrowth in an extensional accretionary orogen: The Tasmanides, eastern Australia. *Earth and Planetary Science Letters* **284**, 455-466.

Kemp, A. I. S., Wormald, R. J., Whitehouse, M. J. & Price, R. C. (2005). Hf isotopes in zircon reveal contrasting sources and crystallization histories for alkaline to peralkaline granites of Temora, southeastern Australia. *Geology* **33**, 797-800.

Kesler, S. E. & Wilkinson, B. H. (2006). The role of exhumation in the temporal distribution of ore deposits. *Economic Geology* **101**, 919-922.

Kinny, P. D. & Maas, R. (2003). Lu-Hf and Sm-Nd isotope systems in zircon. In: Hanchar, J. & Hoskin, P. W. O. (ed.) *Zircon*, 327-341.

Kirsch, M., Keppie, J. D., Murphy, B. J. & Solari, L. A. (2012). Permian–Carboniferous arc magmatism and basin evolution along the western margin of Pangea: Geochemical and geochronological evidence from the eastern Acatlán Complex, southern Mexico. *Geological Society of America Bulletin* **124**, 1607-1628.

Klemperer, S. L. & Matthews, D. H. (1987). Iapetus Suture Located beneath the North-Sea by Birps Deep Seismic-Reflection Profiling. *Geology* **15**, 195-198.

Klemperer, S. L., Ryan, P. D. & Snyder, D. B. (1991). A deep seismic-reflection transect across the Irish Caledonides *Journal of the Geological Society* **148**, 149-164.

Klimm, K., Blundy, J. D. & Green, T. H. (2008). Trace element partitioning and accessory phase saturation during H2O-saturated melting of basalt with implications for subduction zone chemical fluxes. *Journal of Petrology* **49**, 523-553.

Kneller, B. C. (1991). A Foreland Basin on the Southern Margin of Iapetus. *Journal of the Geological Society* **148**, 207-210.

Lackey, J. S., Valley, J. W. & Hinke, H. J. (2006a). Deciphering the source and contamination history of peraluminous magmas using $d^{18}O$ of accessory minerals: examples from garnet-bearing plutons of the Sierra Nevada batholith. *Contributions to Mineralogy and Petrology* **151**, 20-44.

Lackey, J. S., Valley, J. W. & Hinke, H. J. (2006b). Deciphering the source and contamination history of peraluminous magmas using delta(18)0 of accessory minerals: examples from garnet-bearing plutons of the Sierra Nevada batholith. *Contributions to Mineralogy and Petrology* **151**, 20-44.

Lackey, J. S., Valley, J. W. & Saleeby, J. B. (2005). Supracrustal input to magmas in the deep crust of Sierra Nevada batholith: Evidence from high-delta O-18 zircon. *Earth and Planetary Science Letters* **235**, 315-330.

Lapworth, C. (1876). On Scottish Monograptidæ. Geological Magazine :308, 350, 499, 544. *Geological Magazine* **3**, 308-321.

Lapworth, C. (1878). The Moffat Shale. *Quarterly Journal of the Geological Society of London* **34**, 240-346.

Lapworth, C. (1889). On the Ballantrae rocks of the south of Scotland and their place in the upland sequence. *Geological Magazine* **26**, 20-24; 59-69.

Larsen, E. S., Keevil, N. B. & Harrison, H. C. (1952). Method for for determining the age of igneous rocks using the accessory minerals. *Geological Society of America Bulletin* **63**, 1045-1052.

Laul, J. C., Wakita, H. & Showalter, D. L. (1972). Bulk, rare earth, and other trace elements in Apollo 14 and 15 and Luna 16 samples. *Proceedings of the Lunar Sciecne Conference* **3**, 1181-1200.

Lee, C.-T. A., Luffi, P., Le Roux, V., Dasgupta, R., Albarede, F. & Leeman, W. P. (2010). The redox state of arc mantle using Zn/Fe systematics. *Nature* **468**, 681-685.

Lee, M. R., Waldron, K. A. & Parsons, I. (1995). Exsolution and alteration microtextures in alkali feldspar phenocrysts from the Shap granite. *Mineralogical Magazine* **59**, 63-78.

Leggett, J. K., McKerrow, W. S. & Eales, M. H. (1979). The Southern Uplands of Scotland: a Lower Palaeozoic accretionary prism. *Journal of the Geological Society, London* **136**, 755-770.

Leggett, J. K., McKerrow, W. S. & Soper, N. J. (1983). A model for the crustal evolution of Southern Scotland *Tectonics* **2**, 187-210.

Lintern, B. C., Barnes, R. P. & Stone, P. (1992). Discussion on the Silurian and Early Devonian sinistral deformation of the Ratagain Granite, Scotland: constraints on the age of Caledonian movements on the Great Glen system. *Journal of the Geological Society* **149**, 858-858.

Lipman, P. W. (2007). Incremental assembly and prolonged consolidation of Cordilleran magma chambers: Evidence from the Southern Rocky Mountain volcanic field. *Geosphere* **3**, 42-70.

London, D. (1992). Phosphorus in S-type magmas: the P_2O_5 content of feldspars from peraluminous granites, pegmatites, and rhyolites. *American Mineralogist* **77**, 126-145.

London, D., Evensen, J.M, Fritz, E., Icehower, J.P., Morgan, G.B. VI., Wolf, M.B. (2001). Enrichemnt and accommodation of manganese in granite-pegmatite systems. *11th Annual Goldschmidt Conference Abstract 3369*.

Lowe, D. R. & Tice, M. M. (2004). Geologic evidence for Archean atmospheric and climatic evolution: Fluctuating levels of CO_2, CH_4, and O_2 with an overriding tectonic control *Geology* **32**, 493-496.

Ludwig, K. R. (2003). Isoplot 3.00. *Berkeley Geochronology Center Special Publication* **4**.

Maas, R., Kinny, P. D., Williams, I. S., D.O, F. & W, C. (1992). The Earth's oldest known crust—A geochronological and geochemical study of 3900–4200 Ma old detrital zircons from Mt. Narryer and Jack Hills. *Geochimica Et Cosmochimica Acta* **56**, 1281-1300.

Maclennan, J. (2008). Lead isotope variability in olivine-hosted melt inclusions from Iceland. *Geochimica et Cosmochimica Acta* **72**, 4159-4176.

Mahood, G. & Hildreth, W. (1983). An experimental study of the partitioning of copper between pyrrhotite and a high-silica rhyolitic melt. *Geochimica Et Cosmochimica Acta* **47**, 11-30.

Mallmann, G. & O'Neill, H. S. C. (2009). The Crystal/Melt Partitioning of V during Mantle Melting as a Function of Oxygen Fugacity Compared with some other Elements (Al, P, Ca, Sc, Ti, Cr, Fe, Ga, Y, Zr and Nb). *Journal of Petrology* **50**, 1765-1794.

Mange, M. A., Dewey, J. F. & Floyd, J. D. (2005). The origin, evolution and provenance of the Northern Belt (Ordovician) of the Southern Uplands terrane, Scotland: A heavy mineral perspective. *Proceedings of the Geologists' Association* **116**, 251-280.

Marschall, H. R., Hawkesworth, C. J., Storey, C. D., Dhuime, B., Leat, P. T., Meyer, H.-P. & Tamm-Buckle, S. (2010). The Annandagstoppane Granite, East Antarctica: Evidence for Archaean Intracrustal Recycling in the Kaapvaal-Grunehogna Craton from Zircon O and Hf Isotopes. *Journal of Petrology* **51**, 2277-2301.

Martel, C., Pichavant, M., Holtz, F., Scaillet, B., Bourdier, J.-L. & Traineau, H. (1999). Effects of fO_2 and H_2O on andesite phase relations between 2 and 4 kbar. *Jornal of Geophysical Research* **104**, 29453-29470.

Matzel, J. E. P., Bowring, S. A. & Miller, R. B. (2006). Time scales of pluton construction at differing crustal levels: Examples from the Mount Stuart and Tenpeak intrusions, North Cascades, Washington. *Geological Society of America Bulletin* **118**, 1412-1430.

McKerrow, W. S., Leggett, J. K. & Eales, M. H. (1977). Imbricate thrust model of the Southern Uplands of Scotland. *Nature* **267**, 237-239.

McCubbin, F. M., Steele, A., Nekvasil, H., Schnieders, A., Rose, T., Fries, M., Carpenter, P. K. & Jolliff, B. L. (2010). Detection of structurally bound hydroxyl in fluorapatite from Apollo Mare basalt 15058,128 using TOF-SIMS. *American Mineralogist* **95**, 1141-1150.

McCulloch, M. T. & Chappell, B. W. (1982). Nd isotopic characteristics of S-type and I-type granites *Earth and Planetary Science Letters* **58**, 51-64.

McDonough, W. F. & Sun, S. S. (1995). The compositions of the Earth. *Chemical Geology* **120**, 223-253.

McKenzie, D. (1984). The Generation and Compaction of Partially Molten Rock. *Journal of Petrology* **25**, 713-765.

Miller, C., Wooden JF, Bennett VC, Wright JE, Solomon GC, Hurst & RW (eds.) (1990). *Petrogenesis of the composite peraluminousmetaluminous Old Woman-Piute Range batholith, southeastern California; isotopic constraint*. Boulder: Memoir of the Geological Society of America

Miller, C. F., McDowell, S. M. & Mapes, R. W. (2003). Hot and cold granites? Implications of zircon saturation temperatures and preservation of inheritance. *Geology* **31**, 529-532.

Miller, C. F., Rapp, R. P. & Watson, E. B. (1986). AFM mineral-felsic liquid phase relations: Potential for elucidation of the origin and evolution of felsic magmas. *Geological Society of America Abstracts with Programs* **18**, 695.

Miller, C. F., Wooden J.F, Bennett VC, Wright JE, Solomon GC & R.W., H. (eds.) (1990). *Petrogenesis of the composite peraluminousmetaluminous Old Woman-Piute Range batholith, southeastern California; isotopic constraint*. Boulder: Memoir of the Geological Society of America

Miller, J. S. (2008). Assembling a pluton... one increment at a time. *Geology* **36**, 511-512.

Montel, J. M. (1986). Experimental determination of the solubility of Ce-monazite in SiO_2-Al2O_3-K_2O-Na_2O melts at 800 °C, 2 kbar, under H2O-saturated conditions *Geology* **14**, 659-662.

Moore, G. & Carmichael, I. S. E. (1998). The hydrous phase equilibria (to 3 kbar) of an andesite and basaltic andesite from western Mexico: constraints on water content and conditions of phenocryst growth. *Contributions to Mineralogy and Petrology* **130**, 304-319.

Morris, J. H. (1987). The Northern Belt of the Longford–Down Inlier, Ireland and Southern Uplands: an Ordovician back-arc basin. *Journal of the Geological Society* **144**, 773-786.

Morton, A. & Yaxley, G. (2007). Detrital apatite geochemistry and its application in provenance studies. *GSA Special Paper* **420**, 319-344.

Muntener, O., Kelemen, P. B. & Grove, T. L. (2001). The role of H_2O during crystallization of primitive arc magmas under uppermost mantle conditions and genesis of igneous pyroxenites: an experimental study. *Contributions to Mineralogy and Petrology* **141**, 643-658.

Murphy, J. B., Strachan, R. A., Nance, R. D., Parker, K. D. & Fowler, M. B. (2000). Prota-Avalonia: A 1.2-1.0 Ga tectonothermal event and constraints for the evolution of Rodinia. *Geology* **28**, 1071-1074.

Nagasawa, H. (1970). Rare earth concentrations in zircon and their host dacites and granites. *Earth and Planetary Science Letters* **9**, 359-364.

Nance, R. D., Murphy, J. B., Strachan, R. A., Duncan Keppie, J., Gutierrez-Alonso, G., Fernandez-Suarez, J., Quesada, C., Linnemann, U., D'Lemos, R. & Pisarevsky, S. A. (2008). Neoproterozoic-early Palaeozoic tectonostratigraphy and palaeogeography of the peri-Gondwanan terranes: Amazonian v. West African connections. In: Ennih, N. L. J. P. (ed.) *Boundaries of the West African Craton*, 345-383.

Nance, R. D., Murphy, J.B. (1996). 1996. Basement isotopicsignatures and Neoproterozoic paleogeography of Avalonian–Cadomian and related terranes in the circum-North Atlantic. In: Nance, R. D., Thompson, M.A (ed.) *Avalonian and Related Peri-Gondwanan Terranes of the Circum-North Atlantic*: Geological Society of America, Special Papers, 333-346.

Nash, W. P. (1984). *Phosphate minerals in terrestrial igneous and metamorphic rocks*. Berlin: Spinger-Verlag.

Neilson, J. C., Kokelaar, B. P. & Crowley, Q. G. (2009). Timing, relations and cause of plutonic and volcanic activity of the Siluro-Devonian post-collision magmatic episode in the Grampian Terrane, Scotland. *Journal of the Geological Society* **166**, 545-561.

Norrish, K. & Hutton, J. T. (1969). An accurate X-ray spectrographic method for the analysis of a wide range of geological samples. *Geochimica et Cosmochimica Acta* **33**, 431-453.

Nutman, A. P. & Hiess, J. (2009). A granitic inclusion suite within igneous zircons from a 3.81 Ga tonalite (W. Greenland): Restrictions for Hadean crustal evolution studies using detrital zircons. *Chemical Geology* **261**, 76-81.

O'Nions, R. K., Evensen, N. M. & Hamilton, P. J. (1979). Geochemical modeling of mantle differentiation and crustal growth. *Journal of Geophysical Research* **84**, 6091-6101.

O'Nions, R. K., Evensen, N. M. & Hamilton, P. J. (1980). Differentiation and evolution of the mantle. *Philosophical Transactions of the Royal Society of London* **297**, 479-493.

O'Nions, R. K., Hamilton, P. J. & Hooker, P. J. (1983a). A Nd Isotope Investigation of Sediments Related to Crustal Development in the British-Isles. *Earth and Planetary Science Letters* **63**, 229-240.

O'Nions, R. K., Hamilton, P. J. & Hooker, P. J. (1983b). A Nd isotope investigation of sediments related to crustal development in the British Isles. *Earth and Planetary Science Letters* **63**, 229-240.

O'Reilly, B. M., Hauser, F. & Readman, P. W. (2012). The fine-scale seismic structure of the upper lithosphere within accreted Caledonian lithosphere: implications for the origins of the 'Newer Granites'. *Journal of the Geological Society* **169**, 561-573.

Oliver, G. J. H., Wilde, S. A. & Wan, Y. S. (2008). Geochronology and geodynamics of Scottish granitoids from the late Neoproterozoic break-up of Rodinia to Palaeozoic collision. *Journal of the Geological Society* **165**, 661-674.

Pan, Y. M. & Fleet, M. E. (2002). Compoistions of the Apatite-Group Minerals: Substitution Mechamisms and Controlling Factors. In: Kohn, M. J., Rakovan, J, and Hughes, J.M. (ed.) *Phosphates: Geochemical, Geobiological, and Materials Importance*: Mineralogical Society of America, 13-49.

Parrish, R., Noble, SR. (2003). Zircon U-Pb geochronology by isotope dilution - thermal ionisation mass spectrometry (ID-TIMS) In: Hanchar, J. M. H. P. W. O. (ed.) *Zircon*, 183-213.

Parslow, G. R. (1968). The physical and structural features of the Cairnsmore of Fleet granite and its aureole. *Scottish Journal of Geology* **9**, 91-108.

Parslow, G. R. a. R., B. A. O. (1973). A gravity survey of the Cairnsmore of Fleet and its environs. *Scottish Journal of Geology* **9**, 219-231.

Patchett, S. R., Kouvo, O., Hedge, C. E. & Tatsumo, M. (1981). Evolution of continental crust and mantle heterogeneity evidence from Hf isotopes. *Contributions to Mineralogy and Petrology* **79**, 279-297.

Paterson, S. R. & Fowler, T. K. (1993a). Extensional pluton-emplacement models: Do they work for large plutonic complexes? *Geology* **21**, 781-784.

Paterson, S. R. & Fowler, T. K. (1993b). Re-examining pluton emplacement process. *Journal of Structural Geology* **15**, 191-206.

Paterson, S. R., Fowler, T. K. & Miller, R. B. (1996). Pluton emplacement in arcs: A crustal-scale exchange process. *Transactions of the Royal Society of Edinburgh-Earth Sciences* **87**, 115-123.

Patiño Douce, A. E. & Beard, J. S. (1995). Dehydration-melting of Biotite Gneiss and Quartz Amphibolite from 3 to 15 kbar. *Journal of Petrology* **36**, 707-738.

Patiño Douce, A. E. & Harris, N. (1998). Experimental constraints on Himalayan anatexis. *Journal of Petrology* **39**.

Peach, B. N. & Horne, J. (1899). The Silurian Rocks of Britain, Volume 1. Scotland. *Memoir of the Geological Survey of the United Kingdom*.

Pearce, N. J. G., Perkins, W. T., Westgate, J. A., Gorton, M. P., Jackson, S. E., Neal, C. R. & Chenery, S. P. (1997). A compilation of new and published major and trace element data for NIS T SRM 6 10 and NIST SRM 6 12 glass reference material. *The Journal of Geostandards and Geoanalysis* **21**, 115-144.

Peck, W. H., Valley, J. W. & Graham, C. M. (2003). Slow oxygen diffusion rates in igneous zircons from metamorphic rocks. *American Mineralogist* **88**, 1003-1014.

Peck, W. H., Valley, J. W., Wilde, S. A. & Graham, C. M. (2001). Oxygen isotope ratios and rare earth elements in 3.3 to 4.4 Ga zircons: Ion microprobe evidence for high delta O-18 continental crust and oceans in the Early Archean. *Geochimica Et Cosmochimica Acta* **65**, 4215-4229.

Petford, N. (2003). Rheology of granitic magmas during ascent and emplacement. *Annual Review of Earth and Planetary Sciences* **31**, 399-427.

Petford, N., Kerr, R. C. & Lister, J. R. (1993). Dike transport of granitoid magmas. *Geology* **21**, 845-848.

Phillips, E. R., Barnes, R. P., Boland, M. P., Fortey, N. J. & McMillan, A. A. (1995). The Moniaive Shear Zone: a major zone of sinistral strike-slip deformation in the Southern Uplands of Scotland. *Scottish Journal of Geology* **31**, 139-149.

Phillips, E. R., Evans, J. A., Stone, P., Horstwood, M. S. A., Floyd, J. D., Smith, R. A., Akhurst, M. C. & Barron, H. F. (2003). Detrital Avalonian zircons in the Laurentian Southern Uplands terrane, Scotland. *Geology* **31**, 625-628.

Phillips, W. J. (1956). The Criffel-Dalbeattie granodiorite complex. *Jounral of the Geological Society of London* **112**, 221-240.

Piccoli, P. & Candela, P. (1994). Apatite in felsic rocks: a model for the estimation of initial halogen concentrations in the Bishop Tuff (Long Valley) and Tuolumne Intrusive Suite (Sierra Nevada Batholith) magmas. *American Journal of Science* **294**, 92-135.

Pidgeon, R. T. & Aftalion, M. (1978). Cogenetic and inherited zircon U-Pb systems in granites: Palaeozoic granites of Scotland and England, in Bowes, D.R., Leake,

B.E., Crustal evolution in northwestern Britain and adjacent regeions. *Geological Journal Special Issue*, 183-220.

Pietranik, A., Storey, C., Dhuime, B., Tyszka, R. & Whitehouse, M. (2011). Decoding whole rock, plagioclase, zircon and apatite isotopic and geochemical signatures from variably contaminated dioritic magmas. *Lithos* **127**, 455-467.

Pietranik, A. B., Hawkesworth, C. J., Storey, C. D., Kemp, A. I. S., Sircombe, K. N., Whitehouse, M. J. & Bleeker, W. (2008). Episodic, mafic crust formation from 4.5 to 2.8 Ga: New evidence from detrital zircons, Slave craton, Canada. *Geology* **36**, 875-878.

Pinto, V. M. & Hartmann, L. A. (2011). Flow-by-flow chemical stratigraphy and evolution of thirteen Serra Geral Group basalt flows from Vista Alegre, southernmost Brazil. *Anais Da Academia Brasileira De Ciencias* **83**, 425-440.

Pitcher, W. S. & Berger, A. R. (1972). *The geology of Donegal : a study of granite emplacment and unroofing* New York: Wiley-Interscience

Prouteau, G. & Scaillet, B. (2003). Experimental constraints on the origin of the 1991 Pinatubo dacite. *Journal of Petrology* **44**, 2203-2241.

Prowatke, S. & Klemme, S. (2006). Trace element partitioning between apatite and silicate melts. *Geochimica Et Cosmochimica Acta* **70**, 4513-4527.

Qin, L. & Humayun, M. (2008). The Fe/Mn ratio in MORB and OIB determined by ICP-MS. *Geochimica Et Cosmochimica Acta* **72**, 1660-1677.

Read, H. (1961). Aspects of the Caledonian magmatism in Scotland. *Proceedings of the Liverpool and Manchester Geological Society* **2**, 653-683.

Repcheck, J. (2003). *The Man Who Found Time: James Hutton And The Discovery Of Earth's Antiquity*. London: Simon & Schuster.

Reubi, O. & Blundy, J. (2009). A dearth of intermediate melts at subduction zone volcanoes and the petrogenesis of arc andesites. *Nature* **461**, 1269-1273.

Reymer, A. & Schubert, G. (1984). Phanerozoic addition rates to the continental crust and crustal growth. *Tectonics* **3**, 63-77.

Reynolds, R. C. (1963). Matrix corrections in trace element analysis by X-ray fluorescence: estimation of the mass absorption coefficient by Compton scattering. *American Mineralogist* **48**, 1133-1143.

Riley, J. P. (1958). The rapid analysis of silicate rocks and minerals. *Analytica Chimica Acta* **19**, 413-428.

Rino, S., Komiya, T., Windley, B. F., Katayama, I., Motoki, A. & Hirata, T. (2004). Major episodic increases of continental crustal growth determined from zircon ages of river sands; implications for mantle overturns in the Early Precambrian. *Physics of the Earth and Planetary Interiors* **146**, 369-394.

Rino, S., Kon, Y., Sato, W., Maruyama, S., Santosh, M. & Zhao, D. (2008). The Grenvillian and Pan-African orogens: World's largest orogenies through geologic time, and their implications on the origin of superplume. *Gondwana Research* **14**, 51-72.

Roberts, N. (2012). Increased loss of continental crust during supercontinent amalgamation. *Gondwana Research* **21**.

Robock, A. (2000). Volcanic eruptions and climate. *Reviews of Geophysics* **38**, 191-219.

Rock, N. M. S., Gaskarth, J. W. & Rundle, C. C. (1986). Late Caledonian Dyke-Swarms in Southern Scotland - a Regional Zone of Primitive K-Rich Lamprophyres and Associated Vents. *Journal of Geology* **94**, 505-522.

Rudnick, R. L. (1995). Making Continental-Crust. *Nature* **378**, 571-578.

Rudnick, R. L. & Gao, S. (2003). *Composition of the continental crust*. Amsterdam: Elsevier.

Rundle, C. C. (1992). Review and assessment of isotopic ages from the English Lake District. *British Geological Survey Technical Report* No. WA/92/38.

Rutherford, M. J. & Devine, J. D. (2003). Magmatic conditions and magma ascent as indicated by hornblende phase equilibria and reactions in the 1995-2002 Soufriere Hills magma. *Journal of Petrology* **44**, 1433-1454.

Ruzicka, A., Snyder, G. A. & Taylor, L. A. (2001). Comparative geochemistry of basalts from the Moon, Earth, HED asteroid, and Mars: Implications for the origin of the Moon. *Geochimica Et Cosmochimica Acta* **65**, 979-997.

Sano, Y., Terada, K. & Fukuoka, T. (2002). High mass resolution ion microprobe analysis of rare earth elements in silicate glass, apatite and zircon: lack of matrix dependency. *Chemical Geology* **184**, 217-230.

Sawka, W. N. (1988). REE and trace element variations in accessory minerals and hornblende from the strongly zoned McMurray Meadows Pluton, Califirnia. *Transactions of the Royal Society of Edinburgh-Earth Sciences* **79**, 157-168.

Scaillet, B., Clemente, B., Evans, B. W. & Pichavant, M. (1998). Redox control of sulfur degassing in silicic magmas. *Journal of Geophysical Research-Solid Earth* **103**, 23937-23949.

Scaillet, B. & Evans, B. W. (1999). The 15 June 1991 eruption of Mount Pinatubo. I. Phase equilibria and pre-eruption P-T-fO_2-fH_2O conditions of the dacite magma. *Journal of Petrology* **40**, 381-411.

Scaillet, B. & Gaillard, F. (2011). Redox state of early magmas. *Nature* **480**, 48-49.

Scaillet, B. & MacDonald, R. (2001). Phase relations of peralkaline silicic magmas and petrogenetic implications. *Journal of Petrology* **42**, 825-845.

Scherer, E., Munker, C. & Mezger, K. (2001). Calibration of the lutetium-hafnium clock. *Science* **293**, 683-687.

Schnetzler, C. C. & Philpott, J. A. (1970). Partition coefficients of rare-earth elements between igneous matrix material and rock-forming mineral phenocrysts 2. *Geochimica Et Cosmochimica Acta* **34**, 331-340.

Scholl, D. W. & von Huene, R. (2007). Crustal recycling at modern subduction zones applied to the past-Issues of growth and preservation of continental basement crust, mantle geochemistry, and supercontinent reconstruction. In: Hatcher, R. D., Carlson, M. P., McBride, J. H. & Catalan, J. R. M. (eds.) *4-D Framework of Continental Crust*, 9-32.

Scholl, D. W. & Von Huene, R. (2009). Implications of estimated magmatic additions and recycling losses at the subduction zones of accretionary (non-collisional) and collisional (suturing) orogens In: Cawood, P. & Kroner, A. (eds.) *Earth Accretionary Systems in Space and Time*. London: Geological Society of London, Special Publications, 105-125.

Segal, I., Halicz, L. & Platzner, I.T. (2003). Accurate isotope ratio measurements of ytterbium by multi-collector inductively coupled plasma mass spectrometry applying

erbium and hafnium in an improved double external normalisation procedure. *Journal of Analytical Atomic Spectrometry* **18**.

Sha, L. K. & Chappell, B. W. (1999). Apatite chemical composition, determined by electron microprobe and laser-ablation inductively coupled plasma mass spectrometry, as a probe into granite petrogenesis. *Geochimica Et Cosmochimica Acta* **63**, 3861-3881.

Shannon, W. M., Barnes, C. G. & Bickford, M. E. (1997). Grenville magmatism in west Texas: Petrology and geochemistry of the Red Bluff granitic suite. *Journal of Petrology* **38**, 1279-1305.

Shaw, S. E. & Flood, R. H. (2009). Zircon Hf Isotopic Evidence for Mixing of Crustal and Silicic Mantle-derived Magmas in a Zoned Granite Pluton, Eastern Australia. *Journal of Petrology* **50**, 147-168.

Shirey, S. B. & Richardson, S. H. (2011). Start of the Wilson Cycle at 3 Ga Shown by Diamonds from Subcontinental Mantle. *Science* **333**, 434-436.

Shnukov, S. E., Cheburkin, A. K. & Andreev, A. V. (1989). Geochemistry of wide-spread coexisting accessory minerals and their role in investigation of endogenic and exogenic processes. *Geological Journal* **2**, 107-114.

Sinton, J. M. & Detrick, R. S. (1992). Mid-ocean ridge magma chambers. *Journal of Geophysical Research-Solid Earth* **97**, 197-216.

Sisson, T. W. (1994). Hornblende-Melt Trace-Element Partitioning Measured by Ion Microprobe. *Chemical Geology* **117**, 331-344.

Soper, N. J. (1986). The Newer Granite Problem - a Geotectonic View. *Geological Magazine* **123**, 227-236.

Soper, N. J. (1987). The Ordovician Batholith of the English Lake District. *Geological Magazine* **124**, 481-482.

Soper, N. J. & Kneller, B. C. (1990). Cleaved microgranite dykes of the Shap swarm in the Silurian of NW England. *Geological Journal* **25**, 161-170.

Soper, N. J., Strachan, R. A., Holdsworth, R. E., Gayer, R. A. & Greiling, R. O. (1992). Sinistral transpression and the Silurian closure of Iapetus *Journal of the Geological Society* **149**, 871-880.

Soper, N. J. & Woodcock, N. H. (2003). The lost Lower Old Red Sandstone of England and Wales: a record of post-Iapetan flexure or Early Devonian transtension? *Geological Magazine* **140**, 627-647.

Stephens, W. E. (1988). Granitoid plutonism in the Caledonian orogen of Europe. In: Harris, A., Fettes, DJ (ed.) *The Caledonian-Appalachian Orogen*: Geological Society of London, Special Publication, 389-403.

Stephens, W. E. (1992). Spatial, Compositional and Rheological Constraints on the Origin of Zoning in the Criffell Pluton, Scotland. *Transactions of the Royal Society of Edinburgh-Earth Sciences* **83**, 191-199.

Stephens, W. E. (1999). Late Silurian and Devonian granitic intrusions of Scotland. In: Stephenson, D., Bevins, RE, Millward, D, Highton, AJ, Parsons, I, Stone, P, Wadsworth, WJ (ed.) *Caledonian Igneous Rocks of Britain*, 456-460.

Stephens, W. E. & Halliday, A. N. (1980a). Discontinuities in the composition surface of a zoned pluton, Criffel, Scotland. *Geological Society of America Bulletin* **91**, 165-170.

Stephens, W. E. & Halliday, A. N. (1980b). Discontinuities in the Composition Surface of a Zoned Pluton, Criffell, Scotland. *Geological Society of America Bulletin* **91**, 165-170.

Stephens, W. E. & Halliday, A. N. (1984). Geochemical contrasts between late Caledonian granitoid plutons of northern, central and southern Scotland. *Transactions of the Royal Society of Edinburgh-Earth Sciences* **75**, 259-273.

Stephens, W. E., Whitley, J. E., Thirwall, M. F. & Halliday, A. N. (1985). The Criffell zoned pluton: correlated behaviour of rare earth element abundances with isotopic systems. *Contributions to Mineralogy and Petrology* **89**, 226-238.

Stephens, W. E., Whitley, J. E., Thirwall, M.F. and Halliday, A. N. (1985). The Criffell zoned pluton: correlated behaviour of rare earth element abundances with isotopic systems. *Contributions to Mineralogy and Petrology* **89**, 226-238.

Stephenson, D. B. (1999). *Caledonian Igneous Rocks of Great Britain*: Joint Nature Conservation Committee.

Stone, P. (1999). Shoulder O' Craig. In: Stephenson, D., Bevins, R E, Millward, D, Highton, A J, Parsons, I, Stone P, and Wadsworth, W J. GCR Series (ed.) *Caledonian igneous rocks*, 556-559.

Stone, P. & Evans, J. A. (1995). Nd isotope study of provenance patterns across the British sector of the Iapetus suture. *Geological Magazine* **132**, 571-580.

Stone, P., Floyd, J. D., Barnes, R. P. & Lintern, B. C. (1987). A sequential back-arc and foreland basin thrust duplex model for the Southern Uplands of Scotland. *Journal of the Geological Society* **144**, 753-764.

Stone, P. & Evans, J. A. (1997). A comparison of the Skiddaw and Manx groups (English Lake District and Isle of Man) using neodymium isotopes. *Proceedings of the Yorkshire Geological Society* **51**, 343-347.

Taylor, S. R. & McLennan, S. M. (1985). *The Continental Crust: Its Composition and Evolution*. Oxford: Blackwells.

Taylor, S. R. & McLennan, S. M. (1991). Sedimentary Rocks and Crustal Evolution: Tectonic Setting and Secular Trends. *Journal of Geology* **99**, 1-21.

Taylor, S. R. & McLennan, S. M. (1995). The geochemical evolution of the continental crust. *Reviews of Geophysics* **33**, 241-265.

Teyssier, C., Tikoff, B. & Markley, M. (1995). Oblique plate motions and continental tectonics *Geology* **23**, 447-450.

Thirlwall, M. F. (1981). Implications for Caledonian Plate Tectonic Models of Chemical-Data from Volcanic-Rocks of the British Old Red Sandstone. *Journal of the Geological Society* **138**, 123-138.

Thirlwall, M. F. (1982). Systematic variations in chemistry and Nd and Sr isotopes across a Caledonian calc-alkaline volcanic arc - implications for source materials *Earth and Planetary Science Letters* **58**, 27-50.

Thirlwall, M. F. (1983). Isotope geochemistry and origin of calc alkaline lavas from a Caledonian continental margin volcanic arc *Journal of Volcanology and Geothermal Research* **18**, 589-631.

Thirlwall, M. F. (1986). Lead isotope evidecne for the nature of the mantle beneath Caledonian Scotland *Earth and Planetary Science Letters* **80**, 55-70.

Thirlwall, M. F. (1989a). Movement on proposed terane boundaries in northern Britain: constrains from Ordovician-Devonian igneous rocks *Journal of the Geological Society, London* **146**, 373-376.

Thirlwall, M. F. (1989b). Movement on proposed terrane boundaries in northern Britain: constraints from Ordovician-Devonian igneous rocks *Journal of the Geological Society, London* **146**, 373-376.

Thomas, J. B., Bodnar, R. J., Shimizu, N. & Sinha, A. K. (2002). Determination of zircon/melt trace element partition coefficients from SIMS analysis of melt inclusions in zircon. *Geochimica Et Cosmochimica Acta* **66**, 2887-2901.

Thomas, L. J., Harmon, R.S., Oliver, G.J.H. (1985). Stable isotope composition of alteration fluids in low-grade Lower Palaeozoic Rocks, English Lake District. *Mineralogical Magazine* **49**.

Thorogood, E. J. (1990). Provenance of the pre-Devonian sediments of England and Wales: Sm-Nd isotopic evidence. *Journal of the Geological Society* **147**, 591-594.

Tiepolo, M., Oberti, R. & R, V. (2002). Trace-element incorporation in titanite: constraints from experimentally determined solid/liquid partition coefficients. *Chemical Geology* **191**, 105-119.

Tikoff, B. & Teyssier, C. (1992). Crustal-scale, en echelon "P-shear" tensional bridges: A possible solution to the batholithic room problem. *Geology* **20**, 927-930.

Toghill, P. (1970). The south-east limit of the Moffat Shales in the upper Ettrick Valley region, Selkirkshire. *Scottish Journal of Geology* **6**, 233-242.

Trail, D., Watson, E. B. & Tailby, N. D. (2011). The oxidation state of Hadean magmas and implications for early Earth's atmosphere. *Nature* **480**, 79-82.

Tuttle, O., F. & Bowen, N. L. (1958). Origin of granite in the light of experimental studies in the system $NaAlSi_3O_8$-$KAlSi_3O_8$-SiO_2-H_2O. *Geological Scoiety and America Memoir* **74**, 153.

Tuttle, O. F. a. B., N.L. (1958). Origin of granite in the light of experimental studies in the system $NaAlSi_3O_8$-$KAlSi_3O_8$-SiO_2-H_2O. *The Geological Society of America Memoir* **74**.

Ulmer, P. (2007). Differentiation of mantle-derived calc-alkaline magmas at mid to lower crustal levels: experimental and petrologic constraints. *Periodico di Mineralogia* **76**, 309-325.

Valley, J. W., Chiarenzelli, J. R. & McLelland, J. M. (1994). Oxygen-Isotope Geochemistry of Zircon. *Earth and Planetary Science Letters* **126**, 187-206.

Valley, J. W., Graham, C. M., Harte, B., Eiler, J. M. & Kinny, P. D. (1998a). *Ion microprobe analysis of oxygen, carbon and hydrogen isotope ratios*: *Reviews in Economic* Geology, **7**, 73-98.

Valley, J. W., Kinny, P. D., Schulze, D. J. & Spicuzza, M. J. (1998b). Zircon megacrysts from kimberlite: oxygen isotope variability among mantle melts. *Contributions to Mineralogy and Petrology* **133**, 1-11.

Valley, J. W., Lackey, J. S., Cavosie, A. J., Clechenko, C. C., Spicuzza, M. J., Basei, M. A. S., Bindeman, I. N., Ferreira, V. P., Sial, A. N., King, E. M., Peck, W. H., Sinha, A. K. & Wei, C. S. (2005). 4.4 billion years of crustal maturation: oxygen isotope ratios of magmatic zircon. *Contributions to Mineralogy and Petrology* **150**, 561-580.

Van Saal, C. R., Dewey, J. F., MacNicaill, C. & McKerrow, W. S. (1998). The Cambrian-Silurian tectonic evolution of the northern Appalachians and British Caledonides. In: Blundell, D. J., and Scott, A.C. (ed.) *The Past Is the Key to the Present*: Geological Society of London Special Publications, 199-242.

Veizer, J. & Compston, W. (1976). $^{87}Sr/^{86}Sr$ in Precambrian carbonates as an index of crustal evolution. *Geochimica et Cosmochimica Acta* **40**, 905-914.

Vervoort, J. D., Patchett, P. J., Blichert-Toft, J. & Albarede, F. (1999). Relationships between Lu-Hf and Sm-Nd isotopic systems in the global sedimentary system. *Earth and Planetary Science Letters* **168**, 79-99.

Vervoort, J. D., Patchett, P.J., Söderlund, U. & Baker, M. (2004). The isotopic composition of Yb and the precise and accurate determination of Lu concentrations and Lu/Hf ratios by isotope dilution using MC-ICPMS. *Geochemistry, Geophysics, Geosystems*.

Wadge, A. J., Gale, N. H., Beckinsale, R. D. & Rundle, C. C. (1978). A Rb-Sr isochron age for the Shap Granite. *Proceedings of the Yorkshire Geological Society* **42**, 297-305.

Waldron, J. W. F., Floyd, J. D., Simonetti, A. & Heaman, L. M. (2008). Ancient Laurentian detrital zircon in the closing lapetus Ocean, Southern Uplands terrane, Scotland. *Geology* **36**, 527-530.

Wark, D. A. & Miller, C. F. (1993). Accessory mineral behaviour during differentiation of a granite suite: monazite, xenotime and zircon in the Sweetwater Wash pluton, southeastern California, U.S.A. *Chemical Geology* **110**, 49-67.

Waters, J. W. (1909). Radioactive minerals in common rocks. *Philosphical Magazine* **18**, 677-679.

Waters, J. W. (1910). Radioactive minerals in common rocks. *Philosphical Magazine* **19**, 903-904.

Watson, E. B. & Harrison, T. M. (1983a). Zircon Saturation Revisited - Temperature and Composition Effects in a Variety of Crustal Magma Types. *Earth and Planetary Science Letters* **64**, 295-304.

Watson, E. B. & Harrison, T. M. (1983b). Zircon saturation revisited: Temperature and composition effects in a variety of crustal magma types. *Earth and Planetary Science Letters* **64**, 295-304.

Weinberg, R. F., Sial, A. & Mariano, G. (2004). Close spatial relationship between plutons and shear zones. *Geology* **32**, 377-380.

White, D. E., Barron, H. F., Barnes, R. P. & Lintern, B. C. (1992). Biostratigraphy of late Llandovery (Telychian) and Wenlock turbidite sequence in the SW Southern Uplands, Scotland. *Transactions of the Royal Society of Edinburgh: Earth Sciences* **82**, 297-322.

Wiebe, R. A. & Collins, W. J. (1998). Depositional features and stratigraphic sections in granitic plutons: implications for the emplacement and crystallization of granitic magma. *Journal of Structural Geology* **20**, 1273-1289.

Wiedenbeck, M., Alle, P., Corfu, F., Griffin, W. L., Meier, M., Oberli, F., Vonquadt, A., Roddick, J. C. & Speigel, W. (1995). 3 Natural zircon standards for U-Th-Pb, Lu-Hf, trace elements and REE analyses *Geostandards Newsletter* **19**, 1-23.

Wiedenbeck, M., Hanchar, J. M., Peck, W. H., Sylvester, P., Valley, J., Whitehouse, M., Kronz, A., Morishita, Y., Nasdala, L., Fiebig, J., Franchi, I., Girard, J. P., Greenwood, R. C., Hinton, R., Kita, N., Mason, P. R. D., Norman, M., Ogasawara,

M., Piccoli, R., Rhede, D., Satoh, H., Schulz-Dobrick, B., Skar, O., Spicuzza, M. J., Terada, K., Tindle, A., Togashi, S., Vennemann, T., Xie, Q. & Zheng, Y. F. (2004). Further characterisation of the 91500 zircon crystal. *Geostandards and Geoanalytical Research* **28**, 9-39.

Wilde, S. A., Valley, J. W., Peck, W. H. & Graham, C. M. (2001). Evidence from detrital zircons for the existence of continental crust and oceans on the Earth 4.4 Gyr ago. *Nature* **409**, 175-178.

Windley, B. F. (1995). *The Evolving Continents*: Wiley.

Wones, D. R. (1966). Mineralogical indicators of relative oxidation states of magmatic systems. *Transactions American Geophysical Union (Abstract)* **47**, 216.

Yang, J.-H., Wu, F.-Y., Wilde, S. A., Xie, L.-W., Yang, Y.-H. & Liu, X.-M. (2007). Tracing magma mixing in granite genesis: in situ U-Pb dating and Hf-isotope analysis of zircons. *Contributions to Mineralogy and Petrology* **153**, 177-190.

Zandt, G., Leidig, M., Chmielowski, J., Baumont, D. & Yuan, X. H. (2003). Seismic detection and characterization of the Altiplano-Puna magma body, central Andes. *Pure and Applied Geophysics* **160**, 789-807.

Zhang, Y. X. & Zindler, A. (1993). Distribution and evolution of carbon and nitrogen in Earth. *Earth and Planetary Science Letters* **117**, 331-345.

Zindler, A. & Hart, S. (1986). Chemical Geodynamics. *Annual Review of Earth and Planetary Sciences* **14**, 493-571.

Appendix A

Detrital mineral constraints on the tectonic evolution of the Southern Uplands Terrane

The structure, provenance and detrital mineral content of the lower Palaeozoic sediments of the Southern Uplands have provided valuable insights into the timing, duration and geometry of Laurentian and Avalonian convergence and Iapetus Ocean closure. However, a comprehensive model remains elusive, reflecting competing interpretations for the terrane.

A.1 Tectonic models for the Southern Uplands

The early geological surveys of the 1870s were limited by poor inland exposure and a lack of stratigraphic markers such as way-up indicators. Subsequent developments in biostratigraphy (Lapworth, 1876; 1878; 1889) allowed far greater refinement of stratigraphical and structural models of the Southern Uplands Terrane. Peach and Horne (1899) later sub-divided the area into three strike-parallel belts: The Ordovician Northern belt, a Central Belt with interleaved Ordovician and Silurian units and the Silurian Southern Belt. Crucially, Peach and Horne (1899) recognised the importance of the Moffat Shale as a key stratigraphic horizon, which is overlain by progressively younger turbidite sequences to the south. The interpretation of continuous deposition of marine shales coeval with southwards extending deposition of terrigenous material continues to be accepted to the present day (Barnes and Stone, 1999). However, despite overwhelming biostratigraphic evidence for an overall south-eastwards younging (see Toghill, 1970), a new method for determining way-up indicators developed by Craig and Walton (1959) found local but frequent evidence of northwards younging. These authors recognised the structural contradiction that arose from sequences which at outcrop are northward younging, but which overall young southwards. McKerrow et al. (1977) were the first to propose a large-scale interpretation of the area in terms of a supra-subduction zone

accretionary prism on the Laurentian margin of the Iapetus. The model was further developed by Leggett et al. (1979), who proposed that strike-parallel faults define individual tracts, within which sand-rich turbidites were deposited on top of black shales, with the boundary between shales and turbidites become younger to the southeast.

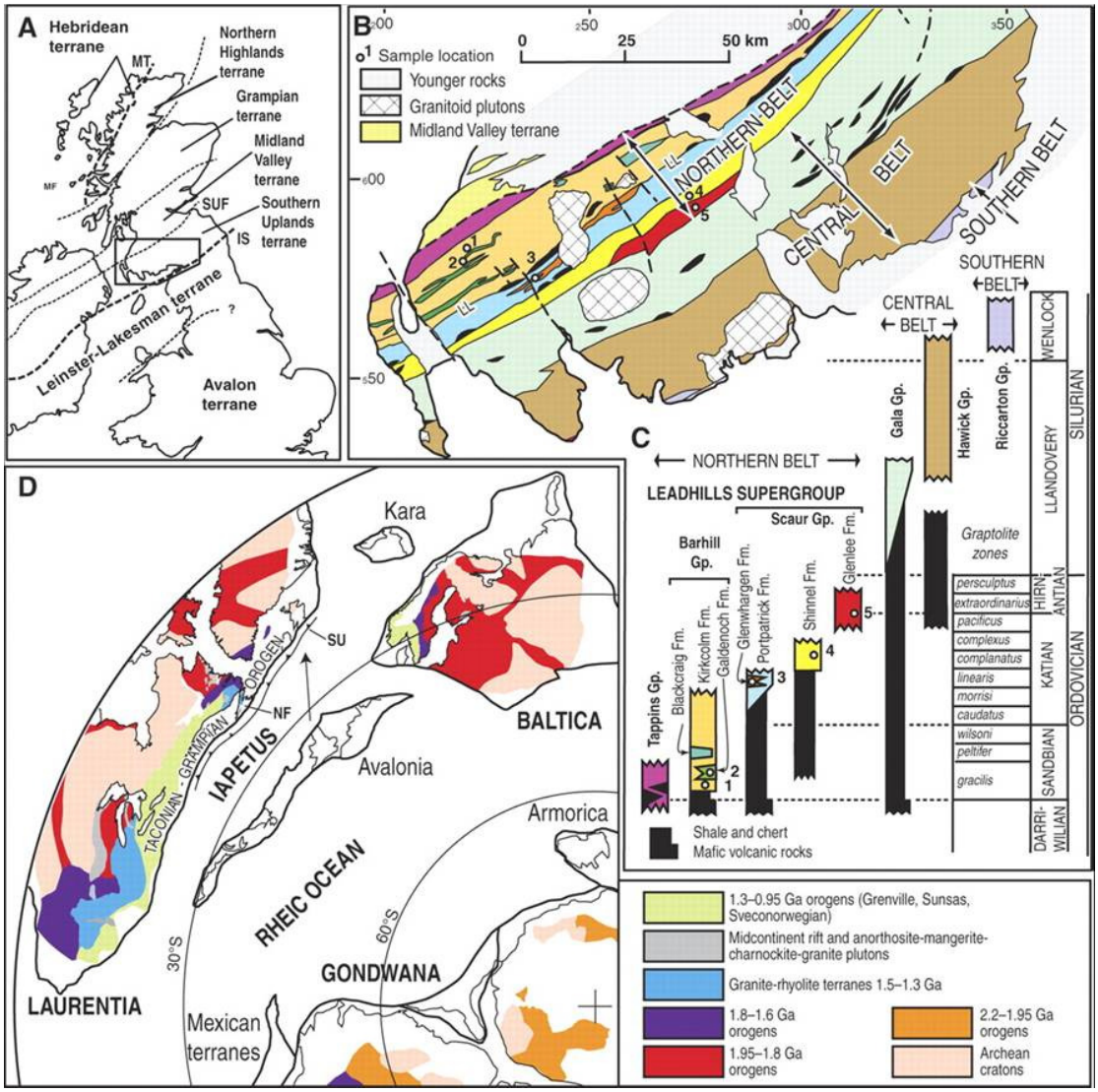

Fig. A1 Adapted from Waldron et al. (2008). A) Map of the principle terranes of Northern Britain. MT – Moine Thrust; SUF – Southern Upland Fault; IS – Iapetus Suture. B) Map of Western Southern Uplands terrane. LL – Leadhills Line. C) Schematic stratigraphic columns after Floyd (2001). Note SE-younging of sediments. Wider columns match units depicted on map in B. C) Paleocontinental reconstruction at 450 Ma showing principle crustal ages in Laurentia, Baltica and NW Gondwana.

More recent studies have demonstrated that despite the significant volumes of turbidites in each tract, they span only a limited age range relative to the Moffat

Shale, which may represent up to 25 Ma of deposition in some areas (Barnes and Stone, 1999). Importantly, it has also been demonstrated that variations in the age of the base of the turbidite sequences require syn-depositional deformation (Barnes et al. 1989; Barnes, 1999; Barnes and Walton, 1999). The processes of syn-depositional deformation remain controversial, but require an active tectonic margin.

Subsequent to the accretionary model proposed by McKerrow et al. (1977) and Leggett, (1979) two alternative tectonic models have been proposed for the Southern Uplands Terrane. Morris (1987) and Stone et al. (1987) suggest that the terrane represents a back-arc basin that became deformed in a foreland fold-and-thrust belt. Armstrong et al. (1996) and Armstrong and Owen (2001) propose that the northern part of the terrane formed in response to extension on a continental margin, with major normal faults later inverted during collision.

A crucial deviation of these models is their differing interpretation of Caradocian to Llandoverian andesite-bearing sandstones, particularly in the northern belt. Proponents of the back-arc model point out that paleocurrent analysis indicates derivation of this detritus from the south (Morris, 1987; Stone et al. 1987). In support of a proximal arc, abundant detrital heavy minerals, lawsonite and sodic amphibole have been found in quartzofeldspathic sandstones (Mange at al. 2005). Furthermore, andesitic material is remarkably fresh (Phillips et al. 2003), with radiogenic εNd values between ~ -2 and -4 (Stone and Evans, 1995). More felsic material is thought to originate from sources located to the north in the Grampian orogen of Scotland and Ireland (Waldron et al. 2008) or from Newfoundland (Elders, 1987).

The presence of a volcanic arc, active contemporaneously with sedimentation in the Southern Uplands is however difficult to reconcile with a lack of any identifiable volcanic source (Phillips et al. 2003). Kelley and Bluck (1989) identified further problems with the back-arc model when Ar-Ar dating of detrital hornblende provided late Neoproterozoic to early Cambrian ages (530 to 560 Ma). Phillips et al. (2003) used high precision thermal ionisation mass spectrometry (TIMS), U-Pb and laser ablation ages of detrital zircons to further confound the back-arc model. These

authors revealed a predominance of ca. 550 Ma and 1 Ga zircon ages in the andesite-bearing sandstones, suggesting that andesitic detritus was derived from an older Neoproterozoic arc on Grenvillian basement in Avalonia.

Waldron et al. (2008) questioned the derivation of detrital material from Avalonia and analysed approximately 100 detrital zircons from five different sandstones from the northern belt of the Southern Uplands. Age peaks at 2.7, 1.8 and 1.1 Ga (Fig. A3) coincide with major episodes of apparent crustal growth on Laurentia (Hoffman, 1989). Furthermore, a Laurentian source was favoured by an absence of Paleoarchean sources in peri-Gondwana terranes (Waldron et al. 2008). Paleoproterozoic (1.9-1.8 Ga) and early Mesoproterozoic (1.55 to 1.0 Ga) sources are also present in Laurentia but are rare in Avalonia. The 1 Ga zircons are attributed to the Grenville orogen sources in Laurentia. However, like Phillips et al. (2003), Waldron et al. (2008) also found a large number of grains with ages of 550 and 615 Ma (Fig. A3). The former authors attributed these peaks to Avalonian arcs, supported by paleocurrant evidence of northwards flow. The latter authors however point out that such detritus could be derived from intrusions in Laurentia formed during late Proterozoic Iapetan rifting (Cawood et al. 2001), and does not detract from the overwhelming Laurentian signature of most grains. Northward directed turbidity currents have been interpreted as meanders in a more general southerly directed series of turbidity currents.

Detrital zircon ages therefore provide a powerful method for distinguishing different tectonic settings, which in turn lead to different predications of sandstone provenance. In addition to identifying syn-depositional active arcs, detrital mineral ages may also be used to test the hypothesis of an extensional and rifted margin. This latter scenario would be expected to result in a transition from local sources to more broadly distributed sources as rift margins subsided (Cawood et al. 2007; Waldron et al. 2008). By contrast, Waldron et al. (2008) suggest that accretionary models would result in progressive changes in detritus sources during denudation of the Grampian orogen on the Laurentian margin. There is a striking similarity in the U-Pb ages of detrital zircons from all five samples which span multiple tracts, and is suggested to

indicate a progressively unitary model. At present, these conclusions are limited to units exposed in the northern tract of the Southern Uplands, with little investigation of the Southern tracts. Although not directly sampled, volcanic vents situated within the southern tract and sampled as part of this study, contain abundant detrital zircons from the surrounding sediments and offer a potential means of investigating the sedimentary detrital mineral record.

A.2 The Shoulder O'Craig volcanic vent and associated detrital minerals

In an attempt to examine the accessory mineral content of Devonian volcanic material, which is of limited exposure in the Southern Uplands, the Shoulder O'Craig volcanic vent was sampled. The outcrop lies on the western side of the River Dee estuary at Clinking Haven, 4 km south of Kirkcudbright. The area is predominantly composed of intrusion breccia, interpreted as a volcanic vent (Rock et al. 1986; Stone 1999) and is cut by a later basalt intrusion. The vent complex intrudes vertically inclined Silurian sandstone turbidites of the Carghidwon Formation (Hawick Group). These sediments have been shown to contain graptolite fauna of late Llandovery age at nearby localities (White et al. 1992). The vent is post-tectonic, cross-cutting slaty cleavage which is sub-parallel to bedding in the surrounding country rocks. The breccia is composed of rounded to sub-angular clasts of sandstone, siltstone and rare basaltic or microdioritic lithologies in a fine-grained matrix, and is interpreted as an intrusion breccia (Rock et al. 1986; Stone (1999). At the western end of the vent, near Clinking Haven, the vent is cut by a lamprophyric biotite-olivine basalt with both sharp and gradational contacts with the breccia. Rock et al. (1986) suggest that oval, pillow-like textures and possible flow fractures in the basalt are indicative of intrusion in a semi-solid state. Kersanitic lamprophyre dykes cross-cut the vent and have been dated using K-Ar in biotite at 410 ± 10 Ma by Rock et al. (1986).

Six zircon U-Pb ages were obtained from zircons separated from the basalt using a CAMECA 1270 ion microprobe with the same analytical set-up outlined in Chapter 5 and Appendix F. U and Pb isotope compositions were measured using a beam size of ~ 20 μm. Common lead was below 15 ppb for all zircons and was mostly below

0.5 ppb. $^{206}Pb/^{238}U$ ages are reported due to their lower uncertainty and are reported at 2σ. One Neoarchean (2.8-2.5 Ga) grain yields an age of 2552 ± 42 Ma, two grains are Mesoproterozoic (~ 1.55 to 1.0 Ga), one is Neoproterozoic (542 Ma to 1.0 Ga) and two are Paleozoic in age. No age is consistent with the depositional age of the Carghidwon Formation. One Paleozoic age of 414 ± 8 Ma is consistent with the age of the vent (Fig. A2).

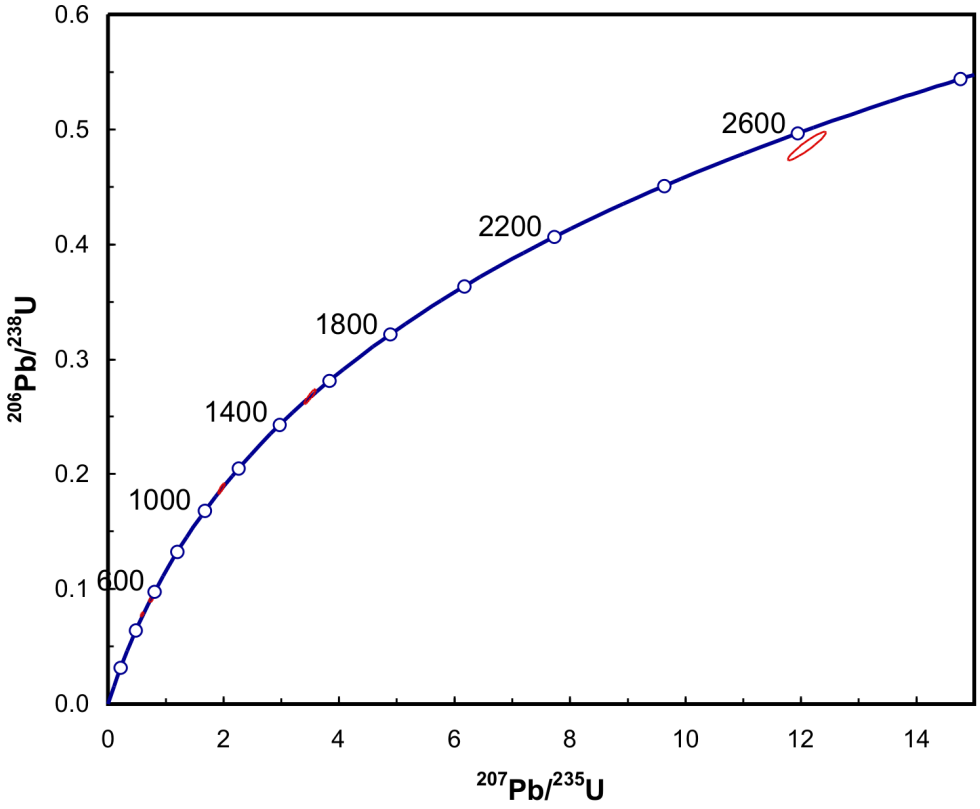

Fig. A2 Concordia diagram for all detrital zircons from the Shoulder O'Craig basalt

Despite the limited size of the data set, the ages show striking similarities with the U-Pb ages measured across multiple tracts of the northern belt (Fig. A3). The continued similarity of ages across both tracts and belts provides further evidence for a progressive unitary model for all belts. As proposed by Waldron et al. (2008), this contrasts with models where tracts are assigned to different tectonic environments (Morris, 1987). It is also inconsistent with a model where different tracts correlate with distinct terranes (van Saal et al. 1998). Although insufficient data are available to assign peaks of ages, the ages obtained coincide with age peaks in the northern belt and in Laurentian rocks (Fig. A3). Mesoproterosoic ages such as the 1528 ± 28 Ma grain are common in Laurentia but not in Avalonia (Waldron et al. 2008). These

same authors ascribe Early Mesoproterozoic grains such as the 1106 ± 22 Ma grain to Laurentian material derived from the Grenville orogen, and are common in areas of Western Newfoundland and in the Dalradian of Scotland (Fig. A3). The youngest two Neoproterozoic grains are broadly consistent with clusters of similar ages found by Phillips et al. (2003) and Waldron et al. (2008). These ages have been ascribed to possible sources on Avalonia by the former authors. The latter authors emphasise that such ages may also be related to Laurentian intrusions associated with late Iapetan rifting.

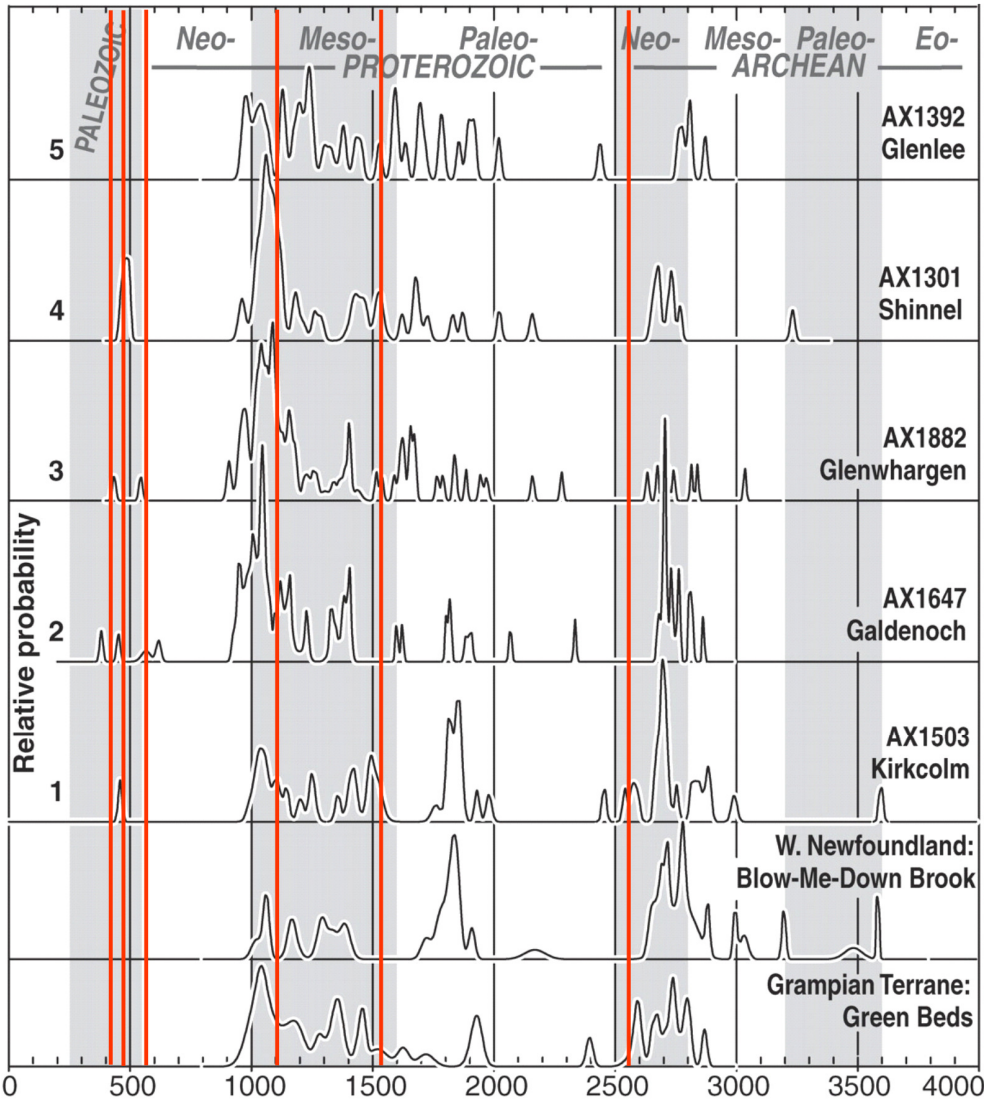

Fig. A3 U-Pb detrital zircon relative probability distributions for sandstone samples from the northern tract of the Southern Uplands from Waldron et al. (2008). The lower panels show comparisons with samples from the Blow-Me-Down Brook Formation, Western Newfoundland (after Cawood and Nemchin, 2001), and the Green Beds, Dalradian Supergroup, Grampian terrane of Scotland (after Cawood et al. 2003). Red vertical lines are U-Pb ages for zircon grains derived from the central tract and separated from the Shoulder O'Craig basalt.

Crucially, there is no abundance of Silurian grains that would support the existence of an active oceanward arc during the development of the terrane in an associated back-arc. The lack of any transition from restricted to more broadly distributed sources across the northern and central belts is also inconsistent with an extensional rifted margin (Cawood et al. 2007; Waldron et al. 2008). Our data for the central belt, though limited in abundance, is similar to that from the northern belt and is most consistent with an active-margin trench environment.

Appendix B

Analytical Set-ups

B.1 Whole-rock major and trace element analysis: XRF[†]

Major-element concentrations were determined after fusion with a lithium borate flux containing La_2O_3 as a heavy absorber, by a method similar to that developed by Norrish and Hutton (1969). Rock powder was dried at 110°C for at least 1 hour, and a nominal but precisely-weighed 1-g aliquot ignited at 1100°C to determine loss on ignition (LOI). The residue was then mixed with Johnson Matthey Spectroflux™ 105 in a sample:flux ratio of 1:5, based on the *unignited* sample mass, and fused in a muffle furnace in a Pt5%Au crucible. After the initial fusion, the crucible was reweighed and any flux weight loss was made up with extra flux. After a second fusion over a Meker burner, the molten mixture was swirled several times to ensure homogeneity, cast onto a graphite mold, and flattened with an aluminium plunger into a thin disk. The mold and plunger were maintained at a temperature of 220°C on a hotplate.

Trace-element concentrations were determined on pressed-powder samples. Eight grams of rock powder were mixed thoroughly with eight drops of a 2% aqueous solution of polyvinyl alcohol. The mixture was loaded into a 40-mm diameter aluminium cup in a stainless steel die and compressed against a polished tungsten carbide disc in a hydraulic press at 0.6 tons/cm^2.

The fused and pressed samples were analyzed using a PANalytical PW 2404 automatic X-ray fluorescence spectrometer with a Rh-anode X-ray tube. Trace-element background positions were placed as close as possible to peaks, and long count times were used at both peak and background positions. Where background count rates were measured on either side of the peak, as in most trace-element

[†] XRF analytical conditions provided by Godfrey Fitton (pers. comm.).

determinations, the count time was divided between the two positions. Analytical conditions are given in Fitton et al. (1998) and Fitton and Godard (2004).

Corrections for matrix effects on the intensities of major-element lines were made using theoretical alpha coefficients calculated on-line using the PANalytical software. The coefficients were calculated to allow for the amount of extra flux replacing volatile components in the sample so that analytical totals should be 100% less the measured LOI. Intensities of the longer wavelength trace-element lines (La, Ce, Nd, Cu, Ni, Co, Cr, V, Ba, and Sc) were corrected for matrix effects using alpha coefficients based on major-element concentrations measured at the same time on the powder samples. Matrix corrections were applied to the intensities of the other trace-element lines by using the count rate from the RhK_a Compton scatter line as an internal standard (Reynolds, 1963). Line-overlap corrections were applied using synthetic standards.

B.2 Whole-rock oxygen isotopes: Laser fluorination

Oxygen isotope analyses of whole-rock samples were carried out at the Scottish Universities Environmental Research Centre (SUERC) at East Kilbride. The method followed the Macaulay et al. (2000) modification of the laser fluorination method of Sharp (1990). 1mg of powdered sample was reacted with ClF_3 using a CO_2 laser. Resultant oxygen was purified and converted to CO_2 on platinised graphite, and the yield measured with a capacitance manometer. A Micromass PRISM 3 duel inlet, triple collector mass spectrometer was used to analyse the oxygen isotope composition of the CO_2, with a working standard gas calibrated against international reference standard NBS28. The accuracy and precision were ±0.4‰ (2σ), and NBS28 gave a value of 9.56‰.

B.3 Zircon

B.3.1 Zircon crystal reparation

Rock samples of approximately 5 kg from different zones of all the plutons studied were crushed and sieved to < 500 μm prior to density separation using a Wilfley Table at the University of St Andrews separation facility. Heavy liquids, including Tetrabromoethane (TBE) and methylene iodide were used for further mineral separation. Non-magnetic fractions were separated by Frantz magnetic separators at the Universities of St Andrews and Edinburgh. Approximately 100 zircon crystals were picked from each sample and mounted in epoxy (Araldite/Epothin) blocks with fragments of 91500 zircon standard positioned at the centre of each block. Polished mounts were imaged by back-scattered electron and cathodoluminescence (CL) using a Phillips XL30CP Scanning Electron Microscope (SEM) at the University of Edinburgh to establish the positions of inclusions, cracks and internal compositional zoning.

B.3.2 Zircon oxygen isotope analysis: SIMS

Zircon oxygen isotope analyses were carried out using a Cameca ims 1270 ion microprobe at the University of Edinburgh following the methods of Cavosie et al. (2005) and Kemp et al. (2006b) with data reported as per mil (‰) values relative to Vienna Standard Mean Ocean Water (VSMOW). A primary $^{133}Cs^{+}$ ion beam of approximately 20 μm was used at 6nA. A normal-incidence electron flood gun was used for charge neutralisation, with secondary ions extracted at 10 kV. Both $^{18}O^{-}$ and $^{16}O^{-}$ ions were monitored simultaneously on dual Faraday cups. Total acquisition times of ~ 200 seconds included secondary ion beam centring, pre-sputtering for 50 seconds and data collection over 10 cycles, each lasting 4 seconds. Instrumental drift was corrected daily by normalising all unknown samples to zircon standard 91500 ($\delta^{18}O$ = 9.86 ‰) (Wiedenbeck et al. 2004). Bracketing analyses of 91500 were used to obtain linearly interpolated values of $^{18}O/^{16}O$ that were subsequently used to normalise the $^{18}O/^{16}O$ ratios of unknown samples. Analyses of 91500 in groups of 5 to 10 were carried out after every 10 to 15 analyses of unknowns. Following

corrections for instrument drift, unknown zircon analyses were normalised to an average daily $^{18}O/^{16}O$ value for zircon standard 91500.

HfO_2 concentrations in unknown zircon samples were determined using Cameca SX100 electron microprobes at the Universities of Bristol and Edinburgh. Variations in the instrumental mass fractionation (IMF) during $^{18}O/^{16}O$ analysis by ion microprobe have been shown to reflect variations in HfO_2, particularly analyses at high energy offset using a Cameca ims 4f (Peck et al. 2001). IMF corrections were not required in this study due to the use of a Cameca ims 1270 (which does not require high energy offset) and the small measured variations in HfO_2 (generally < 0.5 wt%).

Analytical precision from session to session was generally between 0.3 and 0.6 ‰.

B.3.3 Zircon U-Th-Pb analysis: SIMS

U-Th-Pb dating was carried out following oxygen isotope analysis using a Cameca ims 1270 ion microprobe at the University of Edinburgh. A 4 to 5 nA primary O^{2-} beam was used for zircon analysis with 22.5 keV impact energy following the method of Kelly et al. (2008). Resulting analytical pits were ~ 25 μm and ellipsoidal in shape following beam focusing and alignment under Köhler illumination, with further spatial resolution achieved using of a field aperture. U, Th and Pb were analysed at a mass resolution ($M/\Delta M$) of > 4000R using a peak switching routine. No energy centring was carried out and an energy window of 60 eV was used throughout. Pb ion yields were increased by a factor of ~ 2 by flooding the sample surface with oxygen. Any effects from surface contamination were minimised by pre-rastering a ~ 15 μm surface area for 120 seconds prior to analysis. Pb/U ratios were calibrated using a slope factor of 2.6 between ln (Pb/U) vs. ln (UO_2/U). U/Pb ratios were calibrated against measured ratios of zircon standard 91500 with an age of ~1062.5 Ma and assuming a $^{206}Pb/^{238}U$ ratio of 0.17917 (Wiedenbeck et al. 1995). Standard analyses were carried out after every 3 to 4 unknown analyses. Calculated Th/U ratios in all unknown samples were obtained by comparison to measured Th/U ratios (Th/U = 0.362) and $^{206}Pb/^{238}U$ in zircon standard 91500 assuming closed

system behaviour. U and Hf concentrations of 81.2 ppm and 5880 ppm respectively in the standard were assumed and elemental concentrations determined based on the observed oxide ratios of the standard (UO_2/Zr_2O_2 and HfO/Zr_2O_2).

Corrections for dead time (51 ns), detector background (~ 0.01-0.03 counts per second) and common Pb were carried out. Measurements with $^{204}Pb > 10$ ppb were discarded because of large common Pb corrections. Uncertainties in the U/Pb ratio of 91500 are approximately 0.8 % greater than those expected from counting statistics alone and are assumed to be random errors (Ireland, 2003). These random errors have been propagated in the standards and unknowns together with the observed variations in Pb/U ratios for each analysis (typically close to the counting errors). Measurements carried out on zircon standard 91500 are typically between 0.7 and 1.0 % per analysis. Observed variations in $^{207}Pb/^{206}Pb$ ratios from cycle to cycle during each analysis approach those expected from counting statistics. Quoted uncertainties on individual ages are 1SD while those on calculated group ages are quoted as 2 SD.

B.3.4 Zircon Hf isotope analysis: Laser ICP-MS

Zircon Lu-Hf isotope compositions were obtained using a ThermoFinnigan Neptune multicollector inductively-coupled plasma mass spectrometer (MC-ICP-MS) coupled with a New Wave Research UP193HE laser at the University of Bristol. Similar sites to those used for oxygen isotope analyses were chosen using a spot size of 40 or 50μm. Ablation was carried out in helium and later mixed with argon and nitrogen using a pulsed laser at 4 Hz with an energy density of ~ 6 J/cm^2 over 60s. Total analysis times were ~ 90s, including 30s of background measurements. Corrections for interferences and mass bias followed the University of Bristol procedure outlined by Hawkesworth and Kemp (2006) and Kemp (2009). Mass bias effects with interference-free ^{171}Yb were corrected using an exponential law and $^{173}Yb/^{171}Yb = 1.130172$ (Segal et al. 2003). A $^{176}Yb/^{171}Yb$ value of 0.897145 was used to calculate the ^{176}Yb interference on ^{176}Hf (Segal et al. 2003) with mass bias-corrected ^{171}Yb monitored during the run. Mass bias effects on interference-free ^{175}Lu were conducted assuming $\beta Lu = \beta Yb$ and using an exponential law. Mass bias-corrected

^{176}Lu was monitored during the run and the magnitude of the ^{176}Lu interference on ^{176}Hf was calculated using ^{176}Lu/^{175}Lu = 0.02655 (Vervoort et al. 2004). An exponential law was used to correct for mass bias on interference corrected ^{176}Hf/^{177}Hf values before normalising to Hf standard JMC-475 = 0.282160. The accuracy and long term reproducibility of the measurements was estimated by analysing two zircon reference standards, including Plesovice (^{176}Hf/^{177}Hf = 0.282476 (25), *n = 29* with a 40μm beam; ^{176}Hf/^{177}Hf = 0.282474 (17), *n = 36* with a 50 μm beam) and Mud Tank (^{176}Hf/^{177}Hf = 0.282503 (27), *n = 27* with a 40μm beam; ^{176}Hf/^{177}Hf = 0.282501 (18), *n = 30* with a 50μm beam) (errors are reported at 2 SD). Initial εHf values for all samples were calculated using the mean ^{206}Pb/^{238}U ages for each zone. Epsilon values are reported relative to initial Chondritic Uniform Reservoir (CHUR) values calculated from present day values of ^{176}Lu/^{177}Hf = 0.0336 and ^{176}Hf/^{177}Hf = 0.282785 (Bouvier et al. 2008). A ^{176}Lu decay constant of $\lambda = 1.867 \times 10^{-11}$ yr^{-1} (Scherer et al. 2001) was used.

B.3.5 Zircon trace element analysis: SIMS

A Cameca ims-4f was used to measure trace element (including REE) concentrations at the EIMF. Analytical methods and procedures followed those described by Hinton and Upton (1991). A 14.5 keV primary O^- beam was used at 5 nA, with secondary ions measured at ~ 120 V offset. Ten cycles were made through the selected masses because of the low concentrations of some REE in zircon. Analyses were standardised against NIST SRM-610 glass standard and concentrations were referenced against Si. Zircon standard 91500 was used a secondary standard. Corrections were made for $ZrSiO^+$ overlap on $^{138}Ba^+$, $^{139}La^+$, $^{140}Ce^+$ and $^{141}Pr^+$ using count rates measure at mass 134. The interference of LREE on HREE and Hf^{2+} on Y were corrected based on analysis of zircon standard 91500.

B.4 Apatite trace element analysis: EPMA and SIMS

Apatite compositions were determined primarily by a Cameca SX-100 electron probe supported for comparative purposes by ion microprobe analyses using a Cameca ims 4f at the University of Edinburgh Ion Microprobe Facility (EIMF). Good agreement was observed between the two methods. Zircon-hosted apatite was analysed in

zircons mounted in epoxy blocks. Back-scattered electron (BSE) and cathodoluminescence (CL) images were taken on polished surfaces using a Philips XL30P Scanning Electron Microscope (SEM) at the University of Edinburgh. Apatite hosted by other phases was analysed directly in polished thin sections.

A wavelength dispersive method (WDS) was used for electron probe analysis of apatite using PC0, LTAP, LPET and LIF dispersion crystals. Beam conditions were 20 kV and 60 nA for trace and most major elements, with a 10 nA defocused beam used to minimise loss of alkalis during analysis.

Apatite inclusions were analysed using the Cameca ims4f ion microprobe, with a 5 nA $^{16}O^-$ primary ion beam with 15 keV net impact energy and a spot size of approximately 15 µm. Only high energy secondary ions (100-140 eV) were measured in order to reduce molecular ion overlap. F/Ca ion yields were determined using Durango and Wilberforce apatite standards. The very small size of some apatite inclusions in zircon resulted in the need for tests for beam overlap with zircon. The very low concentration of Zr in apatite relative to zircon means the magnitude of any overlap can be estimated by taking the ratio of an average zircon Zr concentration (~ 420,000 ppm) and that of the apatite analysed. Grains that showed evidence for overlap were discounted. Data obtained by both analytical methods (ion probe and electron probe) are similar.

B.5 Quartz oxygen isotope analysis: SIMS

The oxygen isotope compositions of quartz grains were determined on polished thin sections using the Cameca ims 1270 ion microprobe, using the same instrument set-up as that used for zircon oxygen isotope analyses. Unknown quartz analyses were normalised to grains of Bogola quartz standard ($\delta^{18}O$ = 12.3 ± 0.3 ‰; Elsenheimer and Valley, 1993), which were analysed after every 5 to 10 unknowns. Internal precision (~ 0.2 ‰) was calculated from the Bogola quartz standard. External precision varies between 0.2 ‰ and 0.4 ‰ from session to session. In general, heterogeneity within and between quartz crystals exceeded the external analytical precision (intra grain 2σ variations are between ~ 0.6 and 2.1 ‰). Where possible,

multiple analyses were made on single crystals in order to identify oxygen isotope zonation caused by alteration around crystal edges or due to changing magmatic compositions.

B.6 Amphibole analysis: EPMA

Amphiboles were analysed in polished thin sections using a wavelength dispersive method (WDS) on a Cameca SX-100 electron probe using LTAP, TAP and PET dispersion crystals. Beam conditions were 25 kV and 10 nA for Na, Mg, Al, Si, K, Ca and Fe, and 15 kV and 100 nA for Ti and Mn.

Appendix C

Petrography

Detailed petrographic descriptions and OS grid references are provided for each of the mineralogical zones of the Criffell, Fleet and Shap plutons together with any accompanying mafic enclaves. The petrography of mafic rocks from the Shoulder O'Craig site are also described.

C.1The Criffell Pluton

C.1.1 Outer Quartz Diorite (AM0936)

– [NX 83797 51722] - Found at the margins of the Criffell pluton at Almorness Point, the rock is medium grained and often altered with a pinkish-grey colour. Larger K-spar and white plagioclase crystals are visible in hand specimen together with mafic clots composed of biotite and amphibole. In thin section (Fig. C1a-e), the rock consists of plagioclase (~40 modal %) (An_{37}-An_{20}; BGS survey book for maps 5W, E and 6E), hornblende (<5 modal %), biotite (<5 modal %), quartz (~20 modal %) and K-feldspar (~10 modal %). Most feldspar is either completely or partly altered to sericite but some concentric zoning is still visible, particularly around the margins of larger phenocrysts. Perthite exsolution textures are visible in some K-spar crystals. Ferromagnesian mineral define a weak foliation throughout the rock and are often altered to chlorite. Small amounts of relic clinopyroxene (cpx) may be found in the centres of hornblende crystals set amongst larger mafic clots. The 'groundmass' is composed mainly of rounded and interlocking quartz crystals with accessory sphene, apatite, magnetite and zircon.

C.1.2 Granodiorites

C.1.2.1 Zone 1: Clinopyroxene-biotite-hornblende granodiorite (AM0917)

– [NX 89700 68500] - This is the outer and most primitive zone of the Criffell pluton. The dominance of plagioclase gives the rock on overall white colour with hornblende and biotite phenocrysts, all of which define a moderate foliation. The granodiorite consists of inequigranular zoned plagioclase (An_{15}- An_{35}, BGS

survey book for maps 5W, E and 6E) ~50 modal %), quartz (~ 20 modal %), biotite (~10 modal %), K-spar (~10 modal %) and hornblende (~ 5 modal %). Hornblende occasionally contains cores of relic cpx (Fig. C1c). Accessories include sphene, apatite, opaque oxides and zircon. Disc-shaped, ~10cm mafic enclaves within the granodiorite also define the foliation and are composed of similar minerals to the host granodiorite (Fig. C1b), with greater proportions of biotite and plagioclase. Small amounts of kinking in some biotite crystals and recrystallisation of quartz around larger plag crystals has produced a mortar texture (circled in Fig C1d), indicative of deformation most likely related to the foliation.

C.1.2.2 Zone 2: Biotite-hornblende granodiorite (AM0918) – [NX 89650 68490] A gradational transition occurs from the more mafic cpx bearing zone, with a gradual reduction in the proportions of hornblende and a larger proportions of biotite. The main phases are again plagioclase (~50 modal %), quartz (~20 modal %), K-spar (10 modal %), biotite (~15 modal %) and hornblende (< 5 modal %) (Fig. C1f). K-spar crystals are, like plagioclase, often altered to sericite but show ghost simple twinning and often have myrmekitic textures at their boundaries. Some also show cross-hatched twinning, indicative of microcline. Accessories include sphene, apatite, magnetite and zircon. Dioritic mafic enclaves occur, though in smaller numbers than in the more mafic zone.

C.1.3 Granites

C.1.3.1 Zone 3: Biotite granite (AM0921) – [NX 83910 60950] - This zone is missing from the northern side of the Criffell pluton but is exposed around Dalbeattie. Later intrusion of this granite is evident from the lack of foliation and a discontinuity in mineralogy and bulk-rock compositions (Stephenson, 1999) relative to the earlier granodiorites. Large K-spar megacrysts are visible and often show signs of exsolution in thin section. Further evidence for exsolution is seen from myrmekitic textures adjacent to some K-spar megacrysts. Zoned plagioclase crystals are often seen within these large megacrysts. Modal mineral proportions are approximately: K-spar ~ 30%, plag ~30 %, quartz ~ 25%, biotite ~10%. Ferromagnesian minerals are

often altered to chlorite. Accessories include sphene, apatite, magnetite, ilmenite (?) and zircon. Small numbers of mafic, dioritic enclaves may be found.

C.1.3.2 Zone 4: Muscovite-biotite granite (AM0919, AM0922) – [NX 84379 60301] - Subhedral phenocrysts of K-spar become increasingly common on approach to the more evolved core of Criffell, with primary muscovite appearing in this zone. Muscovite is present as small laths, primarily associated with biotite. In general, the granite consists of approximately 40 modal % plag, 30 modal % k-spar, 25 modal % quartz and 5% biotite, which is often altered to chlorite. Feldspars are frequently altered making compositional estimates difficult, though the presence of simple twinning and lamellar twins is indicative of ternary compositions. Small, wart-like myrmekite textures can be seen around the margins of K-spar crystals, which may suggest a late stage alteration caused by fluids. Accessories include muscovite, ilmenite, apatite and zircon.

C.1.3.3 Zone 5: Biotite-muscovite granite (AM1008) – [NX 91050 66900] Poorly exposed and restricted to the centre of the Criffell pluton, this zone represents the most evolved zone of the intrusion. Muscovite (~5 modal %) is clearly more abundant, forming larger laths than in the mu-bt zone. Plagioclase (~ 40 modal %) is extensively altered and may be distinguished from K-spar by this means. Unlike other zone, some K-spar (~30 modal %) has transformed to microcline with characteristic cross-hatched twins. Plagioclase margins are often the least altered, indicating a progressive evolution in melt compositions, with greater disequilibrium with what may be more Ca-rich cores. The inclusion of muscovite and biotite (~5 modal %) in plagioclase crystals and their expulsion to the margins of quart crystals suggests they began crystallising early on during magmatic evolution. Accessories include apatite, ilmenite and zircon and monazite in mineral separates.

Fig. C1 Photomicrographs of a representative selection of thin sections from the Criffell pluton. Sample numbers of listed in the top right and mineral names are abbreviated as follows: Qtz – quartz, K-Spar – K-feldspar, plag – plagioclase, bt- biotite, hb – hornblende, mu – muscovite, sp – sphene, mag – magnetite, ap – apatite, zr – zircon. XP and PPL refer to crossed polarised and plane polarised light respectively. Circled areas mark zones of re-crystallised quartz forming mortar textures.

C.2The Fleet Pluton

C.2.1 Zone 1: Coarse grained biotite granite (AM0933) –

[NX54800 75400] This is the outer and most primitive of the Fleet zones and is composed predominantly of K-spar (~50%), most of which with is microcline (Fig. C2a). Quartz is also common (~30%) both as large crystals up to 1mm but also as the product of re-crystallisation, present as mortar textured bands. These, in addition to smaller amounts of aligned biotite (often chloritised) (5%) define a prominent foliation within the rock around larger feldspar crystals. These areas are also associated with spectacular myrmekitic textures. Most muscovite (5%) is of a secondary nature, often forming as a break down product of K-spar. Plagioclase (10%) is noticeably less common in the Fleet granites than in Criffell, tending to form smaller crystals. Sphene and opaque oxides are noticeably absent in the Fleet samples, and higher values of SiO_2 have resulted in reduced amounts of zircon saturation.

C.2.2 Zone 2: Coarse grained biotite-muscovite granite (AM0934) –

[NX 58233 72519] Modal mineralogy in this intermediate granite is similar to the outer biotite granite except for the addition of ~5% primary muscovite and a reduced proportion of biotite (Fig. C2b). The amount of foliation is also reduced, with no re-crystallisation of quartz. Myrmekitic textures are also present.

C.2.3 Zone 3: Fine grained biotite-muscovite granite (AM0935)

– [NX 57586 68755] Predominantly composed of microcline, this intermediate grained rock is the most evolved of the Fleet zones (Fig. C2c). Mineral proportions are broadly similar to the outer zone but with further reductions in the proportions of biotite, again chloritised, and an increase in the proportions and size of muscovite plates. Myrmekitic textures are less common and there is no evidence of foliation.

C.3 The Shap Pluton

C.3.1 Outer Stage 1 granite – [NX 55505 08291] - This granite is primarily distinguished from the stage 2 granite by lower numbers of K-spar megacrysts (~15 %), some of which reach 5cm in size. These megacrysts have frequent Carlsbad twins and show evidence for exsolution, resulting in perthite intergrowths of albite within the orthoclase host, verified by use of the Becke Line Test. Their late stage formation is indicated by the inclusion of all other mineral phases present in the host granite, but a progressive increase in the size of mainly quartz, biotite and plagioclase inclusions towards the rims may be indicative of a magmatic origin and simultaneous crystallisation with other phases. Some plagioclase laths that transcend the K-spar megacrysts boundaries show evidence for continued growth only around areas that remained outside of the growing megacrysts, again supportive of simultaneous growth from a magmatic system. Others have reported zonal alignment of inclusions within the megacrysts (Stephenson, 1999). The granite is composed of plagioclase (~30%), orthoclase (~40%) (zoned from andesine to albite; Stephenson, 1999), quartz (~20%) and biotite (~10%), often altered to chlorite (Fig. C2d). Accessories include abundant sphene, apatite, magnetite, pyrite and zircon.

C.3.2 Stage 2 granite – [NX 55810 08480] - The second stage granite is broadly similar to the stage 1 granite in terms of mineralogy but has up to ~30% Carlsbad twinned, perthitic orthoclase megacrysts and slightly less biotite. The groundmass is composed of orthoclase, zoned plagioclase, quartz and biotite (Fig C2e). Accessory minerals include sphene, apatite, magnetite, pyrite, zircon and allanite (?).

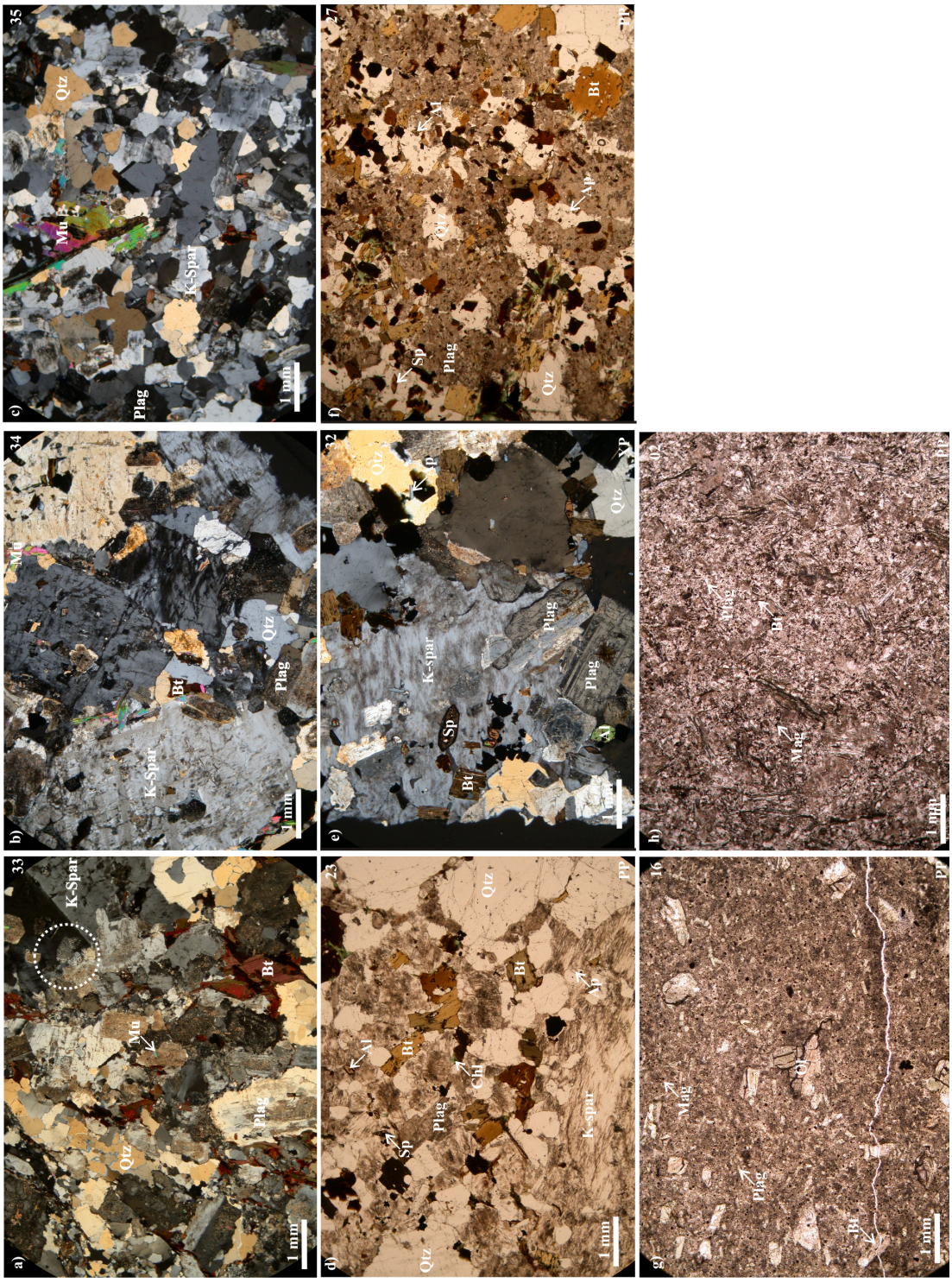

Fig. C2 Photomicrographs of a representative selection of thin sections from the Fleet (a-c), Shap (d-f) plutons and lamprophyre samples from Shoulder O'Craig. Sample numbers of listed in the top right and mineral names are abbreviated as follows: Qtz – quartz, K-Spar – K-feldspar, plag – plagioclase, bt- biotite, hb – hornblende, mu – muscovite, sp – sphene, mag – magnetite, ap – apatite, zr – zircon, Al - allanite. XP and PPL refer to crossed polarised and plane polarised light respectively. Circled area in (a) shows myrmekitic texture.

C.4 Mafic Rocks

C.4.1 Basalt (AM0916) – [NX 66276 49089] - The rock is extensively altered and has pillow basalt-like expression in the field, said to indicate intrusion in a semi-solid state (Rock et al, 1986). Pseudomorphed olivine (< 5 modal %) is identified on the basis of ghost crystal shape and extensive alteration around what were once curving cracks. Augite has previously been identified as an additional pseudomorphed phase by Stephenson (1999). Laths that show more abundant green chlorite are likely to have been biotite. Other larger laths are indicative of plagioclase crystals now altered to clays, in much the same manner as most of the groundmass. Opaque oxides are also common in the clay-dominated groundmass (Fig. C2g).

C.4.2 Lamprophyre (AM0902) – [NX 66380 49170] - Unlike the hornblende lamprophyres reported from around the Criffell pluton, the Shoulder O'Craig Loch Ness Monster kersantite lamprophyre dyke is mica-bearing and has abundant and altered plag. The dyke is mainly fine grained with pale globular structures up to 0.5mm and relic mica phenocrysts all set in a pale grey groundmass. In thin section, the groundmass is mostly dominated by altered plagioclase crystals (Fig.C2h). Pseudomorphed biotite phenocrysts have undergone almost complete kaolinitisation, but other authors report undulose extinction, suggesting early crystallisation and deformation prior to and during final emplacement (Rock et al 1986). Other features identified in biotite include pale cores and darker rims, indicative of increased substitution of Fe for Mg. The overall light to reddish brown colour of fresher biotite crystals also indicates high Ti contents (BGS survey book for maps 5W, E and 6E). High relief apatite crystals are still present within the groundmass along with opaque oxides and small amounts of epidote. Epidote is likely to be the breakdown product of feldspar and biotite. Small amounts of carbonate are also alteration products of the originally feldspathic groundmass. Globular structures up to 1mm also occur throughout the rock and are composed of carbonate, feldspar (now altered) and possibly quartz. These may represent an immiscible carbonate phase in the magma, and have been identified by other authors

(BGS survey book for maps 5W, E and 6E) as having chlorite, epidote and occasional cores of sulphides, mostly pyrite.

Appendix D

Whole-rock compositions

CRIFFELL	*Stephens and Halliday 1980; Stephens, et al. 1985*														
Sample	**102**	**108**	**109**	**144**	**146**	**174**	**184**	**205**	**210**	**219**	**243**	**244**	**272**	**274**	**77056**
Zone	**1**	**1**	**1**	**2**	**2**	**4**	**2**	**3**	**4**	**5**	**1**	**2**	**5**	**4**	**2**
Major elements wt %															
SiO_2	63.08	63.66	61.09	69.08	65.80	73.01	67.91	68.68	71.98	71.88	65.06	64.35	70.32	71.35	68.16
TiO_2	0.77	0.73	0.84	0.44	0.56	0.10	0.48	0.48	0.27	0.26	0.64	0.57	0.32	0.21	0.47
Al_2O_3	16.40	16.12	16.35	15.47	16.04	14.65	16.16	15.76	15.07	15.22	15.50	16.23	15.10	15.39	15.73
Fe_2O_3	2.35	2.19	2.40	2.58	1.66	0.28	1.48	1.64	0.95	0.85	1.74	1.70	1.11	0.00	2.61
FeO	1.84	1.87	2.07		1.41	0.30	1.12	0.99	0.74	0.76	1.58	1.66	0.64	1.33	
MnO	0.07	0.07	0.09	0.05	0.06	0.02	0.06	0.06	0.05	0.05	0.06	0.07	0.04	0.04	0.06
MgO	2.93	2.88	3.12	1.39	2.12	0.41	1.65	1.56	0.93	0.61	2.46	2.50	1.04	0.97	1.47
CaO	4.02	4.00	4.38	2.32	3.78	0.47	1.63	1.56	1.08	1.20	2.97	3.83	1.25	0.90	2.74
K_2O	3.71	3.55	3.38	4.27	4.15	5.12	4.50	4.60	4.26	4.27	3.75	3.50	4.33	4.70	4.36
Na_2O	4.02	4.14	5.42	3.89	3.39	3.92	4.38	4.04	4.16	4.40	3.63	3.96	4.19	3.84	3.90
P_2O_5	0.30	0.28	0.34	0.21	0.28	0.08	0.22	0.22	0.13	0.14	0.23	0.30	0.21	0.10	0.21
LoI	0.00	0.00	0.00		0.00	1.20	0.00	0.00	0.00	0.00	1.20	1.20	1.20	2.00	
Total	99.49	99.49	99.48	99.70	99.25	99.56	99.59	99.59	99.62	99.64	98.82	99.87	99.75	100.83	99.71
Trace elements (ppm)															
Nb	13	12	14	10	12	7	10	11	11	10	7	10	7	7	
Zr	173	188	191	151	62	45	97	162	127	100	127	96	107	94	
Y	15	15	16	12	11	3	12	12	11	11	12	15	11	10	
Sr	725	689	765	495	818	153	526	592	247	275	634	902	237	186	
Rb	133	134	129	174	126	268	165	187	234	243	140	120	177	245	
Th	17	15	18	17	7	0	19	23	14	1	29	20	18	13	
Zn	58	56	62	46	52	23	52	46	47	53	52	56	45	50	
Cu	14	15	6	2	15	7	44	6	4	13	10	14	10	7	
Ni	37	34	34	18	31	5	23	20	5	6	31	40	13	7	
Cr	79	68	73	35	42	0	36	37	13	1	48	53	13	2	
V	99	93	104	48	74	10	54	53	28	24	75	78	32	21	
Ba	867	962	1009	733	1231	631	1118	971	508	577	880	1333	876	662	
Ce	96	91	104	73	97	22	65	80	57	47	79	97	59	41	
La	46	46	52	37	63	14	48	39	23	30	63	65	40	26	
Sc															
Nd															
U															
Pb															
M†	2.24	2.26	2.62	1.67	2.06	1.16	1.50	1.46	1.30	1.36	1.86	2.11	1.38	1.22	
T(zrc sat)/°C†	734	739	716	762	669	701	738	783	774	750	734	697	754	755	

	This study								
Sample	**10_07**	**09_17**	**09_18**	**09_21**	**09_22**	**09_19**	**09_20**	**10_08**	**10_50**
Zone	**1**	**1**	**2**	**3**	**4**	**4**	**5**	**5**	**4**
Major elements wt %									
SiO_2	58.85	63.92	66.04	69.52	68.81	71.65	71.21	72.51	69.74
TiO_2	0.96	0.58	0.53	0.36	0.31	0.23	0.16	0.23	0.37
Al_2O_3	16.99	15.75	15.33	15.10	14.13	14.67	15.23	14.58	14.97
Fe_2O_3	5.29	3.60	3.04	2.10	1.98	1.56	1.19	1.54	2.16
FeO									4.99
MnO	0.10	0.06	0.05	0.04	0.05	0.03	0.02	0.04	0.05
MgO	3.48	2.51	1.97	0.93	1.09	0.72	0.39	0.78	1.29
CaO	4.30	3.82	2.67	2.02	1.05	0.56	0.49	0.60	1.26
K_2O	2.92	3.35	3.86	4.20	4.20	4.37	4.94	4.51	4.99
Na_2O	4.60	4.12	3.99	3.84	3.68	3.83	3.72	3.85	3.52
P_2O_5	0.38	0.29	0.26	0.17	0.15	0.13	0.11	0.11	0.18
LoI	1.51	1.05	1.10	0.91	2.72	1.17	1.67	0.82	0.90
Total	99.38	99.05	98.84	0.00	98.16	98.92	99.13	99.57	99.43

	This study								
Sample	**10_07**	**09_17**	**09_18**	**09_21**	**09_22**	**09_19**	**09_20**	**10_08**	**10_50**
Zone	**1**	**1**	**2**	**3**	**4**	**4**	**5**	**5**	**4**
Trace elements (ppm)									
Nb	18	11	11	10	11	10	9	9	
Zr	215	146	140	129	124	101	74	104	
Y	26	11	9	8	9	8	8	8	
Sr	784	927	583	415	292	160	177	237	
Rb	98	129	147	185	212	238	262	234	
Th	9	14	12	12	14	11	6	9	
Zn	66	50	46	42	38	40	21	35	
Cu	9	8	8	8	6	15	3	11	
Ni	35	34	20	6	3	0	0	1	
Cr	49	36	15	0	0	0	0	0	
V	110	70	53	33	25	17	13	22	
Ba	837	977	841	715	505	377	387	427	
Ce	89	84	67	52	49	39	34	0	
La	41	50	42	28	26	16	15	0	
Sc	12	8	6	4	4	2	0	3	
Nd	42	32	23	21	20	14	15	0	
U	3	5	4	3	2	8	4	5	
Pb	21	29	27	38	29	28	43	30	

FLEET	*Ed Stephens (pers. comm.)*															*This study*			
Sample	**58-76**	**61-75**	**49-67**	**54-66**	**63-75**	**53-65**	**62-68**	**50-68**	**54-68**	**59-69**	**59-71**	**56-68**	**52-66**	**56-70**	**57-69**	**10_12**	**09_33**	**09_34**	**09_35**
Major elements wt %																			
SiO_2	68.43	69.39	70.22	71.33	71.92	72.04	72.22	72.92	73.22	73.83	74.18	74.25	75.37	75.65	76.23	73.77	68.78	71.24	
TiO_2	0.51	0.41	0.4	0.27	0.33	0.27	0.28	0.3	0.15	0.16	0.14	0.16	0.17	0.11	0.06	0.16	0.45	0.30	
Al_2O_3	15.79	15.36	14.72	14.93	14.89	14.43	14.55	14.69	14.45	14.89	14.63	15.14	13.21	15.35	14.81	14.18	14.51	14.21	
Fe_2O_3	2.86	2.69	2.28	1.72	1.92	1.68	1.78	1.82	1.22	1.2	1.08	1.13	1.02	0.8	0.63	1.21	2.57	1.81	
MnO	0.05	0.06	0.05	0.05	0.05	0.05	0.05	0.05	0.05	0.04	0.05	0.04	0.03	0.04	0.05	0.04	0.04	0.05	
MgO	1.03	0.89	0.73	0.56	0.45	0.39	0.51	0.49	0.3	0.09	0.09	0.05	0.17	0	0	0.38	1.18	0.60	
CaO	1.89	1.45	1.66	1.09	1.58	1.14	0.77	0.99	0.41	0.83	0.65	0.6	0.92	0.59	0.35	0.41	1.28	1.06	
Na_2O	2.91	3.09	3.8	3.14	3.62	3.36	3.64	3.51	3.37	3.44	3.86	3.29	3	3.56	4.39	3.25	3.07	3.15	
K_2O	4.91	5.56	4.96	5.4	4.77	5.01	5.26	5.51	5.23	5.07	5.19	5.5	4.89	4.86	4.39	5.38	4.93	5.07	
P_2O_5	0.17	0.16	0.15	0.11	0.12	0.14	0.11	0.13	0.09	0.12	0.09	0.14	0.1	0.15	0.13	0.11	0.16	0.13	
LoI	1.2	0.8	0.4	1.6	0.8	1	0.8	0.4	0.6	0.4	0.4	1	0.8	1	0.2	0.76	1.36	1.04	
Total	99.96	100.05	99.53	100.33	100.59	99.64	100.12	100.96	99.2	100.18	100.46	101.4	99.77	102.2	101.3	99.66	100.64	100.28	
Trace elements (ppm)																			
Nb	13	12	16	11	15	13	15	12	10	9	15	8	8	10	18	13	15	14	11
Zr	244	240	203	136	164	136	160	151	87	93	82	81	91	58	20	103	229	144	94
Y	15	11	16	13	17	14	18	14	9	8	14	7	13	7	2	15	15	20	12
Sr	282	242	223	164	194	141	232	221	107	110	97	116	104	117	29	113	208	165	102
Rb	212	239	259	299	264	307	272	301	311	286	317	339	256	310	432	258	261	277	267
Th	25	24	24	21	28	18	29	24	17	17	20	15	16	11	4	17	28	22	19
Zn	60	59	58	50	48	50	51	53	40	45	41	53	34	41	23	36	45	45	31
Cu	13	14	8	7	8	5	7	9	2	6	6	8	5	5	5	7	9	7	4
Ni	10	11	11	8	7	8	6	7	6	7	6	5	6	6	4	2	3	0	0
Cr	12	7	10	0	0	0	0	0	0	0	0	0	0	0	0	0	0	0	0
V	47	41	38	25	29	23	28	30	17	15	14	10	17	11	9	10	36	21	4
Ba	898	759	563	451	441	387	484	473	373	358	288	268	231	196	0	462	676	427	428
Ce	168	145	96	78	96	78	99	97	62	62	52	60	50	40	25	39	85	83	46
La	96	79	55	42	51	41	53	50	33	29	25	27	25	14	2	18	47	42	24
Hf	6	5	6	4	5	3	4	4	3	3	3	3	3	3	2				
Pb	17	30	30	35	35	27	40	34	36	42	42	38	35	33	16				
$M^{\dagger}$	1.42	1.39	1.55	1.27	1.44	1.31	1.25	1.32	1.09	1.18	1.21	1.11	1.25	1.06			1.34	1.29	
T(zrc sat)/$^{o}C^{\dagger}$	823	823	796	782	785	778	797	787	757	756	744	750	750	727	714	856	823	785	

SHAP	***This study***		
Sample	**09_23**	**09_32**	**09_26**
Major elements wt %			
SiO_2	66.98	69.054	59.74
TiO_2	0.63	0.54366	1.674
Al_2O_3	14.47	14.3208	13.79
Fe_2O_3	2.72	2.4684	4.78
MnO	0.064	0.04692	0.112
MgO	1.41	1.2954	3.3
CaO	2.03	1.7646	2.71
Na_2O	5.039	4.75932	4.82
K_2O	3.35	3.4476	3.08
P_2O_5	0.273	0.2346	0.806
LoI	1.01	1.45	1.85
Total	100.423456	32.0087063	100.963044
Trace elements (ppm)			
Nb	17.3	16	29.2
Zr	193	193.5	477.4
Y	15.1	14.8	20.1
Sr	510.7	371.7	455.8
Rb	239.3	251.7	259.3
Th	28.1	30.8	38.1
Zn	41	27	94.4
Cu	6.7	5.6	10.7
Ni	12.6	10.7	46.2
Cr	7.7	2.4	58.4
V	51.3	41.2	104.3
Ba	737.8	534.8	1208.7
Ce	122	107.6	265.2
La	68	61.9	149.2
Sc	6.1	4.5	7.9
Nd	43.2	41.2	94.9
U	4	9.7	8.4
Pb	40.1	38.8	35.4
$M^{\dagger}$	1.22	1.45	1.39
T(zrc sat)/$^{o}C^{\dagger}$	817	799	891

Appendix E

Criffell pluton apatite compositions

SX 100 electron probe and ims 4f ion probe (italic) results. EPMA concentrations converted to ppm from oxide wt%.

Abbreviations: Zrc- zircon, Hb – hornblende, Bt – biotite, K-Spar – K feldspar, Qtz – Quartz, Plag – Plagioclase.

Zone	Sample	Host	F	Na	Ca	P	Si	Mg	Cl	Mn	Fe	Sr	Y	La	Ce
1	17A_2	**Zrc**	25872	136	379757	173257	5804	39	391	246	101	737	330	492	1423
	17A_25	**Zrc**	28957	75	386385	181404	1716	21	51	281	148	711	269	1855	3352
	17A_43	**Zrc**	23658	554	390118	176133	1786	47	337	323	245	462	155	1109	2150
	17A_43_2	**Zrc**	25805	172	390415	177065	1592	43	147	433	158	459	367	1444	2916
	17A_60	**Zrc**	29115	189	386571	176680	3252	52	306	426	6	503	358	970	2228
	17A_93	**Zrc**	*26900*	*521*	*400220*	*195500*	*3951*		*954*			*536*	*388*	*1357*	*3058*
	17A_93_2	**Zrc**	*29838*	*502*	*400220*	*213520*	*2781*		*903*			*501*	*385*	*1314*	*3010*
	17A_43	**Zrc**	*27660*	*366*	*400220*	*215380*	*2724*		*483*			*506*	*265*	*1142*	*2503*
	17A_65	**Zrc**	28519	152	391341	182849	1041	50	158	288	129	692	125	761	1588
	17A_hb1	**Hb**	29582	210	388092	179203	2246	45	547	430	1941	368	566	1779	3979
	17A_hb2	**Hb**	28528	337	387427	179467	1815	62	465	382	2796	546	386	1563	3356
	17A_hb3	**Hb**	27300	182	388699	180215	1478	40	654	582	1639	555	299	1849	3533
	17A_hb4	**Hb**	28715	280	388544	180399	1408	65	593	423	2573	504	299	1429	2763
	17A_hb5	**Hb**	27213	819	388302	179528	1641	42	709	433	2433	523	263	1373	2567
	17A_hb6	**Hb**	27564	100	390213	179617	1498	34	384	439	1717	621	335	1101	2423
	17A_hb7	**Hb**	32125	29	392403	180358	334	15	155	323	720	588	200	277	573
	17A_hb8	**Hb**	*30311*	*279*	*400220*	*212920*	*2383*		*591*			*447*	*295*	*1122*	*2478*
	17A_hb9	**Hb**	*32059*	*428*	*400220*	*213580*	*2383*		*583*			*450*	*267*	*1260*	*2735*
	17A_hb10	**Hb**	*31494*	*182*	*400220*	*214400*	*2765*		*359*			*438*	*372*	*1259*	*2829*
	17A_bt1	**Bt**	25570	330	388246	178542	1390	39	816	417	1546	551	444	1879	3931
	17A_bt3	**Bt**	29884	277	388215	178135	1272	98	574	501	4592	228	434	956	2157
	17A_bt4	**Bt**	27470	240	387306	178242	1746	73	620	454	3784	357	662	1386	2917
	17A_bt5	**Bt**	29256	503	387903	179523	1600	141	560	377	3641	448	639	1220	2604
	17A_bt6	**Bt**	30038	659	391080	181337	804	38	412	305	3107	505	14	404	521
	17A_bt7	**Bt**	26187	355	387192	176239	1483	30	623	503	2367	308	582	1484	3085
	17A_bt8	**Bt**	*28405*	*345*	*400220*	*214420*	*3636*		*840*			*378*	*262*	*714*	*1576*
	17A_bt9	**Bt**	*27977*	*251*	*400220*	*211850*	*2317*		*1054*			*389*	*328*	*1414*	*3040*
	17A_bt10	**Bt**	*28930*	*247*	*400220*	*215550*	*1947*		*610*			*382*	*210*	*646*	*1378*
	17A_bt11	**Bt**	*28999*	*399*	*400220*	*213140*	*2274*		*659*			*362*	*417*	*973*	*2229*
	17A_bt12	**Bt**	*28726*	*186*	*400220*	*219290*	*1300*		*686*			*359*	*193*	*482*	*1083*
	17A_bt13	**Bt**	*31169*	*297*	*400220*	*217830*	*44811*		*478*			*362*	*489*	*1045*	*2412*
	17A_kspar1	**K-Spar**	27101	264	384994	179702	1905	7	616	397	204	519	273	1954	3156
	17A_kspar2	**K-Spar**	30989	429	385206	179046	6389	97	520	369	258	668	258	766	1858
	17A_kspar3	**K-Spar**	28277	567	376551	172911	4828	29	303	422	249	324	594	1328	2992
	17A_kspar4	**K-Spar**	31288	84	389823	179764	1212	50	434	351	1060	522	291	953	1953
	17A_kspar5	**K-Spar**	28819	431	388481	180705	1653	44	543	368	291	653	246	1788	3013
	17A_qtz1	**Qtz**	32299	395	376136	171682	7172	56	806	397	202	423	307	1833	3358
	17A_qtz2	**Qtz**	26245	172	390436	180415	1250	2	409	418	142	234	1605	683	1903
	17A_qtz3	**Qtz**	30882	98	391880	180030	890	40	499	387	793	573	143	416	889
	17A_qtz4	**Qtz**	*29591*	*252*	*400220*	*207140*	*3784*		*946*			*463*	*572*	*2677*	*5519*
	17A_qtz5	**Qtz**	*28019*	*254*	*400220*	*212140*	*2121*		*879*			*470*	*253*	*1400*	*2785*
	17A_qtz6	**Qtz**	*29572*	*387*	*400220*	*213420*	*28071*		*706*			*434*	*258*	*802*	*1915*
	17A_qtz7	**Qtz**	*30997*	*595*	*400220*	*215230*	*2160*		*744*			*443*	*230*	*943*	*2013*
	17A_plag2	**Plag**	33497	339	388630	178708	1728	0	338	299	123	528	324	1526	3132
	17A_plag3	**Plag**	26143	181	386707	176832	2046	31	564	190	26	454	407	1467	3006
	17A_plag4	**Plag**	30964	1056	386959	176177	1916	44	563	500	769	390	267	1100	2491
	17A_plag5	**Plag**	31505	329	387340	174941	2274	96	683	509	1588	491	496	1825	3900

Zone	Sample	Host	F	Na	Ca	P	Si	Mg	Cl	Mn	Fe	Sr	Y	La	Ce
2	18A_10	**Zrc**	19470	1521	374526	174934	23336	34	2876	471	144	259	344	1093	1922
	18A_10_2	**Zrc**	25285	759	381673	174845	1828	44	3349	628	237	473	194	1156	1971
	18A_19	**Zrc**	29324	87	389478	182131	914	47	298	525	146	433	193	1468	2105
	18A_19_2	**Zrc**	19646	353	383110	178220	3981	100	3483	1076	313	614	335	1636	3423
	18A_68	**Zrc**	30808	697	387715	176258	1742	61	319	531	282	316	382	1300	2022
	18A_60	**Zrc**	28916	685	391224	178546	1808	75	320	518	107	179	220	1115	1903
	18A_77	**Zrc**	21991	428	383472	175888	1357	97	3629	861	328	606	243	1297	2961
	18A_80	**Zrc**	27138	238	388586	183054	1094	55	350	362	202	392	306	1289	2197
	18A_86	**Zrc**	24578	1033	375955	172005	12391	42	3252	789	158	308	325	1191	2279
	18A_68	**Zrc**	*31212*	*422*	*400220*	*215550*	*5807*		*287*			*319*	*239*	*1196*	*2111*
	18A_hb1	**Hb**	33349	251	388428	178905	663	101	361	748	1631	427	231	1781	2019
	18A_hb2	**Hb**	34768	433	388253	176202	825	184	205	583	2650	468	369	1477	2397
	18A_hb3	**Hb**	*29615*	*272*	*400220*	*230070*	*1482*		*451*	*514*		*322*	*165*	*1189*	*1873*
	18A_hb4	**Hb**	*28525*	*268*	*400220*	*227950*	*1695*		*697*	*465*		*322*	*203*	*1316*	*2179*
	18A_bt1	**Bt**	31811	337	389920	179817	629	47	570	531	714	399	183	1506	1808
	18A_bt2	**Bt**	35845	591	391089	179843	690	11	25	336	1115	406	109	625	532
	18A_bt3	**Bt**	31271	439	389405	178948	841	73	198	471	3418	412	46	850	1206
	18A_bt4	**Bt**	40692	1230	387215	177118	1096	0	304	478	1354	414	26	755	729
	18A_bt5	**Bt**	33644	334	388705	179756	949	51	324	562	3297	332	182	1351	1518
	18A_bt6	**Bt**	36945	17	391017	181883	304	63	172	564	3121	399	0	781	939
	18A_bt7	**Bt**	33644	340	390199	180478	452	27	370	617	1789	355	164	1247	1423
	18A_bt8	**Bt**	26909	286	390323	178625	679	65	597	506	542	325	205	1368	2264
	18A_bt9	**Bt**	33886	233	389617	173961	914	95	292	536	1874	362	246	1594	2165
	18A_bt10	**Bt**	32557	163	389159	176232	1091	32	430	651	581	459	258	2053	3105
	18A_bt11	**Bt**	28512	442	384248	173859	6068	97	195	456	4076	351	22	588	873
	18A_bt12	**Bt**	24761	235	388576	175820	1363	66	524	523	2155	356	469	2187	3608
	18A_bt13	**Bt**	34839	70	389069	176308	834	6	297	564	2442	281	152	1595	1773
	18A_bt14	**Bt**	28088	251	388573	174894	1045	113	383	505	3809	443	175	1304	1745
	18A_bt15	**Bt**	40078	504	393409	186021	830	86	397	508	3776	344	59	1241	690
	18A_bt16	**Bt**	39054	493	390575	180663	1075	91	715	533	2357	427	154	1345	1026
	18A_bt17	**Bt**	*28442*	*209*	*400220*	*226780*	*1328*		*705*	*432*		*336*	*149*	*1142*	*1956*
	18A_bt18	**Bt**	*30829*	*179*	*400220*	*230240*	*1426*		*294*	*404*		*341*	*79*	*858*	*1351*
	18A_bt19	**Bt**	*27458*	*351*	*400220*	*227090*	*1157*		*832*	*579*		*319*	*105*	*956*	*1566*
	18A_bt20	**Bt**	*28588*	*286*	*400220*	*224690*	*1602*		*665*	*506*		*323*	*194*	*1415*	*2507*
	18A_bt21	**Bt**	*28895*	*264*	*400220*	*226290*	*1928*		*699*	*520*		*330*	*186*	*1644*	*2725*
	18A_bt22	**Bt**	*29579*	*647*	*400220*	*227330*	*1726*		*677*	*494*		*348*	*94*	*1031*	*1577*
	18A_bt23	**Bt**	*30782*	*584*	*400220*	*228070*	*1721*		*311*	*356*		*355*	*82*	*606*	*1006*
	18A_bt24	**Bt**	*30563*	*554*	*400220*	*228280*	*2520*		*209*	*372*		*348*	*89*	*612*	*1027*
	18A_bt25	**Bt**	*30967*	*1174*	*400220*	*227220*	*2054*		*607*	*373*		*349*	*93*	*811*	*1349*
	18A_bt26	**Bt**	*30017*	*1365*	*400220*	*228120*	*1577*		*559*	*429*		*349*	*52*	*593*	*874*
	18A_bt27	**Bt**	*28950*	*208*	*400220*	*228570*	*1879*		*581*	*503*		*321*	*154*	*1508*	*2440*
	18A_bt28	**Bt**	*27979*	*200*	*400220*	*229100*	*1737*		*733*	*522*		*320*	*153*	*1459*	*2400*
	18A_bt29	**Bt**	*28783*	*194*	*400220*	*230980*	*3392*		*586*	*500*		*328*	*106*	*1200*	*1843*
	18A_bt30	**Bt**	*28215*	*238*	*400220*	*229320*	*1806*		*695*	*567*		*323*	*169*	*1519*	*2494*
	18A_bt31	**Bt**	*30909*	*250*	*400220*	*236530*	*1378*		*501*	*527*		*313*	*95*	*1033*	*1646*
	18A_kspar1	**K-Spar**	32790	1036	389542	177334	1171	0	181	552	316	349	152	569	780
	18A_kspar2	**K-Spar**	28767	106	391589	182246	501	6	238	565	513	365	194	934	1202
	18A_kspar3	**K-Spar**	38594	213	389848	177616	575	26	131	527	152	352	69	1302	1362
	18A_kspar4	**K-Spar**	31037	78	388922	177581	1528	4	309	433	201	320	125	1016	1165
	18A_kspar5	**K-Spar**	40058	419	393842	182507	1193	78	410	533	273	317	169	2067	1877
	18A_kspar6	**K-Spar**	34509	501	388505	174587	1398	0	128	605	104	411	287	2290	2796
	18A_qtz1	**Qtz**	28382	702	389489	176002	2828	47	191	363	543	303	174	1340	2022
	18A_qtz2	**Qtz**	28389	1188	389245	176305	784	37	793	443	284	345	164	928	1171
	18A_qtz3	**Qtz**	26596	695	387094	176038	664	63	1054	577	59	308	125	1294	1765
	18A_qtz4	**Qtz**	31355	488	390533	178748	880	0	295	705	304	346	187	1559	2447
	18A_qtz5	**Qtz**	28775	760	385733	168462	15888	21	813	421	100	246	255	1055	1986
	18A_qtz6	**Qtz**	43716	504	391040	182872	968	71	374	514	1314	285	216	1680	1321
	18A_qtz7	**Qtz**	40814	320	387509	183615	1104	68	261	457	716	380	35	1529	1331
	18A_qtz8	**Qtz**	*30097*	*1030*	*400220*	*229530*	*1989*		*930*	*448*		*340*	*83*	*820*	*1271*
	18A_qtz9	**Qtz**	*29920*	*835*	*400220*	*230400*	*1590*		*759*	*418*		*342*	*69*	*651*	*1007*
	18A_plag1	**Plag**	35719	225	390529	181877	278	13	243	441	212	304	151	898	1048

Zone	Sample	Host	F	Na	Ca	P	Si	Mg	Cl	Mn	Fe	Sr	Y	La	Ce
3	21A_40	**Zrc**	23348	837	385979	180338	2729	147	2350	938	401	120	61	1144	1863
	21A_48	**Zrc**	26959	762	382525	179685	1234	196	1909	921	417	674	352	982	1323
	21A_60	**Zrc**	21350	1017	381729	175742	1521	108	4502	1306	455	690	262	1614	2925
	21A_74	**Zrc**	28122	286	388030	183870	459	111	782	1634	336	157	387	748	1770
	21A_78	**Zrc**	24958	840	382121	175977	2119	62	4277	1870	360	576	560	1577	3235
	21A_89	**Zrc**	24037	272	388494	180547	772	85	1739	1344	425	362	65	906	1338
	21A_74	**Zrc**	*27590*	*512*	*400220*	*212790*	*5244*		*697*			*195*	*619*	*913*	*2458*
	21A_74	**Zrc**	*27960*	*389*	*400220*	*215440*	*1430*		*649*			*190*	*475*	*747*	*1978*
	21A_96	**Zrc**	22714	438	377872	181983	664	86	2216	1522	347	479	414	775	1971
	21A_bt1	**Bt**	33542	393	386164	178078	1053	79	54	1264	2102	201	1599	731	1482
	21A_bt2	**Bt**	36345	1691	380369	174044	1063	54	164	1442	1579	195	1715	791	1844
	21A_bt3	**Bt**	34595	1603	385063	178291	739	175	203	1565	1525	129	1596	827	2052
	21A_bt4	**Bt**	36847	618	383756	177674	995	153	63	1480	1808	387	3107	472	1265
	21A_bt5	**Bt**	32392	307	386676	175385	531	85	95	1200	2696	135	1418	484	1014
	21A_bt6	**Bt**	36136	400	385320	177861	759	191	142	1325	1851	151	1497	1079	2354
	21A_bt7	**Bt**	39904	2142	379905	171189	1539	72	96	1268	2545	192	2306	1031	2516
	21A_bt8	**Bt**	37408	665	385686	175909	358	129	112	1254	4095	233	1287	760	1395
	21A_bt9	**Bt**	39045	492	387661	175045	167	57	82	1197	689	205	1160	691	1183
	21A_bt10	**Bt**	35684	851	375903	171228	969	117	96	1251	666	181	1663	833	1973
	21A_bt11	**Bt**	34484	2643	383401	175527	931	107	181	1267	2101	258	954	819	1268
	21A_bt12	**Bt**	31186	947	389274	180593	470	81	36	1440	2284	308	824	890	994
	21A_bt13	**Bt**	32457	913	384934	174489	496	76	51	1221	2600	203	895	694	808
	21A_bt14	**Bt**	30866	1096	386535	175513	621	108	56	1338	2478	291	1096	651	1032
	21A_bt15	**Bt**	27851	872	384553	176977	794	114	79	1185	3307	276	1142	651	1133
	21A_bt16	**Bt**	27521	676	392152	178708	313	78	159	1120	711	132	736	1034	824
	21A_bt17	**Bt**	31590	634	384989	174891	713	91	87	1402	2314	124	1099	710	1373
	21A_bt18	**Bt**	30854	937	389900	176456	239	88	116	1259	2411	317	684	631	669
	21A_bt19	**Bt**	33597	2264	386743	169709	762	108	106	1203	3885	170	824	917	812
	21A_bt20	**Bt**	32008	833	389610	170506	508	97	157	1281	1118	197	808	916	1007
	21A_bt21	**Bt**	31470	992	389055	169739	366	74	0	1096	2311	168	620	669	877
	21A_bt22	**Bt**	30463	1447	387676	167954	929	289	48	981	4741	115	747	356	594
	21A_bt23	**Bt**	*72859*	*737*	*400220*	*209170*	*645*		*313*			*362*	*1511*	*249*	*1222*
	21A_bt24	**Bt**	*74845*	*1034*	*400220*	*203680*	*2183*		*371*			*428*	*2725*	*399*	*2143*
	21A_bt25	**Bt**	*72894*	*1016*	*400220*	*204400*	*2500*		*339*			*467*	*2537*	*339*	*1852*
	21A_bt26	**Bt**	*73373*	*979*	*400220*	*207290*	*1535*		*358*			*388*	*2196*	*383*	*1885*
	21A_kspar1	**K-Spar**	38127	1821	379200	181630	8830	92	133	1212	256	226	1562	698	1880
	21A_kspar2	**K-Spar**	32469	708	380541	173391	1147	48	122	1339	429	177	1567	537	1247
	21A_kspar3	**K-Spar**	34875	1197	384954	177123	1220	8	57	1206	199	224	1824	484	1620
	21A_kspar4	**K-Spar**	39760	894	385933	177321	503	57	65	1153	661	223	1384	692	1317
	21A_kspar5	**K-Spar**	33582	673	387551	180461	886	43	106	1266	227	156	1389	726	1650
	21A_kspar6	**K-Spar**	25513	989	391202	180908	438	98	95	1255	781	131	803	673	1160
	21A_kspar7	**K-Spar**	26336	712	386706	176331	337	109	156	1481	505	351	342	827	939
	21A_kspar8	**K-Spar**	30432	671	387281	173107	1418	87	54	985	174	201	681	501	536
	21A_kspar9	**K-Spar**	44932	1843	383431	173956	1145	18	158	1167	171	226	513	795	1652
	21A_kspar10	**K-Spar**	30542	2424	384925	173412	852	100	177	1488	382	332	865	884	1136
	21A_kspar11	**K-Spar**	*72423*	*638*	*400220*	*210430*	*992*		*425*			*188*	*913*	*556*	*1886*
	21A_kspar12	**K-Spar**	*71766*	*552*	*400220*	*211130*	*1308*		*300*			*191*	*1334*	*376*	*1506*
	21A_kspar13	**K-Spar**	*71807*	*685*	*400220*	*207250*	*1795*		*413*			*188*	*1636*	*700*	*2356*
	21A_kspar14	**K-Spar**	*78198*	*609*	*400220*	*211950*	*1214*		*240*			*193*	*1343*	*294*	*1342*
	21A_kspar15	**K-Spar**	*74074*	*645*	*400220*	*207710*	*1272*		*375*			*196*	*1366*	*388*	*1521*
	21A_qtz1	**Qtz**	29453	545	385303	175479	887	93	99	1275	140	351	1176	647	1088
	21A_qtz2	**Qtz**	32874	957	376493	155329	2101	77	871	1314	463	245	1656	493	1925
	21A_qtz3	**Qtz**	33709	564	386944	174877	1453	4	58	1140	144	233	1239	540	1090
	21A_qtz4	**Qtz**	30581	424	387047	175650	7309	53	55	1099	844	246	1165	390	1019
	21A_qtz5	**Qtz**		*970*	*400220*	*208740*	*1710*					*372*	*2285*	*402*	*1974*
	21A_qtz6	**Qtz**		*1066*	*400220*	*206530*	*20207*					*416*	*2142*	*298*	*1586*
	21A_qtz7	**Qtz**	*74736*	*1002*	*400220*	*204670*	*1349*		*330*			*362*	*1848*	*341*	*1650*
	21A_qtz8	**Qtz**	*72782*	*2018*	*400220*	*201380*	*2748*		*531*			*403*	*2550*	*406*	*2051*
	21A_qtz9	**Qtz**	*73335*	*1136*	*400220*	*204900*	*1860*		*355*			*408*	*2223*	*315*	*1694*
	21A_plag1	**Plag**	28445	965	388734	177360	549	96	55	1311	590	273	1012	770	957
	21A_plag2	**Plag**	35785	363	390040	179046	189	21	102	1426	248	360	276	743	1111
	21A_plag3	**Plag**	28650	588	389387	176042	373	104	459	1299	336	178	710	485	803
	21A_plag4	**Plag**	25636	776	388807	175592	363	98	336	1199	352	84	597	528	944
	21A_plag5	**Plag**	27973	760	392662	174314	433	72	209	1145	303	291	802	703	789

Zone	Sample	Host	F	Na	Ca	P	Si	Mg	Cl	Mn	Fe	Sr	Y	La	Ce
4	22A_7	**Zrc**	30604	748	383910	179590	1101	80	158	2991	258	263	2579	483	1203
	22A_7	**Zrc**	31101	791	382649	181451	1609	146	111	2778	450		2927	535	1169
	22A_7	**Zrc**	29551	415	382273	182235	1357	80	94	2861	628	164	3054	477	1345
	22A_7	**Zrc**	30581	663	358238	170958	1572	74	90	2808	546	74	2916	391	1263
	22A_31	**Zrc**	30459	395	384525	184140	570	124	354	3941	589	50	730	603	1590
	22A_62	**Zrc**	32651	629	382022	179003	1113	78	91	2834	515	96	2822	364	1231
	22A_bt1	**Bt**	30880	666	383824	173707	516	122	79	3570	2255	154	2076	559	1348
	22A_bt2	**Bt**	32693	909	384099	172502	518	214	103	4145	2065	181	1710	670	1805
	22A_bt3	**Bt**	26219	542	385965	182059	61	132	114	3957	1174	146	1506	353	815
	22A_bt4	**Bt**	36822	411	383529	181379	488	169	85	3676	4152	79	1930	628	1322
	22A_bt5	**Bt**	37149	883	380630	181345	901	153	114	3723	2446	132	2183	920	2101
	22A_bt6	**Bt**	38332	1110	382870	180401	541	93	134	2837	2167	222	1583	612	1303
	22A_bt7	**Bt**	32769	794	382675	179903	503	239	111	4164	1972	292	1971	839	1609
	22A_bt8	**Bt**	31956	397	382267	177858	1085	145	122	4181	4306	146	2836	713	1358
	22A_bt9	**Bt**	32396	661	386218	182307	248	115	116	2950	865	175	815	658	847
	22A_bt10	**Bt**	41217	884	382343	182150	151	217	106	3905	2892	242	1647	523	524
	22A_bt11	**Bt**	39379	1236	387007	180217	674	203	141	3665	2712	90	1956	509	804
	22A_bt12	**Bt**	38697	2187	380913	177679	1410	226	128	3373	4001	62	2567	425	684
	22A_bt13	**Bt**	39109	871	385768	181275	276	161	89	3275	3857	175	1927	196	443
	22A_bt14	**Bt**	39535	989	387977	178779	967	244	153	3963	1422	313	1225	1079	1325
	22A_bt15	**Bt**	39065	1226	382277	180038	734	310	181	4405	1577	186	1199	851	1123
	22A_bt16	**Bt**	37307	1169	389610	179981	212	146	123	3321	3310	37	1783	436	431
	22A_bt17	**Bt**	38273	1197	385048	176915	632	137	263	3304	890	31	2152	421	500
	22A_bt18	**Bt**	41772	2255	383056	176247	667	226	93	4205	1647	105	2142	554	763
	22A_bt19	**Bt**	39562	1278	379715	180113	836	235	158	4007	1667	132	2408	617	697
	22A_bt20	**Bt**	38186	930	383614	176985	661	159	89	3659	1426	181	2152	538	591
	22A_bt21	**Bt**	32351	717	384713	180021	420	175	90	3571	1190	33	1722	496	522
	22A_bt22	**Bt**	41456	1076	383221	178117	631	210	48	3876	1727		2144	713	785
	22A_bt23	**Bt**	37877	1271	383100	177972	639	221	100	4046	2258	177	2106	702	920
	22A_bt24	**Bt**	38477	1140	386604	180842	140	176	90	3815	1380	137	1497	419	396
	22A_kspar1	**K-Spar**	37528	395	386499	180643	243	166	110	3943	1244	140	1732	684	1309
	22A_kspar2	**K-Spar**	38077	517	383616	182101	72	168	135	3771	1476	204	1311	482	751
	22A_kspar3	**K-Spar**	30013	722	383133	180273	697	185	135	3557	506	94	2779	635	1756
	22A_kspar4	**K-Spar**	31133	654	383704	178722	445	140	124	3776	553	126	2208	667	1550
	22A_kspar5	**K-Spar**	34843	537	384866	180380	271	182	190	3740	629	147	1288	819	1333
	22A_kspar6	**K-Spar**	37372	1180	382796	178682	647	207	132	3354	525	301	965	838	1232
	22A_kspar7	**K-Spar**	42221	996	386767	177374	792	202	115	4032	1344	259	1257	958	971
	22A_kspar8	**K-Spar**	39610	1451	383790	180626	429	236	168	4286	1679	93	1729	469	614
	22A_kspar9	**K-Spar**	39050	470	388176	181460	583	304	255	1807	937	252	383	900	851
	22A_kspar10	**K-Spar**	36691	380	387773	179869	783	290	222	3473	1097	352	752	935	1184
	22A_kspar11	**K-Spar**	39472	1272	384153	179019	678	239	147	4178	1066	111	2005	732	855
	22A_kspar12	**K-Spar**	37883	1006	388560	180961	532	181	80	3842	786	230	1569	690	721
	22A_kspar13	**K-Spar**	39684	1602	385035	177979	896	133	268	3621	741	97	2290	762	892
	22A_kspar14	**K-Spar**	42522	1082	390086	179043	571	27	236	1713	550	174	1347	480	525
	22A_kspar15	**K-Spar**	40727	1978	385637	176276	950	149	186	2883	542	164	2384	616	522
	22A_kspar16	**K-Spar**	37639	1112	385653	179400	651	152	137	3258	641	86	2317	568	452
	22A_kspar17	**K-Spar**	42820	959	392602	181218	475	63	62	2016	379	206	1785	484	361
	22A_kspar18	**K-Spar**	38996	798	387830	180392	477	149	171	3614	755	202	1602	654	613
	22A_kspar19	**K-Spar**	39365	1141	390197	179313	398	345	40	3548	716	233	1665	545	501
	22A_qtz1	**Qtz**	37441	548	384432	173653	701	117	56	2886	800	188	2378	528	1131
	22A_plag1	**Plag**	34951	619	383359	180945	518	132	104	3937	751	154	2162	511	1281
	22A_plag2	**Plag**	27422	816	382627	181378	610	145	171	3985	516	164	1712	782	1914
	22A_plag3	**Plag**	37844	715	387982	179898	437	88	680	2264	433	389	571	668	513
	22A_plag4	**Plag**	40986	832	387257	180702	461	235	77	4205	1562	278	1746	790	710
	22A_plag5	**Plag**	37214	1058	381396	178404	395	209	122	4168	1588	114	1643	574	457
	22A_plag6	**Plag**	32990	418	385730	179330	413	250	79	3132	457	241	1552	842	1251

Zone	Sample	Host	F	Na	Ca	P	Si	Mg	Cl	Mn	Fe	Sr	Y	La	Ce
5	08A_bt1	Bt	*34639*	*839*	*400220*	*214430*	*961*		*45*			*123*	*2087*	*232*	*819*
	08A_bt2	Bt	*35096*	*1731*	*400220*	*213870*	*4891*		*48*			*132*	*2645*	*279*	*951*
	08A_bt3	Bt	*33617*	*632*	*400220*	*217460*	*775*		*64*			*137*	*1677*	*252*	*779*
	08A_bt4	Bt	*35375*	*582*	*400220*	*217930*	*14931*		*87*			*127*	*2129*	*193*	*669*
	08A_qtz1	Qtz	*35110*	*1481*	*400220*	*216870*	*2598*		*96*			*133*	*2218*	*178*	*667*
	08A_qtz2	Qtz	*34900*	*1277*	*400220*	*217390*	*1413*		*48*			*159*	*1627*	*323*	*1137*
	08A_qtz3	Qtz	*34338*	*675*	*400220*	*214550*	*588*		*57*			*139*	*1705*	*232*	*748*
	08A_qtz4	Qtz	*33147*	*640*	*400220*	*215830*	*659*		*74*			*137*	*1680*	*248*	*803*
	08A_qtz5	Qtz	*34662*	*1207*	*400220*	*217660*	*3224*		*119*			*130*	*1994*	*259*	*906*
	08A_qtz6	Qtz	*31709*	*699*	*400220*	*219970*	*77177*		*359*			*137*	*1399*	*115*	*443*

Electron probe two sigma analytical errors (ppm)

4000	350	5500	4000	50	40	120	150	130	200	140	200	200

Electron probe three sigma detection limits (ppm)

2737	359	433	1129	73	41	140	166	129	265	176	239	218

Apatite major, trace and REE element concentrations in the Criffell pluton (ims 4f ion microprobe).

Zone	1	1	1	1	1	1	1	1	1	1	1	1	1	1	1
Sample	17_93A.DAT	17_93A2.DAT	17_43A.DAT	17A_hb8	17A_hb9	17A_hb10	17A_bt8	17A_bt9	17A_bt10	17A_bt11	17A_bt12	17A_bt13	17A_qtz4	17A_qtz5	17A_qtz6	17A_qtz7
Host	Zrc	Zrc	Zrc	Hb	Hb	Hb	Bt	Bt	Bt	Bt	Bt	Bt	Qtz	Qtz	Qtz	Qtz
F	26900	29838	27660	30311	32059	31494	28405	27977	28930	28999	28726	31169	29591	28019	29572	30997
Na	521	502	366	279	428	182	345	251	247	399	186	297	252	254	387	595
Si	3951	2781	2724	2383	2383	2765	3636	2317	1947	2274	1300	44811	3784	2121	28071	2160
P	195500	213520	215380	212920	213580	214400	214420	211850	215550	213140	219290	217830	207140	212140	213420	215230
Cl	954	903	483	591	583	359	840	1054	610	659	686	478	946	879	706	744
Ca	400220	400220	400220	400220	400220	400220	400220	400220	400220	400220	400220	400220	400220	400220	400220	400220
Sr	536	501	506	447	450	438	378	389	382	362	359	362	463	470	434	443
Y	90	89	101	295	267	372	262	328	210	417	193	489	572	253	258	230
Zr	3827	278	368	1	1	2	1	1	1	1	0	2	5	2	1	1
Ba	6	1		1	1	0	3	0	2	1	2	52	0	0	1	0
La	1357	1314	1142	1122	1260	1259	714	1414	646	973	482	1045	2677	1400	802	943
Ce	3057	3010	2503	2478	2735	2829	1576	3040	1378	2229	1083	2412	5519	2785	1915	2013
Pr	350	339	260	272	286	313	171	314	148	246	121	271	556	278	217	208
Nd	1443	1386	1119	1108	1167	1356	705	1232	618	1044	526	1118	2211	1121	947	899
Sm	220	213	154	189	183	215	108	181	93	180	83	186	307	167	156	126
Eu	47	46	39	41	38	49	27	45	24	40	20	44	83	40	34	35
Gd	123	156	120	126	128	169	75	144	72	139	70	169	228	110	123	127
Tb	18	21	16	17	15	18	12	19	10	20	9	23	34	14	13	12
Dy	91	79	52	62	55	70	49	64	43	86	36	97	121	44	56	49
Ho	14	14	9	12	9	12	8	12	7	13	8	18	20	9	8	8
Er	42	40	24	25	21	27	23	28	17	31	16	40	49	25	23	22
Tm	5	5	3	4	3	4	3	4	3	5	3	7	7	3	2	2
Yb	40	37	26	21	21	28	21	31	18	33	11	37	41	18	22	19
Lu	5	5	2	3	2	4	3	4	2	3	2	4	6	3	3	3
Pb	107	73	40	41	66	29	66	71	86	133	62	122	84	101	37	53
Th	99	90	102	90	69	71	38	124	29	103	19	90	261	71	57	77
U	89	55	55	95	55	119	29	75	46	88	42	118	151	53	79	60

2SD analytical errors on analyses are ~ 10%

Zone	2	2	2	2	2	2	2	2	2	2	2	2	2	2	2	2	2	2
Sample	18_68A	18A_hb3	18A_hb4	18A_bt17	18A_bt18	18A_bt19	18A_bt20	18A_bt21	18A_bt22	18A_bt23	18A_bt24	18A_bt25	18A_bt26	18A_bt27	18A_bt28	18A_bt29	18A_bt30	18A_bt31	18A_qtz8	18A_qtz9
Host	Zrc	Hb	Hb	Bt	Bt	Bt	Bt	Bt	Bt	Bt	Bt	Bt	Bt	Bt	Bt	Bt	Bt	Bt	Qtz	Qtz
F	31212	29615	28525	28442	30829	27458	28588	28895	29579	30782	30563	30967	30017	28950	27979	28783	28215	30909	30097	29920
Na	422	272	268	209	179	351	286	264	647	584	554	1174	1365	208	200	194	238	250	1030	835
Si	5807	1482	1695	1328	1426	1157	1602	1928	1726	1721	2520	2054	1577	1879	1737	3392	1806	1378	1989	1590
P	215550	230070	227950	226780	230240	227090	224690	226290	227330	228070	228280	227220	228120	228570	229100	230980	229320	236530	229530	230400
Cl	287	451	697	705	294	832	665	699	677	311	209	607	559	581	733	586	695	501	930	759
Ca	400220	400220	400220	400220	400220	400220	400220	400220	400220	400220	400220	400220	400220	400220	400220	400220	400220	400220	400220	400220
Sr	319	322	322	336	341	319	323	330	348	355	348	349	349	321	320	328	323	313	340	342
Y	28	165	203	149	79	105	194	186	94	82	89	93	52	154	153	106	169	95	83	69
Zr	11811	1	1	1	0	0	1	1	1	1	1	2	0	1	1	1	1	0	1	0
Ba	1	6	7	4	4	5	7	12	4	5	5	5	4	8	7	8	9	7	6	4
La	1196	1189	1316	1142	858	956	1415	1644	1031	606	612	811	593	1508	1459	1200	1519	1033	820	651
Ce	2110	1873	2179	1956	1351	1566	2507	2725	1577	1006	1027	1349	874	2440	2400	1843	2494	1646	1271	1007
Pr	204	163	191	175	109	137	238	235	130	89	94	115	72	205	207	147	218	136	107	82
Nd	835	648	796	684	379	481	898	877	457	356	378	432	248	754	727	524	825	487	393	299
Sm	126	92	108	88	44	60	124	109	52	43	49	51	25	88	81	57	101	55	48	35
Eu	23	21	24	20	18	14	23	28	17	11	11	13	9	27	25	18	24	16	14	11
Gd	109	74	92	85	37	58	103	92	46	40	48	50	19	59	60	39	64	30	43	31
Tb	13	9	11	11	6	8	14	13	7	5	6	7	4	10	9	6	10	6	6	5
Dy	47	27	33	31	14	20	50	40	21	14	15	21	8	22	24	12	24	11	15	14
Ho	9	5	6	6	2	4	7	7	3	3	3	3	2	5	5	3	5	3	3	2
Er	21	13	15	11	6	9	16	16	7	7	8	9	3	10	10	6	12	6	8	6
Tm	2	1	1	1	1	1	2	2	1	1	1	1	0	1	1	1	1	1	1	1
Yb	17	13	14	15	5	8	13	16	9	5	7	10	5	10	11	8	10	8	7	5
Lu	2	1	1	2	1	1	2	2	1	1	1	1	0	1	0	0	1	0	1	0
Pb	73																			
Th	56	34	41	29	40	19	31	51	27	23	19	21	16	55	41	35	40	27	20	18
U	93	46	34	16	65	54	15	26	22	38	42	15	11	49	44	44	15	45	38	30

Zone	3	3	3	3	3	3	3	3	3	3	3	3	3	3	3
Sample	21_74A1.DAT	21_74A2.DAT	21A_qtz5	21A_qtz6	21A_qtz7	21A_qtz8	21A_qtz9	21A_bt23	21A_bt24	21A_bt25	21A_bt26	21A_kspar11	21A_kspar12	21A_kspar13	21A_kspar14	21A_kspar15
Host	Zrc	Zrc	Qtz	Qtz	Qtz	Qtz	Qtz	Bt	Bt	Bt	Bt	K-Spar	K-Spar	K-Spar	K-Spar	K-Spar
F	27590	27960			74736	72782	73335	72859	74845	72894	73373	72423	71766	71807	78198	74074
Na	512	389	970	1066	1002	2018	1136	737	1034	1016	979	638	552	685	609	645
Si	5244	1430	1710	20207	1349	2748	1860	645	2183	2500	1535	992	1308	1795	1214	1272
P	212790	215440	208740	206530	204670	201380	204900	209170	203680	204400	207290	210430	211130	207250	211950	207710
Cl	697	649			330	531	355	313	371	339	358	425	300	413	240	375
Ca	400220	400220	400220	400220	400220	400220	400220	400220	400220	400220	400220	400220	400220	400220	400220	400220
Sr	195	190	372	416	362	403	408	362	428	467	388	188	191	188	193	196
Y	41	32	2285	2142	1848	2550	2223	1511	2725	2537	2196	913	1334	1636	1343	1366
Zr	6345	433	1	1	1	2	1	1	3	2	2	1	1	1	1	1
Ba	2	1	2	2	1	3	2	3	4	4	6	3	2	4	1	1
La	913	747	402	298	341	406	315	249	399	339	383	556	376	700	294	388
Ce	2457	1978	1974	1586	1650	2051	1694	1222	2143	1852	1885	1886	1506	2356	1342	1521
Pr	341	275	406	347	338	431	363	256	467	404	392	290	257	374	240	261
Nd	1706	1363	2631	2310	2152	2884	2469	1689	3082	2753	2587	1483	1481	2104	1452	1518
Sm	381	313	920	847	754	1018	904	595	1052	1014	889	385	488	629	488	514
Eu	66	55	63	59	51	69	61	41	79	80	61	45	55	65	52	55
Gd	370	254	744	715	608	855	746	484	815	837	692	247	398	483	399	412
Tb	34	25	104	98	85	116	102	66	114	113	95	34	58	67	56	56
Dy	137	119	566	543	441	645	554	358	642	619	522	177	294	355	296	300
Ho	24	18	92	87	74	106	91	61	111	104	89	30	50	61	52	51
Er	49	37	202	189	169	226	198	129	247	112	65	72	113	136	116	115
Tm	7	7	26	24	22	30	26	17	33	14	8	11	15	18	16	16
Yb	45	42	168	150	135	189	166	115	211	85	39	85	119	140	118	121
Lu	6	6	15	15	13	19	15	10	20	5	0	8	12	15	12	12
Pb	43	44	226	195	164	260	216	229	242	104	61	64	129	125	149	122
Th	56	33	31	16	19	29	21	7	61	24	15	20	20	31	10	19
U	69	36	19	18	15	13	20	5	25	14	8	14	20	19	19	21

Zone	5	5	5	5	5	5	5	5	5	5
Sample	08A_bt1	08A_bt2	08A_bt3	08A_bt4	08A_qtz1	08A_qtz2	08A_qtz3	08A_qtz4	08A_qtz5	08A_qtz6
Host	Bt	Bt	Bt	Bt	Qtz	Qtz	Qtz	Qtz	Qtz	Qtz
F	34639	35096	33617	35375	35110	34900	34338	33147	34662	31709
Na	839	1731	632	582	1481	1277	675	640	1207	699
Si	961	4891	775	14931	2598	1413	588	659	3224	77177
P	214430	213870	217460	217930	216870	217390	214550	215830	217660	219970
Cl	45	48	64	87	96	48	57	74	119	359
Ca	400220	400220	400220	400220	400220	400220	400220	400220	400220	400220
Sr	123	132	137	127	133	159	139	137	130	137
Y	2087	2645	1677	2129	2218	1627	1705	1680	1994	1399
Zr	1	4	1	2	2	2	0	1	3	9
Ba	0	3	1	13	0	2	1	1	3	4
La	232	279	252	193	178	323	232	248	259	115
Ce	819	951	779	669	667	1137	748	803	906	443
Pr	136	165	129	120	123	186	119	129	156	80
Nd	803	968	764	696	740	1108	679	727	963	547
Sm	414	479	355	378	438	440	326	351	458	300
Eu	37	50	37	43	47	44	33	29	40	32
Gd	541	658	430	548	606	513	435	407	572	412
Tb	80	99	60	85	96	68	64	65	78	64
Dy	456	567	354	445	516	353	357	349	423	323
Ho	68	94	56	76	80	58	58	61	71	53
Er	114	139	82	102	130	84	88	115	109	77
Tm	19	22	15	17	21	14	16	17	17	11
Yb	123	167	98	112	125	99	103	115	117	73
Lu	9	12	5	7	8	6	6	9	6	4
Pb	35	19	37	19	30	29	23	99	60	90
Th	2	4	2	6	3	3	1	2	3	4
U	6	2	7	16	16	7	6	13	3	5

Appendix F

Zircon $\delta^{18}O$ compositions

Pluton	Zone	Sample	$^{18}O/^{16}O$	% 2SD	1 s.e.m	$\delta^{18}O$	2SD	1 s.e.m
Session 1 (26.01.2010)								
Shap	2	32_1c	0.002012			7.6		
	2	32_13c	0.002011			7.5		
	2	32_1r	0.002011			7.6		
	2	32_2m	0.002012			7.8		
	2	32_4m	0.002012			7.9		
	2	32_10c	0.002012			7.9		
	2	32_7c	0.002012			7.8		
	2	32_7r	0.002012			7.8		
	2	32_6c	0.002012			7.7		
	2	32_11c	0.002012			7.9		
		91500	0.002012	0.02499	0.004627	9.6	0.26	0.058138
Shap	2	32_12c	0.002011			7.3		
	2	32_14c	0.002011			7.7		
	2	32_14r	0.002015			9.7		
	2	32_20m	0.002011			7.5		
	2	32_18m	0.002011			7.6		
	2	32_18r	0.002011			7.8		
	2	32_16m	0.00201			7.2		
	2	32_21m	0.00201			7.3		
	2	32_22c	0.002011			7.4		
	2	32_25c	0.002012			7.9		
		91500	0.002011	0.027332	0.006112	9.5	0.44	0.100287
Shap	1	23_1c	0.002012			7.9		
	1	23_4c	0.002011			7.3		
	1	23_4m	0.002012			8.1		
	1	23_5r	0.002012			7.8		
	1	23_10m	0.002012			8.0		
	1	23_8m	0.002012			7.9		
	1	23_7c	0.002011			7.3		
	1	23_12r	0.002012			7.7		
	1	23_14m	0.002012			7.7		
	1	23_18m	0.002012			7.9		
	1	23_17c	0.002012			7.8		
	1	23_17r	0.002012			8.0		
	1	23_16c	0.002012			7.7		
	1	23_28m	0.002012			7.8		
	1	23_26c	0.002013			8.3		
		91500	0.002012	0.033114	0.008278	8.0	0.34	0.17
Shap	1	23_39c	0.002012			8.5		
	1	23_38c	0.002011			7.8		
	1	23_37m	0.002011			8.0		
	1	23_39c	0.002011			7.8		
	1	23_49c	0.002011			8.0		
	1	23_49m	0.002011			8.0		
	1	23_46m	0.002011			7.8		
	1	23_51c	0.00201			7.6		
	1	23_58c	0.002012			8.3		

Pluton	Zone	Sample	$^{18}O/^{16}O$	% 2SD	1 s.e.m	$\delta^{18}O$	2SD	1 s.e.m
	1	23_56c	0.00201			7.5		
		91500	0.002011	0.032968	0.007372	9.6	0.9	0.402492
Session 2 (27.01.2010)								
Shap	E1	25_2c	0.002013			7.4		
	E1	25_3c	0.002014			7.9		
	E1	25_3r	0.002013			7.7		
	E1	25_4c	0.002013			7.4		
	E1	25_5m	0.002013			7.7		
	E1	25_9m	0.002014			7.9		
	E1	25_7m	0.002014			8.0		
	E1	25_13c	0.002013			7.8		
	E1	25_20m	0.002014			7.9		
	E1	25_28c	0.002014			8.0		
	E1	25_28r	0.002014			8.0		
	E1	25_25c	0.002014			8.1		
	E1	25_25r	0.002013			7.7		
	E1	25_32c	0.002013			7.8		
		91500	0.002014	0.020014	0.004475	9.6	0.5	0.11339
Shap	E1	25_35c	0.002012			7.3		
	E1	25_34c	0.002012			7.1		
	E1	25_48c	0.002013			7.3		
	E1	25_48m	0.002013			7.4		
	E1	25_59c	0.002013			7.7		
	E1	25_75c	0.002015			8.3		
	E1	25_74c	0.002013			7.6		
	E1	25_73c	0.002013			7.7		
	E1	25_73r	0.002014			7.9		
	E1	25_78c	0.002013			7.4		
		91500	0.002013	0.022778	0.005093	9.8	0.54	0.121005
Shap	E2	26_1c	0.002014			7.9		
	E2	26_1r	0.002014			8.1		
	E2	26_2c	0.002013			7.4		
	E2	26_9c	0.002014			8.2		
	E2	26_8c	0.002013			7.3		
	E2	26_8r	0.002012			7.1		
	E2	26_7c	0.002011			6.8		
	E2	26_15m	0.002013			7.6		
	E2	26_15r	0.002013			7.7		
	E2	26_22r	0.002014			8.2		
	E2	26_26m	0.002014			7.8		
	E2	26_31c	0.002013			7.5		
	E2	26_31r	0.002014			7.8		
	E2	26_33m	0.002014			8.0		
	E2	26_38c	0.002013			7.4		
		91500	0.002013	0.022544	0.005041	9.9	0.28	0.062021
Shap	E2	26_47m	0.002014			7.8		
	E2	26_46c	0.002015			8.4		

Pluton	Zone	Sample	$^{18}O/^{16}O$	% 2SD	1 s.e.m	$\delta^{18}O$	2SD	1 s.e.m
	E2	26_45m	0.002014			7.8		
	E2	26_44m	0.002013			7.6		
	E2	26_48m	0.002014			7.9		
	E2	26_51c	0.002015			8.3		
	E2	26_56m	0.002014			7.9		
	E2	26_55c	0.002014			7.9		
	E2	26_55r	0.002014			7.8		
	E2	26_53c	0.002014			8.2		
		91500	0.002014	0.022964	0.005135	10.2	0.26	0.056937
Session 3 (28.01.2010)								
Criffell	1	17_43m	0.002007			5.2		
	1	17_54c	0.002008			5.7		
	1	17_54r	0.002008			5.7		
	1	17_53c	0.002008			5.9		
	1	17_56c	0.002008			5.5		
	1	17_60m	0.002008			5.6		
	1	17_68m	0.002009			6.3		
	1	17_68r	0.002007			5.3		
	1	17_76c	0.00201			6.6		
	1	17_81c	0.002009			5.9		
	1	17_83m	0.002009			6.1		
	1	17_85c	0.002009			6.0		
	1	17_86r	0.002007			5.3		
		91500	0.002008	0.031483	0.00704	9.4	0.56	0.125635
Criffell	3	21_21c	0.002009			6.2		
	3	21_21r	0.00201			6.6		
	3	21_30c	0.00201			6.6		
	3	21_30r	0.00201			6.6		
	3	21_34c	0.002013			8.1		
	3	21_33c	0.00201			6.6		
	3	21_37c	0.002009			6.4		
	3	21_37r	0.00201			6.5		
	3	21_38c	0.00201			6.7		
	3	21_39c	0.00201			6.8		
	3	21_39r	0.002009			6.1		
		91500	0.00201	0.028174	0.0063	9.7	0.38	0.083622
Criffell	4	22_40m	0.002011			7.4		
	4	22_40r	0.002011			7.4		
	4	22_39m	0.002012			7.8		
	4	22_38c	0.002007			5.1		
	4	22_38r	0.00201			6.8		
	4	22_37c	0.002011			7.4		
	4	22_37r	0.00201			6.9		
	4	22_43c	0.002011			7.1		
	4	22_42r	0.00201			6.6		
	4	22_50c	0.00201			6.7		
	4	22_50r	0.00201			6.8		
	4	22_49c	0.002011			7.5		
	4	22_48c	0.002011			7.1		

Pluton	Zone	Sample	$^{18}O/^{16}O$	% 2SD	1 s.e.m	$\delta^{18}O$	2SD	1 s.e.m
	4	22_47c	0.002012			7.7		
		91500	0.002011	0.035816	0.008009	9.8	0.02	0.002775
Session 4 (29.01.2010)								
Criffell	4	22_46c	0.002017			8.4		
	4	22_46r	0.002012			6.2		
	4	22_52c	0.002015			7.7		
	4	22_53m	0.002014			7.2		
	4	22_54m	0.002014			7.1		
	4	22_55c	0.002013			6.5		
	4	22_55r	0.002014			7.2		
	4	22_60m	0.002016			8.0		
	4	22_60r	0.002014			7.0		
	4	22_58c	0.002016			8.1		
	4	22_62m	0.002017			8.7		
	4	22_63c	0.002014			7.2		
	4	22_69r	0.002014			7.1		
	4	22_67c	0.002015			7.6		
		91500	0.002015	0.039488	0.00883	9.7	0.7	0.154636
Criffell	3	21_44c	0.002012			6.1		
	3	21_44r	0.002012			6.2		
	3	21_42c	0.002013			6.9		
	3	21_42r	0.002013			6.6		
	3	21_41m	0.002013			6.7		
	3	21_46c	0.002013			7.0		
	3	21_46r	0.002011			6.0		
	3	21_48c	0.002012			6.1		
	3	21_53c	0.002011			5.8		
	3	21_51m	0.002013			6.7		
		91500	0.002012	0.02544	0.005689	9.6	0.46	0.205718
Criffell	2	18_75c	0.002012			6.3		
	2	18_75r	0.00201			5.5		
	2	18_80m	0.00201			5.4		
	2	18_79c	0.00201			5.5		
	2	18_76c	0.002011			6.1		
	2	18_81c	0.002013			6.9		
	2	18_83c	0.002012			6.2		
	2	18_85c	0.002011			6.1		
	2	18_90c	0.002011			5.8		
	2	18_95m	0.00201			5.2		
	2	18_95r	0.002011			5.8		
	2	18_92m	0.002012			6.4		
	2	18_68m	0.002011			6.0		
		91500	0.002011	0.005488		9.6	0.7	0.157371
Session 5 (01.02.2010)								
Criffell	E1	17E_1c	0.002012			6.2		
	E1	17E_1r	0.002011			6.1		
	E1	17E_2c	0.002012			6.5		

Pluton	Zone	Sample	$^{18}O/^{16}O$	% 2SD	1 s.e.m	$\delta^{18}O$	2SD	1 s.e.m
	E1	17E_3c	0.002012			6.5		
	E1	17E_3m	0.002012			6.5		
	E1	17E_4m	0.002013			6.7		
	E1	17E_5c	0.002012			6.3		
	E1	17E_7m	0.002012			6.6		
	E1	17E_9m	0.002012			6.2		
	E1	17E_14c	0.002011			6.0		
	E1	17E_14m	0.002011			5.8		
	E1	17E_13m	0.002011			6.1		
	E1	17E_11c	0.002012			6.3		
	E1	17E_10m	0.002012			6.3		
	E1	17E_15c	0.002012			6.2		
		91500	0.002012	0.022095	0.004941	9.9	0.46	0.103506
Criffell		36_1c	0.002012			6.6		
		36_1r	0.002012			6.4		
		36_2c	0.002012			6.2		
		36_2r	0.002012			6.3		
		36_3m	0.002012			6.6		
		36_4c	0.002012			6.1		
		36_5m	0.002012			6.3		
		36_6m	0.002013			6.6		
		36_11m	0.002012			6.6		
		36_23m	0.002013			6.7		
		36_21m	0.002013			6.7		
		36_26c	0.002012			6.4		
		36_26r	0.002012			6.6		
		36_20c	0.002013			6.8		
		36_16r	0.002012			6.4		
		91500	0.002012	0.00481		10.0	0.38	0.087072
Criffell	E2	18E_2c	0.002012			6.3		
	E2	18E_2r	0.002012			6.1		
	E2	18E_3c	0.002012			6.6		
	E2	18E_5c	0.002012			6.5		
	E2	18E_10c	0.002012			6.4		
	E2	18E_14c	0.002012			6.4		
	E2	18E_16c	0.002011			5.9		
	E2	18E_18c	0.002012			6.2		
	E2	18E_19c	0.002012			6.2		
	E2	18E_19r	0.002012			6.5		
	E2	18E_22c	0.002012			6.1		
	E2	18E_23m	0.002012			6.1		
	E2	18E_29c	0.002011			5.9		
	E2	18E_29r	0.002012			6.2		
	E2	18E_27c	0.002012			6.1		
		91500	0.002012	0.021158	0.004731	9.8	0.56	0.125724
Fleet	1	33_1c	0.002013			6.7		
	1	33_1r	0.002014			7.5		
	1	33_12c	0.002014			7.3		
	1	33_14c	0.002014			7.5		

Pluton	Zone	Sample	$^{18}O/^{16}O$	% 2SD	1 s.e.m	$\delta^{18}O$	2SD	1 s.e.m
	1	33_15c	0.002013			6.9		
	1	33_19m	0.002013			6.9		
	1	33_18c	0.002013			6.6		
	1	33_27m	0.002012			6.5		
	1	33_26c	0.002013			7.0		
	1	33_26r	0.002012			6.5		
	1	33_24c	0.002012			6.4		
	1	33_29c	0.002012			6.1		
	1	33_31c	0.002013			6.7		
	1	33_37c	0.002013			7.0		
	1	33_35c	0.002013			6.7		
		91500	0.002013	0.006707		9.8	0.14	0.03323
Fleet	2	34_22m	0.002013			7.0		
	2	34_21c	0.002013			7.0		
	2	34_28m	0.002013			6.7		
	2	34_47c	0.002014			7.4		
	2	34_47r	0.002014			7.1		
	2	34_39c	0.002012			6.4		
	2	34_39m	0.002014			7.4		
	2	34_50c	0.002011			6.1		
	2	34_49c	0.002013			7.0		
	2	34_52c	0.00201			5.4		
	2	34_52r	0.002016			8.1		
	2	34_54c	0.002015			7.6		
	2	34_65m	0.002015			7.7		
	2	34_67c	0.002016			8.2		
	2	34_68c	0.002013			6.8		
		91500	0.002015	0.004474		9.8	0.16	0.034897
Fleet	3	35_1c	0.002012			6.1		
	3	35_6m	0.002015			7.8		
	3	35_13c	0.002011			5.8		
	3	35_11m(lower)	0.002013			7.0		
	3	35_10c	0.002013			6.7		
	3	35_9c	0.002013			6.9		
	3	35_14c	0.002012			6.4		
	3	35_15c	0.002009			4.7		
	3	35_17m	0.00201			5.5		
	3	35_18c	0.002013			6.7		
		91500	0.002011	0.025039	0.005599	10.1	0.4	0.088573

c denotes crystal core, r denotes crystal rim.

Appendix G

Zircon U-Pb ages

Pluton	Zone	Sample	U ppm wt	Th ppm wt	Pb ppm wt	Th/U atomic	^{204}Pb ppb wt	f206 (%)	^{204}Pb/^{206}Pb	Corrected ^{207}Pb/^{206}Pb	1σ	^{208}Pb/^{206}Pb	1σ	Ages ^{206}Pb/^{238}Pb	1σ	^{207}Pb/^{235}Pb	1σ	^{207}Pb/^{206}Pb	1σ	% dis
Criffell	1	17_63	283	237	22	0.86	0.24	0.03	1.5E-05	0.0552	0.0004	0.2712	0.0036	415	5	416	5	419	14	-1
		17_76	320	205	23	0.66	1.08	0.11	5.9E-05	0.0535	0.0005	0.2055	0.0023	409	4	400	5	350	20	17
		17_81	268	209	20	0.80	1.26	0.15	8.2E-05	0.0548	0.0005	0.2482	0.0041	414	5	413	5	403	19	3
		17_82	231	139	16	0.62	2.90	0.41	2.2E-04	0.0546	0.0005	0.1934	0.0022	410	5	407	5	395	22	4
		17_83	255	145	18	0.58	0.61	0.08	4.3E-05	0.0539	0.0004	0.1831	0.0011	402	4	397	4	367	16	9
		17_91	461	249	32	0.55	0.49	0.04	1.9E-05	0.0554	0.0003	0.1747	0.0017	406	4	409	4	426	14	-5
		17_93	377	284	28	0.77	0.51	0.04	2.4E-05	0.0539	0.0004	0.2416	0.0019	414	4	406	4	365	17	13
		17_98	260	137	18	0.54	0.86	0.11	5.8E-05	0.0554	0.0005	0.1705	0.0009	409	4	412	5	429	18	-5
		17_96	285	218	20	0.79	3.12	0.37	2.0E-04	0.0543	0.0008	0.2454	0.0015	394	4	392	6	383	32	3
Criffell	2	18_7	370	204	26	0.56	0.50	0.04	2.4E-05	0.0557	0.0003	0.1780	0.0016	412	4	416	4	440	11	-6
		18_12	225	86	15	0.39	0.66	0.09	5.1E-05	0.0536	0.0005	0.1260	0.0010	415	4	406	5	354	21	17
		18_22	368	133	25	0.37	3.94	0.35	1.9E-04	0.0551	0.0004	0.1165	0.0006	412	4	413	4	414	15	0
		18_34	678	294	47	0.45	0.75	0.04	1.9E-05	0.0545	0.0003	0.1387	0.0007	419	5	415	5	391	13	7
		18_68	438	198	29	0.46	0.79	0.06	3.2E-05	0.0549	0.0004	0.1450	0.0007	403	4	404	4	408	17	-1
		18_75	343	133	23	0.40	0.68	0.07	3.6E-05	0.0539	0.0003	0.1246	0.0007	402	4	397	4	366	14	10
		18_79	917	608	67	0.68	0.33	0.01	6.4E-06	0.0552	0.0002	0.2132	0.0023	413	4	414	4	419	10	-1
		18_81	437	335	32	0.79	4.81	0.37	2.0E-04	0.0548	0.0004	0.2466	0.0008	403	4	403	4	405	15	0
		18_83	317	192	22	0.62	0.57	0.06	3.3E-05	0.0548	0.0003	0.1938	0.0013	398	4	399	4	402	13	-1
Criffell	3	21_34	373	244	27	0.67	0.13	0.01	5.8E-06	0.0549	0.0005	0.2068	0.0010	415	4	414	5	407	18	2
		21_33	314	107	21	0.35	0.69	0.07	3.8E-05	0.0552	0.0004	0.1094	0.0015	410	4	412	4	420	16	-2
		21_35	484	190	33	0.40	1.08	0.07	3.8E-05	0.0538	0.0004	0.1264	0.0020	419	4	410	4	361	19	16
		21_37	856	283	57	0.34	2.67	0.10	5.4E-05	0.0552	0.0002	0.1063	0.0003	413	4	414	4	418	8	-1
		21_38	591	220	39	0.38	0.68	0.04	2.0E-05	0.0541	0.0004	0.1187	0.0006	410	4	405	4	376	15	9
		21_39	559	316	40	0.58	0.82	0.05	2.5E-05	0.0544	0.0004	0.1807	0.0008	421	4	416	4	388	14	8
		21_41	616	257	41	0.43	1.47	0.08	4.2E-05	0.0544	0.0004	0.1361	0.0008	407	4	404	4	387	18	5
Criffell	4	22_39	540	137	35	0.26	1.96	0.12	6.4E-05	0.0548	0.0005	0.0795	0.0020	409	5	409	5	404	21	1
		22_38	514	239	35	0.48	0.89	0.06	3.0E-05	0.0549	0.0005	0.1500	0.0022	413	5	412	6	407	21	2
		22_30	591	377	43	0.66	2.99	0.16	8.8E-05	0.0549	0.0002	0.2036	0.0006	412	4	412	4	408	10	1
		22_32	548	166	36	0.31	1.33	0.08	4.2E-05	0.0551	0.0003	0.0959	0.0006	415	4	415	4	415	12	0
Criffell	E1	17E_1	277	158	19	0.58	1.39	0.17	8.9E-05	0.0534	0.0004	0.1799	0.0009	409	4	400	4	343	19	19
		17E_2	434	264	31	0.62	0.37	0.03	1.5E-05	0.0549	0.0003	0.1932	0.0011	414	4	413	4	406	11	2
		17E_3	250	151	18	0.62	0.53	0.07	3.7E-05	0.0549	0.0005	0.1927	0.0014	415	4	414	5	407	19	2
		17E_4	324	251	24	0.79	1.59	0.16	8.6E-05	0.0536	0.0005	0.2469	0.0016	411	4	403	5	355	22	16
		17E_5	538	461	41	0.88	3.84	0.23	1.3E-04	0.0555	0.0003	0.2356	0.0009	411	4	414	4	432	14	-5
		17E_7	309	167	22	0.55	2.90	0.31	1.6E-04	0.0547	0.0005	0.1733	0.0008	411	4	409	5	398	20	3
		17E_9	422	302	31	0.73	0.12	0.01	5.0E-06	0.0541	0.0004	0.2331	0.0012	411	4	406	4	374	16	10
		17E_14	294	144	20	0.50	2.16	0.24	1.3E-04	0.0544	0.0005	0.1570	0.0008	407	4	404	4	386	19	5
		17E_13	291	178	20	0.63	3.78	0.43	2.3E-04	0.0564	0.0005	0.1989	0.0009	406	4	415	4	466	18	-13

Pluton	Zone	Sample	U	Th	Pb	Th/U	^{204}Pb	f206		Corrected				Ages						
			ppm wt	ppm wt	ppm wt	atomic	ppb wt	(%)	^{204}Pb/^{206}Pb	^{207}Pb/^{206}Pb	1σ	^{208}Pb/^{206}Pb	1σ	^{206}Pb/^{238}Pb	1σ	^{207}Pb/^{235}Pb	1σ	^{207}Pb/^{206}Pb	1σ	% dis
		17E_11	333	237	24	0.73	0.26	0.03	1.3E-05	0.0557	0.0004	0.2273	0.0011	411	4	416	4	440	18	-7
Criffell	E2	18E_3	500	249	36	0.51	0.70	0.04	2.4E-05	0.0553	0.0004	0.1583	0.0020	425	5	425	5	424	14	0
		18E_5	522	261	37	0.51	7.56	0.46	2.5E-04	0.0561	0.0004	0.1667	0.0015	418	4	424	5	455	17	-8
		18E_10	560	226	39	0.41	6.44	0.36	2.0E-04	0.0545	0.0004	0.1266	0.0008	422	4	418	4	393	15	7
		18E_19	637	336	45	0.54	2.85	0.14	7.7E-05	0.0548	0.0004	0.1697	0.0009	418	4	416	4	403	15	4
		18E_22	565	340	41	0.62	0.27	0.02	8.3E-06	0.0553	0.0004	0.1958	0.0011	422	4	422	4	422	16	0
		18E_23	423	242	30	0.59	0.93	0.07	3.8E-05	0.0544	0.0006	0.1816	0.0009	413	4	409	5	387	24	7
Criffell	QD	36_1	259	128	18	0.51	1.21	0.15	8.1E-05	0.0541	0.0004	0.1570	0.0012	414	4	408	4	376	17	10
		36_2	389	249	28	0.66	0.91	0.08	4.1E-05	0.0537	0.0004	0.2065	0.0010	412	4	404	4	359	17	15
		36_3	363	214	26	0.60	0.83	0.07	4.0E-05	0.0549	0.0004	0.1887	0.0007	417	4	416	5	407	19	3
		36_4	326	182	23	0.57	1.37	0.14	7.3E-05	0.0546	0.0005	0.1808	0.0009	417	4	414	5	395	21	6
		36_5	380	239	28	0.64	0.79	0.07	3.6E-05	0.0539	0.0006	0.1978	0.0009	418	4	411	5	368	24	14
		36_6	299	177	21	0.61	8.09	0.88	4.7E-04	0.0529	0.0005	0.1895	0.0023	412	4	399	4	326	20	26
		36_11	399	218	29	0.56	1.70	0.14	7.3E-05	0.0545	0.0004	0.1752	0.0007	420	4	415	5	391	18	7
		36_16	339	189	24	0.57	0.79	0.08	4.0E-05	0.0536	0.0005	0.1769	0.0007	416	4	407	5	353	22	18
		36_26c	333	255	25	0.78	0.94	0.09	4.9E-05	0.0543	0.0004	0.2449	0.0016	416	4	412	4	384	17	8
		36_26r	226	123	16	0.56	0.98	0.14	7.7E-05	0.0537	0.0005	0.1726	0.0013	404	4	398	5	358	23	13
Fleet	1	33_1	659	262	45	0.41	2.72	0.13	7.2E-05	0.0544	0.0005	0.1275	0.0018	414	7	410	6	388	19	7
		33_2	894	327	59	0.37	0.90	0.03	1.8E-05	0.0549	0.0003	0.1183	0.0013	406	4	407	4	408	11	0
		33_7	747	192	48	0.26	4.03	0.18	9.5E-05	0.0549	0.0004	0.0837	0.0013	410	5	409	5	406	15	1
		33_6	166	150	13	0.93	0.48	0.10	5.1E-05	0.0551	0.0006	0.2905	0.0067	410	44	411	37	414	26	-1
Fleet	2	34_10	1292	240	77	0.19	0.70	0.02	1.0E-05	0.0548	0.0002	0.0619	0.0052	385	5	388	4	405	7	-5
		34_24	574	318	38	0.57	1.90	0.12	6.2E-05	0.0544	0.0003	0.1739	0.0014	385	4	385	4	387	14	-1
		34_30	464	535	35	1.18	3.19	0.24	1.3E-04	0.0541	0.0004	0.3697	0.0013	382	4	381	4	374	16	2
		34_47	954	1061	72	1.14	3.60	0.13	7.0E-05	0.0541	0.0003	0.3630	0.0039	387	4	385	4	374	12	4
		34_61	1016	1531	84	1.55	2.55	0.09	4.6E-05	0.0543	0.0003	0.4877	0.0014	390	4	389	4	382	14	2
		34_68	205	153	14	0.76	0.77	0.13	7.2E-05	0.0544	0.0004	0.2348	0.0014	379	4	381	4	387	17	-2
		34_67	824	357	53	0.44	0.33	0.01	7.4E-06	0.0544	0.0003	0.1392	0.0006	390	4	390	4	388	12	0
Fleet	3	35_2	1379	1475	105	1.10	1.30	0.03	1.7E-05	0.0544	0.0002	0.3443	0.0016	394	4	393	4	385	9	2
		35_13	545	333	37	0.63	2.74	0.17	9.2E-05	0.0546	0.0003	0.1959	0.0009	393	4	393	4	397	13	-1
		35_9	1235	659	81	0.55	2.60	0.07	3.9E-05	0.0551	0.0003	0.1708	0.0008	387	4	391	4	416	11	-7
Shap	1	23_1	1458	857	108	0.60	0.76	0.02	8.7E-06	0.0545	0.0003	0.1895	0.0015	428	4	422	4	390	12	10
		23_4	585	654	47	1.15	6.98	0.39	2.1E-04	0.0546	0.0005	0.3522	0.0044	407	4	405	5	396	22	3
		23_5	589	251	41	0.44	0.59	0.03	1.7E-05	0.0547	0.0005	0.1399	0.0009	418	4	416	5	400	21	5
		23_10	764	659	59	0.88	0.95	0.04	2.1E-05	0.0551	0.0004	0.2736	0.0008	420	4	420	4	415	16	1
		23_8	561	352	40	0.64	1.60	0.09	5.0E-05	0.0547	0.0005	0.2017	0.0009	413	4	411	5	398	22	4
		23_7	524	614	43	1.20	6.77	0.42	2.3E-04	0.0542	0.0004	0.3787	0.0015	413	4	408	4	380	15	9
		23_18	1324	673	93	0.52	0.86	0.02	1.1E-05	0.0552	0.0002	0.1644	0.0004	417	4	418	4	419	10	0

Pluton	Zone	Sample	U	Th	Pb	Th/U	^{204}Pb	f206		Corrected				Ages						
			ppm wt	ppm wt	ppm wt	atomic	ppb wt	(%)	^{204}Pb/^{206}Pb	^{207}Pb/^{206}Pb	1σ	^{208}Pb/^{206}Pb	1σ	^{206}Pb/^{238}Pb	1σ	^{207}Pb/^{235}Pb	1σ	^{207}Pb/^{206}Pb	1σ	% dis
Shap	2	32_11	1092	448	74	0.42	1.00	0.03	1.6E-05	0.0548	0.0003	0.1328	0.0003	413	4	412	4	404	11	2
		32_14	929	512	66	0.57	0.00	0.00	2.0E-08	0.0550	0.0002	0.1761	0.0007	416	4	415	4	410	9	1
		32_16	1121	730	81	0.67	7.75	0.22	1.2E-04	0.0548	0.0003	0.2095	0.0007	413	4	411	4	402	11	3
		32_21	1144	729	83	0.65	1.19	0.03	1.8E-05	0.0549	0.0003	0.2041	0.0028	414	4	413	4	406	12	2
Shap	E1	25_3	739	752	59	1.04	8.89	0.39	2.1E-04	0.0539	0.0003	0.3239	0.0061	416	4	409	4	368	14	13
		25_5	423	554	36	1.34	0.66	0.05	2.7E-05	0.0545	0.0003	0.4142	0.0084	419	4	415	4	390	12	8
		25_20	1264	649	89	0.53	0.90	0.02	1.2E-05	0.0547	0.0003	0.1655	0.0008	416	4	413	4	398	10	5
		25_28	395	151	27	0.39	0.61	0.05	2.7E-05	0.0547	0.0005	0.1219	0.0007	413	4	411	5	399	22	4
		25_25	1428	723	102	0.52	0.14	0.00	1.7E-06	0.0546	0.0003	0.1627	0.0005	425	4	420	4	397	14	7
		25_32	1135	692	83	0.63	0.30	0.01	4.6E-06	0.0552	0.0002	0.1950	0.0008	421	4	421	4	421	8	0
		25_38	1143	702	82	0.63	3.85	0.11	5.9E-05	0.0551	0.0002	0.1957	0.0007	415	4	415	4	416	10	0
Shap	E2	26_2	591	415	44	0.72	0.91	0.05	2.6E-05	0.0548	0.0004	0.2249	0.0020	420	4	418	4	405	15	4
		26_7	1383	1285	109	0.95	4.86	0.11	6.0E-05	0.0550	0.0003	0.2968	0.0011	419	4	418	4	411	12	2
		26_8	718	576	54	0.82	9.70	0.43	2.3E-04	0.0549	0.0005	0.2554	0.0011	417	4	415	5	407	19	2
		26_15	562	1193	56	2.18	9.13	0.52	2.8E-04	0.0541	0.0004	0.6728	0.0023	415	4	409	4	375	16	11
		26_26	917	388	63	0.43	15.30	0.54	2.9E-04	0.0549	0.0003	0.1350	0.0007	413	4	412	4	407	11	2
SO'C	Bas	16_12	332	67	173	0.21	12.49	0.17	8.9E-05	0.1807	0.0007	0.0580	0.0004	2552	22	2612	10	2659	6	-4
		16_1	495	227	47	0.47	14.65	0.70	3.8E-04	0.0595	0.0010	0.1448	0.0022	560	5	565	8	586	35	-4
		16_4	139	61	11	0.45	0.39	0.08	4.2E-05	0.0550	0.0007	0.1377	0.0015	484	5	471	6	411	29	18
		16_5	175	113	36	0.67	0.39	0.03	1.4E-05	0.0761	0.0004	0.1965	0.0028	1106	11	1103	8	1097	10	1
		16_13	276	172	20	0.64	1.22	0.14	7.7E-05	0.0552	0.0006	0.2004	0.0014	414	4	415	5	420	22	-1
		16_11	231	156	69	0.69	0.12	0.00	2.3E-06	0.0948	0.0004	0.2034	0.0006	1528	14	1527	9	1524	9	0

SO'C - Shoulder O'Craig
Bas. - Basalt
QD - Quartz Diorite

Appendix H

Zircon Hf isotope compositions

	Zone	Sample	Spot size	Age Ma	$\delta^{18}O$ [‰]	±2σ	$^{176}Hf/^{177}Hf$	±2σ	$^{176}Lu/^{177}Hf$	±2σ	$^{176}Yb/^{177}Hf$	$^{176}Hf/^{177}Hf_T$	±2σ	εHf_T	±2σ	$T(DM)^c_{felsic}Ma^\dagger$
Criffell																
	1	Spl17-68	50µ	408	5.3	0.4	0.282598	0.000015	0.000683	0.000030	0.022168	0.282593	0.000015	2.3	0.5	1234
		Spl17-76	50µ	408	6.6	0.4	0.282627	0.000016	0.000735	0.000029	0.023293	0.282622	0.000016	3.3	0.6	1168
		Spl17-81	50µ	408	5.9	0.4	0.282616	0.000016	0.000631	0.000012	0.019783	0.282611	0.000016	2.9	0.6	1192
		Spl17-83	50µ	408	6.1	0.4	0.282619	0.000017	0.000746	0.000034	0.023554	0.282613	0.000017	3.0	0.6	1187
		Spl17-85	50µ	408	6.0	0.4	0.282633	0.000020	0.001063	0.000143	0.035365	0.282625	0.000020	3.4	0.7	1161
		Spl17-58	50µ	408			0.282607	0.000015	0.000652	0.000032	0.020993	0.282602	0.000015	2.6	0.5	1213
		Spl17-63	50µ	408			0.282604	0.000018	0.000680	0.000035	0.021978	0.282599	0.000018	2.5	0.7	1220
		Spl17-64	50µ	408			0.282620	0.000015	0.000521	0.000011	0.016026	0.282616	0.000015	3.1	0.5	1182
		Spl17-67	50µ	408			0.282613	0.000015	0.000730	0.000018	0.023551	0.282608	0.000015	2.8	0.5	1200
		Spl17-82	50µ	408			0.282617	0.000015	0.000583	0.000017	0.018579	0.282613	0.000015	3.0	0.5	1188
	2	Spl18-7	50µ	409			0.282636	0.000019	0.000819	0.000019	0.024739	0.282630	0.000019	3.6	0.7	1150
		Spl18-8	50µ	409			0.282623	0.000016	0.000715	0.000048	0.021986	0.282617	0.000016	3.2	0.6	1178
		Spl18-12	50µ	409			0.282644	0.000019	0.000600	0.000024	0.018362	0.282640	0.000019	4.0	0.7	1127
		Spl18-21	50µ	409			0.282651	0.000017	0.000722	0.000021	0.022191	0.282646	0.000017	4.2	0.6	1114
		Spl18-22	50µ	409			0.282646	0.000025	0.000775	0.000018	0.022537	0.282640	0.000025	4.0	0.9	1127
		Spl18-75	50µ	409	6.3	0.6	0.282642	0.000017	0.000633	0.000019	0.018277	0.282638	0.000017	3.9	0.6	1132
		Spl18-76	50µ	409	6.1	0.6	0.282643	0.000018	0.000921	0.000036	0.028345	0.282636	0.000018	3.8	0.6	1136
		Spl18-79	50µ	409	5.5	0.6	0.282645	0.000018	0.000826	0.000036	0.024354	0.282639	0.000018	3.9	0.6	1130
		Spl18-80	50µ	409	5.4	0.6	0.282635	0.000018	0.000577	0.000023	0.017273	0.282630	0.000018	3.6	0.6	1148
		Spl18-81	50µ	409	6.9	0.6	0.282646	0.000020	0.000713	0.000057	0.022998	0.282640	0.000020	4.0	0.7	1127
	3	Spl21-21	50µ	414	6.6	0.4	0.282632	0.000022	0.000578	0.000042	0.017660	0.282627	0.000022	3.6	0.8	1153
		Spl21-30	50µ	414	6.6	0.4	0.282634	0.000027	0.000670	0.000023	0.019287	0.282629	0.000027	3.7	1.0	1149
		Spl21-32	50µ	414			0.282639	0.000027	0.001005	0.000071	0.030986	0.282632	0.000027	3.8	1.0	1143
		Spl21-33	50µ	414	6.6	0.4	0.282633	0.000022	0.000615	0.000014	0.018473	0.282628	0.000022	3.7	0.8	1151
		Spl21-34	50µ	414	8.1	0.4	0.282655	0.000020	0.000770	0.000019	0.022973	0.282649	0.000020	4.4	0.7	1104
		Spl21-37	50µ	414	6.4	0.4	0.282619	0.000022	0.000609	0.000017	0.018306	0.282614	0.000022	3.2	0.8	1181
		Spl21-38	50µ	414	6.7	0.4	0.282642	0.000023	0.000550	0.000018	0.017631	0.282638	0.000023	4.0	0.8	1129
		Spl21-39	50µ	414	6.8	0.4	0.282641	0.000022	0.000704	0.000007	0.021559	0.282635	0.000022	3.9	0.8	1135
		Spl21-41	50µ	414	6.7	0.6	0.282625	0.000019	0.000751	0.000016	0.023234	0.282619	0.000019	3.3	0.7	1171
		Spl21-42	50µ	414	6.9	0.6	0.282615	0.000025	0.000598	0.000008	0.017905	0.282610	0.000025	3.0	0.9	1191
	4	Spl22-37	50µ	412	7.4	0.4	0.282614	0.000017	0.000767	0.000041	0.023793	0.282608	0.000017	2.9	0.6	1196
		Spl22-38	50µ	412	5.1	0.4	0.282618	0.000018	0.000674	0.000032	0.020686	0.282613	0.000018	3.1	0.6	1186
		Spl22-39	50µ	412			0.282615	0.000020	0.001135	0.000229	0.037478	0.282607	0.000020	2.9	0.7	1200

	Zone	Sample	Spot size	Age Ma	$\delta^{18}O$ [‰]	±2σ	$^{176}Hf/^{177}Hf$	±2σ	$^{176}Lu/^{177}Hf$	±2σ	$^{176}Yb/^{177}Hf$	$^{176}Hf/^{177}Hf_T$	±2σ	εHf_T	±2σ	$T(DM)^c$ $_{felsic}Ma^\dagger$
Criffell																
		Spl22-40	50µ	412	7.4	0.4	0.282622	0.000018	0.000716	0.000015	0.022161	0.282617	0.000018	3.2	0.6	1177
		Spl22-42	50µ	412	6.6	0.4	0.282616	0.000013	0.000810	0.000033	0.025660	0.282610	0.000013	3.0	0.5	1192
		Spl22-46	50µ	412	8.4	0.6	0.282624	0.000020	0.000898	0.000042	0.028040	0.282617	0.000020	3.2	0.7	1176
		Spl22-58	50µ	412	8.1	0.6	0.282611	0.000018	0.000589	0.000018	0.017327	0.282606	0.000018	2.9	0.6	1201
		Spl22-59	50µ	412			0.282608	0.000015	0.000517	0.000052	0.017227	0.282604	0.000015	2.8	0.5	1206
		Spl22-62	50µ	412	8.7	0.6	0.282629	0.000020	0.000665	0.000033	0.019988	0.282624	0.000020	3.5	0.7	1160
		Spl22-63	50µ	412	7.2	0.6	0.282628	0.000019	0.000748	0.000035	0.022895	0.282622	0.000019	3.4	0.7	1165
	E1	Spl17E-1	50µ	411	6.2	0.4	0.282613	0.000016	0.000515	0.000006	0.016347	0.282610	0.000016	2.9	0.6	1194
		Spl17E-3	50µ	411	6.5	0.4	0.282608	0.000017	0.000617	0.000014	0.020193	0.282603	0.000017	2.7	0.6	1209
		Spl17E-5	50µ	411	6.3	0.4	0.282606	0.000017	0.000790	0.000038	0.026178	0.282600	0.000017	2.6	0.6	1215
		Spl17E-10	50µ	411	6.3	0.4	0.282631	0.000023	0.000622	0.000050	0.020541	0.282626	0.000023	3.5	0.8	1158
		Spl17E-11	50µ	411	6.3	0.4	0.282618	0.000018	0.000726	0.000044	0.021399	0.282613	0.000018	3.1	0.6	1187
		Spl17E-7	50µ	411	6.6	0.4	0.282627	0.000017	0.000429	0.000007	0.013965	0.282623	0.000017	3.4	0.6	1163
		Spl17E-9	50µ	411	6.2	0.4	0.282621	0.000020	0.000625	0.000032	0.019892	0.282617	0.000020	3.2	0.7	1178
		Spl17E-13	50µ	411	6.1	0.4	0.282623	0.000023	0.000589	0.000020	0.018909	0.282618	0.000023	3.3	0.8	1174
		Spl17E-14	50µ	411	5.8	0.4	0.282615	0.000015	0.000538	0.000010	0.017051	0.282611	0.000015	3.0	0.5	1192
		Spl17E-15	50µ	411	6.2	0.4	0.282639	0.000017	0.000887	0.000028	0.028744	0.282632	0.000017	3.7	0.6	1143
		Spl18E-5	50µ	420	6.5	0.4	0.282636	0.000017	0.000616	0.000012	0.017727	0.282631	0.000017	3.9	0.6	1140
	E2	Spl18E-10	50µ	420	6.4	0.4	0.282643	0.000019	0.000934	0.000047	0.027254	0.282636	0.000019	4.1	0.7	1130
		Spl18E-14	50µ	420	6.4	0.4	0.282635	0.000016	0.000583	0.000012	0.016939	0.282630	0.000016	3.9	0.6	1141
		Spl18E-18	50µ	420	6.2	0.4	0.282646	0.000017	0.000651	0.000013	0.019279	0.282641	0.000017	4.3	0.6	1117
		Spl18E-19	50µ	420	6.2	0.4	0.282637	0.000019	0.000608	0.000036	0.016861	0.282632	0.000019	4.0	0.7	1137
		Spl18E-22	50µ	420	6.1	0.4	0.282653	0.000015	0.000794	0.000007	0.022259	0.282647	0.000015	4.5	0.5	1104
		Spl18E-23	50µ	420	6.1	0.4	0.282642	0.000016	0.000562	0.000014	0.015745	0.282638	0.000016	4.1	0.6	1125
		Spl18E-27	50µ	420	6.1	0.4	0.282619	0.000016	0.000775	0.000010	0.022170	0.282613	0.000016	3.3	0.6	1181
		Spl18E-28	50µ	420			0.282632	0.000019	0.000877	0.000017	0.025806	0.282625	0.000019	3.7	0.7	1155
		Spl18E-29	50µ	420	5.9	0.4	0.282628	0.000019	0.000852	0.000028	0.024906	0.282622	0.000019	3.6	0.7	1161
		Spl36-1	50µ	415	6.6	0.4	0.282600	0.000017	0.000675	0.000016	0.021528	0.282595	0.000017	2.5	0.6	1225
		Spl36-2	50µ	415	6.2	0.4	0.282622	0.000017	0.000532	0.000007	0.016803	0.282617	0.000017	3.3	0.6	1174
		Spl36-3	50µ	415	6.6	0.4	0.282591	0.000019	0.000665	0.000010	0.021559	0.282585	0.000019	2.2	0.7	1246
		Spl36-4	50µ	415	6.1	0.4	0.282611	0.000020	0.000790	0.000030	0.024462	0.282605	0.000020	2.9	0.7	1202
		Spl36-5	50µ	415	6.3	0.4	0.282623	0.000020	0.000506	0.000032	0.015474	0.282619	0.000020	3.4	0.7	1169
		Spl36-6	50µ	415	6.6	0.4	0.282628	0.000020	0.000544	0.000009	0.017226	0.282624	0.000020	3.5	0.7	1160

	Zone	Sample	Spot size	Age Ma	$\delta^{18}O$ [‰]	±2σ	$^{176}Hf/^{177}Hf$	±2σ	$^{176}Lu/^{177}Hf$	±2σ	$^{176}Yb/^{177}Hf$	$^{176}Hf/^{177}Hf_T$	±2σ	εHf_T	±2σ	$T(DM)^c$ $^{felsic}Ma^\dagger$
Criffell		Spl36-11	50µ	415	6.6	0.4	0.282621	0.000021	0.000740	0.000015	0.023862	0.282615	0.000021	3.2	0.8	1179
		Spl36-21	50µ	415	6.7	0.4	0.282626	0.000022	0.000726	0.000024	0.023396	0.282620	0.000022	3.4	0.8	1168
		Spl36-23	50µ	415	6.7	0.4	0.282629	0.000020	0.000714	0.000017	0.022302	0.282624	0.000020	3.5	0.7	1160
		Spl36-26	50µ	415	6.4	0.4	0.282601	0.000017	0.000689	0.000024	0.021368	0.282596	0.000017	2.6	0.6	1223
Fleet																
	1	Spl33-1	50µ	410	6.7	0.4	0.282547	0.000024	0.000861	0.000091	0.028257	0.282540	0.000024	0.5	0.9	1352
		Spl33-12	50µ	410	7.3	0.4	0.282566	0.000022	0.001118	0.000021	0.038014	0.282557	0.000022	1.1	0.8	1313
		Spl33-19	50µ	410	6.9	0.4	0.282559	0.000019	0.000919	0.000049	0.032529	0.282552	0.000019	0.9	0.7	1325
		Spl33-24	50µ	410	6.4	0.4	0.282542	0.000021	0.001214	0.000044	0.043476	0.282533	0.000021	0.2	0.7	1368
		Spl33-26	50µ	410	6.5	0.4	0.282575	0.000017	0.001197	0.000038	0.041366	0.282566	0.000017	1.4	0.6	1294
		Spl33-27	50µ	410	6.5	0.4	0.282547	0.000018	0.000878	0.000031	0.030872	0.282540	0.000018	0.5	0.6	1351
		Spl33-29	50µ	410	6.1	0.4	0.282553	0.000017	0.001095	0.000162	0.040487	0.282545	0.000017	0.6	0.6	1341
		Spl33-31	50µ	410	6.7	0.4	0.282538	0.000016	0.000853	0.000019	0.029576	0.282532	0.000016	0.2	0.6	1370
		Spl33-35	50µ	410	6.7	0.4	0.282522	0.000021	0.001012	0.000026	0.035542	0.282515	0.000021	-0.4	0.8	1408
		Spl33-37	50µ	410	7.0	0.4	0.282584	0.000020	0.001384	0.000117	0.049875	0.282574	0.000020	1.7	0.7	1276
	2	Spl34-21	40µ	386	7.0	0.4	0.282565	0.000026	0.001242	0.000053	0.041683	0.282556	0.000026	0.5	0.9	1330
		Spl34-22	40µ	386	7.0	0.4	0.282583	0.000030	0.001175	0.000067	0.038605	0.282575	0.000030	1.1	1.1	1289
		Spl34-39	40µ	386	7.4	0.4	0.282151	0.000029	0.000790	0.000081	0.028919	0.282145	0.000029	-14.1	1.0	2247
		Spl34-47	50µ	386	7.1	0.4	0.282529	0.000021	0.001528	0.000027	0.051960	0.282518	0.000021	-0.9	0.8	1416
		Spl34-52	40µ	386	5.4	0.4	0.282251	0.000035	0.001279	0.000025	0.049211	0.282242	0.000035	-10.6	1.3	2033
		Spl34-54	40µ	386	7.6	0.4	0.282559	0.000075	0.001796	0.000033	0.063571	0.282546	0.000075	0.1	2.7	1354
		Spl34-67	40µ	386	8.2	0.4	0.282562	0.000027	0.002123	0.000051	0.068518	0.282547	0.000027	0.2	1.0	1351
		Spl34-68	40µ	386	6.8	0.4	0.282541	0.000025	0.000963	0.000054	0.031054	0.282534	0.000025	-0.3	0.9	1380
		Spl34-69	40µ	386			0.282581	0.000020	0.000910	0.000086	0.030607	0.282574	0.000020	1.1	0.7	1290
		Spl34-70	40µ	386			0.282516	0.000019	0.000993	0.000029	0.031360	0.282509	0.000019	-1.2	0.7	1437
	3	Spl35-1	40µ	391	6.1	0.4	0.282593	0.000027	0.000918	0.000018	0.030812	0.282586	0.000027	1.7	1.0	1260
		Spl35-10	40µ	391	6.7	0.4	0.282556	0.000028	0.001608	0.000051	0.053868	0.282544	0.000028	0.2	1.0	1354
		Spl35-11	40µ	391	7.0	0.4	0.282555	0.000024	0.001291	0.000048	0.042111	0.282546	0.000024	0.2	0.9	1350
		Spl35-13	40µ	391			0.282622	0.000021	0.000782	0.000025	0.023845	0.282616	0.000021	2.8	0.7	1191
		Spl35-6	40µ	391	7.8	0.4	0.282583	0.000024	0.001571	0.000169	0.054083	0.282572	0.000024	1.2	0.9	1292

	Zone	Sample	Spot size	Age Ma	$\delta^{18}O$ [‰]	±2σ	$^{176}Hf/^{177}Hf$	±2σ	$^{176}Lu/^{177}Hf$	±2σ	$^{176}Yb/^{177}Hf$	$^{176}Hf/^{177}Hf_T$	±2σ	εHf_T	±2σ	$T(DM)^c$ $^{felsic}Ma^{\dagger}$
Shap	1	Spl23-1	50µ	417	7.9	0.3	0.282524	0.000019	0.001094	0.000015	0.034901	0.282515	0.000019	-0.3	0.7	1403
		Spl23-4	50µ	417	7.3	0.3	0.282528	0.000021	0.000850	0.000020	0.027888	0.282521	0.000021	0.0	0.7	1389
		Spl23-5	50µ	417	7.8	0.3	0.282537	0.000019	0.000702	0.000039	0.023794	0.282532	0.000019	0.3	0.7	1365
		Spl23-7	50µ	417	7.3	0.3	0.282530	0.000018	0.000944	0.000013	0.032536	0.282522	0.000018	0.0	0.6	1387
		Spl23-8	50µ	417	7.9	0.3	0.282503	0.000016	0.000571	0.000046	0.017755	0.282499	0.000016	-0.8	0.6	1440
		Spl23-10	50µ	417	8.0	0.3	0.282519	0.000020	0.000693	0.000049	0.022644	0.282513	0.000020	-0.3	0.7	1407
		Spl23-12	50µ	417	7.7	0.3	0.282509	0.000017	0.001061	0.000025	0.035695	0.282501	0.000017	-0.8	0.6	1435
		Spl23-14	50µ	417	7.7	0.3	0.282534	0.000025	0.001681	0.000066	0.056324	0.282521	0.000025	0.0	0.9	1389
		Spl23-17	50µ	417	7.8	0.3	0.282525	0.000019	0.000949	0.000018	0.029853	0.282517	0.000019	-0.2	0.7	1398
		Spl23-18	50µ	417	7.9	0.3	0.282526	0.000018	0.000926	0.000094	0.028093	0.282518	0.000018	-0.1	0.6	1396
	2	Spl32-1	50µ	414	7.6	0.3	0.282535	0.000016	0.000873	0.000076	0.032063	0.282528	0.000017	0.1	0.6	1376
		Spl32-2	50µ	414	7.6	0.3	0.282509	0.000018	0.000755	0.000014	0.025159	0.282503	0.000018	-0.8	0.7	1432
		Spl32-4	50µ	414	7.8	0.3	0.282534	0.000020	0.001154	0.000023	0.039832	0.282526	0.000020	0.0	0.7	1382
		Spl32-6	50µ	414	7.8	0.3	0.282520	0.000015	0.000925	0.000094	0.033079	0.282512	0.000015	-0.4	0.5	1411
		Spl32-5	50µ	414			0.282531	0.000015	0.000889	0.000038	0.030664	0.282524	0.000015	0.0	0.5	1384
		Spl32-10	50µ	414	7.9	0.3	0.282518	0.000020	0.000707	0.000017	0.023417	0.282512	0.000020	-0.4	0.7	1411
		Spl32-11	50µ	414	7.7	0.3	0.282478	0.000022	0.000835	0.000107	0.028968	0.282472	0.000022	-1.9	0.8	1502
		Spl32-12	50µ	414	7.3	0.3	0.282535	0.000016	0.000581	0.000042	0.019640	0.282530	0.000016	0.2	0.6	1370
		Spl32-14	50µ	414	7.7	0.3	0.282517	0.000017	0.000940	0.000026	0.030635	0.282510	0.000017	-0.5	0.6	1417
		Spl32-16	50µ	414	7.2	0.3	0.282529	0.000015	0.001040	0.000015	0.035566	0.282521	0.000015	-0.1	0.5	1392
	E1	Spl25-2	50µ	418	7.4	0.3	0.282522	0.000022	0.000869	0.000056	0.029546	0.282515	0.000022	-0.2	0.8	1402
		Spl25-3	50µ	418	7.7	0.3	0.282516	0.000019	0.001103	0.000053	0.035054	0.282508	0.000019	-0.5	0.7	1419
		Spl25-5	50µ	418	7.7	0.3	0.282514	0.000016	0.000437	0.000016	0.012745	0.282511	0.000016	-0.4	0.6	1412
		Spl25-7	50µ	418	8.0	0.3	0.282508	0.000015	0.000981	0.000015	0.030472	0.282500	0.000015	-0.8	0.5	1436
		Spl25-9	50µ	418	7.9	0.3	0.282515	0.000019	0.001102	0.000025	0.036378	0.282506	0.000019	-0.6	0.7	1423
		Spl25-20	50µ	418	7.9	0.3	0.282492	0.000014	0.000680	0.000040	0.018528	0.282487	0.000014	-1.2	0.5	1466
		Spl25-25	50µ	418	7.7	0.3	0.282508	0.000018	0.000915	0.000028	0.029826	0.282501	0.000018	-0.7	0.6	1434
		Spl25-28	50µ	418	8.0	0.3	0.282519	0.000012	0.000365	0.000020	0.011371	0.282516	0.000012	-0.2	0.4	1400
		Spl25-32	50µ	418	7.8	0.3	0.282518	0.000014	0.000636	0.000022	0.018836	0.282513	0.000014	-0.3	0.5	1408

† - $T(DM)^c$ = model ages assuming felsic crust and depleted mantle values of $^{176}Lu/^{177}Hf$ = 0.0384, $^{176}Hf/^{177}Hf$ = 0.283250 (Nowell et al 1998).

^{176}Lu decay constant = 1.867×10-11y-1 (Soderlund et al 2004).

Appendix I

Zircon trace element concentrations

	Criffell										
Zone	1	1	1	1	1	1	1	1	1	2	2
Sample	17_9	17_12	17_60	17_93	17_94	17_92	17_85	17_63	17_68	18_10	18_19
Si	140230	140230	140230	140230	140230	140230	140230	140230	140230	140230	140230
P	64	56	203	144	134	135	143	125	82	236	215
Ca	2	3	3	7	8	2	3	10	18	7	4
Ti	3	3	5	7	7	7	7	6	3	4	4
Y	870	408	1096	835	821	931	917	708	566	598	532
Zr	471600	469670	453720	471940	470660	469630	475410	445870	453380	458010	452870
Ba	0.0	0.0	0.4	0.1	0.2	0.3	0.3	0.3	0.2	0.2	0.0
La	0.2	0.2	0.3	0.2	0.2	0.1	0.1	0.0	0.0	0.1	0.1
Ce	42.2	23.9	48.0	44.7	43.9	47.4	43.3	37.2	30.8	27.3	25.9
Pr	0.2	0.1	0.3	0.2	0.3	0.3	0.2	0.1	0.1	0.1	0.1
Nd	3.8	1.6	4.6	2.5	3.9	3.6	5.1	1.7	0.6	1.1	1.9
Sm	4.1	1.8	5.5	3.5	5.1	5.8	5.5	3.4	2.3	2.4	1.7
Eu	1.7	0.5	2.0	0.9	1.4	1.7	1.6	0.8	0.6	0.6	0.7
Gd	15.4	5.7	25.8	16.0	19.5	24.3	23.5	15.6	10.2	9.2	7.0
Tb	6.0	2.2	8.5	5.9	6.2	8.1	7.4	5.6	3.8	3.5	3.2
Dy	61.4	25.7	92.2	66.9	71.1	86.4	85.7	58.2	41.2	41.2	37.6
Ho	24.2	11.1	34.9	25.8	26.2	30.1	29.2	21.9	16.9	16.0	14.7
Er	122.0	56.8	150.4	112.8	117.7	123.0	130.4	96.3	75.3	77.5	71.9
Tm	30.0	13.7	36.5	25.0	24.1	27.5	27.8	21.8	18.1	17.2	16.9
Yb	295.2	145.5	305.8	221.8	218.4	235.7	241.1	191.8	175.6	179.1	163.2
Lu	78.2	41.2	69.0	54.3	49.9	53.2	56.0	39.4	40.3	38.1	40.6
Hf	12011	12389	11589	10908	10211	9926	10135	9506	11629	8554	8493
Pb	1076	792	405	645	532	434	515	552	704	368	412
Th	527	190	367	222	220	254	232	166	160	129	136
U	1329	604	526	356	317	338	309	245	481	359	349
T(Zrc)/°C[†]	666	666	716	742	740	746	741	725	665	694	688
Eu/Eu*	0.6	0.4	0.5	0.4	0.4	0.4	0.4	0.3	0.4	0.4	0.6
Ce/Ce*	57	42	37	52	42	52	60	144	186	114	71
***f*O$_2$**[*]	5.43E-18	4.11E-19	8.25E-17	3.25E-14	4.93E-15	5.69E-14	1.12E-13	3.31E-11	1.28E-13	8.97E-14	6.45E-16
D FMQ	0.7	-0.4	0.6	2.5	1.7	2.6	3.1	5.9	5.1	4.2	2.2

	Criffell										
Zone	2	2	2	2	2	2	2	2	3	3	3
Sample	18_16	18_35	18_60	18_76	18_83	18_7	18_22	18_21	21_48	21_60	21_73
Si	140230	140230	140230	140230	140230	140230	140230	140230	140230	140230	140230
P	196	189	123	85	142	97	104	78	207	105	133
Ca	9	7	5	4	6	16	13	22	8	6	2
Ti	5	5	6	3	7	3	3	3	6	3	2
Y	1237	2104	880	388	941	723	719	509	1003	575	508
Zr	456020	452950	477080	465120	474780	449920	448000	443450	455670	459860	462490
Ba	0.3	0.2	0.0	-0.2	0.4	0.0	0.3	0.2	0.3	0.1	0.4
La	0.2	2.3	0.1	0.1	0.1	0.1	0.0	0.1	0.2	0.3	0.0
Ce	46.1	101.7	36.0	24.1	46.5	35.4	41.4	29.2	63.2	41.3	27.0
Pr	0.3	1.7	0.3	0.1	0.3	0.1	0.1	0.1	0.4	0.3	0.1
Nd	5.2	17.6	3.7	0.9	4.0	1.6	1.7	0.7	3.8	2.8	0.8
Sm	6.5	15.0	6.0	1.4	6.2	3.1	2.3	1.2	3.7	2.3	1.5
Eu	1.8	5.3	1.5	0.5	1.2	0.9	0.9	0.5	0.9	0.8	0.7
Gd	27.6	48.6	20.5	6.2	25.4	14.5	9.6	7.1	16.3	8.9	7.5
Tb	9.6	16.4	6.5	2.4	7.7	5.1	3.9	2.3	5.8	3.6	3.3
Dy	99.4	167.4	71.8	28.1	81.8	55.5	51.6	32.2	75.7	39.5	37.0
Ho	35.1	60.9	26.5	11.9	29.9	20.8	19.7	13.4	29.8	16.2	14.2
Er	157.4	269.9	115.4	53.0	128.2	92.5	97.7	68.6	141.2	74.9	69.3
Tm	35.3	56.1	25.3	13.4	28.0	21.0	21.9	15.8	31.8	17.7	15.2
Yb	302.6	504.5	233.9	130.8	246.1	186.8	225.0	156.5	294.5	173.6	142.8
Lu	66.8	108.5	56.5	32.9	56.9	42.2	51.7	40.8	69.6	43.1	37.1
Hf	8787	7987	10066	10447	10185	9606	9266	10129	7930	10386	9330
Pb	423	727	566	481	582	558	608	605	539	710	424
Th	326	750	234	92	264	172	183	137	392	312	111
U	511	1081	362	301	353	345	485	438	658	949	324
T(Zrc)/°C[†]	721	712	727	680	750	681	677	661	739	669	657
Eu/Eu*	0.4	0.6	0.4	0.5	0.3	0.4	0.6	0.5	0.4	0.5	0.7
Ce/Ce*	48	12	49	54	70	85	175	56	55	33	207
fO_2[*]	1.62E-15	2.79E-21	3.47E-15	2.42E-17	1.09E-12	1.45E-15	3.86E-13	2.34E-18	3.61E-14	7.73E-20	1.18E-13
D FMQ	1.7	-3.8	1.9	1.0	3.8	2.7	5.3	0.5	2.6	-1.2	5.3

	Criffell										
Zone	3	3	3	3	3	3	4	4	4	4	4
Sample	21_78	21_92	21_69	21_37	21_38	21_46	22_7	22_62	22_92	22_33	22_32
Si	140230	140230	140230	140230	140230	140230	140230	140230	140230	140230	140230
P	158	101	155	85	128	129	163	210	112	283	199
Ca	12	3	2	16	57	64	30	9	7	8	6
Ti	5	1	5	3	3	3	3	3	1	3	3
Y	650	689	1045	658	1018	673	799	705	528	1036	713
Zr	460060	462170	453610	453440	451520	450780	462410	462760	456220	465360	460410
Ba	0.6	0.3	0.2	0.3	0.0	0.0	0.6	0.2	0.2	0.2	-0.1
La	0.9	0.1	0.1	0.5	0.4	0.2	0.6	0.2	0.3	0.0	0.0
Ce	35.5	20.6	62.5	37.0	39.3	49.0	24.6	15.8	13.8	61.7	24.2
Pr	0.6	0.1	0.1	0.3	0.3	0.2	0.6	0.1	0.2	0.1	0.1
Nd	4.7	0.6	2.0	2.9	4.2	1.5	5.3	0.9	1.4	1.6	0.5
Sm	3.2	0.9	3.4	2.7	5.6	1.8	4.0	1.2	0.9	3.7	1.4
Eu	0.9	0.3	1.0	1.0	2.4	0.8	1.6	0.4	0.5	1.3	0.6
Gd	9.5	5.2	15.4	10.5	23.1	11.9	14.3	8.0	3.3	18.1	10.5
Tb	4.0	2.1	5.8	3.5	8.0	4.4	5.7	3.5	1.9	5.9	4.0
Dy	43.9	32.9	77.0	44.5	82.9	50.0	58.8	43.9	28.1	70.9	50.3
Ho	17.7	14.9	31.0	17.6	30.6	18.9	22.4	19.3	11.9	27.9	20.2
Er	91.1	90.8	145.2	88.2	131.3	89.1	110.6	90.4	71.4	133.2	95.6
Tm	20.8	24.6	33.1	20.3	27.4	19.1	23.8	22.8	17.7	30.0	21.7
Yb	207.6	279.1	297.8	198.5	252.0	187.8	225.1	225.6	211.2	290.9	200.6
Lu	50.7	87.3	70.9	49.7	54.1	43.2	50.7	53.6	57.5	65.9	51.4
Hf	9166	11829	8455	9863	9119	9421	11215	12203	11806	8781	9748
Pb	560	1104	479	641	537	687	733	828	749	585	682
Th	251	366	316	158	253	331	236	179	189	381	203
U	643	1810	699	446	449	665	1061	1259	1233	770	791
T(Zrc)/°C[†]	708	610	717	671	678	676	671	674	599	671	663
Eu/Eu*	0.5	0.4	0.4	0.6	0.6	0.5	0.6	0.4	0.9	0.5	0.5
Ce/Ce*	11	62	161	22	30	64	10	30	14	465	134
***f*O$_2$**[*]	1.18E-21	3.14E-21	3.09E-11	3.52E-21	1.05E-19	6.21E-17	2.69E-24	6.47E-20	1.29E-27	7.89E-10	6.13E-15
D FMQ	-4.1	-0.8	6.1	-2.6	-1.3	1.5	-5.7	-1.4	-6.9	8.8	3.9

	Criffell											
Zone	4	4	4	4	4	E1	E1	E1	E1	E1	E2
Sample	22_29	22_30	22_37	22_38	22_47	17E_14	17E_21	17E_1	17E_3	17E_5	18E_15
Si	140230	140230	140230	140230	140230	140230	140230	140230	140230	140230	140230
P	153	130	153	173	281	213	109	142	148	203	134
Ca	24	18	6	12	10	4	2	8	12	13	2
Ti	3	5	2	3	2	10	4	7	8	10	6
Y	774	1114	734	628	846	1415	391	455	465	948	561
Zr	463140	457150	460300	455200	459350	468680	472990	449830	457070	447350	475720
Ba	0.5	0.2	0.3	0.1	0.2	0.5	0.1	0.0	0.5	0.0	0.3
La	0.4	1.1	0.1	0.0	0.2	0.4	0.2	0.0	0.0	0.1	0.3
Ce	23.1	65.9	20.2	32.0	25.2	53.9	23.6	25.2	29.5	88.3	54.8
Pr	0.5	0.9	0.1	0.0	0.2	1.0	0.2	0.1	0.1	0.2	0.3
Nd	2.4	7.4	0.4	0.7	3.1	12.6	2.2	0.5	1.2	5.0	4.1
Sm	2.2	5.4	1.7	1.8	3.1	11.8	1.9	2.1	2.2	6.3	4.1
Eu	1.1	1.9	0.6	0.8	1.1	4.7	0.8	0.5	0.6	1.8	1.1
Gd	8.3	19.5	8.6	9.5	14.1	40.5	6.3	7.2	8.7	24.0	12.9
Tb	3.8	6.8	4.0	4.1	5.3	11.1	2.2	2.7	3.4	7.0	4.0
Dy	46.1	78.9	48.9	46.1	65.6	118.4	27.6	35.7	37.2	77.3	45.7
Ho	20.4	31.3	19.6	18.0	23.3	44.6	11.4	13.4	13.5	28.4	16.7
Er	99.1	150.3	100.3	87.9	110.5	194.7	56.5	59.5	61.4	124.9	79.0
Tm	23.5	33.9	23.6	20.3	25.0	43.1	13.7	13.6	13.3	25.4	17.7
Yb	238.5	314.4	232.5	204.9	236.8	385.2	131.8	131.7	122.6	235.6	162.8
Lu	62.3	75.4	60.1	49.5	52.0	95.3	33.3	28.9	29.1	50.7	40.5
Hf	11043	8958	11431	9551	11361	7538	12155	9106	9022	8617	10614
Pb	823	596	292	613	885	551	541	360	336	417	644
Th	265	334	242	188	216	460	75	90	126	642	402
U	1280	786	1315	519	1093	417	240	199	233	625	552
T(Zrc)/°C[†]	681	714	620	659	649	780	697	750	764	783	737
Eu/Eu*	0.8	0.6	0.5	0.6	0.5	0.6	0.7	0.4	0.4	0.4	0.5
Ce/Ce*	11	16	81	227	26	21	26	141	132	184	40
***f*O$_2$**[*]	3.28E-23	3.98E-20	1.64E-19	3.56E-13	5.20E-22	9.45E-16	4.52E-19	5.01E-10	1.43E-09	1.92E-07	1.94E-15
D FMQ	-4.9	-2.7	0.6	5.7	-2.8	0.1	-1.2	6.5	6.6	8.3	1.4

	Criffell								
Zone	E2	E2	QD	QD	QD	QD	QD	QD	QD
Sample	18E_5	18E_10	36_5	36_6	36_26	36_21	36_1	36_2	36_3
Si	140230	140230	140230	140230	140230	140230	140230	140230	140230
P	116	141	257	156	120	140	150	180	145
Ca	17	30	3	2	3	3	13	15	22
Ti	4	5	6	7	6	7	6	6	10
Y	1023	1597	665	596	731	430	500	764	1044
Zr	456920	459480	471130	471970	471080	475160	448990	453370	455060
Ba	0.2	0.4	0.0	0.1	0.2	0.2	0.3	0.0	0.2
La	0.3	3.6	0.1	0.1	0.1	0.1	0.0	0.0	4.6
Ce	44.4	99.3	32.7	32.5	37.0	35.8	37.7	43.1	70.8
Pr	0.3	2.9	0.2	0.1	0.1	0.1	0.1	0.1	3.1
Nd	5.1	23.7	2.0	1.8	2.5	1.5	1.1	1.4	20.4
Sm	6.2	15.2	2.7	2.9	3.5	2.2	2.1	2.4	9.6
Eu	1.7	4.8	0.7	0.8	0.8	0.4	0.6	0.8	2.7
Gd	22.4	40.2	12.3	11.7	15.2	8.3	9.0	11.9	26.8
Tb	7.5	12.1	4.3	3.7	5.8	2.8	3.1	4.3	8.5
Dy	81.8	128.4	49.0	44.4	59.2	31.5	36.3	55.1	90.6
Ho	29.3	45.4	19.8	17.4	22.3	13.2	14.1	22.0	32.1
Er	128.4	197.2	90.9	83.5	103.2	57.2	67.4	103.4	143.4
Tm	29.9	43.3	20.7	19.5	22.2	14.1	14.7	24.1	30.5
Yb	270.6	377.1	197.9	196.1	189.1	124.1	138.6	222.2	263.1
Lu	60.9	86.3	47.4	47.1	47.7	30.4	32.9	53.9	59.7
Hf	9564	9012	10076	9622	10359	11091	9704	9368	9930
Pb	564	646	489	424	488	564	412	428	454
Th	306	519	145	158	161	156	143	171	552
U	527	707	294	319	252	330	278	361	467
T(Zrc)/°C[†]	697	715	735	750	732	739	737	739	780
Eu/Eu*	0.4	0.6	0.4	0.4	0.3	0.2	0.4	0.5	0.5
Ce/Ce*	35	7	53	62	65	84	146	203	4
***f*O$_2$**[*]	5.24E-18	5.86E-23	2.00E-14	4.19E-13	7.91E-14	1.66E-12	1.54E-10	3.18E-09	1.36E-21
D FMQ	-0.1	-5.6	2.5	3.4	3.1	4.3	6.3	7.6	-5.8

	Fleet											
Zone	1	1	1	1	2	2	2	2	2	3	3	3
Sample	33_41	33_1	33_12	33_19	34_80	34_47	34_52	34_54	34_65	35_15	35_12	35_6
Si	140230	140230	140230	140230	140230	140230	140230	140230	140230	140230	140230	140230
P	309	399	232	106	283	524	1148	375	154	78	156	1633
Ca	23	36	29	23	5	46	1374	269	34	3	7	2011
Ti	5	3	14	3	6	11	23	7	4	2	11	3
Y	1021	1173	1807	422	1421	3877	2391	1670	701	334	489	4684
Zr	466540	452070	449670	444860	469450	459240	438920	431230	441880	466780	474880	433800
Ba	0.1	0.4	0.3	0.4	-0.2	0.6	0.4	0.9	0.2	0.1	0.4	1.3
La	1.9	1.7	0.4	0.0	0.1	3.6	6.1	1.1	0.8	0.1	0.2	6.3
Ce	21.9	18.8	30.9	15.5	43.3	188.6	38.7	39.9	27.3	3.2	26.2	19.2
Pr	1.2	0.7	0.7	0.1	0.6	3.0	4.3	0.7	0.4	0.1	0.2	1.6
Nd	9.0	5.0	11.7	0.7	5.9	28.6	26.6	7.0	2.7	0.7	2.7	6.6
Sm	7.3	4.8	12.2	1.0	8.4	25.5	13.1	9.7	2.7	0.9	2.5	5.3
Eu	1.1	0.6	2.6	0.3	1.4	5.7	0.8	1.3	0.4	0.3	0.6	0.5
Gd	21.7	17.3	44.8	5.0	31.3	103.1	39.4	38.6	10.6	3.6	10.0	32.7
Tb	6.7	7.1	15.1	2.5	11.5	33.0	16.6	13.2	4.2	1.4	3.7	19.9
Dy	79.8	83.4	155.5	29.2	121.1	358.0	186.5	143.4	55.5	16.5	39.2	310.2
Ho	30.0	34.2	55.3	11.9	44.0	127.4	70.9	52.1	20.7	8.9	14.6	131.8
Er	137.4	163.8	236.8	56.1	194.3	522.1	329.3	223.7	95.3	52.9	66.1	685.1
Tm	29.6	36.3	46.6	12.9	41.1	106.1	72.0	44.3	21.1	14.6	14.9	175.9
Yb	275.8	324.9	413.6	123.7	344.1	853.9	635.5	383.3	195.4	168.8	134.8	1766.4
Lu	65.2	72.8	84.2	28.2	76.7	178.8	136.5	82.9	43.3	47.8	32.3	390.4
Hf	11603	10810	8112	9986	10177	9652	10779	8261	10849	10630	9265	16461
Pb	697	794	399	490	530	869	1211	498	540	448	489	3749
Th	182	217	251	64	215	1435	401	318	175	25	91	173
U	614	779	222	158	311	1294	2045	410	423	85	177	7282
T(Zrc)/°C[†]	721	667	813	669	725	795	869	747	697	654	787	674
Eu/Eu*	0.3	0.2	0.3	0.3	0.3	0.3	0.1	0.2	0.2	0.4	0.4	0.1
Ce/Ce*	3	4	14	91	35	14	2	11	11	8	32	1
fO_2^*	2.15E-25	6.16E-28	1.18E-15	4.52E-16	1.54E-16	1.08E-16	3.79E-21	1.03E-19	2.29E-22	5.67E-26	7.43E-14	2.66E-31
D FMQ	-8.2	-9.3	-0.6	2.6	0.6	-1.2	-7.2	-3.1	-4.5	-6.9	1.8	-12.8

	Fleet		Shap								
Zone	3	3	1	1	1	2	2	2	E1	E1	E2
Sample	35_13	35_17	23_7	23_5	23_19	32_12	32_18	32_16	25_5	25_28	26_8
Si	140230	140230	140230	140230	140230	140230	140230	140230	140230	140230	140230
P	194	320	93	212	197	44	129	219	160	155	189
Ca	29	31	12	19	200	18	16	165	15	23	15
Ti	7	13	4	7	8	3	9	7	4	3	5
Y	577	1264	938	992	1617	396	1444	1680	912	1173	1595
Zr	445420	443060	445280	447740	443320	436490	441950	449200	445350	453530	442040
Ba	0.2	0.3	0.2	0.4	0.9	0.0	0.3	0.2	0.0	0.2	0.1
La	0.0	1.3	0.0	0.9	58.4	0.1	0.4	0.9	0.0	0.4	0.1
Ce	34.9	85.1	39.0	54.0	137.7	29.6	65.7	98.0	47.4	30.2	62.0
Pr	0.1	0.8	0.1	0.5	5.7	0.3	0.9	0.6	0.1	0.3	0.3
Nd	1.2	8.3	2.7	5.1	26.2	3.3	11.5	8.4	1.8	1.8	5.7
Sm	2.4	6.4	4.7	6.1	7.9	3.7	13.4	11.8	3.4	3.8	8.8
Eu	0.7	1.9	1.2	1.9	3.0	1.2	4.3	3.8	1.2	1.1	2.8
Gd	11.3	26.2	19.0	24.5	26.3	12.8	48.2	46.6	17.7	20.7	36.3
Tb	3.9	7.9	6.6	7.8	10.0	3.7	14.2	14.3	6.8	8.7	12.4
Dy	44.0	96.3	72.8	84.5	114.4	39.0	137.6	141.8	70.4	99.1	136.3
Ho	16.5	37.0	25.5	28.5	43.9	12.4	44.8	49.6	26.0	35.7	47.2
Er	76.6	164.0	111.4	116.2	211.9	52.0	172.4	208.2	116.2	155.7	198.8
Tm	16.7	35.7	25.7	24.9	49.2	11.1	33.6	44.7	24.9	33.1	42.7
Yb	156.3	278.0	233.1	218.6	460.9	99.1	284.2	386.2	220.6	278.2	364.9
Lu	37.2	62.5	56.2	47.0	104.3	22.4	54.0	83.6	49.1	60.7	76.1
Hf	8539	8102	11564	10178	11718	10782	9609	10301	11160	12333	10607
Pb	454	540	362	221	720	281	197	404	309	337	339
Th	138	493	374	261	1342	272	352	801	328	342	559
U	254	570	596	321	2056	368	306	852	542	695	607
T(Zrc)/°C[†]	751	804	689	749	763	681	769	746	689	664	720
Eu/Eu*	0.4	0.4	0.4	0.5	0.6	0.5	0.5	0.5	0.5	0.4	0.5
Ce/Ce*	141	19	132	20	2	37	25	31	251	22	109
fO_2^*	5.89E-10	6.08E-15	1.74E-13	1.64E-17	7.79E-26	1.18E-18	1.20E-15	6.01E-16	4.63E-11	1.02E-21	1.51E-12
D FMQ	6.5	0.3	4.6	-1.0	-9.6	-0.4	0.4	0.7	7.0	-3.0	4.7

	Shap	
Zone	E2	E2
Sample	26_15	26_22
Si	140230	140230
P	128	191
Ca	13	33
Ti	14	10
Y	2609	1384
Zr	439830	439970
Ba	0.0	0.4
La	1.4	0.3
Ce	162.7	77.6
Pr	2.5	0.8
Nd	28.5	12.8
Sm	31.6	15.4
Eu	10.6	3.7
Gd	99.3	49.7
Tb	26.3	14.7
Dy	249.5	137.4
Ho	78.0	42.2
Er	311.1	158.6
Tm	60.8	30.7
Yb	495.9	249.3
Lu	103.1	49.9
Hf	7920	8376
Pb	240	218
Th	1082	455
U	558	406
T(Zrc)/°C[†]	819	781
Eu/Eu*	0.6	0.4
Ce/Ce*	20	38
fO_2^*	4.3E-14	1.9E-13
D FMQ	0.9	2.4

[†]Ti-in-zircon thermometer, Ferry and Watson (2007) after Watson and Harrison (2005)
Oxygen fugacity calculated using the Ce/Ce calibration of Trail et al (2011)

Appendix J

Quartz $\delta^{18}O$ compositions

Pluton	Zone	Sample	$^{18}O/^{16}O$	% 2SD	1 s.e.m	$\delta^{18}O$	2SD	1 s.e.m	comment
Session 1 (14.06.2012)									
Criffell	1	17_1	0.00200977			*9.0*			edge
	1	17_2	0.00201025			9.2			
	1	17_3	0.00201046			9.3			400µm
	1	17_4	0.00201013			9.2			traverse
	1	17_5	0.00201074			9.5			
	1	17_6	0.00201099			9.6			middle
	1	17_7	0.00201114			9.7			
	1	17_8	0.00201121			9.7			
	1	17_9	0.00201333			*10.8*			edge
	1	17_10	0.00201265			*10.4*			edge
		Bog.	0.00201632	0.01733424	0.00387605	12.3	0.24	0.05166259	
	1	17_11	0.00200597			*7.1*			*edge*
	1	17_12	0.00201174			10.0			
	1	17_13	0.00201195			10.1			300µm
	1	17_14	0.00201131			9.7			traverse
	1	17_15	0.00201096			9.6			
	1	17_16	0.00201002			9.1			
	1	17_17	0.0020098			9.0			middle
	1	17_18	0.00200838			*8.3*			crack
	1	17_19	0.00201042			9.3			
	1	17_20	0.00201123			9.7			edge
		Bog.	2.02E-03	1.98E-02	0.00442755	12.4	0.26	0.05923275	
	1	17_21	0.00201149			9.8			Multiple
	1	17_22	0.00201196			10.0			small grains
	1	17_23	0.00201069			9.4			
	1	17_24	0.00201039			9.2			
	1	17_25	0.00201084			9.5			
	1	17_26	0.00201022			9.2			
	1	17_27	0.00200925			8.7			
	1	17_28	0.00201047			9.3			
	1	17_29	0.0020141			*11.1*			crack
	1	17_30	0.00201753			*12.8*			crack
		Bog.	2.02E-03	1.91E-02	0.0042693	12.3	0.28	0.06458754	
	1	17_31	0.00200999			9.0			Multiple
	1	17_32	0.00200969			8.9			small grains
	1	17_33	0.00201112			9.6			
	1	17_34	0.00200821			*8.1*			inclusion
	1	17_35	0.0020117			9.9			
	1	17_36	0.00201176			9.9			
	1	17_37	0.00200971			8.9			
	1	17_38	0.0020101			9.1			
	1	17_39	0.00201006			9.0			
	1	17_40	0.00201004			9.0			
		Bog.	2.02E-03	1.58E-02	0.00354326	12.4	0.24	0.0523048	

Pluton	Zone	Sample	$^{18}O/^{16}O$	% 2SD	1 s.e.m	$\delta^{18}O$	2SD	1 s.e.m	comment
Session 2 (14.06.2012)									
		Bog.	2.02E-03	1.63E-02	0.00363445	12.8	0.22	0.04908714	
	3	21_1	0.00201102			10.3			edge
	3	21_2	0.00201047			10.0			
	3	21_3	0.00201025			9.9			700µm
	3	21_4	0.00201004			9.8			traverse
	3	21_5	0.00200985			9.7			
	3	21_6	0.00201056			10.1			middle
	3	21_7	0.00201052			10.1			
	3	21_8	0.00201012			9.9			
	3	21_9	0.00201016			9.9			
	3	21_10	0.00201037			10.0			edge
		Bog.	0.0020151	0.01807573	0.00404186	12.3	0.14	0.03036172	
	3	21_11	0.002009			9.3			Multiple
	3	21_12	0.00200966			9.6			small grains
	3	21_13	0.00200908			9.3			
	3	21_14	0.00200907			9.3			
	3	21_15	0.00201086			10.2			
	3	21_16	0.00200891			9.2			
	3	21_17	0.0020082			*8.9*			crack
	3	21_18	0.0020088			9.2			
	3	21_19	0.00201031			9.9			
	3	21_20	0.00201081			10.2			
		Bog.	0.00201503	0.01670714	0.00373583	11.6	0.38	0.08671581	
	3	21_21	0.00200846			9.0			edge
	3	21_22	0.00200651			*8.0*			inclusion
	3	21_23	0.00200614			*7.8*			inclusion
	3	21_24	0.00200781			8.6			300µm
	3	21_25	0.00200722			8.3			traverse
	3	21_26	0.00200732			8.4			middle
	3	21_27	0.00200716			8.3			
	3	21_28	0.00200816			8.8			
	3	21_29	0.00200692			8.2			
	3	21_30	0.00200689			8.2			edge
		Bog.	0.00201496	0.01524267	0.00340836	12.2	0.48	0.10881411	
	3	21_31	0.00200953			9.5			edge
	3	21_32	0.00200831			*8.8*			crack
	3	21_33	0.00200936			9.4			600µm
	3	21_34	0.00200946			9.4			traverse
	3	21_35	0.00201028			9.8			
	3	21_36	0.00201011			9.7			middle
	3	21_37	0.00200948			9.4			
	3	21_38	0.00201034			9.8			
	3	21_39	0.00201042			9.9			
	3	21_40	0.00201056			10.0			edge
		Bog.	0.00201541	0.01955497	0.00437262	12.4	0.26	0.05742788	

Pluton	Zone	Sample	$^{18}O/^{16}O$	% 2SD	1 s.e.m	$\delta^{18}O$	2SD	1 s.e.m	comment
Session 3 (15.06.2012)									
Fleet	1	33_1	0.00201231			12.8			Multiple
	1	33_2	0.002009			11.1			small grains
	1	33_3	0.00200781			10.5			
	1	33_4	0.00200758			10.4			
	1	33_5	0.00200902			11.1			
	1	33_6	0.00200858			10.9			
	1	33_7	0.00201045			11.9			
	1	33_8	0.00201035			11.8			
	1	33_9	0.00200968			11.5			
	1	33_10	0.00200762			10.4			
		Bog.	0.00201116	0.02021531	0.00452028	12.3	0.16	0.03632075	
	1	33_11	0.00200987			11.6			Multiple
	1	33_12	0.00200899			11.2			small grains
	1	33_13	0.00201069			12.1			
	1	33_14	0.00201083			12.1			
	1	33_15	0.00200986			11.7			
	1	33_16	0.0020095			11.5			
	1	33_17	0.00200976			11.6			
	1	33_18	0.00200929			11.4			
	1	33_19	0.00200943			11.5			
	1	33_20	0.00200928			11.4			
		Bog.	0.00201067	0.02062482	0.00461185	12.0	0.44	0.09875622	
	1	33_21	0.00200905			11.3			Multiple
	1	33_22	0.00200827			10.9			small grains
	1	33_23	0.00200967			11.7			
	1	33_24	0.00200998			11.8			
	1	33_25	0.00201018			11.9			
	1	33_26	0.00200762			10.6			
	1	33_27	0.00200762			10.7			
	1	33_28	0.0020089			11.3			
	1	33_29	0.00201725			*15.5*			crack
	1	33_30	0.00201247			*13.1*			edge
		Bog.	0.00201107	0.01982332	0.00443263	12.2	0.4	0.08970081	
Session 4 (15.06.2012)									
		Bog.	0.00201044	0.0214041	0.0047861	12.4	0.14	0.03000358	
	2	34_1	0.00201285			13.5			edge
	2	34_2	0.00200888			11.5			
	2	34_3	0.00200849			11.3			600µm
	2	34_4	0.00200803			11.1			traverse
	2	34_5	0.00200738			10.8			
	2	34_6	0.00200429			9.2			
	2	34_7	0.00200577			10.0			
	2	34_8	0.00200688			10.5			
	2	34_9	0.00200737			10.8			
	2	34_10	0.00200669			10.4			middle

Pluton	Zone	Sample	$^{18}O/^{16}O$	% 2SD	1 s.e.m	$\delta^{18}O$	2SD	1 s.e.m	comment
		Bog.	0.00201038	0.01965224	0.00439438	12.3	0.41	0.09260205	
	2	34_11	0.00200836			11.3			Multiple
	2	34_12	0.00200813			11.2			small grains
	2	34_13	0.00200785			11.0			
	2	34_14	0.00200786			11.1			
	2	34_15	0.00200818			11.2			
	2	34_16	0.00200728			10.8			
	2	34_17	0.00200783			11.0			
	2	34_18	0.00200835			11.3			
	2	34_19	0.00200773			11.0			
	2	34_20	0.00201212			13.2			edge
		Bog.	0.0020103	0.02464301	0.00551034	12.3	0.58	0.12948235	
	2	34_21	0.00200772			11.0			edge
	2	34_22	0.00200747			10.9			
	2	34_23	0.00200756			11.0			500µm
	2	34_24	0.00200756			11.0			traverse
	2	34_25	0.0020123			13.3			crack
	2	34_26	0.00200752			10.9			middle
	2	34_27	0.00200774			11.1			
	2	34_28	0.00200093			*7.6*			inclusion
	2	34_29	0.00200746			10.9			
	2	34_30	0.00200522			9.8			edge
		Bog.	0.00201017	0.02579514	0.00576797	12.2	0.3	0.06690055	

edge and middle are used to denot positions of traverses within single grains
italic figures were excluded when calcualting mean compositions due to edge or crack effects

Appendix K

Amphibole compositions

Electron probe amphibole compoistions (Zone 1 Criffell pluton)

	Na_2O	MgO	Al_2O_3	SiO_2	K_2O	CaO	FeO	TiO_2	MnO	Total	P (kbar)*	Depth (km)**	T/C†	P (kbar)×	Depth (km)×	Comment
AM0917	1.22	13.50	6.65	47.39	0.70	11.81	14.33	1.21	0.43	97.23	1.5	5.5	688	2.36	8.91	17_Amph1a
	1.03	13.46	6.29	48.13	0.58	12.25	14.44	0.98	0.42	97.58	1.2	4.4	675	2.16	8.15	17_Amph1b
	1.07	13.44	6.17	47.80	0.57	11.94	14.77	0.94	0.41	97.12	1.1	4.2	677	2.06	7.78	17_Amph1c
	1.11	13.84	6.25	48.14	0.58	12.30	13.88	1.10	0.43	97.65	1.1	4.3	679	2.09	7.89	17_Amph2a
	0.98	13.75	6.32	48.14	0.62	12.15	13.86	1.05	0.42	97.30	1.2	4.5	674	2.18	8.25	17_Amph2b
	1.04	13.70	6.20	47.63	0.64	12.11	13.85	1.04	0.41	96.63	1.1	4.3	679	2.10	7.91	17_Amph2c
	1.13	13.56	6.32	47.92	0.66	11.86	14.50	1.05	0.44	97.45	1.2	4.5	678	2.16	8.14	17_Amph2d_edge
	1.22	13.47	6.72	47.12	0.68	11.93	14.62	1.05	0.43	97.24	1.5	5.7	692	2.38	8.99	17_Amph3a_edge
	1.15	13.40	6.40	47.65	0.61	11.75	14.61	1.03	0.43	97.05	1.3	4.8	679	2.24	8.44	17_Amph3b
	1.10	12.98	6.64	47.24	0.71	11.87	15.37	1.01	0.44	97.36	1.5	5.5	687	2.37	8.95	17_Amph3_core
	0.98	13.40	6.28	47.62	0.66	12.03	14.36	1.04	0.43	96.80	1.2	4.5	678	2.16	8.17	17_Amph4c_core
	1.24	14.16	5.83	48.05	0.63	11.78	13.64	1.12	0.42	96.88	0.8	3.2	675	1.78	6.73	17_Amph4d_core
	1.32	13.75	6.62	47.35	0.72	11.78	13.96	1.23	0.42	97.15	1.4	5.4	690	2.32	8.74	17_Amph4e_edge
	1.24	13.86	6.30	47.78	0.66	11.70	13.75	1.28	0.40	96.98	1.2	4.5	681	2.13	8.04	17_Amph5a_core
	1.23	14.08	6.21	47.91	0.64	11.59	13.42	1.26	0.41	96.75	1.1	4.2	677	2.08	7.85	17_Amph5b_core
	1.21	14.10	6.13	47.84	0.59	11.81	13.99	1.01	0.42	97.09	1.1	4.0	681	1.98	7.48	17_Amph5c_middle
	1.15	13.84	6.12	47.89	0.63	11.86	14.00	0.98	0.43	96.89	1.1	4.0	676	2.03	7.65	17_Amph5d_edge
	1.14	13.72	6.46	47.30	0.60	11.83	14.05	1.20	0.43	96.74	1.3	5.0	687	2.23	8.41	17_Amph6a_core
	1.24	13.64	6.36	47.55	0.66	11.69	14.04	1.21	0.43	96.81	1.3	4.7	682	2.19	8.27	17_Amph6b_middle
	1.31	13.78	6.47	47.43	0.72	11.71	13.73	1.24	0.40	96.79	1.3	5.0	685	2.25	8.50	17_Amph6c_edge

* Al-in-hornblende barometer (Johnson and Rutherford, 1989)

** Depth conversions calculated assuming crustal density of 2700kgm^{-3}

†Amphibole-plagioclase barometer of Blundy and Holland (1990). Plagioclase composition: An_{25} (Ab_{75}) (BGS memoir for maps 5W, E and 6E)

× Amphibole barometer of Anderson and Smith (1995), depth conversions calculated assuming crustal density of 2700kgm^{-3}

Appendix L

Allanite EDS Spectra